

ANISOTROPIC NEUTRON TRANSPORT ANALYSIS

ANISOTROPIC NEUTRON TRANSPORT ANALYSIS

by

EL-TANTAWY A. ATTIA, B.Sc., M.Sc., M.Eng.

A Thesis

Submitted to the School of Graduate Studies

in Partial Fulfilment of the Requirements

for the Degree

Doctor of Philosophy

McMaster University

July 1976

DOCTOR OF PHILOSOPHY (1976)  
(Physics).

MCMASTER UNIVERSITY  
Hamilton, Ontario.

TITLE: Anisotropic Neutron Transport Analysis

AUTHOR: El-Tantawy A. Attia, B.Sc. (University of Alexandria)  
M.Sc. (University of Alexandria)  
M.Eng. (McMaster University)

SUPERVISOR: Dr. A.A. Harms

NUMBER OF PAGES: xxii, 233

## ABSTRACT

This study is concerned with the analysis of the neutron transport equation with anisotropic phenomena. The mathematical method chosen for this analysis is the partial-range orthogonal function for the representation of the angular dependence of the pertinent angular neutronic functions. These functions are the neutron angular flux and the external sources of neutrons as well as the scattering functions. Of the several existing models of neutron transport analysis, the time-independent one-group neutron transport equations for plane and spherical geometries have been selected.

The partial-range Legendre polynomials, which represent an orthogonal set of functions over an arbitrary range of the angular variable, have been used for the analysis in this research. The reproduction of the partial-range polynomials using the Gram-Schmidt orthogonalization theorem as well as the linear transformation of variables is mathematically examined; moreover, the properties of orthogonality, the recurrence relations, and the full-range integrations have been established. The distinguishing feature of this mathematical formalism is that it combines the features of both methods of the discrete ordinate methods and the spherical harmonics approximations for the neutron transport analysis. The features of the discrete ordinate methods are incorporated by the arbitrary segmentation of the angular variable into a number of intervals. Then, the features

of the spherical harmonics methods are included by expanding the neutronic functions in terms of the partial-range Legendre polynomials over these intervals. Hence, this formalism is very appropriate for the transport problems involving highly varying angular fluxes and strong anisotropic scattering.

For plane geometry, two different partial-range formalisms have been systematically developed. In both formalisms, the neutron angular flux and the external sources of neutrons are expanded in terms of partial-range Legendre polynomials. In the first formalism, which is designated by the  $NP_L$  approximation, the scattering function has been represented in terms of full-range Legendre polynomials; in the second formalism, which is designated by the  $NP_L$ - $MP_K$  approximation, the scattering function is reconstructed using the partial-range Legendre polynomials. The two formalisms allow for discontinuities in the angular flux as well as the external sources of neutrons at arbitrary points of the angular variable. However, it is only the second formalism of the partial-range scattering functions which allows for such discontinuities in the scattering functions at arbitrary points of the scattering angular variables. This permits the representation of the scattering function to a high accuracy with few terms.

An indication of the computational usefulness of these formalisms was obtained by calculating some neutronic parameters using low-order approximations. The  $NP_L$  approximations have been used to calculate the eigenvalues associated with the homogeneous neutron transport equation which gives the diffusion length. Moreover, the end point, the linear

extrapolation length and the ratio of the asymptotic flux to the total flux associated with the vacuum boundary of the Milne's problem in plane geometry have been examined. It has been found that this formalism of the partial-range analysis is better than the conventional methods of analysis especially for highly absorbing media and strong anisotropic scattering processes. In a certain sense, the low-order  $2P_0$  approximation doubles the range of  $c$  for the same accuracy compared to the usual double- $P_0$  approximation; the constant  $c$  is the average number of secondary neutrons per collision.

Three different low-order approximations of the  $NP_L$ - $MP_K$  analysis have been examined and compared with each other as well as with the alternative methods of the same complexity. A highly anisotropic scattering function, for which the exact eigenvalue is known, has been used for the comparison. It has been found that the  $DP_L$ - $2P_K$  approximation is very adequate for the analysis of problems with highly anisotropic scattering. Moreover, the  $DP_0$ - $DP_0$  approximation is used to examine the critical thickness of a bare slab reactor. For practical compositions of the critical reactors, the critical thickness changes considerably with the degree of anisotropy. The effect of anisotropic scattering, therefore, must be considered in the analysis and design of nuclear reactors especially when strong anisotropic scattering is involved.

A general formalism, which allows for discontinuities in the neutron angular flux and its angular derivatives at position dependent points of the angular variables, has been established for spherical geometry. This formalism is exact and free of any functional assumptions

and exactly represents the actual behaviour of the discontinuities in the angular flux, and hence it satisfies the boundary conditions exactly. The low-order  $2P_0$  approximation has been used to study the spherical Milne's problem. The results show discontinuities in the angular flux at position dependent angular points which are expected from the physical processes of the problem. The important feature of this formalism is that the  $2P_0$  approximation, which is of the same computational complexity as the diffusion theory, gives the total flux with much higher accuracy especially close to the surface of the sphere.

Finally, the partial-range formalism has been used to study some reactor physics problems of current practical interest. This is concerned with the reconstruction of elastic scattering cross sections as well as the group-to-group transfer cross sections. For a numerical illustration, the elastic scattering cross sections of 14.0 MeV neutrons of  $U^{238}$  and  $Bi^{209}$ , which are highly anisotropic, have been reconstructed. The results show improvement over the usual full-range representation of the scattering function. Further, the group-to-group cross sections of hydrogen, oxygen and water from (3.3287-3.0119) MeV to (2.7253-2.4600) MeV have been reconstructed using low-order representation. The results are in good agreement with the exact values and more accurate compared to the full-range Legendre polynomials approximation; the reason for this is that the group-to-group cross section is well-behaved only over certain ranges of the scattering angular variables. Moreover, this representation provides an additional degree of freedom: it is not necessary to employ the same order of approximation over the various allowable directional

ranges of the scattering angular variable. The order can be varied according to the extent of anisotropy of the scattering cross section, over each range. This suggests that the partial-range approximation of the scattering functions and the group-to-group cross sections represents a potentially useful representation redundant in the neutron transport analysis with highly anisotropic scattering; a case in hand is the fast breeder reactor, the calculation of the blanket of the proposed fusion reactors, and detailed neutronic calculation in interface regions of thermal reactors.



## ACKNOWLEDGEMENTS

The author gratefully acknowledges the useful comments and suggestions as well as the supervision of Dr. A.A. Harms during the course of this work. Helpful discussions with Dr. S.A. Kushneriuk, Theoretical Physics Branch, Chalk River Nuclear Laboratories, Chalk River, Ontario, are appreciated.

The author also wishes to thank Dr. A.B. Volkov and Dr. J.E. Robinson, the members of the supervisory committee, for their counsel and advice. The cooperation of all the members of the theoretical physics group at that time is sincerely appreciated. Also, financial support of the NRC is gratefully acknowledged.

The author would also like to thank Miss Beverley Erskine for the final typing of the thesis and Mr. Essam Allam for the drafting of the graphs.

Finally, thanks are due to the author's wife, Soheir Attia, for providing a home environment conducive to academic endeavours and for the typing of the preliminary draughts of this dissertation.

## TABLE OF CONTENTS

	<u>Page No.</u>
ABSTRACT	111
ACKNOWLEDGEMENTS	v111
TABLE OF CONTENTS	ix
LIST OF FIGURES	x11
LIST OF TABLES	xx1
CHAPTER I: INTRODUCTION	1
1.1 Preface	1
1.2 Neutron Transport Equation	5
1.3 Anisotropy: Sources and Effects	8
1.4 Scope of This Thesis	14
CHAPTER II: PARTIAL-RANGE SPHERICAL HARMONICS FORMULATION	19
2.1 Introduction	19
2.2 Reproduction of Partial-Range Spherical Harmonics	21
2.3 Properties of Partial-Range Legendre Polynomials	24
2.4 Partial-Range Expansion of Full-Range Legendre Polynomials	26
2.5 Generalization of Partial-Range Orthogonal Polynomials	28
CHAPTER III: PLANE GEOMETRY: FULL-RANGE SCATTERING FUNCTIONS	33
3.1 Introduction	33
3.2 Solution Formulation	35

	<u>Page No.</u>
3.3 Special Cases	39
3.3.1 Isotropic Scattering	39
3.3.2 Double Spherical Harmonics Approximation	41
3.4 $NP_L$ Approximation	42
3.5 $NP_0$ Approximation and the Eigenvalues	43
3.6 $2P_0$ Approximation	45
3.7 Necessary Numbers of Partial-Range Spherical Harmonics	54
3.8 $NP_1$ Approximation	56
3.9 The Angular Flux and the Milne Problem	66
CHAPTER IV: PLANE GEOMETRY: PARTIAL-RANGE SCATTERING FUNCTIONS	77
4.1 Introduction	77
4.2 Solution Formalism	79
4.3 Special Case: Full-Range Scattering Functions	85
4.4 $NP_L$ - $MP_K$ Approximation	87
4.5 $DP_0$ - $DP_0$ Approximation	88
4.5.1 The Eigenvalues	92
4.5.2 Diffusion Approximation	97
4.5.3 Critical Bare Slab Reactor	98
4.6 $DP_0$ - $2P_0$ Approximation	105
4.7 $2P_0$ - $2P_0$ Approximation	116
4.8 Comparison Between the $DP_0$ - $DP_0$ , $DP_0$ - $2P_0$ and $2P_0$ - $2P_0$ Approximations	131
CHAPTER V: SPHERICAL GEOMETRY: POSITION DEPENDENT POINTS OF DISCONTINUITIES	142

	<u>Page No.</u>
5.1 Introduction	142
5.2 Solution Formalism	145
5.3 Partial-Range Spatial Moments	153
5.4 Two-Range Approximation	156
5.5 Computational Analysis	158
CHAPTER VI: SCATTERING KERNELS: REPRESENTATION AND APPLICATIONS	168
6.1 Introduction	168
6.2 Partial-Range Expansion of Scattering Kernels	169
6.2.1 One-Group Neutron Transport	169
6.2.2 Multi-Group Neutron Transport	174
6.3 Examples of Applications	179
6.3.1 Scattering Function Calculations	179
6.3.2 Group-to-Group Transfer Cross Section Calculations	186
CHAPTER VII: SUMMARY AND CONCLUSIONS	191
APPENDIX A: THE $B_0^\alpha$ INTEGRALS OF THE $DP_0$ - $DP_0$ APPROXIMATION	199
APPENDIX B: INTEGRALS OF THE $DP_0$ - $2P_0$ APPROXIMATION	204
B.1. Non Symmetrical Spherical Surface Integral	204
B.2 The $B_0^\beta$ Integrals	206
B.3 The $A_0^\beta$ Constants	214
APPENDIX C: INTEGRALS OF THE $2P_0$ - $2P_0$ APPROXIMATION	217
C.1 The $B_0^\gamma$ Integrals	217
C.2 The $A_0^\gamma$ Integrals	224
REFERENCES	228

LIST OF FIGURES

	<u>Page No.</u>
Figure 1.1: Milne's problem in spherical geometry.	10
Figure 1.2: Differential cross section of 14.0 MeV neutrons elastically scattered from $U^{238}$ .	12
Figure 1.3: Differential cross section of 14.1 MeV neutrons elastically scattered from $Bi^{209}$ .	13
Figure 1.4: Main lines of directed research to be pursued in this study to develop methods of partial-range analysis for anisotropic neutron transport.	18
Figure 3.1: Domain of real and complex eigenvalues as a function of angular segmentation and the number of secondary neutrons using the $2P_0$ approximation.	49
Figure 3.2: Eigenvalue spectra as a function of angular segmentation for $c = 0.9$ using the $2P_0$ approximation.	51
Figure 3.3: Eigenvalue spectra as a function of angular segmentation for $c = 0.5$ using the $2P_0$ approximation.	52

- Figure 3.4: Number of secondary neutrons as a function of angular segmentation for various values of  $1/v_0$  for isotropic scattering using the  $2P_0$  approximation. 55
- Figure 3.5: Number of secondary neutrons as a function of angular segmentation for various values of  $1/v_0$  for forward scattering using the  $2P_0$  approximation. 57
- Figure 3.6: Number of secondary neutrons as a function of angular segmentation for various values of  $1/v_0$  for backward scattering using the  $2P_0$  approximation. 58
- Figure 3.7: Asymptotic relaxation constant as a function of the free angular variable for various values of anisotropy and  $c = 0.5$  using the  $3P_1$  approximation. 67
- Figure 3.8: End point of asymptotic flux as a function of the free angular variable for various values of anisotropy and  $c = 0.5$  using the  $3P_1$  approximation. 74
- Figure 3.9: Linear extrapolation length as a function of the free angular variable for various values of anisotropy and  $c = 0.5$  using

	<u>Page No.</u>
Figure 3.9: the $3P_1$ approximation. (cont'd)	75
Figure 3.10: Ratio of asymptotic flux to the total flux as a function of the free angular variable for various values of anisotropy and $c = 0.5$ using the $3P_1$ approximation.	76
Figure 4.1: Neutron directions before and after a collision.	81
Figure 4.2: The $DP_0$ - $DP_0$ representation of (a) angular flux and (b) scattering function.	89
Figure 4.3: Double- $P_0$ representation of scattering function: (a) complete forward scattering; (b) isotropic scattering; and (c) complete backward scattering.	94
Figure 4.4: Eigenvalue as a function of degree of anisotropy and number of secondaries for the $DP_0$ - $DP_0$ approximation.	96
Figure 4.5: Slab reactor thickness as a function of anisotropy for different values of $c$ using the $DP_0$ - $DP_0$ approximation.	100
Figure 4.6: Illustration showing $c$ - $\Delta f$ domain of real and finite reactor thickness in the context of the $DP_0$ - $DP_0$ approximation.	102

Figure 4.7:	Critical half-thickness of slab reactor as function of number of secondaries.	104
Figure 4.8:	The $DP_0-2P_0$ representation of (a) angular flux and (b) scattering function.	106
Figure 4.9:	Representation of the integral $B_{00}^{22}(\mu)$ for the $DP_0-2P_0$ approximation.	108
Figure 4.10:	The function $B_{00}^{22}(\mu)$ as a function of $\theta$ and $\theta_{s1}$ for the $DP_0-2P_0$ approximation.	110
Figure 4.11:	The function $B_{00}^{22}(\mu)$ as a function of $\mu$ for various values of $\mu_{s1}$ for the $DP_0-2P_0$ approximation.	111
Figure 4.12:	Eigenvalue as a function of degree of anisotropy, scattering angular segmentation and number of secondaries using the $DP_0-2P_0$ approximation.	115
Figure 4.13:	The $2P_0-2P_0$ representation of (a) angular flux and (b) scattering function.	117
Figure 4.14:	Representation of the integral of $B_{00}^{22}(\mu)$ for the $2P_0-2P_0$ approximation.	119



Figure 4.15: The integral  $B_{00}^{22}(\mu)$  as a function of  $\theta$  and  $\theta_1$  for the  $2P_0-2P_0$  approximation. 120

Figure 4.16: The integral  $B_{00}^{22}(\mu)$  as a function of the angular variable  $\mu$  for various values of angular segmentation  $\mu_1$  for the  $2P_0-2P_0$  approximation. 121

Figure 4.17: Eigenvalue spectrum as a function of angular segmentation for  $c = 0.5$  and  $\Delta f = +1$  and  $-1$ , respectively. 127

Figure 4.18: Eigenvalue spectrum as a function of the degree of anisotropy for  $c = 0.95$  and various values of angular segmentation using the  $2P_0-2P_0$  approximation. 128

Figure 4.19: Eigenvalue spectrum as a function of the degree of anisotropy for  $c = 0.5$  and various values of angular segmentation using the  $2P_0-2P_0$  approximation. 129

Figure 4.20: Eigenvalue spectrum as a function of the degree of anisotropy for  $c = 0.1$  and various values of angular segmentation using the  $2P_0-2P_0$  approximation. 130

	<u>Page No.</u>
Figure 4.21: The scattering function $f^{N+}(\mu_s)$ for various orders of anisotropy.	132
Figure 4.22: Eigenvalue spectra as a function of scattering segmentation for $c = 0.95$ using the $DP_0 - 2P_0$ approximation.	139
Figure 4.23: Eigenvalue spectra as a function of angular segmentation for $c = 0.95$ using the $2P_0 - 2P_0$ approximation.	140
Figure 5.1: Absorbing sphere in an infinite moderating medium.	144
Figure 5.2: Concentric spherical system possessing three directional discontinuities.	146
Figure 5.3: Calculated directionally discontinuous flux $\psi(r, \mu)$ at positions $r = 2.0, 2.5$ and $3.0$ measured in units of mean-free-path from the center of the absorbing sphere.	164
Figure 5.4: Total flux in the moderating medium normalized to unity at the surface of an absorbing sphere possessing a radius of two mean-free-paths.	167

- Figure 6.1: Representation of energy groups  $g$  and  $g'$  illustrating neutron down scattering. 176
- Figure 6.2: Illustrative comparison between the experimental  $U^{238}$  cross section (14 MeV neutrons) and its partial-range Legendre representation for  $L = 0$  while  $N = 1, 2$  and  $3$ . 181
- Figure 6.3: Illustrative comparison between the experimental  $U^{238}$  cross section (14 MeV neutrons) and its partial-range Legendre representation for  $L = 2$  and  $3$  while  $N = 3$ . 183
- Figure 6.4: Illustrative comparison between the experimental  $Bi^{209}$  cross section (14.1 MeV neutrons) and its partial-range Legendre representation for  $L = 0, 2$  and  $4$  while  $N = 3$ . 185
- Figure 6.5: Comparison of the oxygen group-to-group elastic scattering cross section from (3.3287-3.0119) MeV to (2.7253-2.4660) MeV for  $L = 0, 1$  and  $3$  in the partial-range Legendre representation. 187
- Figure 6.6: Comparison of the hydrogen group-to-group cross section from (3.3287-3.0119) MeV to (2.7253-2.4660) MeV for  $L = 0, 2$  and  $4$  in the partial-range Legendre representation. 189

Figure 6.7:	Comparison of water group-to-group elastic scattering cross section from (3.3287-3.0119) MeV to (2.7253-2.4660) MeV using $L = 3$ for oxygen domain and $L = 4$ for the hydrogen domain in the partial-range Legendre representation.	190
Figure A.1:	Geometrical configuration used in the $DP_0$ - $DP_0$ approximation.	200
Figure A.2:	One direction projection of the integrals $B_{00}^{22}(\mu)$ and $B_{00}^{21}(\mu)$ of the $DP_0$ - $DP_0$ approximation.	202
Figure B.1:	Graphical representation of a non symmetrical spherical integral.	205
Figure B.2:	Graphical representation of the integral $B_{00}^{22}(\mu)$ of the $DP_0$ - $2P_0$ approximation.	207
Figure B.3:	Different ranges of $\theta$ and $\theta_{s1}$ for the derivation of $B_{00}^{22}(\mu)$ of the $DP_0$ - $2P_0$ approximation.	209
Figure B.4:	The integral $B_{00}^{22}(\mu)$ as a function of $\theta$ and $\theta_{s1}$ for the $DP_0$ - $2P_0$ approximation.	213
Figure C.1:	Graphical representation of the $B_{00}^{22}(\mu)$ of the $2P_0$ - $2P_0$ approximation for $\theta/2 \leq \theta_1 \leq \pi - \theta/2$ .	218

Figure C.2: Graphical representation of the  $B_{00}^{22}(\mu)$  of the  $2P_0-2P_0$  approximation for  $\theta_1 \leq \theta/2$ . 220

Figure C.3: Graphical representation of the  $B_{00}^{22}(\mu)$  of the  $2P_0-2P_0$  approximation for  $\theta_1 \geq \pi - \theta/2$ . 221

Figure C.4: The integral  $B_{00}^{22}(\mu)$  as a function of  $\theta$  and  $\theta_1$  for the  $2P_0-2P_0$  approximation. 222

## LIST OF TABLES

	<u>Page No.</u>
Table 2.1: Recurrence relationship of the integrals $a_{n,\ell,\lambda}$ of partial-range Jacobi polynomials.	32
Table 3.1: Calculated eigenvalue $1/v_0$ as a function of number of secondary neutrons and anisotropy using $2P_0$ approximation.	53
Table 3.2: The $\underline{D}$ -matrix of the $2P_1$ approximation with a linear full-range scattering function.	61
Table 4.1: Critical half-thickness of slabs for isotropic scattering and various values of the mean number of secondaries per collision.	103
Table 4.2: The constants $A_0^B$ of the $DP_0-2P_0$ approximation for various values of $\mu_{s1}$ .	113
Table 4.3: The constants $A_0^Y$ of the $2P_0-2P_0$ approximation for various values of $\mu_1$ .	125
Table 4.4: The parameters $\mu_{s1}$ , $f_{1,0}$ and $f_{2,0}$ for the $2P_0$ approximation of the scattering function $f^{H+}(\mu_s)$ .	134

Table 4.5:	Comparison of the eigenvalue $(1/v)^{\pm}$ for the tenth-order scattering function $f^{N\pm}(\mu_s)$ and $c = 0.95$ .	136
Table 5.1:	The one-group neutron transport equation in spherical geometry expressed in terms of position dependent partial-range Legendre polynomials.	152
Table 5.2:	System of equations of partial-range spatial moments $\phi_{n,\ell}(r)$ for $\mu \in (\mu_{n-1}, \mu_n)$ .	157
Table 5.3:	System of equations of partial-range spatial moments for $\mu \in (-1, \mu_1)$ .	159
Table 5.4:	System of equations of partial-range spatial moments for $\mu \in (\mu_1, +1)$ .	160
Table 5.5:	Calculated total flux in the moderating medium normalized to unity at the surface of an absorbing sphere possessing a radius of two mean-free-paths.	166
Table 6.1:	Comparison of goodness of fit for $U^{238}$ and $Bi^{209}$ elastic scattering cross sections at 14 MeV neutrons.	184

CHAPTER I  
INTRODUCTION /

1.1. Preface

The characteristics of many neutronic systems of current interest are governed by the distribution of neutrons in space, energy, direction and time. This distribution is adequately described by the neutron transport or the linearized Boltzmann equation either in its partial differential-integral form or its integral form; both of these equations are, of course, equivalent and the choice of which form be used for a given problem is primarily a matter of convenience. In problems of any generality, these equations are impossible to solve analytically and prohibitively expensive to solve numerically. Except in the simplest cases, approximate forms of the transport equation must generally be used.

As neutrons collide with the atomic nuclei of the medium through which they are passing, various reactions such as absorption, scattering and fission are possible depending on the energy of the neutron and the kind of target nucleus. Once these interaction characteristics are known they form the starting point of neutron transport theory the object of which is to predict the average or expected distributions of a large number of neutrons in any neutronic system. This represents one of the central problems in the field of nuclear



reactor physics.

Due to the relative complexity of solving the neutron transport equation analytically, even for simple geometries and isotropic scattering, extensive use is made of numerical and semianalytical methods in its solution<sup>(1-4)</sup>. One of the best known and widely used approximate methods for one-dimensional neutron distributions is the spherical harmonics approximation; indeed, an early citation on spherical harmonics dates back to 1926<sup>(5)</sup>. Since then additional techniques have been developed to solve the neutron transport equation. For example, the discrete ordinate methods in particular have been widely used and have proven very powerful. Yet, the spherical harmonics method and its variations continue to be viable as design and research tools. One of the key characteristics of the spherical harmonics methods is that it describes the angular distribution of neutrons in terms of polynomials up to degree  $N$ . Low-order approximation should, then, be adequate when the angular distribution is not too anisotropic.

The study of anisotropies in neutron transport theory has been of interest for some time. Amaldi and Fermi were concerned with it as early as 1936<sup>(6)</sup>. Other workers have subsequently investigated it from several perspectives<sup>(1,7-9)</sup>. One recent development to solve the neutron transport equation for plane geometry and isotropic scattering, that of singular eigenfunctions, has been pioneered by Case<sup>(10)</sup>. More recently, efforts in this field have been undertaken to extend this method to the cases of anisotropic scattering with modest results<sup>(11-15)</sup>.

The studies of the transport problems for neutron energies and media of highly anisotropic scattering and strong angular dependence of the neutron angular flux have, however, invariably introduced a number of constraining conditions associated with the directional dependence of the angular flux as well as the scattering function and the transfer cross section within the context of the multi-group formalism. In some cases, effective specialized approaches have been employed for the treatment of the angular flux; among these we cite the use of double Legendre polynomials for plane geometry<sup>(16-18)</sup> and spherical geometry<sup>(19-21)</sup>, application of asymmetric quadrature sets<sup>(22)</sup> and the use of free parameters<sup>(23,24)</sup>.

The scattering kernels as well as the group-to-group transfer cross sections are widely represented by the full-range Legendre polynomials<sup>(1,2)</sup>. The truncation induced oscillation leading to negative values for the neutron flux<sup>(25,26)</sup> has prompted the introduction of large number of Legendre coefficients<sup>(27)</sup> and other ad-hoc methods<sup>(28)</sup>. On the other hand, the singular eigenfunctions solution of the transport equation for plane geometry with anisotropic scattering yields multiple discrete eigenvalues in highly absorbing media<sup>(11,29)</sup>. Indeed, the more forward peaked the anisotropy, the larger the multiplicity of the discrete eigenvalues. This result has required the introduction of large numbers of Legendre coefficients of the scattering function in certain approximations of the neutron angular flux<sup>(29)</sup>.

Very recently the group-to-group cross section has been calculated without Legendre expansions and then used within the context

of  $S_N$ -method<sup>(3,30)</sup> for transport calculations<sup>(31)</sup>. The reason for this is the inadequacy of the Legendre expansion in reconstructing the transfer cross section. However, this new method necessitates large data storage requirements and computer storage limitations preclude its wide use<sup>(31)</sup>. The approximate methods using conventional representation of the scattering function and the group-to-group transfer cross section, are clearly inadequate in cases of strongly anisotropic scattering functions and anisotropic transfer cross sections.

To overcome some of the traditional problems associated with anisotropies, a new solution formalism based on the partial-range analysis has been suggested<sup>(32,33)</sup>. It has been found that, for the case of isotropic scattering, this formalism does permit the calculation of some neutronic transport parameters to a high degree of accuracy even in low-order approximations<sup>(32)</sup>. The associate problem of specifying suitable angular segmentation in accordance with the partial-range functional representations did not appear to be a severe limitation<sup>(34)</sup>.

Here we will develop a formalism which combines the features of both the discrete ordinate methods and the spherical harmonics methods for the solution of neutron transport equation with strong anisotropies. This new formalism is very adequate for cases of highly anisotropic angular distributions of both the angular flux as well as the scattering functions. Our analysis will be restricted to the one-group neutron transport equations for plane and spherical geometries. Of course, one might argue that the one-group neutron transport equation

represents a highly idealized situation. However, for the purpose of adapting and testing the accuracy of a new formalism one would prefer to use model problems for which there are benchmark data to compare with; the one-group neutron transport equations for slabs and spheres are very well suited for this purpose. Moreover, the solution of the one-group transport equation is an essential part of the solution of the energy dependent problem when multi-group techniques are employed. In the latter case, a one-group equation must be solved for each energy group with sources of neutrons owing to the transfer of neutrons from the other groups.

## 1.2 Neutron Transport Equation

In the derivation of the commonly used neutron transport equation the following assumptions have been used<sup>(3)</sup>:

- 1) the neutron is considered to be point particle in the sense that it can be described completely by its position vector and velocity vector;
- 2) delayed neutrons have been neglected;
- 3) neutron-neutron scattering is not included.

Under these assumptions the neutron transport equation takes the form,

$$\frac{1}{v} \frac{\partial \psi(\underline{r}, \underline{\Omega}, E; t)}{\partial t} + \underline{\Omega} \cdot \underline{\nabla} \psi(\underline{r}, \underline{\Omega}, E; t) + \Sigma(\underline{r}, E) \psi(\underline{r}, \underline{\Omega}, E; t) = \int_{E'} \int_{\underline{\Omega}'} \Sigma(\underline{r}, E') f(\underline{r}; \underline{\Omega}', E' \rightarrow \underline{\Omega}, E) \psi(\underline{r}, \underline{\Omega}', E'; t) d\underline{\Omega}' dE' + S(\underline{r}, \underline{\Omega}, E; t) \quad (1.1)$$

where  $\psi(\underline{r}, \underline{\Omega}, E; t)$  represents the neutron angular flux at position  $\underline{r}$  per unit solid angle about the direction  $\underline{\Omega}$  per unit energy about the energy  $E$  at any time  $t$ , the neutron speed is given by  $v$  while the total macroscopic cross section of neutrons having energy  $E$  at position  $\underline{r}$  is denoted by  $\Sigma(\underline{r}, E)$ , the function  $f(\underline{r}; \underline{\Omega}', E' \rightarrow \underline{\Omega}, E)$  represents the probability distribution function of a neutron with direction  $\underline{\Omega}'$  and energy  $E'$  at the position  $\underline{r}$  suffering a collision and subsequently appearing or creating another neutron (or neutrons) with direction  $\underline{\Omega}$  and energy  $E$ , and finally the source term  $S(\underline{r}, \underline{\Omega}, E; t)$  represents all the external neutron sources and gives the number of neutrons supplied to the system at time  $t$  per unit volume at the position  $\underline{r}$  having a direction within unit solid angle about  $\underline{\Omega}$  and unit energy about  $E$  per unit time.

The above equation, Eq. (1.1), represents a balance condition for the various mechanisms by which neutrons of certain energy and direction can be gained or lost from a unit volume at an arbitrary position within the system. The first term of Eq. (1.1) represents the time rate of change of the neutron angular density. The second term represents the net loss of neutrons of interest due to leakage as well as streaming through its surface while the third term represents the loss of neutrons due to collisions with the nuclei; this includes both absorption and scattering collisions. Finally, the right hand side of Eq. (1.1) represents the mechanisms of neutron gain; the first term gives all neutrons, in the unit volume under consideration, of different directions  $\underline{\Omega}'$  and energies  $E'$  suffering

collisions that change  $\underline{\Omega}'$  and  $E'$  to the direction  $\underline{\Omega}$  and the energy  $E$  of interest while the last term represents all the external neutron sources.

Equation (1.1) is the neutron transport equation in its integro-differential form. It is a linear equation in the unknown angular flux  $\psi(\underline{r}, \underline{\Omega}, E; t)$  with seven independent variables  $\underline{r}(x, y, z)$ ,  $\underline{\Omega}(\theta, \omega)$ ,  $E$  and  $t$ . In spite of certain minor limitations, which have been indicated previously, this transport equation has been found to be entirely satisfactory for treating most problems in reactor physics. As indicated previously, this equation can not be solved analytically in its general form. However, it can be simplified by an integration over one or more of the independent variables. For example, the time-independent one-group neutron transport equation for plane symmetry can be written as

$$\mu \frac{\partial \psi(x, \mu)}{\partial x} + \psi(x, \mu) = c \int_{\underline{\Omega}'} f(\underline{\Omega}', \underline{\Omega}) \psi(x, \mu') d\underline{\Omega}' + \frac{1}{\Sigma(x)} S(x, \mu) , \quad (1.2)$$

where now the number of independent variables is two: the spatial variable  $x$ , measured in units of mean free path of the neutron in the medium under consideration, and the angular variable  $\mu$ , as the cosine of the angle between the neutron direction and the  $x$ -axis. The constant  $c$  represents the average number of secondary neutrons per collision and  $\Sigma(x)$  is the total macroscopic cross section which is only function of the position  $x$ . The function  $f(\underline{\Omega}', \underline{\Omega})$  represents the probability density function for the case of a neutron entering a collision with initial direction  $\underline{\Omega}'$  and subsequently emerging with

direction contained in a unit solid angle about the direction  $\underline{\Omega}$ ; it is assumed to be rotationally invariant.

For spherical symmetry, the time-independent one-group neutron transport equation is given by

$$\begin{aligned} & \mu \frac{\partial \psi(r, \mu)}{\partial r} + \frac{1 - \mu^2}{r} \frac{\partial \psi(r, \mu)}{\partial \mu} + \psi(r, \mu) \\ & = c \int_{\underline{\Omega}'} f(\underline{\Omega}', \underline{\Omega}) \psi(r, \mu') d\underline{\Omega}' + \frac{1}{\Sigma(r)} S(r, \mu) \end{aligned} \quad (1.3)$$

Herein,  $r$  represents the distance of neutron from the origin measured in units of mean free path of the neutron and  $\mu$  represents the cosine of the angle between the neutron direction and the radius vector to the point  $r$ . Here, we note that the streaming term of Eq. (1.1) yields two terms, the first and the second term of Eq. (1.3), because the direction cosine depends on the neutron position as well as neutron's direction in spherical geometry.

The study and application of the solutions of Eqs. (1.2) and (1.3) under conditions of anisotropies is the object of this work.

### 1.3 Anisotropy: Sources and Effects

Since this work is concerned with anisotropies in neutron transport analysis, it is important to note the different sources which contribute to neutron anisotropy in any neutronic system. In the following we will summarize the sources of anisotropies as well as their effects.

#### 1) Boundary Conditions:

(a) Plane geometry: Any free surface of a neutronic system with a vacuum introduces anisotropy in the angular flux. The Milne's problem in plane geometry<sup>(1,3)</sup> is an example in which the free surface boundary condition is

$$\psi(x=0, \mu) = 0 \quad ; \quad \mu \geq 0 \quad , \quad (1.4)$$

where the boundary between the medium and the free space is assumed to be at  $x = 0$ . This boundary condition implies that the angular flux is discontinuous with respect to the angular variable at  $\mu = 0$  and hence represents a source of high anisotropy in the angular flux especially close to the surface. Moreover, at the interface between two different media, where the properties of absorption, scattering and fission of the two media differ significantly, there is therefore also a source of anisotropy in the neutron angular flux close to the interface.

(b) Spherical geometry: The free boundary condition in the spherical geometry can introduce discontinuities in either the angular flux or its angular derivative. As an example, consider the spherical Milne's problem<sup>(35,36)</sup>, Fig. 1.1, for which the boundary condition is

$$\psi(R, \mu) = 0 \quad ; \quad \mu \geq 0 \quad , \quad (1.5)$$

where  $R$  is the radius of the neutronically black sphere, Region I in Fig. 1.1. This condition is the same as that for plane geometry. However, we encounter more complicated pathologies in the angular flux. Clearly, the angular flux  $\psi(R, \mu)$  is discontinuous at  $\mu = 0$  while the angular flux at the point  $P$ , with spherical coordinate  $r$ ,



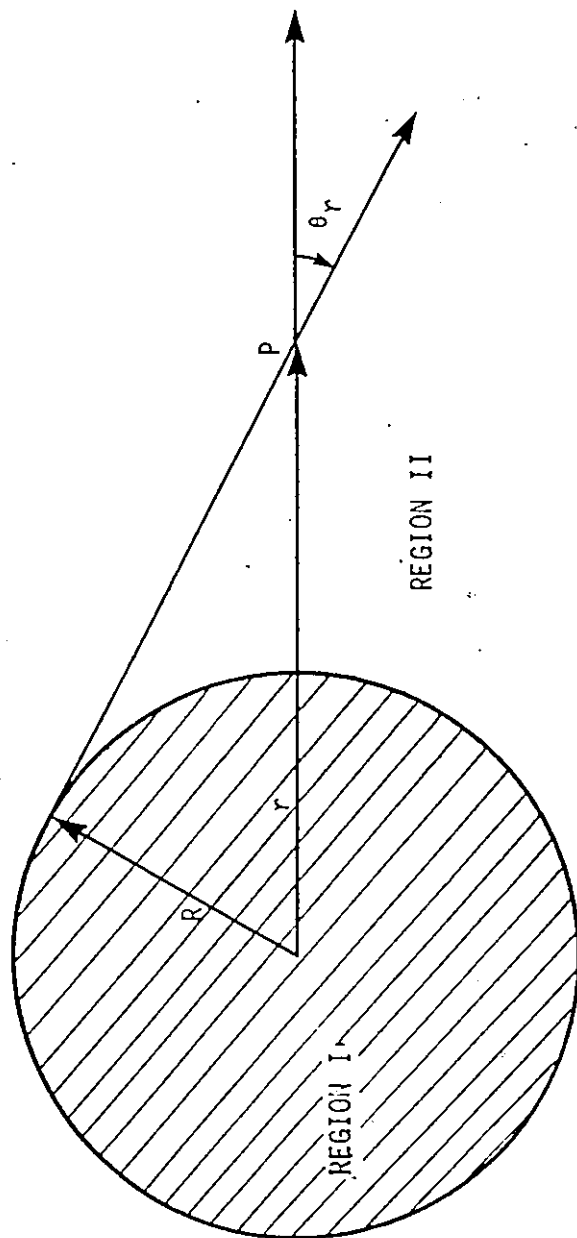


Fig. 1.1: Milne's problem in spherical geometry; Region I: Black absorbing sphere, and Region II: Moderator with a source of neutrons at infinity.

is discontinuous at  $\mu_r$  where

$$\mu_r = \cos^{-1} \theta_r \neq 0 \quad (1.6)$$


Therefore, the location of the discontinuity depends on the position  $r$ . In cases when the central sphere is not neutronically black but has a finite absorption and scattering cross sections, the angular flux is not discontinuous but its derivative with respect to  $\mu$  is discontinuous at  $\mu = 0$  at the interface while the angular flux may change rapidly with  $\mu$  near  $\mu = 0$ . Moreover, such discontinuities in the angular derivative are present at points outside the interface and for direction cosines given by Eq. (1.6) as well<sup>(3,35)</sup>.

### 2) Sources and Sinks of Neutrons:

In regions very close to the neutron sources and sinks the neutron flux changes rapidly with the position. This causes a high anisotropy in the neutron angular flux at these regions:

### 3) Scattering Kernels:

It is known that for high energy neutrons and heavy materials the scattering kernels (elastic as well as inelastic) tend to be very anisotropic<sup>(25,37-39)</sup>. For an example, the elastic scattering cross section of  $U^{238}$  and  $Bi^{209}$  for 14.0 MeV neutrons are shown in Figs. 1.2 and 1.3, respectively. These cross sections are highly anisotropic and peaked in the forward direction. In contrast, for other materials such as beryllium for neutron energy slightly greater than that for the Bragg cut-off energy, the elastic scattering cross section is highly peaked in the backward direction<sup>(40)</sup>.



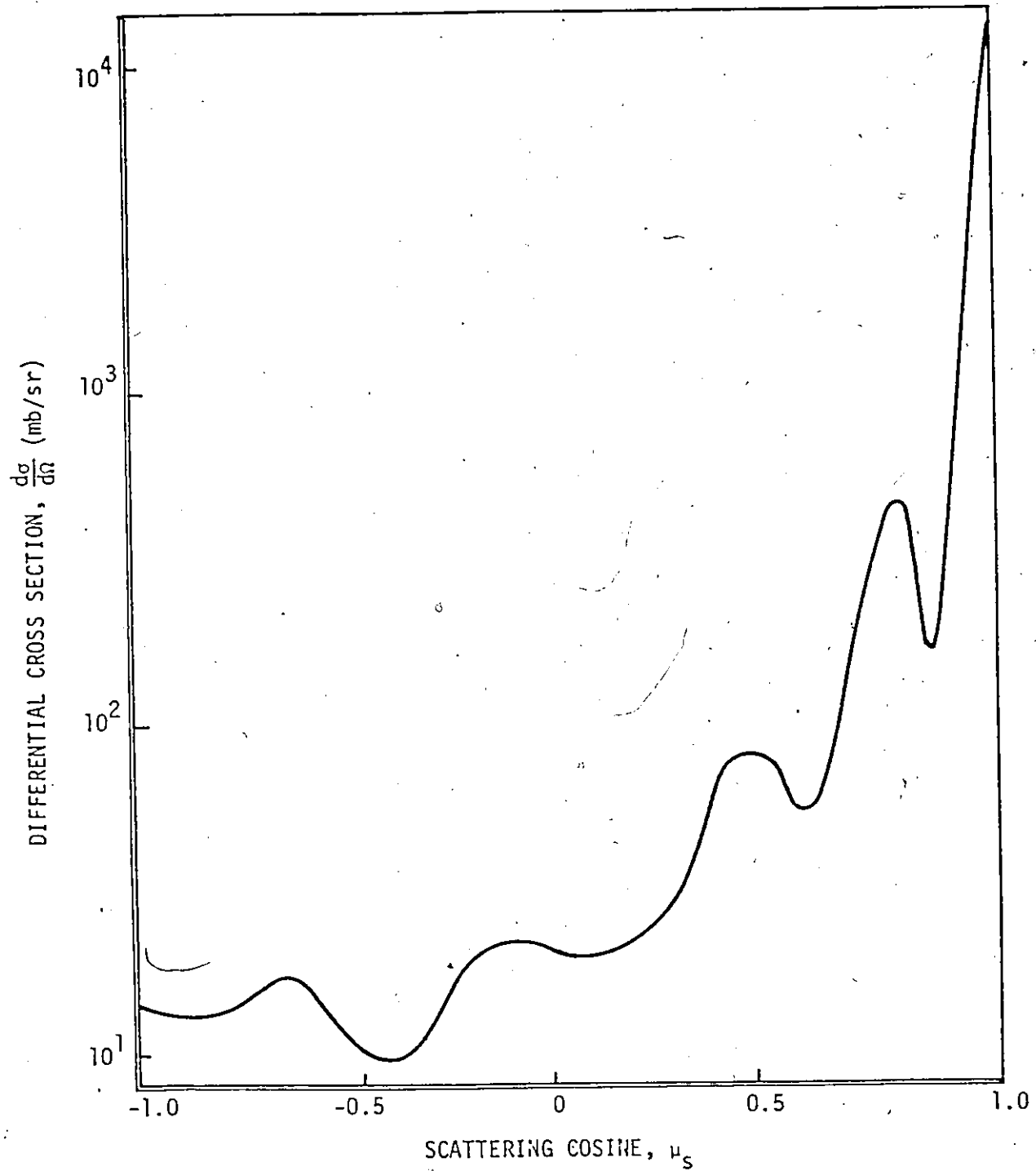


Fig. 1.2: Differential cross section of 14.0 MeV neutrons elastically scattered from  $U^{238}$  as a function of the cosine of the scattering angle in the center-of-mass system (from reference -29).

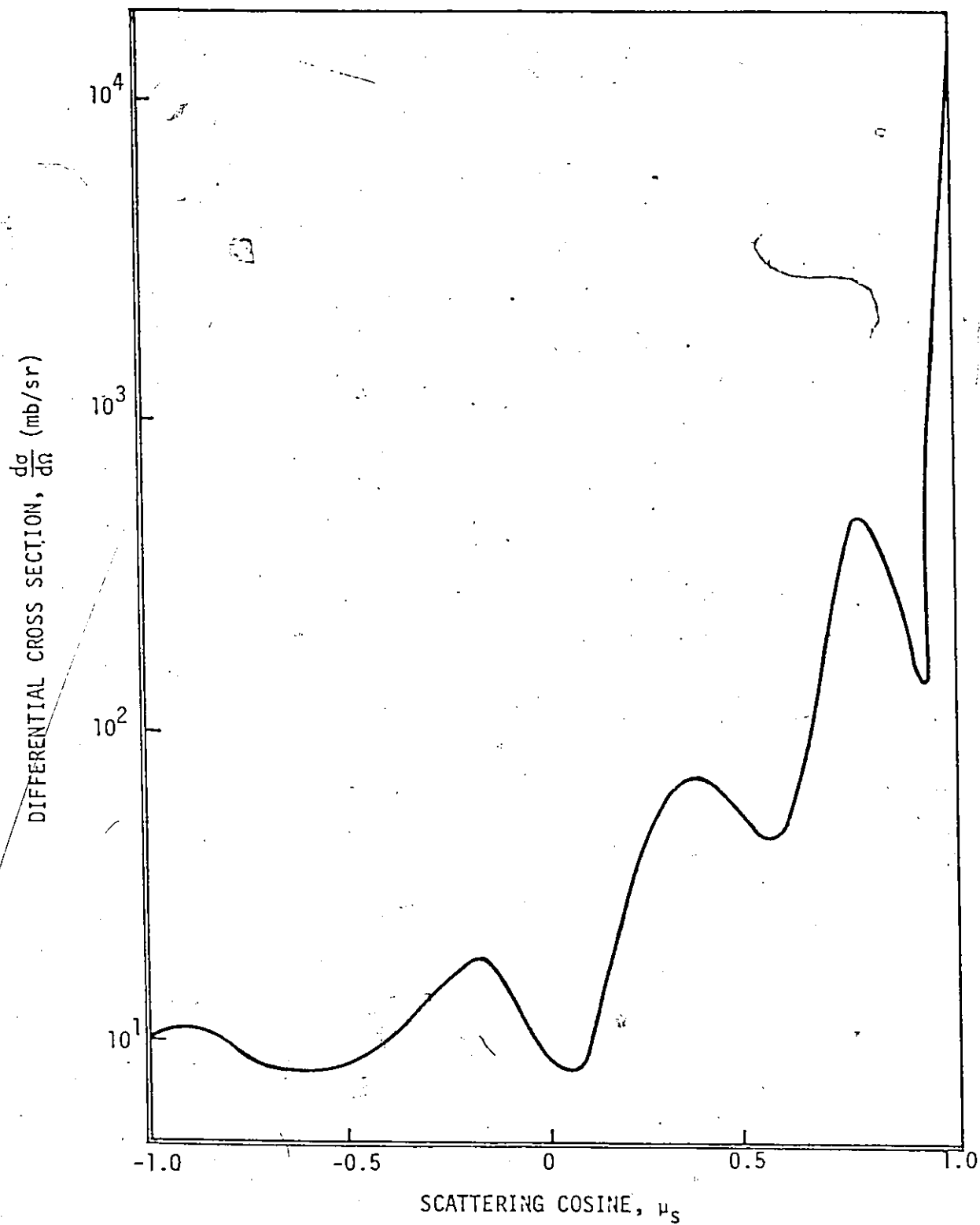


Fig. 1.3: Differential cross section of 14.1 MeV neutrons elastically scattered from  $\text{Bi}^{209}$  as a function of the cosine of the scattering angle in the center-of-mass system (from reference 38).

#### 4) Group-to-Group Transfer Cross Section:

In the multi-group method which is concerned with energy dependent flux calculations of neutrons, the main problem is the consistent determination of group cross sections. The group cross sections in general depend on direction<sup>(3)</sup>. Moreover, the group-to-group transfer cross section is restricted over certain ranges of the cosine of the scattering angle  $\mu_s$ <sup>(31,41-43)</sup>. Therefore, these functions themselves are highly anisotropic and represent a source of anisotropy in the transport problem. More details about the group-to-group transfer cross section will be given in Section 6.2.2.

We interject here to note that outside the field of neutron transport and reactor theory there are many problems which involve anisotropic angular distributions. In the fields of radiative transfer<sup>(44)</sup> and gas kinetics<sup>(45)</sup> we find problems similar to those described above. A series of studies about the radiances in optically deep absorbing media showed very anisotropic phase functions<sup>(44,46,47)</sup>. More examples can be found in references (48-51). Finally, the multi-group Compton scattering cross section of  $\gamma$ -radiation is another example of anisotropic behaviour<sup>(52)</sup>.

#### 1.4 Scope of this Thesis

It is our intent to briefly summarize the various topics to be presented in this thesis. We will limit ourselves to the one dimensional problem for plane and spherical geometries for the case of time-independent and one-group of neutrons representations. Before

we proceed to the partial-range analysis of anisotropic neutron transport equation we shall establish, in Chapter II, the mathematical formalism we will use. These are the definitions and properties of the partial-range spherical polynomials. Also, the properties of some other partial-range orthogonal polynomials, such as Jacobi-, Gegenbauer- and Tschebycheff-polynomials, will be considered.

Plane geometry neutron transport equation with anisotropic scattering will be studied in two chapters. In Chapter III, the angular flux as well as the external neutron sources will be expanded in terms of partial-range Legendre polynomials; the scattering function will be expressed in terms of full-range Legendre polynomials. In Chapter IV, the neutron angular flux and the external sources of neutrons will be represented the same way as in Chapter III. However, the scattering function will be expressed in terms of partial-range Legendre polynomials. In a sense, the study of Chapter IV represents a complete partial-range spherical harmonics analysis for one-group neutron transport equation in plane geometry.

The neutron transport equation in spherical geometry is considered in Chapter V. A distinctive procedure will be used for the analysis in this chapter: the angular flux and the external sources of neutrons will be expanded in terms of partial-range Legendre polynomials. However, the segmentation of the angular variable, associated with the problem, is position dependent.

The general procedure, however, in Chapters III, IV and V is to develop the mathematical formalism and establish a set of equations

governing the partial-range moments of the angular flux. Then, we will discuss some special cases extracted from the literature to provide the continuity between this work and that of other researchers. After that, some low-order approximations will be examined and used for calculational purposes. Neutronic parameter associated with each problem will then be calculated. Some of the parameters calculated in this work are the eigenvalues which are related to the inverse diffusion length, the end point, the linear extrapolation length and the ratio between total and asymptotic fluxes at the boundary associated with the Milne's problem. Also the angular as well as the total fluxes will be considered. A comparison between the results of this formalism, with the results of other approximations as well as the exact results, when they are available, will also be given.

In Chapter VI, the partial-range formalism will be extended to some problems of current practical interest. These are the reconstruction of the scattering function within the context of one-group neutron transport theory and the group-to-group transfer cross section within the context of multi-group theory. As a numerical illustration, the elastic scattering cross sections of 14.0 MeV neutrons of  $U^{238}$  and  $Bi^{209}$ , which are very anisotropic, will be reconstructed by few low-order approximations. For multi-group calculations the water group-to-group transfer cross section from (3.3287-3.0119) MeV to (2.7253-2.4600) MeV will be considered. Also a comparison with the usual full-range representation will be given. Figure 1.4 provides a graphical representation of the main lines of

the research undertaken. Finally, Chapter VII gives a summary with the conclusions of this work.



Anisotropic Neutron Transport Analysis

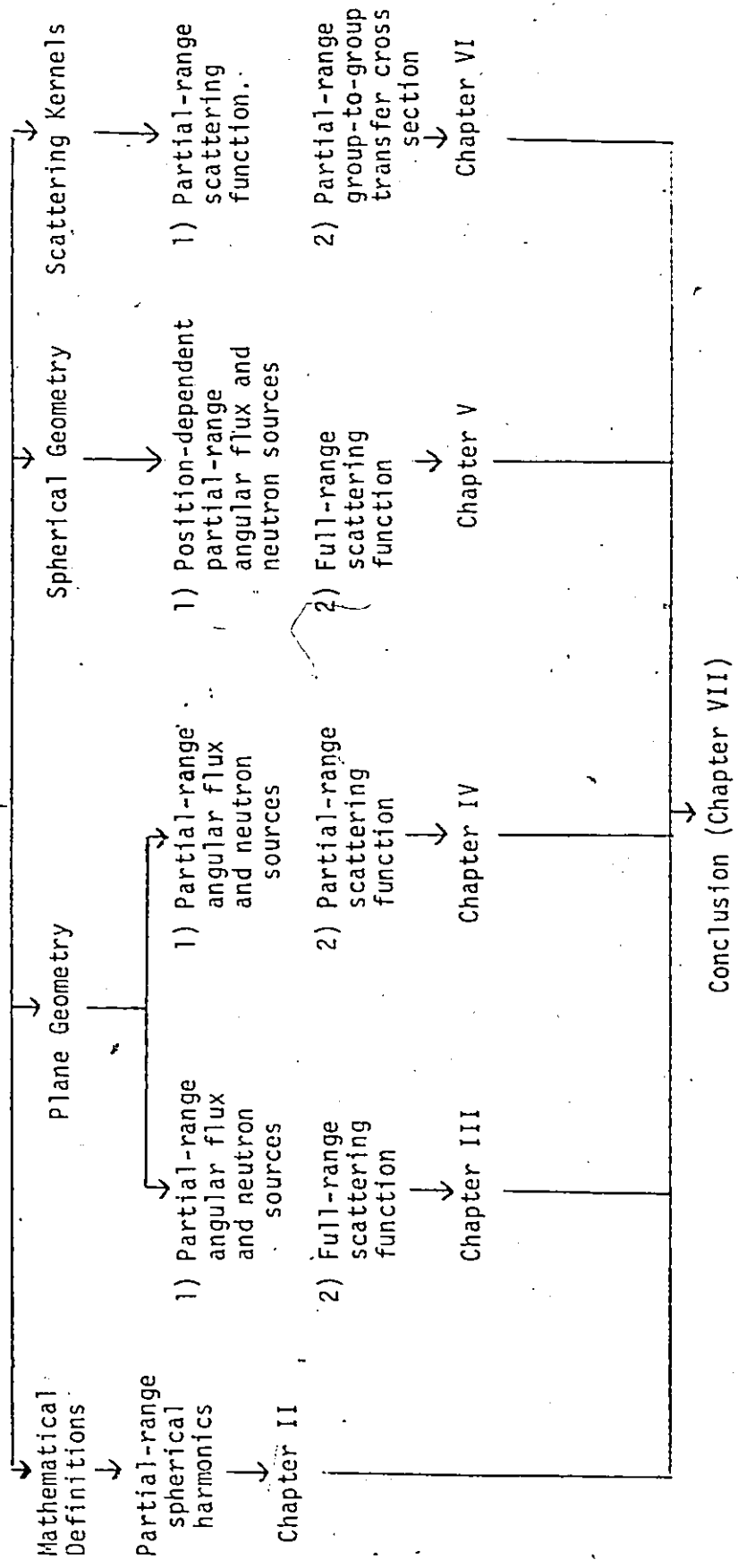


Fig. 1.4: Main lines of directed research redundant pursued in this study to develop methods of partial-range analysis for anisotropic neutron transport.

## CHAPTER II

### PARTIAL-RANGE SPHERICAL HARMONICS FORMULATION

#### 2.1 Introduction

The purpose of this chapter is to define the partial-range spherical harmonics and to establish their properties of orthogonality, recurrence and full-range integrations. The partial-range spherical harmonics is the mathematical tool, in this thesis, to describe the anisotropic angular neutronic functions. The pertinent neutronic functions are the angular flux, the external neutron sources and the scattering kernels. In the present formalism we will combine the features of both the discrete ordinate methods and the spherical harmonics approximations for the solution of the neutron transport equation. In the discrete ordinate methods the neutron transport equation is solved in a discrete set of directions only; angular integrals are then approximated by sums over discrete directions and angular derivatives by differences. In the spherical harmonics methods, the angular neutronic functions are written as infinite sums in terms of an orthogonal complete set of spherical harmonics over the entire direction cosine  $\mu$ .

The basis of this formalism of partial-range spherical harmonics analysis is the segmentation of the angular variable, that is the direction cosine  $\mu$ , into  $N$  number of arbitrary intervals; and then we expand the angular functions in terms of an orthogonal complete set

over every interval. These sets, which are orthogonal and complete over an arbitrary interval of the direction cosine, have been called partial-range orthogonal functions<sup>(32,53,54)</sup>. The method of spherical harmonics approximations will be incorporated by using the partial-range Legendre polynomials. The  $N$  intervals are here specified by the following system of inequalities:

$$-1 \leq \mu_0 < \mu_1 < \dots < \mu_n < \dots < \mu_N \leq +1 \quad (2.1)$$

Furthermore, the partial-range Legendre polynomial of the  $\ell$ 'th order over the  $n$ 'th angular interval is defined by

$$P_{n,\ell}(\mu) = P_\ell(\alpha_n \mu + \beta_n)[H(\mu - \mu_{n-1}) - H(\mu - \mu_n)] \quad (2.2)$$

where  $H$  is the unit step function<sup>(55)</sup>. The interval functions  $\alpha_n$  and  $\beta_n$  are chosen to preserve the orthogonality of the functions  $P_{n,\ell}(\mu)$  over the range  $\mu \in [\mu_{n-1}, \mu_n]$ . The reconstruction of this function as well as the derivation of the interval functions and the properties of orthogonality, recurrence, and full-range integrations will be discussed in latter sections of this chapter.

This orthogonal complete set allows the expansion of any regular function over a partial-range of  $\mu \in [\mu_{n-1}, \mu_n]$ . For example, a function  $f_n(x, \mu)$  may be written as

$$f_n(x, \mu) = \sum_{\ell=0}^{\infty} \frac{2\ell + 1}{\mu_n - \mu_{n-1}} f_{n,\ell}(x) P_{n,\ell}(\mu) \quad (2.3)$$

where  $(2\ell + 1)/(\mu_n - \mu_{n-1})$  represents a normalization factor and the partial-range moments  $f_{n,\ell}(x)$  are given by

$$f_{n,\ell}(x) = \int_{\mu_{n-1}}^{\mu_n} f_n(x,\mu) P_{n,\ell}(\mu) d\mu \quad (2.4)$$

An expansion of a function over the entire range of the direction cosine  $\mu \in [-1,1]$  follows from a summation of such partial-range Legendre polynomials expansion of Eq. (2.3) over the  $N$  angular intervals. Therefore, any function,  $f(x,\mu)$ , can be written as

$$f(x,\mu) = \sum_{n=1}^N \sum_{\ell=0}^{\infty} \frac{2\ell+1}{\mu_n - \mu_{n-1}} f_{n,\ell}(x) P_{n,\ell}(\mu) \quad (2.5)$$

Note that Eq. (2.5) reduces to the usual expansion in terms of full-range Legendre polynomials if we specify  $N = 1$  and full-range description of the function  $f(x,\mu)$ . Moreover, this expansion allows for irregularities at the position of segmentation  $\mu_n$ , such as discontinuities in the angular flux and other neutronic functions.

## 2.2 Reproduction of Partial-Range Spherical Harmonics

The partial-range spherical harmonics are defined one way by Eq. (2.2). However, there are two methods to reproduce the partial-range spherical harmonics. The first one is by using the Gram-Schmidt orthogonalization theorem<sup>(56)</sup> while the second procedure is by linear transformation of variables.

Using the Gram-Schmidt orthogonalization theorem, we can write the following function in the space  $\mu \in [\mu_{n-1}, \mu_n]$

$$u_{n,\ell}(\mu) = P_{\ell}(\mu) - \sum_{\lambda < \ell} \langle P_{\ell}(\mu), \bar{P}_{n,\lambda}(\mu) \rangle \bar{P}_{n,\lambda}(\mu) \quad (2.6)$$

where  $P_\ell(\mu)$  represents the full-range Legendre polynomials which is a linearly independent set in the space  $\mu \in [\mu_{n-1}, \mu_n]$ , then the partial-range Legendre polynomial  $\bar{P}_{n,\ell}(\mu)$  is given by

$$\bar{P}_{n,\ell}(\mu) = \frac{u_{n,\ell}(\mu)}{\|u_{n,\ell}(\mu)\|} \quad (2.7)$$

where  $\langle P_\ell, \bar{P}_{n,\ell} \rangle$  is the inner product defined by

$$\langle P_\ell, \bar{P}_{n,\ell} \rangle = \int_{\mu_{n-1}}^{\mu_n} P_\ell(\mu) \bar{P}_{n,\ell}(\mu) d\mu \quad (2.8)$$

and  $\|u_{n,\ell}(\mu)\|$  is the norm of  $u_{n,\ell}(\mu)$  defined by

$$\|u_{n,\ell}(\mu)\| = \sqrt{\langle u_{n,\ell}, u_{n,\ell} \rangle} \quad (2.9)$$

The partial-range Legendre polynomials set  $\{\bar{P}_{n,\ell}(\mu)\}$ , defined by Eq. (2.7), is orthonormal over the range  $[\mu_{n-1}, \mu_n]$ . The orthonormality can be proven by the Gram-Schmidt orthogonalization theorem. Using this procedure the two leading terms of the resulting set are

$$\bar{P}_{n,0}(\mu) = \frac{1}{(\mu_n - \mu_{n-1})^{1/2}} \quad (2.10)$$

and

$$\bar{P}_{n,1}(\mu) = \frac{1}{A} \left[ \mu - \frac{1}{2} (\mu_n + \mu_{n-1}) \right] \quad (2.11)$$

where

$$A = (\mu_n - \mu_{n-1}) \left[ \frac{1}{3} (\mu_n^2 + \mu_n \mu_{n-1} + \mu_{n-1}^2) + \frac{1}{2} (\mu_n + \mu_{n-1}) \left( \frac{1}{2} - \mu_n - \mu_{n-1} \right) \right] \quad (2.12)$$

A slightly different partial-range Legendre polynomials set can be reproduced from the full-range Legendre polynomials set by a linear transformation as defined by Eq. (2.2). The interval dependent functions  $\alpha_n$  and  $\beta_n$  of Eq. (2.2) are chosen so that  $(\alpha_n \mu + \beta_n) \in [-1, 1]$  for  $\mu \in [\mu_{n-1}, \mu_n]$ . The expressions of  $\alpha_n$  and  $\beta_n$  are then given by<sup>(32)</sup>

$$\alpha_n = \frac{2}{\mu_n - \mu_{n-1}} \quad , \quad (2.13)$$

and

$$\beta_n = - \frac{\mu_n + \mu_{n-1}}{\mu_n - \mu_{n-1}} \quad (2.14)$$

Using this transformation the two leading terms of the  $P_{n,l}(\mu)$  are

$$P_{n,0}(\mu) = 1 \quad , \quad (2.15)$$

and

$$P_{n,1}(\mu) = \frac{2}{\mu_n - \mu_{n-1}} \mu - \frac{\mu_n + \mu_{n-1}}{\mu_n - \mu_{n-1}} \quad (2.16)$$

The Gram-Schmidt orthogonalization theorem is the standard procedure to reproduce the orthonormal set of partial-range spherical harmonics from the set of full-range spherical harmonics. The second method which involves linear transformation of variables is only valid for polynomials of one variable such as Legendre polynomials and Jacobi polynomials; the reason being that it reproduces incomplete sets for polynomials of two variables such as the spherical harmonics<sup>(19)</sup>. In the present study we will use the set defined by Eq. (2.2) because it is easier to use.

### 2.3 Properties of Partial-Range Legendre Polynomials

We will use the properties of orthogonality, recurrence and full-range integration of full-range Legendre polynomials to establish the properties of partial-range Legendre polynomials by performing the appropriate transformation of variables.

#### 1) Orthogonality:

Starting by the known orthogonal property of the full-range Legendre polynomials,

$$\int_{-1}^1 P_{\ell}(\mu)P_{\ell'}(\mu)d\mu = \frac{2}{2\ell + 1} \delta_{\ell\ell'} \quad (2.17)$$

performing the appropriate transformation of variables and changing the functional notation yields

$$\int_{\mu_{n-1}}^{\mu_n} P_{n,\ell}(\mu)P_{n',\ell'}(\mu)d\mu = \frac{2}{\alpha_n(2\ell + 1)} \delta_{\ell\ell'}\delta_{nn'} \quad (2.18)$$

Here,  $\alpha_n$  is given by Eq. (2.13) and  $\delta$  is the Kronecker delta. The above equation, Eq. (2.18), represents the orthogonality relationship of the partial-range Legendre polynomials.

#### 2) Recurrence Relationships:

The recurrence relationships of partial-range Legendre polynomials are useful in the mathematical formulation of the partial-range analysis of the transport problems. These relationships may be established for the partial-range Legendre polynomials by reference to the known recurrence expressions of the full-range Legendre polynomials. First, consider the following recurrence relationship,

$$(2\ell + 1)\mu P_{\ell}(\mu) = (\ell + 1)P_{\ell+1}(\mu) + \ell P_{\ell-1}(\mu), \quad (2.19)$$

and again perform the appropriate change of variables and functional notation to obtain the equivalent relationship for the partial-range Legendre polynomials

$$(2\ell + 1)(\alpha_n \mu + \beta_n)P_{n,\ell}(\mu) = (\ell + 1)P_{n,\ell+1}(\mu) + \ell P_{n,\ell-1}(\mu). \quad (2.20)$$

Secondly, using the recurrence relationship for the derivatives of the full-range Legendre polynomials,

$$P'_{\ell+1}(\mu) = P'_{\ell-1}(\mu) + (2\ell + 1)P_{\ell}(\mu), \quad (2.21)$$

we can obtain the corresponding relationship for the partial-range Legendre polynomials,

$$P'_{n,\ell}(\mu) = P'_{n,\ell-2}(\mu) + \alpha_n(2\ell - 1)P_{n,\ell-1}(\mu), \quad (2.22)$$

where

$$P'_{n,\ell}(\mu) = \frac{dP_{n,\ell}(\mu)}{d\mu} \quad (2.23)$$

### (3) Full- and Partial-Range Integrations:

Another property of interest is the full-range integration defined by

$$I = \int_{-1}^{+1} P_{n,\ell}(\mu) d\mu. \quad (2.24)$$

From the definitions of  $P_{n,\ell}(\mu)$  the above integral can be rewritten as a partial-range integration,



$$I = \int_{\mu_{n-1}}^{\mu_n} P_{n,\ell}(\mu) d\mu \quad (2.25)$$

Using the property  $P_{n,0}(\mu) = 1$  of Eq. (2.15) and the orthogonality of Eq. (2.18) we can write

$$I = \int_{\mu_{n-1}}^{\mu_n} P_{n,0}(\mu) P_{n,\ell}(\mu) d\mu = \frac{2}{\alpha_n} \delta_{\ell 0} \quad (2.26)$$

#### (4) Special Values of Partial-Range Legendre Polynomials:

The final properties of interest are the special values of partial-range Legendre polynomials at the boundaries of the angular interval, i.e. at  $\mu = \mu_n$  and  $\mu = \mu_{n-1}$ , respectively. Using the special values of full-range Legendre polynomials and the definition of  $\alpha_n$  and  $\beta_n$  results in

$$P_{n,\ell}(\mu_n) = P_{\ell}(+1) = 1 \quad , \quad (2.27)$$

and

$$P_{n,\ell}(\mu_{n-1}) = P_{\ell}(-1) = (-1)^{\ell} \quad (2.28)$$

### 2.4 Partial-Range Expansion of Full-Range Legendre Polynomial

A subject of interest to the further development of this study is the expansion of the full-range Legendre polynomial over an arbitrary interval of direction cosine  $\mu \in [\mu_{n-1}, \mu_n]$  in terms of the partial-range Legendre polynomials over this interval. Using the Gram-Schmidt orthogonalization theorem we can write

$$P_\ell(\mu) = \sum_{\lambda=0}^{\ell} \frac{2\lambda + 1}{\mu_n - \mu_{n-1}} a_{n,\ell,\lambda} P_{n,\lambda}(\mu) \quad (2.29)$$

where, using the orthogonality condition of Eq. (2.18), the expansion coefficients  $a_{n,\ell,\lambda}$  are given by

$$a_{n,\ell,\lambda} = \int_{\mu_{n-1}}^{\mu_n} P_\ell(\mu) P_{n,\lambda}(\mu) d\mu \quad (2.30)$$

These integrals are easily evaluated for any value of  $\ell$  and  $\lambda$ . For example

$$a_{n,0,0} = \mu_n - \mu_{n-1} \quad (2.31)$$

$$a_{n,1,0} = \frac{1}{2} (\mu_n^2 - \mu_{n-1}^2) \quad (2.32)$$

and

$$a_{n,1,1} = \frac{1}{6} (\mu_n - \mu_{n-1})^2 \quad (2.33)$$

We have examined these integrals, Eq. (2.30), further and have found that the following recurrence relationship exists

$$\begin{aligned} a_{n,\ell,\lambda+1} &= \frac{\ell(2\lambda+1)\alpha_n}{(\lambda+1)(2\ell+1)} a_{n,\ell-1,\lambda} + \frac{(\ell+1)(2\lambda+1)\alpha_n}{(\lambda+1)(2\ell+1)} a_{n,\ell+1,\lambda} \\ &+ \frac{(2\lambda+1)\beta_n}{(\lambda+1)} a_{n,\ell,\lambda} - \frac{\lambda}{(\lambda+1)} a_{n,\ell,\lambda-1} \end{aligned} \quad (2.34)$$

Moreover, the integral  $a_{n,\ell,0}$  can be shown to be given by

$$\begin{aligned} a_{n,\ell,0} &= \frac{1}{(2\ell+1)} [P_{\ell+1}(\mu_n) - P_{\ell+1}(\mu_{n-1}) \\ &- P_{\ell-1}(\mu_n) + P_{\ell-1}(\mu_{n-1})] \end{aligned} \quad (2.35)$$

By Eqs. (2.34) and (2.35) the entire array  $a_{n,\ell,\lambda}$  can be determined.

Furthermore, it is useful to note that

$$a_{n,\ell,\lambda} = 0 \quad \text{for} \quad \ell < \lambda \quad . \quad (2.36)$$

## 2.5 Generalization of Partial-Range Orthogonal Polynomials

Some other orthogonal polynomials have been used in neutron transport analysis. The orthogonal polynomials employed to a varying extent were Jacobi polynomials, Gegenbauer polynomials and Tschebyscheff polynomials<sup>(57-60)</sup>. Moreover, the partial-range polynomials have been extended to the Jacobi polynomials for the solution of the neutron transport equation<sup>(61)</sup>. In the following we will summarize the definition and properties of partial-range Jacobi polynomials. The Jacobi polynomials are functions of one independent variable  $\mu$ , are orthogonal over the range of  $\mu \in [-1,1]$ , and have the following property

$$\int_{-1}^{+1} \omega(\mu) f_{\ell}(\mu) f_{\ell'}(\mu) d\mu = h_{\ell} \delta_{\ell\ell'} \quad , \quad (2.37)$$

where the  $f_{\ell}(\mu)$  denotes the polynomial and  $\omega(\mu)$  is the weighting function given by

$$\omega(\mu) = (1 - \mu)^{\alpha} (1 + \mu)^{\beta} \quad , \quad (2.38)$$

and  $h_{\ell}$  can be shown to be

$$h_{\ell} = \frac{2^{\alpha+\beta+1} \Gamma(\ell + \alpha + 1) \Gamma(\ell + \beta + 1)}{(2\ell + \alpha + \beta + 1) \ell! \Gamma(\ell + \alpha + \beta + 1)} \quad . \quad (2.39)$$

where  $\Gamma$  denotes the gamma-function<sup>(62)</sup>; it is further required that  $\alpha > -1$  and  $\beta > -1$ . Customarily, these polynomials are denoted by

$P_{\ell}^{\alpha, \beta}(\mu)$  possessing the following recurrence relationship

$$\begin{aligned}
 & 2(\ell + 1)(\ell + \alpha + \beta + 1)(2\ell + \alpha + \beta)P_{\ell+1}^{\alpha, \beta}(\mu) \\
 &= (2\ell + \alpha + \beta + 1)[\mu(2\ell + \alpha + \beta)(2\ell + \alpha + \beta + 2) \\
 &+ (\alpha^2 - \beta^2)]P_{\ell}^{\alpha, \beta}(\mu) \\
 &- 2(\ell + 1)(\ell + \beta)(2\ell + \alpha + \beta + 2)P_{\ell-1}^{\alpha, \beta}(\mu) \quad (2.40)
 \end{aligned}$$

Using the transformation of variables, the partial-range Jacobi polynomials which are orthogonal over an arbitrary range of the direction cosine  $\mu \in [\mu_{n-1}, \mu_n]$  is defined by

$$P_{n, \ell}^{\alpha, \beta}(\mu) = P_{\ell}^{\alpha, \beta}(\alpha_n \mu + \beta_n) [H(\mu - \mu_{n-1}) - H(\mu - \mu_n)] \quad (2.41)$$

where  $\alpha_n$  and  $\beta_n$  are given by Eqs. (2.13) and (2.14), respectively, and  $H$  is the unit step function. Again, using the transformation of variables and Eq. (2.37) we can show that the partial-range Jacobi polynomials, as defined by Eq. (2.41), possess the following orthogonality relationship over their range of definition

$$\begin{aligned}
 & \int_{\mu_{n-1}}^{\mu_n} P_{n, \ell}^{\alpha, \beta}(\mu) P_{n, \ell'}^{\alpha, \beta}(\mu) (\mu_n - \mu)^{\alpha} (\mu - \mu_{n-1})^{\beta} d\mu \\
 &= h_{n, \ell} \delta_{\ell \ell'} \delta_{nn'} \quad (2.42)
 \end{aligned}$$

Here  $\delta$  represents the Kronecker delta and  $h_{n, \ell}$  is a normalization factor given by

$$h_{n, \ell} = \frac{(\mu_n - \mu_{n-1})^{(\alpha+\beta+1)} \Gamma(\ell + \alpha + 1) \Gamma(\ell + \beta + 1)}{(2\ell + \alpha + \beta + 1) \ell! \Gamma(\ell + \alpha + \beta + 1)} \quad (2.43)$$

Using Eq. (2.40), the recurrence relationship of the partial-range Jacobi polynomials can be shown to be given by

$$\begin{aligned}
 & 2(\ell + 1)(\ell + \alpha + \beta + 1)(2\ell + \alpha + \beta)(\mu_n - \mu_{n-1})P_{n,\ell+1}^{\alpha,\beta}(\mu) \\
 &= (2\ell + \alpha + \beta + 1)[(2\ell + \alpha + \beta)(2\ell + \alpha + \beta + 2)(2\mu - \mu_n - \mu_{n-1}) \\
 &+ (\mu_n - \mu_{n-1})(\alpha^2 - \beta^2)]P_{n,\ell}^{\alpha,\beta}(\mu) \\
 &- (\ell + \alpha)(\ell + \beta)(2\ell + \alpha + \beta + 2)(\mu_n - \mu_{n-1})P_{n,\ell-1}^{\alpha,\beta}(\mu). \quad (2.44)
 \end{aligned}$$

Finally, we consider the expansion of the full-range Jacobi polynomials over the range  $\mu[\mu_{n-1}, \mu_n]$  in terms of the partial-range Jacobi polynomials over that range as

$$P_{\ell}^{\alpha,\beta}(\mu) = \sum_{\lambda=0}^{\ell} \frac{a_{n,\ell,\lambda}}{h_{n,\lambda}} P_{n,\lambda}^{\alpha,\beta}(\mu) ; \mu \in [\mu_{n-1}, \mu_n] \quad (2.45)$$

where using the orthogonality condition of Eq. (2.42), the coefficients  $a_{n,\ell,\lambda}$  are given by

$$a_{n,\ell,\lambda} = \int_{\mu_{n-1}}^{\mu_n} P_{\ell}^{\alpha,\beta}(\mu) P_{n,\lambda}^{\alpha,\beta}(\mu) (\mu_n - \mu)^{\alpha} (\mu - \mu_{n-1})^{\beta} d\mu. \quad (2.46)$$

These integrals can be evaluated for arbitrary values of  $\ell$  and  $\lambda$ . For example, several low order terms can be shown to be given by

$$a_{n,0,0} = h_{n,0} \quad (2.47)$$

$$\begin{aligned}
 a_{n,1,0} &= \frac{1}{2} \left[ (\alpha - \beta) \left( 1 - \frac{\mu_n - \mu_{n-1}}{2} \right) \right. \\
 &\quad \left. + (2 + \alpha + \beta) \frac{\mu_n + \mu_{n-1}}{2} \right] h_{n,0} \quad (2.48)
 \end{aligned}$$

and

$$a_{n,1,1} = \frac{1}{8} (\mu_n - \mu_{n-1}) h_{n,1} \quad (2.49)$$

where  $h_{n,\lambda}$  is given by Eq. (2.43). Furthermore, higher order of these integrals have been examined and a recurrence relationship between different orders has been established, Table 2.1.

We note that, if we set  $\alpha = \beta = \delta$  and maintain  $N > 1$  with arbitrary directional segmentation, then the partial-range Gegenbauer orthogonal polynomial emerges; if we specify  $\alpha = \beta = -1/2$  or  $0$  and again admit an arbitrary directional segmentation, then the partial-range Tschebyscheff or the partial-range Legendre polynomials are formed, respectively. These partial-range polynomials may be termed the usual full-range polynomials if we defined the angular segmentation by  $N = 1$  with  $\mu \in [-1,1]$ . Similarly, half-range polynomials can be specified for any of the above polynomial designations if we choose  $N = 2$  with  $(-1,0,+1)$  segmentations of direction cosine  $\mu$ .

$$\begin{aligned}
& 4(\ell + 1)(\ell + \alpha + \beta + 1)(2\ell + \alpha + \beta)(2\lambda + \alpha + \beta)(2\lambda + \alpha + \beta + 1) \\
& (2\lambda + \alpha + \beta + 2)a_{n,\ell+1,\lambda} \\
& -2(2\ell + \alpha + \beta)(2\ell + \alpha + \beta + 1)(2\ell + \alpha + \beta + 2)(\lambda + 1) \\
& (\lambda + \alpha + \beta + 1)(2\lambda + \alpha + \beta)(\mu_n - \mu_{n-1})a_{n,\ell,\lambda+1} \\
& = \{2(2\ell + \alpha + \beta + 1)(\alpha^2 - \beta^2)(2\lambda + \alpha + \beta)(2\lambda + \alpha + \beta + 1) \\
& (2\lambda + \alpha + \beta + 2) - (2\ell + \alpha + \beta)(2\ell + \alpha + \beta + 1)(2\ell + \alpha + \beta + 2) \\
& (2\lambda + \alpha + \beta + 1)[(\mu_n - \mu_{n-1})(\alpha^2 - \beta^2) - (\mu_n + \mu_{n-1}) \\
& (2\lambda + \alpha + \beta)(2\lambda + \alpha + \beta + 2)]\}a_{n,\ell,\lambda} \\
& -4(\ell + \alpha)(\ell + \beta)(2\ell + \alpha + \beta + 1)(2\lambda + \alpha + \beta)(2\lambda + \alpha + \beta + 1) \\
& (2\lambda + \alpha + \beta + 2)a_{n,\ell-1,\lambda} \\
& +2(2\ell + \alpha + \beta)(2\ell + \alpha + \beta + 1)(2\ell + \alpha + \beta + 2)(\lambda + \alpha) \\
& (\lambda + \beta)(2\lambda + \alpha + \beta + 2)(\mu_n - \mu_{n-1})a_{n,\ell,\lambda-1}
\end{aligned}$$

Table 2.1: Recurrence relationship of the integrals  $a_{n,\ell,\lambda}$  of partial-range Jacobi polynomials.

## CHAPTER III

### PLANE GEOMETRY: FULL-RANGE SCATTERING FUNCTIONS

#### 3.1 Introduction

The purpose of this chapter is to explore the solution of the one-group neutron transport equation with anisotropic scattering for plane geometry using partial-range Legendre polynomials as the basis solution formalism. As mentioned in the Introduction, the study of the neutron transport equation for cases of strong angular dependence and anisotropic scattering has, however, invariably introduced a number of constraining conditions associated with the directional dependence of the neutron angular flux. In some cases, effective ad hoc approaches have been employed such as the use of double Legendre polynomials<sup>(16-18)</sup>, asymmetric quadrature sets<sup>(22)</sup>, and the use of free parameters<sup>(23,24)</sup>. Moreover, it has been shown that for the case of isotropic scattering, partial-range solutions do permit the calculation of some neutron transport parameters to a very high degree of accuracy even in low-order approximations<sup>(32,33)</sup>. The associated problem of specifying suitable angular segmentations in accordance with the partial-range functional representations did not appear to be a severe limitation<sup>(34)</sup>.

In the partial-range formalism given in this chapter, the angular flux as well as the external sources of neutrons will be expanded in terms of partial-range Legendre polynomials. The scattering function, however, will be expanded traditionally in terms of the



full-range spherical harmonics. The definition and the properties of the partial-range Legendre polynomials have been given in Chapter II. Again, the basis for the use of the partial-range expansions for the neutron angular flux and the neutron sources is the segmentation of the direction cosine  $\mu$  into  $N$  number of arbitrary intervals. These intervals are, as previously suggested, specified by the following:

$$-1 \leq \mu_0 < \mu_1 < \dots < \mu_n < \dots < \mu_N \leq +1 \quad (3.1)$$

Subsequently, over each interval the angular flux as well as the neutron sources are expanded in terms of the partial-range Legendre polynomials in this range and summed up over all the angular intervals. Hence, the proposed solution of the neutron transport equation, Eq. (1.2), in terms of the set of partial-range Legendre polynomials can be written as a double sum

$$\psi(x, \mu) = \sum_{n=1}^N \sum_{\ell=0}^{\infty} \frac{2\ell + 1}{\mu_n - \mu_{n-1}} \phi_{n,\ell}(x) P_{n,\ell}(\mu) \quad (3.2)$$

where the partial-range moments of the angular flux,  $\phi_{n,\ell}(x)$ , are given by

$$\phi_{n,\ell}(x) = \int_{\mu_{n-1}}^{\mu_n} \psi(x, \mu) P_{n,\ell}(\mu) d\mu \quad (3.3)$$

where  $P_{n,\ell}(\mu)$  are the partial-range Legendre polynomials discussed in Chapter II. The source term of Eq. (1.2),  $S(x, \mu)$ , will similarly be expanded as

$$S(x, \mu) = \sum_{n=1}^N \sum_{\ell=0}^{\infty} \frac{2\ell + 1}{\mu_n - \mu_{n-1}} s_{n,\ell}(x) P_{n,\ell}(\mu) \quad (3.4)$$

where the partial-range coefficients of the source  $s_{n,\ell}(x)$  are given by

$$s_{n,\ell}(x) = \int_{\mu_{n-1}}^{\mu_n} S(x, \mu) P_{n,\ell}(\mu) d\mu \quad (3.5)$$

Finally, the scattering function  $f(\underline{\Omega}', \underline{\Omega})$  can be expanded conventionally in terms of the full-range Legendre polynomials,  $P_{\ell}(\mu_s)$ , as (1,2)

$$f(\underline{\Omega}', \underline{\Omega}) = \sum_{\ell=0}^{\infty} \frac{2\ell + 1}{4\pi} f_{\ell} P_{\ell}(\mu_s) \quad (3.6)$$

where the coefficient  $f_{\ell}$  is given by

$$f_{\ell} = 2\pi \int_{-1}^{+1} f(\underline{\Omega}', \underline{\Omega}) P_{\ell}(\mu_s) d\mu_s \quad (3.7)$$

Here,  $\mu_s$  is the cosine of the scattering angle of the neutron.

### 3.2 Solution Formulation

The time-independent one-group neutron transport equation with anisotropic scattering for the case of plane geometry, Eq. (1.2), is written again here for homogeneous system as

$$\mu \frac{\partial \psi(x, \mu)}{\partial x} + \psi(x, \mu) = c \int_{\underline{\Omega}'} f(\underline{\Omega}', \underline{\Omega}) \psi(x, \mu') d\underline{\Omega}' + \frac{1}{\Sigma} S(x, \mu) \quad (3.8)$$

The notation used here has been defined in Section 1.2. Briefly, the angular flux of neutrons,  $\psi(x, \mu)$ , is a function of the position  $x$  and

the direction cosine  $\mu = \cos\theta$  where  $\theta$  is the angle between the direction of neutron motion and the x-axis. The neutrons source density function is designated by  $S(x, \mu)$ . Here, the constant  $c$  represents the mean number of secondary neutrons per collision and  $\Sigma$  defines the space independent total macroscopic cross section of neutrons. Finally,  $f(\underline{\Omega}', \underline{\Omega})$ , represents the probability density function for the case of a neutron, entering a collision with initial direction  $\underline{\Omega}'$ , and subsequently emerging with direction contained in a unit solid angle about the final direction  $\underline{\Omega}$ .

The neutron transport equation over the  $N$  independent intervals of  $\mu$  which are defined by Eq. (3.1) expressed explicitly in terms of the partial-range Legendre polynomials are obtained by direct substitution of Eqs. (3.2), (3.4) and (3.6) into Eq. (3.8). The resultant equation is given by

$$\begin{aligned} & \sum_{n=1}^N \sum_{\ell=0}^{\infty} \frac{2\ell+1}{\mu_n - \mu_{n-1}} \left[ \mu \frac{d\phi_{n,\ell}(x)}{dx} P_{n,\ell}(\mu) + \phi_{n,\ell}(x) P_{n,\ell}(\mu) \right] \\ &= \sum_{n=1}^N \sum_{\ell=0}^{\infty} \frac{2\ell+1}{\mu_n - \mu_{n-1}} \left[ c \int_{\underline{\Omega}'} \sum_{k=0}^{\infty} \frac{2k+1}{4\pi} f_k P_k(\mu_s) \phi_{n,\ell}(x) P_{n,\ell}(\mu') d\underline{\Omega}' \right. \\ & \left. + \frac{1}{\Sigma} s_{n,\ell}(x) P_{n,\ell}(\mu) \right] \end{aligned} \quad (3.9)$$

Here, the scattering cosine  $\mu_s$  is a function of  $\mu'$  and  $\mu$ , where  $\mu'$  is the cosine of the direction of neutron before collision, and  $\mu$  is the cosine of its direction after collision.

The transformation of the one-group neutron transport equation, Eq. (3.9), into a linear system of equations in terms of the one spatial

variable  $x$  is obtained by multiplication of each term by the partial-range Legendre polynomial,  $P_{n',j}(\mu)$ . Subsequently, an integration over the specified allowable range of the angular variable is performed. The most important term in the resultant equation is the integral associated with the right-hand side of Eq. (3.9). This integral expression, designated by  $I_1$ , is

$$I_1 = \int_{\mu_{n'-1}}^{\mu_{n'}} \int_{\underline{\Omega}'} P_k(\mu_s) P_{n',j}(\mu) P_{n,\ell}(\mu') d\underline{\Omega}' d\mu . \quad (3.10)$$

Using the addition theorem of the spherical harmonics permits us to write the following

$$P_k(\mu_s) = \sum_{m=-k}^k \frac{4\pi}{2k+1} Y_k^{m*}(\underline{\Omega}) Y_k^m(\underline{\Omega}') , \quad (3.11)$$

where  $Y_k^m(\underline{\Omega})$  is the spherical harmonics function which can be expressed in the form<sup>(62,63)</sup>

$$Y_k^m(\underline{\Omega}) = K_k^m(\mu) e^{im\omega} . \quad (3.12)$$

Here the function  $K_k^m(\mu)$  is independent of the azimuthal angle  $\omega$  and  $K_k^0(\mu) = P_k(\mu)$ . Substituting Eq. (3.12) into Eq. (3.11) and then into Eq. (3.10) leads to

$$I_1 = 8\pi^2 \int_{\mu_{n'-1}}^{\mu_{n'}} \int_{-1}^1 P_k(\mu) P_k(\mu') P_{n',j}(\mu) P_{n,\ell}(\mu') d\mu' d\mu . \quad (3.13)$$

To evaluate the integration of Eq. (3.13) it is necessary to obtain the partial-range expansion of the full-range Legendre polynomial

$P_\ell(\mu)$  as discussed in Section 2.4. Using Eq. (2.29) we can write the above equation as

$$I_1 = 8\pi^2 \int_{\mu_{n'-1}}^{\mu_{n'}} \int_{-1}^1 \sum_{\lambda=0}^k \frac{2\lambda+1}{\mu_{n'} - \mu_{n'-1}} a_{n',k,\lambda} P_{n',\lambda}(\mu) \times \sum_{\lambda'=0}^k \frac{2\lambda'+1}{\mu_n - \mu_{n'+1}} a_{n,k,\lambda'} P_{n,\lambda'}(\mu') P_{n',j}(\mu) P_{n,\ell}(\mu') d\mu' d\mu, \quad (3.14)$$

where the coefficients  $a_{n,k,\lambda}$  are defined by Eq. (2.30) and the entire array  $a_{n,k,\lambda}$  has been evaluated in Section 2.4. Employing the orthogonality condition of the partial-range Legendre polynomials, Eq. (2.18), the above integral can be rewritten as

$$I_1 = 8\pi^2 a_{n',k,j} a_{n,k,\ell} \quad (3.15)$$

The second integral of interest is

$$I_2 = \int_{\mu_{n'-1}}^{\mu_{n'}} \mu P_{n',j}(\mu) P_{n,\ell}(\mu) d\mu \quad (3.16)$$

This integral can be evaluated using the recurrence relationship of the partial-range Legendre polynomials, Eq. (2.20), and subsequently the orthogonality condition of Eq. (2.18). The result is given by

$$I_2 = \frac{\mu_{n'} - \mu_{n'-1}}{\alpha_{n'}(2j+1)(2\ell+1)} \delta_{n'n} [(j+1)\delta_{\ell,j+1} + j\delta_{\ell,j-1} + \beta_n(2j+1)\delta_{\ell,j}] \quad (3.17)$$

where the interval functions  $\alpha_n$  and  $\beta_n$  are given by Eqs. (2.13) and

(2.14), respectively. The other integrals resulting from the rest of the terms of Eq. (3.9) involve only the multiplication of two partial-range Legendre polynomials, which is given by their orthogonality condition, Eq. (2.18). Substituting the appropriate integrals into Eq. (3.9), and rearranging we finally obtain

$$\begin{aligned}
 & \frac{2}{\alpha_n(2j+1)} \left[ j \frac{d\phi_{n,j-1}(x)}{dx} + (j+1) \frac{d\phi_{n,j+1}(x)}{dx} \right] \\
 & + \frac{2\beta_n}{\alpha_n} \frac{d\phi_{n,j}(x)}{dx} + 2\phi_{n,j}(x) \\
 & = c \sum_{n'=1}^N \sum_{\ell=0}^{\infty} \sum_{\lambda=0}^{\infty} \frac{(2\ell+1)(2\lambda+1)}{\mu_{n'} - \mu_{n'-1}} f_{\ell}^{a_{n',\ell,\lambda}} a_{n,\ell,j} \phi_{n',\lambda}(x) \\
 & + \frac{2}{\Sigma} s_{n,j}(x); \quad j = 0, 1, \dots, \infty \text{ and } n = 1, 2, \dots, N. \quad (3.18)
 \end{aligned}$$

This system of linear equations represents the condition on the partial-range moments of the angular flux  $\phi_{n,j}(x)$ , which are functions of only one independent variable.

Before proceeding to low-order approximations, numerical tests and calculational studies, we briefly consider several reductions of Eq. (3.18) to illustrate a measure of generality associated with the solution presented here, and to provide its continuity with the previous works in the field.

### 3.3 Special Cases

#### 3.3.1 Isotropic Scattering

We consider first the case of a medium with isotropic scattering.

For this case clearly  $f_\ell = 0$  for all  $\ell \geq 1$  and thus Eq. (3.18), after substituting the values of  $\alpha_n$  and  $\beta_n$  of Eqs. (2.13) and (2.14), respectively, reduces to

$$\begin{aligned}
 & \frac{\mu_n - \mu_{n-1}}{2j+1} \left[ j \frac{d\phi_{n,j-1}(x)}{dx} + (j+1) \frac{d\phi_{n,j+1}(x)}{dx} \right] \\
 & + (\mu_n + \mu_{n-1}) \frac{d\phi_{n,j}(x)}{dx} + 2\phi_{n,j}(x) \\
 & = c \sum_{n'=1}^N \sum_{\lambda=0}^{\infty} \frac{2\lambda+1}{\mu_{n'} - \mu_{n'-1}} a_{n',0,\lambda} a_{n,0,\lambda} \phi_{n',\lambda}(x) \\
 & + \frac{2}{\Sigma} s_{n,j}(x) \quad (3.19)
 \end{aligned}$$

From the normalization of the scattering function we write  $f_0 = 1$  and using Eqs. (2.31) and (2.36) we can write

$$a_{n',0,\lambda} = (\mu_{n'} - \mu_{n'-1}) \delta_{0\lambda} \quad (3.20)$$

and

$$a_{n,0,j} = (\mu_n - \mu_{n-1}) \delta_{0j} \quad (3.21)$$

Substituting Eqs. (3.20) and (3.21) into Eq. (3.19), therefore, yields

$$\begin{aligned}
 & \frac{\mu_n - \mu_{n-1}}{2j+1} \left[ j \frac{d\phi_{n,j-1}(x)}{dx} + (j+1) \frac{d\phi_{n,j+1}(x)}{dx} \right] \\
 & + (\mu_n + \mu_{n-1}) \frac{d\phi_{n,j}(x)}{dx} + 2\phi_{n,j}(x) \\
 & = c (\mu_n - \mu_{n-1}) \sum_{n'=1}^N \phi_{n',0}(x) \delta_{0j} + \frac{2}{\Sigma} s_{n,j}(x) \quad (3.22)
 \end{aligned}$$

This equation agrees with that previously obtained via a different starting point<sup>(32)</sup> but for a source free medium, that is  $s_{n,j}(x) = 0$  for all values of  $n$  and  $j$ .

### 3.3.2 Double Spherical Harmonics Approximation

The double spherical harmonics approximation which is known as Yvon's double- $P_\ell$  approximation<sup>(16-18)</sup> can be obtained as a special case of this general solution by specifying the number of intervals of the angular variable  $N = 2$  and allowing the order of the partial-range Legendre polynomial  $\ell$  to take any arbitrary value. In this case there are two fixed angular intervals specified by  $\mu_0 = -1$ ,  $\mu_1 = 0$ , and  $\mu_2 = +1$ . For  $n = 1$ , Eq. (3.18) reduces to

$$\begin{aligned} & \frac{1}{2j+1} \left[ j \frac{d\phi_{1,j-1}(x)}{dx} + (j+1) \frac{d\phi_{1,j+1}(x)}{dx} \right] \\ & - \frac{d\phi_{1,j}(x)}{dx} + 2\phi_{1,j}(x) \\ & = c \sum_{\ell=0}^{\infty} \sum_{\lambda=0}^{\infty} (2\ell+1)(2\lambda+1) f_{\ell} a_{1,\ell,j} [a_{1,\ell,\lambda} \phi_{1,\lambda}(x) \\ & + a_{2,\ell,\lambda} \phi_{2,\lambda}(x)] + \frac{2}{\Sigma} s_{1,j}(x) \end{aligned} \quad (3.23)$$

and for  $n = 2$  it reduces to

$$\begin{aligned} & \frac{1}{2j+1} \left[ j \frac{d\phi_{2,j-1}(x)}{dx} + (j+1) \frac{d\phi_{2,j+1}(x)}{dx} \right] + \frac{d\phi_{2,j}(x)}{dx} + 2\phi_{2,j}(x) \\ & = c \sum_{\ell=0}^{\infty} \sum_{\lambda=0}^{\infty} (2\ell+1)(2\lambda+1) f_{\ell} a_{2,\ell,j} [a_{1,\ell,\lambda} \phi_{1,\lambda}(x) \\ & + a_{2,\ell,\lambda} \phi_{2,\lambda}(x)] + \frac{2}{\Sigma} s_{2,j}(x) \end{aligned} \quad (3.24)$$



These two equations agree with the results of the double spherical harmonics approximation<sup>(16-18)</sup> if we replace the notation  $\phi_{1,j}(x)$  and  $\phi_{2,j}(x)$  by  $\phi_j^-(x)$  and  $\phi_j^+(x)$ , respectively.

#### 2.4 NP<sub>L</sub> Approximation

In the NP<sub>L</sub> approximation the flux is written in terms of N(L+1) components of the partial-range moments  $\phi_{n,\ell}(x)$ . This condition requires that  $\phi_{n,\ell}(x) = 0$  for  $\ell > L$ ; that is, we truncate the  $P_{n,\ell}(\mu)$  expansion of the angular flux after (L+1) terms only. Thus Eq. (3.2) becomes

$$\psi(x, \mu) = \sum_{n=1}^N \sum_{\ell=0}^L \frac{2\ell + 1}{\mu_n - \mu_{n-1}} \phi_{n,\ell}(x) P_{n,\ell}(\mu) \quad (3.25)$$

and Eq. (3.4) may be written as

$$S(x, \mu) = \sum_{n=1}^N \sum_{\ell=0}^L \frac{2\ell + 1}{\mu_n - \mu_{n-1}} s_{n,\ell}(x) P_{n,\ell}(\mu) \quad (3.26)$$

In the expansion of the scattering function we need to set  $f_\ell = 0$  for  $\ell > L_f$ . This assumes that the scattering function is adequately described by  $(L_f + 1)$  coefficients and therefore we write for Eq. (3.6)

$$f(\underline{\Omega}' \cdot \underline{\Omega}) = \sum_{\ell=0}^{L_f} \frac{2\ell + 1}{4\pi} f_\ell P_\ell(\mu_s) \quad (3.27)$$

Finally, the expansion of the full-range Legendre polynomial, Eq. (2.29) can be approximated by

$$P_\ell(\mu) = \sum_{\lambda=0}^{\text{Min}\{L, \ell\}} \frac{2\ell + 1}{\mu_n - \mu_{n-1}} a_{n,\ell,\lambda} P_{n,\lambda}(\mu) \quad (3.28)$$

Herein, we emphasize that the summation extends to  $L$  or  $\ell$ , whichever is smaller. We note, however, that  $\ell$  can take on a value larger than  $L$  because it is restricted by  $L_f$ .

Using the above approximations finally permits us to write the following condition for the spatial moments

$$\begin{aligned}
 & \frac{\mu_n - \mu_{n-1}}{2j+1} \left[ j \frac{d\phi_{n,j-1}(x)}{dx} + (j+1) \frac{d\phi_{n,j+1}(x)}{dx} \right] \\
 & + (\mu_n + \mu_{n-1}) \frac{d\phi_{n,j}(x)}{dx} + 2\phi_{n,j}(x) \\
 & = c \sum_{n'=1}^N \sum_{\ell=0}^{L_f} \sum_{\lambda=0}^{\text{Min}\{L,\ell\}} \frac{(2\ell+1)(2\lambda+1)}{\mu_{n'} - \mu_{n'-1}} f_{a_{n',\ell,\lambda}} a_{n,\ell,j} \phi_{n',\lambda}(x) \\
 & + \frac{2}{\Sigma} s_{n,j}(x); \tag{3.29}
 \end{aligned}$$

with  $j = 0, 1, \dots, L$  and  $n = 1, 2, \dots, N$ . This equation here represents a system of  $N(L+1)$  linear equations in the  $N(L+1)$  unknown partial-range spatial moments  $\phi_{n,j}(x)$ . It is the starting point for any further approximations and calculational studies in this chapter for the present formalism.

### 3.5 NP<sub>0</sub> Approximation and the Eigenvalues

In this section we will formulate the eigenvalue problem associated with Eq. (3.29). For this purpose we will consider a source-free medium. However, we assume the presence of a source of neutrons at the boundary of the system under consideration to provide the neutrons; thus this source of neutrons can be treated as a boundary condition for the problem. Also, we will consider a

medium with a linear anisotropic scattering. This means that  $L_f = 1$ . In this case the anisotropy is described by two coefficients. The first coefficient is  $f_0$  which is equal to unity from the normalization of the scattering function. The second one is the anisotropy variable  $f_1$  which depends on the medium under consideration and its allowable range<sup>(64)</sup> is  $-1/3 \leq f_1 \leq 1/3$ . As a first approximation, we choose the lowest-order approximation  $L = 0$ . Under these conditions, Eq. (3.29) reduces to

$$\begin{aligned} (\mu_n + \mu_{n-1}) \frac{d\phi_{n,o}(x)}{dx} + 2\phi_{n,o}(x) & \quad (3.30) \\ & = c(\mu_n - \mu_{n-1}) \sum_{n'=1}^N \phi_{n',o}(x) \left[ 1 + \frac{3f_1}{4} (\mu_n + \mu_{n-1})(\mu_{n'} - \mu_{n'-1}) \right]; \end{aligned}$$

with  $n = 1, 2, \dots, N$ , to yield a system of independent linear differential equations possessing  $N$  solutions for the partial-range moments  $\phi_{n,o}(x)$ .

The general solutions of  $\phi_{n,o}(x)$  is given in terms of

$$\phi_{n,o}(x) = A_n e^{-x/\nu} \quad (3.31)$$

where  $A_n$  is a constant governed not only by the usual boundary conditions but by the eigenvalues; in distinction to previous analysis<sup>(1,2)</sup>, the eigenvalues are - as will become clear - dependent upon the chosen angular segmentation. Substituting Eq. (3.31) into Eq. (3.30) leads to a matrix representation for the eigenvalue problem associated with the system of Eq. (3.30) which can be written in the form

$$\underline{\lambda} \underline{A} = \underline{D} \underline{A} \quad (3.32)$$

where  $\underline{\lambda}$  is a diagonal matrix possessing  $1/\nu$  in each element of the diagonal and the vector  $\underline{A}$  is given by

$$\underline{A} = \begin{bmatrix} A_1 \\ A_2 \\ \vdots \\ A_N \end{bmatrix} \quad (3.33)$$

and  $\underline{D}$  is a  $N \times N$  matrix defined by

$$\underline{D} = \begin{bmatrix} y_1(\mu_1) & y_1(\mu_2) & \dots & y_1(\mu_N) \\ y_2(\mu_1) & y_2(\mu_2) & \dots & y_2(\mu_N) \\ \vdots & \vdots & \ddots & \vdots \\ y_N(\mu_1) & y_N(\mu_2) & \dots & y_N(\mu_N) \end{bmatrix} \quad (3.34)$$

where,

$$y_n(\mu_m) = \frac{1}{\mu_n + \mu_{n-1}} \{ 2\delta_{nm} - c(\mu_n - \mu_{n-1}) \times [1 + \frac{3f_1}{4} (\mu_n + \mu_{n-1})(\mu_m + \mu_{m-1})] \}; \quad (3.35)$$

with  $n = 1, 2, \dots, N$  and  $m = 1, 2, \dots, N$ .

Of significant interest here is the observation that all eigenvalues are along the diagonal; this feature, attained by suitable transformation, was not apparent in a related analysis for isotropic scattering medium<sup>(53)</sup>. This represents a usual eigenvalue problem and we can use the standard solution methods of the eigenvalue problem in its solution.

### 3.6 2P<sub>0</sub> Approximation

To proceed further with this study we calculate the asymptotic

relaxation length by this method of partial-range analysis as described here and compare it with other methods of similar complexity. The asymptotic relaxation length is related to the eigenvalue of the problem. Consider the low-order approximation of  $N = 2$  and  $L = 0$  which herein is designated the  $2P_0$  approximation. In this approximation, the angular partitions  $\mu_0$ ,  $\mu_1$  and  $\mu_2$  are variables subjected only to the condition that  $-1 \leq \mu_0 < \mu_1 < \mu_2 \leq +1$ . To contain the complete range of  $\mu = -1$  to  $\mu = +1$ , we impose  $\mu_0 = -1$  and  $\mu_2 = +1$  and retain  $\mu_1$  as a free variable  $-1 < \mu_1 < +1$ . The appearance of a free variable has previously been encountered in the analysis of the one-group neutron transport equation within the context of full-range orthogonal polynomial expansions<sup>(59,60)</sup>; this necessitates a numerical or analytical study to determine how the free variable affects the numerical value of the parameter of interest.

In the approximation treated here, we obtain the following condition on the eigenvalue

$$\begin{vmatrix} y_1(\mu_1) - \frac{1}{v} & y_1(\mu_2) \\ y_2(\mu_1) & y_2(\mu_2) - \frac{1}{v} \end{vmatrix} = 0 \quad (3.36)$$

where the  $y$ 's functions are given by Eq. (3.35) but for the specific values of  $n$  and  $m$ . Equation (3.36) is expanded and by the appropriate substitution of the expressions of the  $y$ 's functions it yields

$$(1 - \mu_1^2)\left(\frac{1}{v}\right)^2 + 4\mu_1(1 - c)\frac{1}{v} - 4(1 - c)\left[1 - \frac{3f_1c}{4}(1 - \mu_1^2)\right] = 0. \quad (3.37)$$

In this case the above equation yields only two eigenvalues given by

$$\left(\frac{1}{v_0}\right)^\pm = -\frac{2\mu_1(1-c)}{1-\mu_1^2} \pm \frac{2}{1-\mu_1^2} \left\{ (1-c)[1-\mu_1^2c] - \frac{3f_1c}{4}(1-\mu_1^2)^2 \right\}^{1/2}, \quad (3.38)$$

both of which depend upon the parameters  $c$ ,  $f_1$  and the free variable  $\mu_1$ . Here,  $v_0$  represents the asymptotic relaxation length of the medium under consideration. From this equation we can recognize the following special cases:

- 1) For  $f_1 = 0$ , we obtain the isotropic scattering case. For this special case Eq. (3.38) reduces to

$$\left(\frac{1}{v_0}\right)^\pm = -\frac{2\mu_1(1-c)}{1-\mu_1^2} \pm \frac{2}{1-\mu_1^2} [(1-c)(1-\mu_1^2c)]^{1/2}. \quad (3.39)$$

This result is in agreement with a previous study for the isotropic case of scattering<sup>(32)</sup>.

- 2) For  $\mu_1 = 0$ , we obtain the formal  $DP_0$  approximation. For this special case of  $\mu_1 = 0$ , Eq. (3.38) yields

$$\left(\frac{1}{v_0}\right)^\pm = \pm 2\sqrt{(1-c)\left(1 - \frac{3f_1c}{4}\right)}. \quad (3.40)$$

This result again agrees with that of the  $DP_0$  approximation<sup>(1,2)</sup>.

Whether the eigenvalues of Eq. (3.38) are real or complex depends on the sign of the discriminant

$$D = (1 - c) \left[ 1 - \mu_1^2 c - \frac{3f_1 c}{4} (1 - \mu_1^2)^2 \right] \quad (3.41)$$

The boundaries between the real and complex eigenvalues are given by the requirement that  $D = 0$  which is satisfied by the following conditions on  $c$  in terms of the free variable  $\mu_1$  and the anisotropic coefficient  $f_1$ .

$$c = \begin{cases} 1, \\ \frac{1}{\mu_1^2 + \frac{3f_1}{4} (1 - \mu_1^2)^2} \end{cases} \quad (3.42)$$

A graphical representation of the properties of the eigenvalues is shown in Fig. 3.1 for three cases of scattering: isotropic ( $f_1 = 0$ ), forward ( $f_1 = +0.3$ ), and backward ( $f_1 = -0.3$ ). From this figure we note that the range of the variables  $c$  and  $\mu_1$ , which gives complex eigenvalues, increases for backward scattering and decreases for forward scattering. This means that the region in the  $c$ - $\mu_1$  space in which a sustained reaction can be obtained is much greater for backward scattering than for forward scattering. Therefore, a criticality can be attained by a smaller volume and mass of fuel when materials with backward scattering are used. The effect of anisotropic scattering on criticality of slab reactors will be studied in Section 4.5.3. It is of interest to note that in an early study of neutron transport with anisotropic scattering Davison<sup>(65)</sup>, employing an entirely different approach, similarly encountered real and complex eigenvalues for  $c > 1$ .

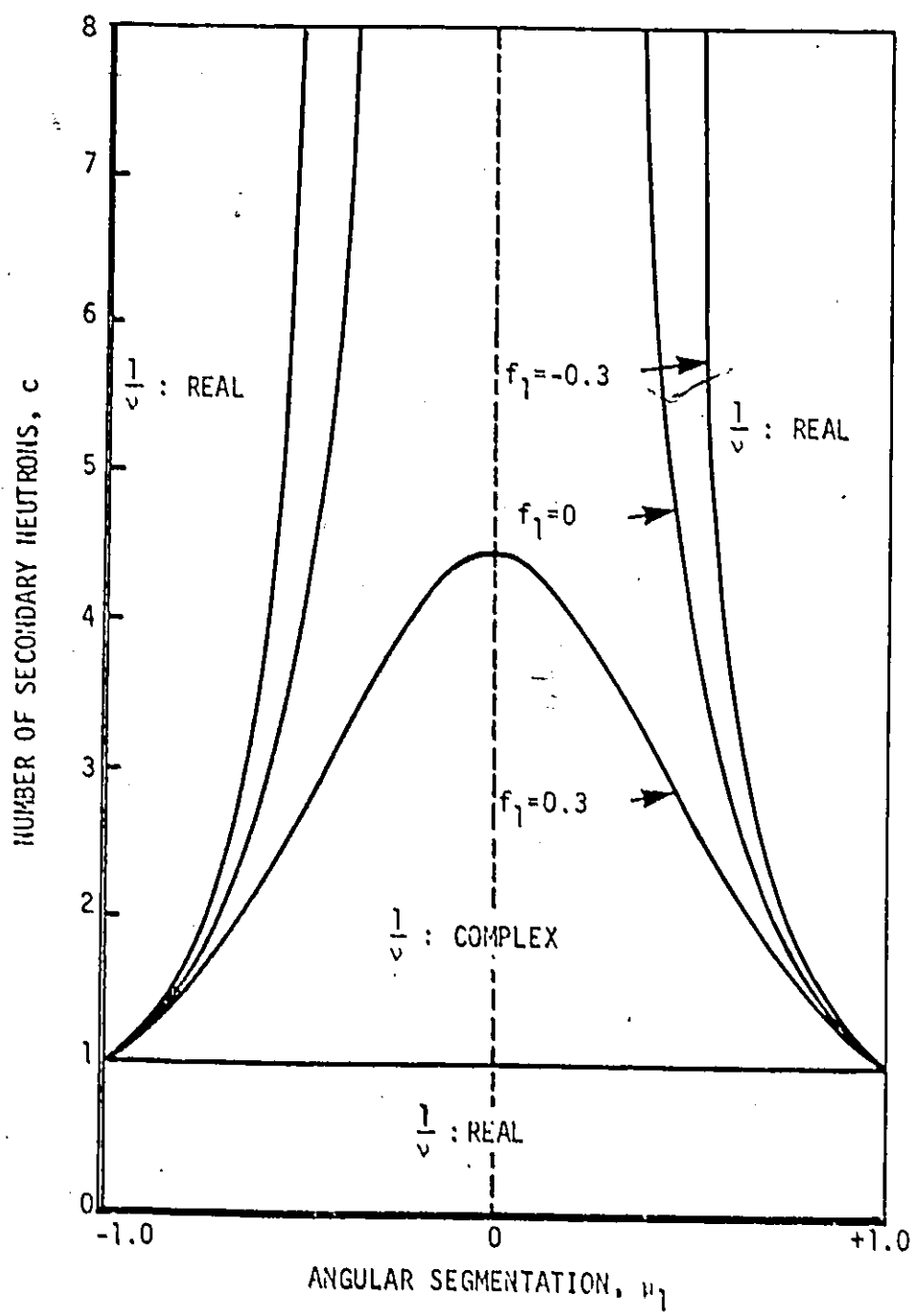


Fig. 3.1: Domain of real and complex eigenvalues as a function of angular segmentation and the number of secondary neutrons using the  $2P_0$  approximation.



The eigenvalue spectra for the same three cases of scattering, as well as  $c = 0.9$  and  $0.5$ , are shown in Figs. 3.2 and 3.3, respectively. From both figures we note that the eigenvalue  $1/v_0$  varies over a wide range as  $\mu_1$  varies inbetween  $-1$  and  $+1$ . It is clearly of interest to determine the angular segmentation  $\mu_1$  which minimizes the error between the exact eigenvalue and that obtained in this low-order approximation ( $N = 2, L = 0$ ) for various cases of linear anisotropy. We have conducted such a search and listed the results on Table 3.1.

In Table 3.1, the eigenvalue  $1/v_0$  as a function of the number of secondary neutrons,  $c$ , and anisotropy,  $f_1$ , have been listed as calculated by exact method,  $2P_0$  approximation of this work, diffusion theory, and double- $P_0$  approximation. The free parameter  $\mu_1$  corresponding to the results obtained by the  $2P_0$  approximation as well as the percentage errors between this result and the exact values have been given as well. The exact eigenvalues have been recalculated using the singular eigenfunctions method<sup>(64)</sup>. The diffusion theory results have been extracted from Case and Zweifel<sup>(2)</sup>, while the double- $P_0$  approximation results have been calculated as a special case of this study using Eq. (3.40). Here we note that this low-order partial-range solution yields very accurate results in the range of small  $c$  where alternative methods are particularly inaccurate. It is also seen that for backward scattering the  $NP_L$  approximation gives essentially better results than for forward scattering. This would suggest that the partial-range approximation may possess considerable merit in highly backward scattering medium with high absorption.

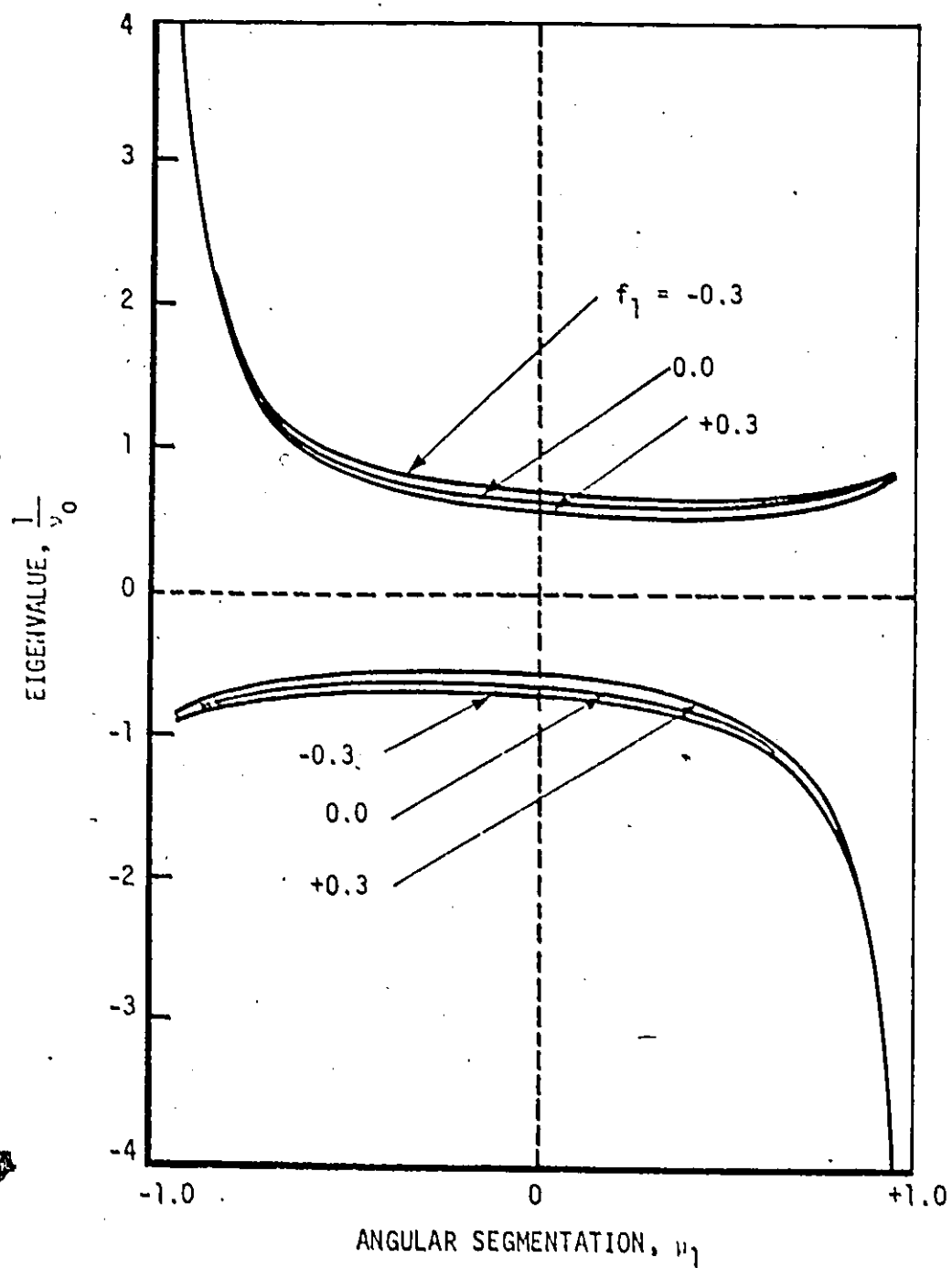


Fig. 3.2: Eigenvalue spectra as a function of angular segmentation for  $c = 0.9$  using the  $2P_0$  approximation.

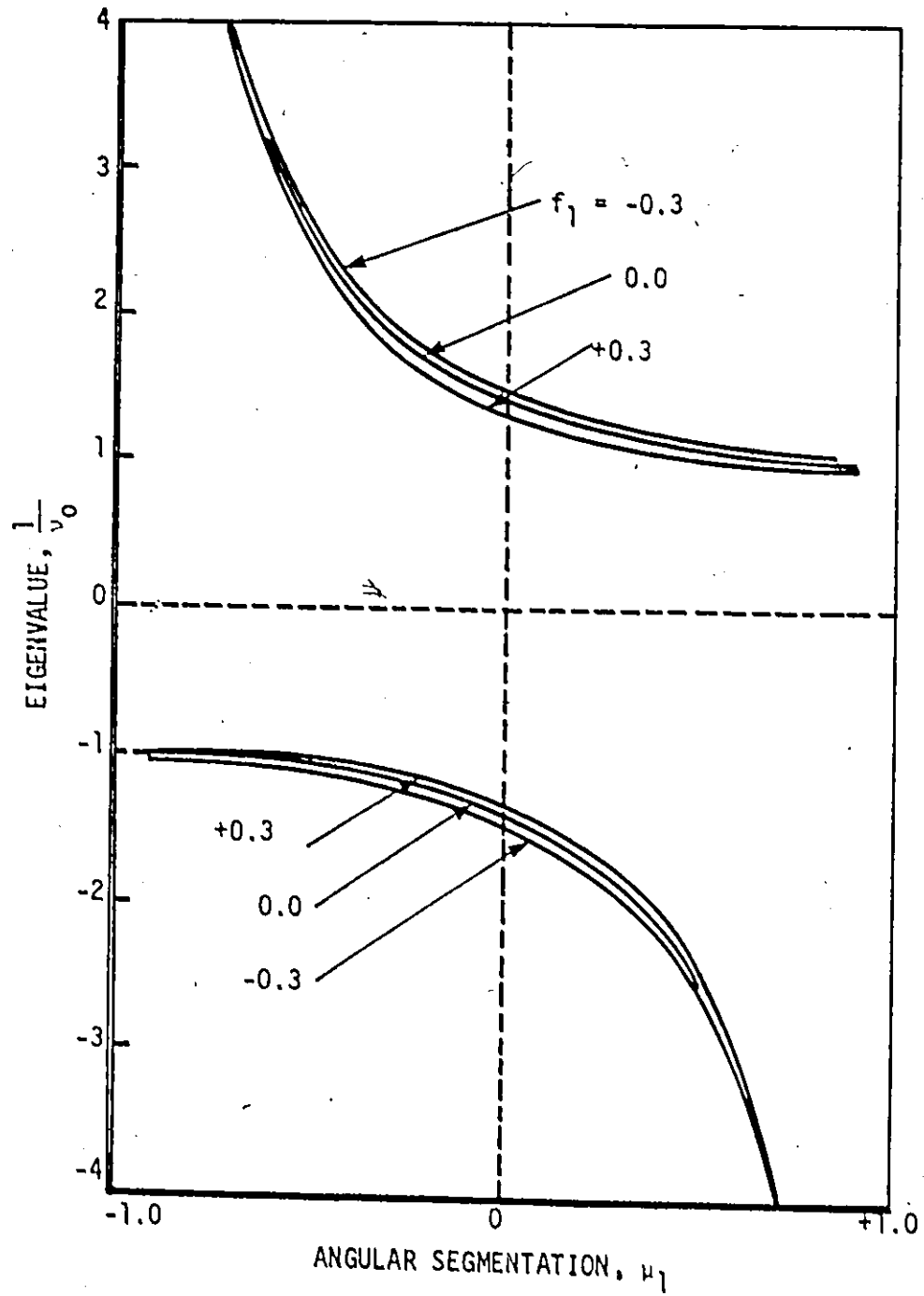


Fig. 3.3: Eigenvalue spectra as a function of angular segmentation for  $c = 0.5$  using the  $2P_0$  approximation.

c	f <sub>1</sub>	Exact Solution	2P <sub>0</sub> (This Work)			Diffusion Theory (P <sub>1</sub> )	Double -P <sub>0</sub>
			1/v <sub>0</sub>	% error	μ <sub>1</sub>		
0	All	1.0000	1.0050	0.50	0.99	1.7320	2.0000
0.5	0	0.9575	1.0000	4.43	0.99	1.2247	1.4142
	0.1	0.9419	0.9975	5.90	0.93	1.1937	1.3874
	0.3	0.9078	0.9819	8.16	0.83	1.1291	1.3323
	-0.1	0.9716	1.0008	3.01	0.99	1.2550	1.4405
	-0.3	0.9928	1.0639	7.16	0.76	1.3134	1.4916
0.7	0	0.8286	0.9165	10.61	0.65	0.9487	1.0954
	0.1	0.8069	0.8962	11.07	0.62	0.9148	1.0663
	0.3	0.7642	0.8517	11.45	0.56	0.8432	1.0055
	-0.3	0.8944	0.9686	8.30	0.78	1.0435	1.1786
0.9	0	0.5254	0.6000	14.20	0.33	0.5477	0.6325
	0.05	0.5193	0.5899	13.60	0.33	0.5352	0.6217
	0.07	0.5169	0.5858	13.33	0.32	0.5302	0.6173
	0.1	0.5132	0.5796	12.94	0.32	0.5225	0.6107
	0.3	0.4897	0.5365	9.56	0.29	0.4680	0.5648
0.98	0	0.2430	0.2800	15.23	0.14	0.2450	0.2828
	0.1	0.2401	0.2695	12.25	0.14	0.2316	0.2726
	0.3	0.2345	0.2472	5.42	0.13	0.2058	0.2497
1.0	All	0.0	0.0	0.0	All	0.0	0.0

Table 3.1: Calculated eigenvalue  $1/v_0$  as a function of number of secondary neutrons,  $c$ , and anisotropy,  $f_1$ . The results obtained with the partial-range analysis (this work) are listed corresponding to the angular segmentation,  $\mu_1$ , which yielded the most accurate results. The percentages errors between the results of this work and the exact ones are listed.

### 3.7 Necessary Numbers of Partial-Range Spherical Harmonics

As an alternative way to test the accuracy of the present formalism of partial-range spherical harmonics we will discuss the necessary numbers of partial-range Legendre polynomials starting by the  $2P_0$  approximation given in the previous section. It is evident that the asymptotic relaxation length  $v_0$  must be at least as large as the mean free path  $\lambda_0 = 1/\Sigma^{(66)}$ , where  $\Sigma$  is the total macroscopic cross section of neutrons. In fact,  $v_0$  is always larger than  $\lambda_0$  with the possible exception of a medium with complete absorption in which both are equal. In the  $NP_L$  approximation this is not fulfilled for all values of the angular variable  $\mu_1$  for specific values of  $c$  and  $f_1$ . It is important to determine the range in the  $c$ - $\mu_1$  space in which the largest eigenvalue  $v_0$  is greater than the mean free path  $\lambda_0 = 1$ , which is chosen in this analysis as the unit of length.

To illustrate this feature let us consider the  $2P_0$  approximation. Starting by Eq. (3.37) which can be rearranged to read

$$\begin{aligned} \frac{3f_1}{4} (1 - \mu_1^2)c^2 + \left[ \frac{\mu_1}{v_0} - 1 - \frac{3f_1}{4} (1 - \mu_1^2) \right] c \\ + 1 - \frac{\mu_1}{v_0} - \frac{1 - \mu_1^2}{4v_0} = 0 \end{aligned} \quad (3.43)$$

The above equation is a second order equation in  $c$  and it can be solved for  $c$  as a function of  $\mu_1$  for specific values of  $f_1$ . In Fig. 3.4,  $c$  is given as function of  $\mu_1$  for the isotropic case of scattering ( $f_1 = 0$ ) and for three values of  $1/v_0 = 1.0, 0.8$  and  $0.6$ , respectively. From the figure, we observe that for values of  $c$  from 0.5 to 1.0 the

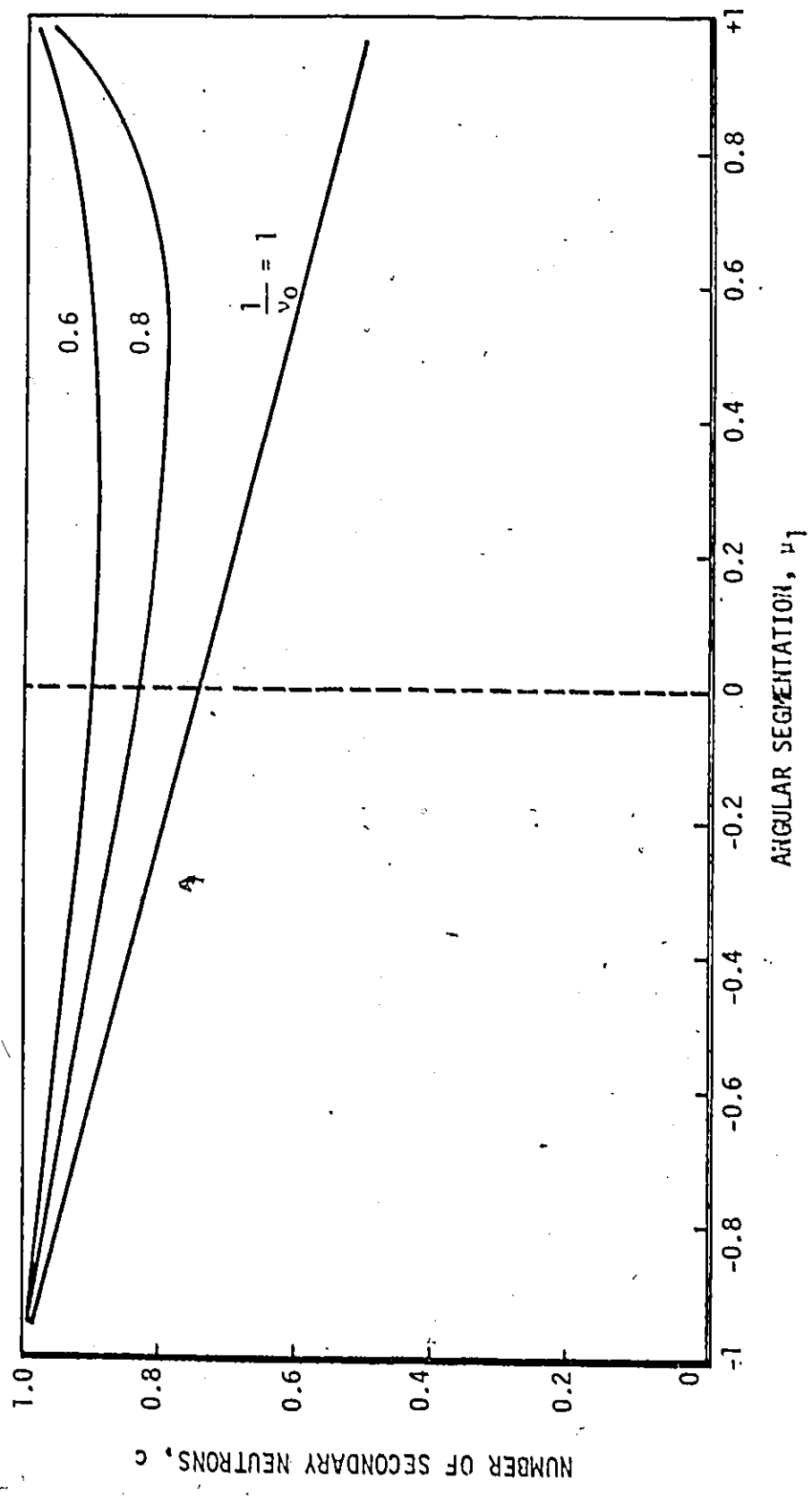


Fig. 3.4: Number of secondary neutrons,  $c$ , as a function of angular segmentation,  $\mu_1$ , for various values of  $1/v_0$  for isotropic scattering ( $f_1 = 0$ ) using the  $2P_0$  approximation.

$2P_0$  approximation gives the characteristic values of  $1/\nu_0$  less than unity. This ensures the separability of the asymptotic partial-range solution from the transient solution. Moreover, from the figure one can also conclude that the traditional double- $P_0$  approximation ( $\mu_1 = 0$ ) gives, for isotropic scattering,  $1/\nu_0$  less than unity for the range of  $c$  from 0.75 to 1.0. In this sense this comparison shows that the  $2P_0$  approximation of the new formalism of partial-range spherical harmonics doubles the range of  $c$  which gives results as accurate as the double- $P_0$  approximations. For values of  $c$  less than 0.5 we have to use higher order approximations such as  $3P_0$  or  $2P_1$  approximations.

In Fig. 3.5 the same set of curves are shown but for forward scattering ( $f_1 = +0.3$ ), while Fig. 3.6 gives the case of backward scattering ( $f_1 = -0.3$ ). Both sets of curves show the same features similar to the isotropic case of scattering.

### 3.8 $NP_1$ Approximation

In this section we consider the higher order approximation of  $L = 1$  while assuming a source free medium with linear anisotropic scattering,  $L_f = 1$ . For this approximation the running variable  $j$  of Eq. (3.29) can have the values of 0 and 1, respectively. For  $j = 0$ , Eq. (3.29) yields,

$$\begin{aligned}
 & (\nu_n - \nu_{n-1}) \frac{d\phi_{n,1}(x)}{dx} + (\nu_n + \nu_{n-1}) \frac{d\phi_{n,0}(x)}{dx} + 2\phi_{n,0}(x) \\
 & = c(\nu_n - \nu_{n-1}) \sum_{n'=1}^N \left\{ \left[ 1 + \frac{3f_1}{4} (\nu_n + \nu_{n-1})(\nu_{n'} + \nu_{n'-1}) \right] \phi_{n',0}(x) \right. \\
 & \left. + \frac{3f_1}{4} (\nu_n + \nu_{n-1})(\nu_{n'} - \nu_{n'-1}) \phi_{n',1}(x) \right\} , \quad (3.44)
 \end{aligned}$$

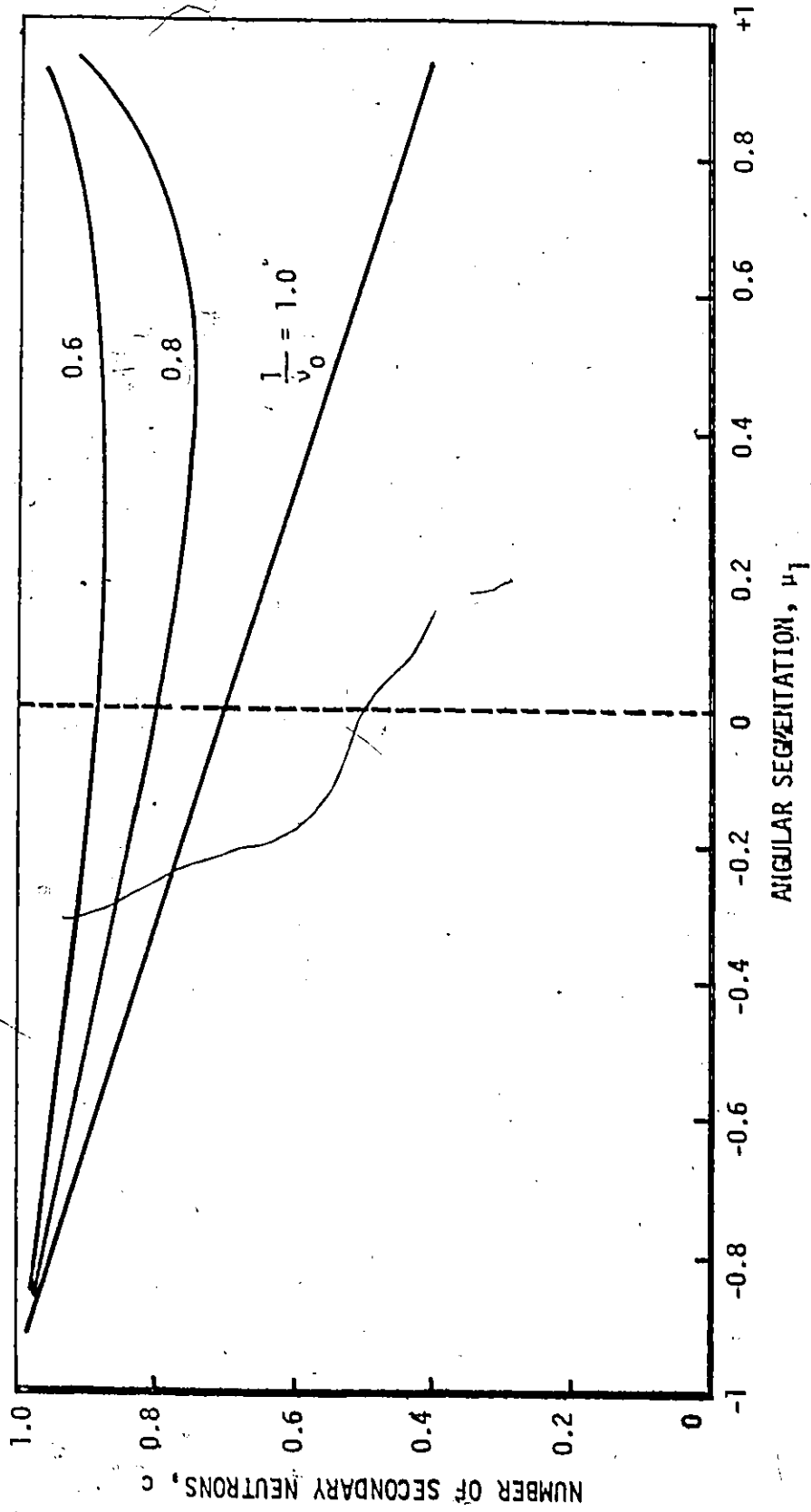


Fig. 3.5: Number of secondary neutrons,  $c$ , as a function of angular segmentation,  $\mu_1$ , for various values of  $1/v_0$  for forward scattering ( $f_1 = 0.3$ ) using the  $2P_0$  approximation.



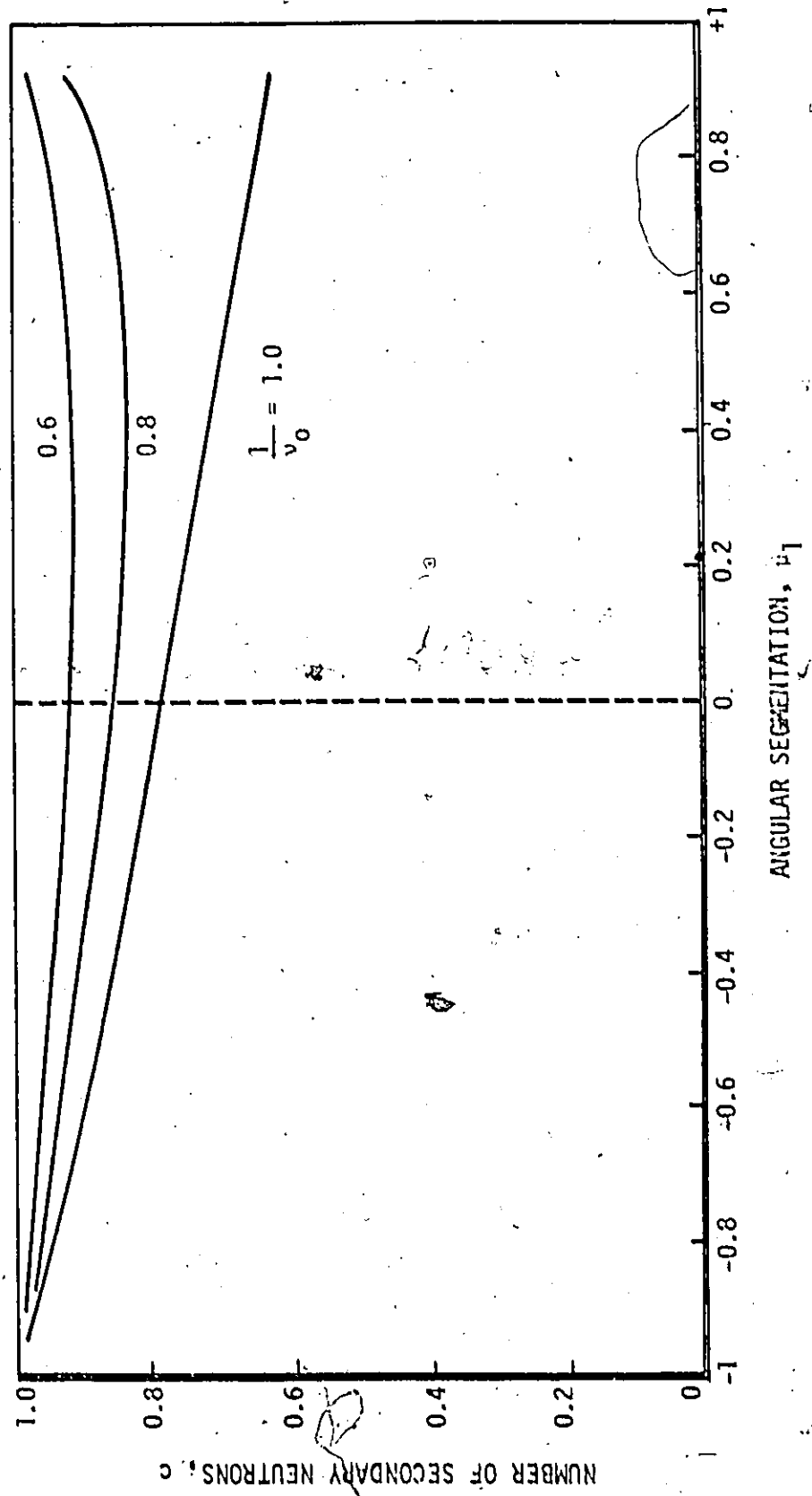


Fig. 3.6: Number of secondary neutrons, c, as a function of angular segmentation,  $\mu_1$ , for various values of  $1/v_0$  for backward scattering ( $f_1 = -0.3$ ) using the  $2P_0$  approximation.

and for  $j = 1$ , it yields

$$\begin{aligned} & \frac{1}{3} (\mu_n - \mu_{n-1}) \frac{d\phi_{n,0}(x)}{dx} + (\mu_n + \mu_{n-1}) \frac{d\phi_{n,1}(x)}{dx} + 2\phi_{n,1}(x) \\ & = \frac{cf_1}{4} (\mu_n - \mu_{n-1})^2 \sum_{n'=1}^N [(\mu_{n'} + \mu_{n'-1})\phi_{n',0}(x) \\ & + (\mu_{n'} - \mu_{n'-1})\phi_{n',1}(x)] ; \end{aligned} \quad (3.45)$$

with  $n = 1, 2, \dots, N$ . Here, we have used the expressions of the integrals  $a_{n,\lambda,\lambda}$  discussed in Section 2.4. Equations (3.44) and (3.45) represent a system of  $2N$  first order coupled differential equations. We seek solutions for this system of equations that have the exponential space dependent form

$$\phi_{n,\lambda}(x) = A_{n,\lambda} e^{-x/v} \quad (3.46)$$

where  $\lambda = 0, 1$  and  $n = 1, 2, \dots, N$ . Here  $A_{n,\lambda}$  are functions of the eigenvalue  $1/v$  as well as the boundary conditions of the problem under consideration. By substituting this ansatz, Eq. (3.46), into Eqs. (3.44) and (3.45) we obtain an eigenvalue problem in the eigenvalue  $1/v$  and the eigenvector  $[A_{n,\lambda}]$ . This eigenvalue problem can be represented in matrix notation by

$$\underline{D}A = 0 \quad (3.47)$$

where,

$$\underline{A} = \begin{bmatrix} A_{1,0} \\ A_{1,1} \\ A_{2,0} \\ A_{2,1} \\ \vdots \\ A_{N,0} \\ A_{N,1} \end{bmatrix} \quad (3.48)$$

and  $\underline{D}$  is a square matrix of size  $2N \times 2N$  with elements containing  $c$ , the angular partitions  $\mu_n$ , the coefficient of anisotropy  $f_1$  and the eigenvalue  $1/\nu$ . As an illustration, consider the two simple cases of  $N = 1$  and  $N = 2$ , respectively. First, for  $N = 1$  with  $\mu_0 = -1$  and  $\mu_2 = 1$ , we obtain the  $TP_1$  approximation which is the formal diffusion approximation. For this approximation the  $\underline{D}$ -matrix is given by

$$\underline{D} = \begin{bmatrix} \frac{1}{3\nu} & 1 - cf_1 \\ (1 - c) & -\frac{1}{\nu} \end{bmatrix} \quad (3.49)$$

The determinant of this matrix must be equal to zero to have non-trivial solution yielding the following eigenvalues

$$\left(\frac{1}{\nu}\right)^{\pm} = \pm \sqrt{3(1 - c)(1 - cf_1)} \quad (3.50)$$

This result agrees with that of the diffusion approximation<sup>(2)</sup>.

Secondly, consider the approximation of  $N = 2$ . Here, the angular partitions are given by  $\mu_0$ ,  $\mu_1$  and  $\mu_2$ . For this approximation, the  $\underline{D}$ -matrix of Eq. (3.47) possesses elements as given in Table 3.2.

$\frac{\mu_1 + \mu_0}{\nu} - 2 + c(\mu_1 - \mu_0)$	$\frac{\mu_1 + \mu_0}{\nu}$ $+ \frac{3cf_1}{4} (\mu_1 - \mu_0)^2 (\mu_1 + \mu_0)$	$c(\mu_1 - \mu_0)$ $+ \frac{3cf_1}{4} (\mu_1 - \mu_0)^2 (\mu_2 + \mu_1)$	$\frac{3cf_1}{4} (\mu_1 - \mu_0)^2 (\mu_2 - \mu_1)$
$\frac{\mu_1 + \mu_0}{3\nu}$ $+ \frac{cf_1}{4} (\mu_1 - \mu_0)^2 (\mu_1 + \mu_0)$	$\frac{\mu_1 + \mu_0}{\nu} - 2$ $+ \frac{cf_1}{4} (\mu_1 - \mu_0)^3$	$\frac{cf_1}{4} (\mu_1 - \mu_0)^2 (\mu_2 + \mu_1)$	$\frac{cf_1}{4} (\mu_1 - \mu_0)^2 (\mu_2 - \mu_1)$
$c(\mu_2 - \mu_1)$ $+ \frac{3cf_1}{4} (\mu_2 - \mu_1)^2 (\mu_1 + \mu_0)$	$\frac{3cf_1}{4} (\mu_2 - \mu_1)^2 (\mu_1 - \mu_0)$	$\frac{\mu_2 + \mu_1}{\nu} - 2 + c(\mu_2 - \mu_1)$ $+ \frac{3cf_1}{4} (\mu_2 - \mu_1) (\mu_2 + \mu_1)^2$	$\frac{\mu_2 - \mu_1}{\nu}$ $+ \frac{3cf_1}{4} (\mu_2 - \mu_1)^2 (\mu_2 + \mu_1)$
$\frac{cf_1}{4} (\mu_2 - \mu_1)^2 (\mu_1 + \mu_0)$	$\frac{cf_1}{4} (\mu_2 - \mu_1)^2 (\mu_1 - \mu_0)$	$\frac{\mu_2 + \mu_1}{3\nu}$ $+ \frac{cf_1}{4} (\mu_2 - \mu_1)^2 (\mu_2 + \mu_1)$	$\frac{\mu_2 + \mu_1}{\nu} - 2$ $+ \frac{cf_1}{4} (\mu_2 - \mu_1)^3$

$\underline{D} =$

Table 3.2: The  $\underline{D}$ -matrix of Eq. (3.47) for the  $2P_1$  approximation with a linear full-range scattering function.

We note that, there are 4 eigenvalues. It is evident that this number is associated with the order of angular segmentation  $N = 2$  and the order of polynomial approximation over each interval  $L = 1$ . The magnitude of the eigenvalue, however is specifically associated with  $c$ , the angular partitions and the degree of anisotropy  $f_1$ . In this approximation the angular partitions  $\mu_0$ ,  $\mu_1$  and  $\mu_2$  are variables subjected only to the condition that  $-1 \leq \mu_0 < \mu_1 < \mu_2 \leq +1$ . For a full-range description it is necessary to specify  $\mu_0 = -1$  and  $\mu_2 = +1$ . Then the 4 eigenvalues are therefore functions of the variable  $\mu_1$ , where  $\mu_1 \in (-1, 1)$ ,  $c$  and  $f_1$ .

A significant characteristic of the matrix of Table 3.2 is that the eigenvalue,  $1/\nu$ , is not restricted to the main diagonal but also appears in ~~the~~ nondiagonal elements. Indeed, this occurs with any higher-order approximation of  $N$ . This unusual form of the eigenvalue problem makes the numerical solution of it rather difficult. In addition, no zero terms appear in the nondiagonal elements. This means that there is a coupling between all the partial-range spatial moments  $\phi_{n,\ell}(x)$ . This is not the case with the traditional spherical harmonics approximation in which there is only coupling between any three successive moments.

Of some interest is the special case of isotropic scattering,  $f_1 = 0$ . Specifying  $f_1 = 0$  in Table 3.2 we get a  $D$ -matrix in agreement with that given in previous work for this special case<sup>(53)</sup>. The only difference is the additional normalization factor  $1/(\mu_n - \mu_{n-1})$  in the expansion of the angular flux, Eq. (3.2).

It is of interest now to write this problem in the usual form of the eigenvalue problem with the eigenvalue appears only in the diagonal elements. This can be done by the following transformation. Multiplying Eq. (3.44) by  $(\mu_n + \mu_{n-1})$  and Eq. (3.45) by  $(\mu_n - \mu_{n-1})$  and then subtracting, subsequently multiplying Eq. (3.44) by  $1/3(\mu_n - \mu_{n-1})$  and Eq. (3.45) by  $(\mu_n + \mu_{n-1})$  and again subtracting. Finally substituting the ansatz of Eq. (3.46) into the resultant equations, the new system can be written in a matrix form given by Eq. (3.47). Herein, the eigenvector,  $\underline{A}$ , is still given by Eq. (3.48) but the  $\underline{D}$  has the following form

$$\underline{D} = \begin{bmatrix} y(1,1) - \frac{1}{v} & y(1,2) & g(1,3) & \dots & g(1,2N) \\ y(2,1) & y(2,2) - \frac{1}{v} & g(2,3) & \dots & g(2,2N) \\ g(3,1) & g(3,2) & y(3,3) - \frac{1}{v} & \dots & g(3,2N) \\ g(4,1) & g(4,2) & y(4,3) & \dots & g(4,2N) \\ \vdots & & & & \vdots \\ g(2N-1,1) & \dots & \dots & \dots & y(2N-1,2N) \\ g(2N,1) & \dots & \dots & \dots & y(2N,2N) - \frac{1}{v} \end{bmatrix}, \quad (3.51)$$

where the elements are given by

$$y(2n-1,2n-1) = \frac{1}{F} (2(\mu_n + \mu_{n-1}) - c(\mu_n^2 - \mu_{n-1}^2)) \\ \times \left[ 1 + \frac{3f_1}{4} (\mu_n + \mu_{n-1})^2 - \frac{f_1}{4} (\mu_n - \mu_{n-1})^2 \right], \quad (3.52)$$

$$y(2n-1, 2n) = -\frac{1}{F} (2(\mu_n - \mu_{n-1}) - \frac{cf_1}{4} [3(\mu_n^2 - \mu_{n-1}^2)^2 - (\mu_n - \mu_{n-1})^4]) \quad (3.53)$$

$$y(2n, 2n-1) = -\frac{1}{3F} (\mu_n - \mu_{n-1}) [2 - c(\mu_n - \mu_{n-1})] \quad (3.54)$$

$$y(2n, 2n) = \frac{2(\mu_n + \mu_{n-1})}{F} \quad (3.55)$$

$$g(2n-1, 2m-1) = \frac{c}{F} ((\mu_n^2 - \mu_{n-1}^2) [1 + \frac{3f_1}{4} (\mu_n + \mu_{n-1})(\mu_m - \mu_{m-1})] - \frac{f_1}{4} (\mu_n - \mu_{n-1})^3 (\mu_m + \mu_{m-1})) \quad (3.56)$$

$$g(2n-1, 2m) = \frac{f_1}{4F} (\mu_m - \mu_{m-1}) [3(\mu_n^2 - \mu_{n-1}^2)(\mu_n + \mu_{n-1}) - (\mu_n - \mu_{n-1})^3] \quad (3.57)$$

$$g(2n, 2m-1) = \frac{c}{3F} \quad (3.58)$$

$$g(2n, 2m) = 0 \quad (3.59)$$

and

$$F = (\mu_n + \mu_{n-1})^2 - \frac{1}{3} (\mu_n - \mu_{n-1})^2 \quad (3.60)$$

for  $n = 1, 2, \dots, N$  and  $m = 1, 2, \dots, N$  with  $n \neq m$ .

The matrix of Eq. (3.51) shows that this problem has been formulated in the form of the traditional eigenvalue problem with the

eigenvalue  $1/v$  appears only in the diagonal. Also, some of the non-diagonal elements have zero values;  $g(2n,2m)$  as given by Eq. (3.59). As a special case, we consider the diffusion approximation again.

The  $\underline{D}$ -matrix of Eq. (3.51) reduces to

$$\underline{D} = \begin{bmatrix} -\frac{1}{v} & 3(1 - cf_1) \\ 1 - c & -\frac{1}{v} \end{bmatrix} \quad (3.61)$$

which is different from that of Eq. (3.49) but gives the same eigenvalues as Eq. (3.50).

Formally, we can take  $N$  as large as we please and obtain an eigenvalue problem of size  $2N \times 2N$ . However, as a calculational test we will consider the case of  $N = 3$ . In this case of approximation, there are three angular partitions ( $\mu_n$ ,  $n = 0,1,2,3$ ). For full range description of the angular flux, we specify  $\mu_0 = -1$  and  $\mu_3 = +1$ . This leaves  $\mu_1$  and  $\mu_2$  as the only variables in specifying the angular intervals; both of these variables will be incorporated into a specified angular segmentation by defining a free angular variable  $\mu_f$  using the following

$$\mu_f = \mu_1 \in (-1,0), \quad \text{for } \mu_2 = 0 \quad (3.62)$$

and

$$\mu_f = \mu_2 \in (0,1), \quad \text{for } \mu_1 = 0 \quad (3.63)$$

We have used this definition for the angular variables and have calculated the corresponding asymptotic relaxation constant. The



results are shown in Fig. 3.7 for  $c = 0.5$  and three cases of anisotropy corresponding to  $f_1 = -0.3, 0$  and  $0.3$ , respectively. The exact results of the eigenvalues are shown in the same figure. These results indicate that it is possible, in this low-order approximation to approach the exact value for the backward scattering and very close to the forward scattering. Again, these results show the superiority of the partial-range formalism for backward scattering.

### 3.9 The Angular Flux and the Milne Problem

In this section the angular flux will be discussed for the Milne problem. The  $HP_1$  approximation discussed so far gives  $2N$  eigenvalues and  $2N$  eigenvectors. Let us denote these  $2N$  eigenvalues by

$$\frac{1}{v_k} \quad ; \quad k = 1, 2, \dots, 2N \quad , \quad (3.64)$$

and the  $2N$  eigenvectors by

$$A_{n,\ell}(v_k) \quad ; \quad n = 1, 2, \dots, N \quad ; \quad \ell = 1, 2 \quad . \quad (3.65)$$

The eigenvectors  $A_{n,\ell}(v_k)$  are only functions of the eigenvalues. In terms of these eigenvectors and eigenvalues the partial-range moments  $\phi_{n,\ell}(x)$  can be written as

$$\phi_{n,\ell}(x) = \sum_{k=1}^{2N} B_k A_{n,\ell}(v_k) e^{-x/v_k} \quad . \quad (3.66)$$

Here,  $B_k$  are constants to be determined from the boundary condition of the problem under consideration. Substituting Eq. (3.66) into the expansion of the angular flux, Eq. (3.25) with  $L = 1$ , yields

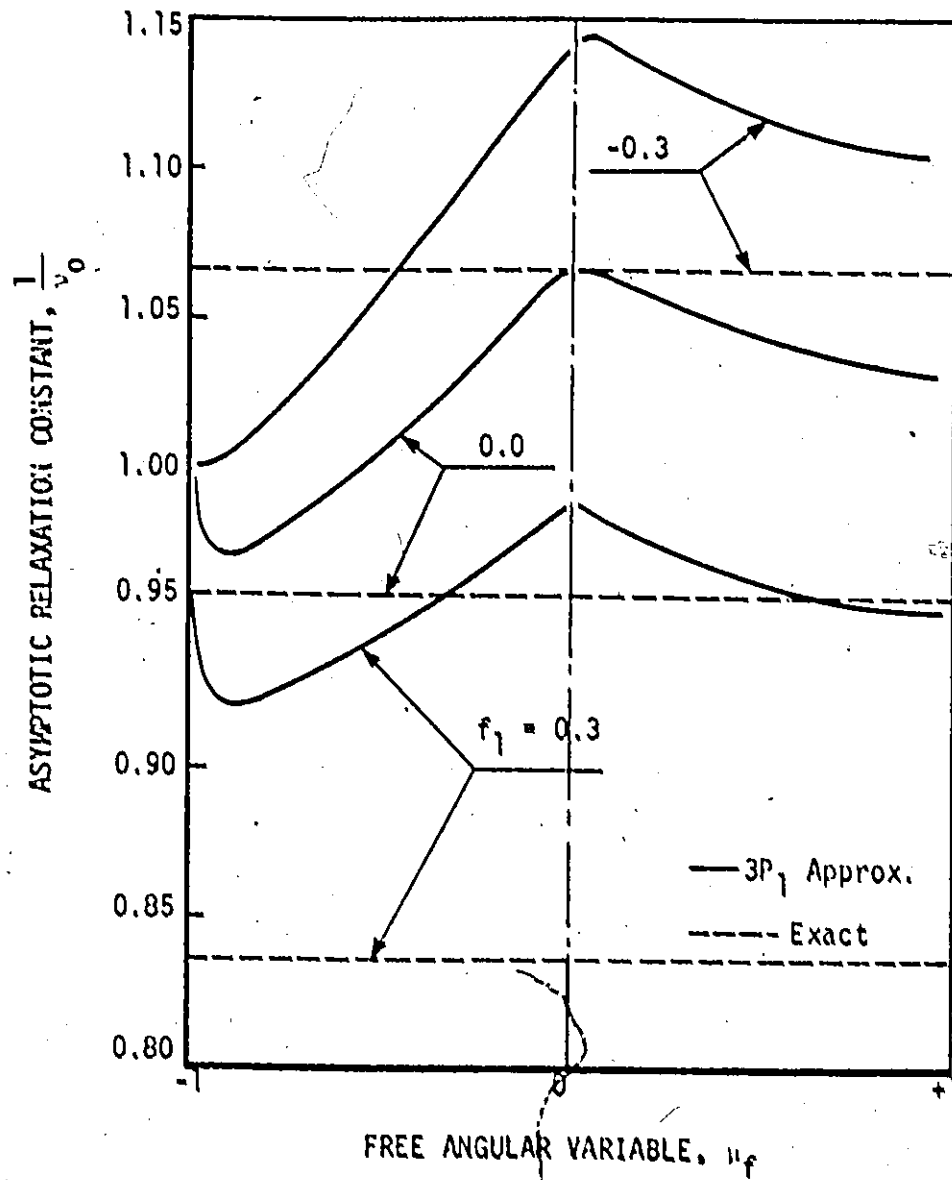


Fig. 3.7: Asymptotic relaxation constant as a function of the free angular variable for various values of anisotropy and  $c = 0.5$ .

$$\psi(x, \mu) = \sum_{n=1}^N \sum_{\ell=0}^1 \frac{2\ell + 1}{\mu_n - \mu_{n-1}} P_{n,\ell}(\mu) \sum_{k=1}^{2N} B_k A_{n,\ell}(v_k) e^{-x/v_k} \quad (3.67)$$

The eigenvalues  $1/v_k$  and the eigenvectors  $A_{n,\ell}(v_k)$  can be determined from Eqs. (3.51) and (3.47), while the constants  $B_k$  are determined from the boundary conditions. As an illustrative example we will consider the Milne problem.

The Milne problem involves the determination of the neutron flux distribution in an infinite source-free half space medium with zero incident flux. Presumably there is a source of neutrons at infinity which provides the neutrons. Far away from this source, but still far away from the boundary at  $x = 0$ , we expect the neutrons to follow the asymptotic flux distribution obtained from plane sources in an infinite medium. This means that the solution rises exponentially with the asymptotic relaxation length  $v_0$  towards the source. Hence, the boundary conditions associated with the Milne problem are

$$1) \quad \lim_{x \rightarrow \infty} \psi(x, \mu) \rightarrow \psi_{0-}(x, \mu) ,$$

$$2) \quad \psi(0, \mu) = 0 \quad ; \quad \mu > 0 .$$

Herein,  $\psi_{0-}(x, \mu)$  is the asymptotic flux distribution.

For the further development of this section, we order the subscript notation of the  $2N$  eigenvalues to yield an ordered sequence defined by

$$\frac{1}{v_1} < \frac{1}{v_2} < \dots < \frac{1}{v_{2N-1}} < \frac{1}{v_{2N}} \quad (3.68)$$

Let us assume that of the  $2N$  eigenvalues there are  $Q$  negative eigenvalues and  $(2N-Q)$  positive eigenvalues. The sequence of the eigenvalues, Eq. (3.68), will be rewritten, for convenience in the following manner

$$\frac{1}{v_1} < \dots < \frac{1}{v_Q} < 0 < \frac{1}{v_{Q+1}} < \dots < \frac{1}{v_{2N}}. \quad (3.69)$$

In the above sequence, Eq. (3.69), the asymptotic eigenvalues are given by

$$\left(\frac{1}{v_0}\right)^- = \frac{1}{v_Q} \quad (3.70)$$

and

$$\left(\frac{1}{v_0}\right)^+ = \frac{1}{v_{Q+1}} \quad (3.71)$$

The first boundary condition of the problem requires that

$$B_k = 0 \quad ; \quad k = Q+2, Q+3, \dots, 2N. \quad (3.72)$$

Note that  $B_{Q+1}$  corresponds to the asymptotic eigenvalue. Equation (3.67) can now be written as

$$\begin{aligned} \psi(x, \mu) = & \sum_{n=1}^N \sum_{\ell=0}^1 \frac{2\ell + 1}{\mu_n - \mu_{n-1}} P_{n,\ell}(\mu) [B_{Q+1} A_{n,\ell}(v_{Q+1}) e^{-x/v_{Q+1}} \\ & + \sum_{k=1}^Q B_k A_{n,\ell}(v_k) e^{-x/v_k}] \quad (3.73) \end{aligned}$$

Moreover, applying the second boundary condition to Eq. (3.73) yields

$$B_{Q+1} A_{n,\ell}(v_{Q+1}) + \sum_{k=1}^Q B_k A_{n,\ell}(v_k) = 0 \quad ; \quad \mu > 0 \quad (3.74)$$

with  $n = 1, 2, \dots, N$ , and  $\epsilon = 0, 1$ .

To ensure that this condition, Eq. (3.74), is satisfied exactly it is necessary to specify one of the  $(N-1)$  angular segmentations  $(\mu_1, \mu_2, \dots, \mu_{N-1})$  equal to zero. We specify  $\mu_i = 0$ , where  $i$  can take any value between 1 and  $(N-1)$ . The angular segmentations, therefore, are

$$-1 < \mu_1 < \dots < \mu_i = 0 < \dots < \mu_{N-1} < 1. \quad (3.75)$$

This partition gives a full-range description for the angular flux. With this specification Eq. (3.74) must be satisfied for the angular intervals number  $(i+1), (i+2), \dots$ , and  $N$ , respectively. In other words, Eq. (3.74) can be written as

$$B_{Q+1} A_{n,\epsilon}(v_{Q+1}) + \sum_{k=1}^Q B_k A_{n,\epsilon}(v_k) = 0, \quad (3.76)$$

for  $n = i+1, i+2, \dots, N$ , and  $\epsilon = 0, 1$ . We further introduce the following normalization

$$B_{Q+1} = 1. \quad (3.77)$$

Then, Eq. (3.76) can be written as

$$\sum_{k=1}^Q B_k A_{n,\epsilon}(v_k) = -A_{n,\epsilon}(v_{Q+1}), \quad (3.78)$$

with  $n = i+1, i+2, \dots, N$ , and  $\epsilon = 0, 1$ . This equation can be written in a matrix form as

$$\begin{bmatrix}
 A_{1+1,0}(v_1) & \dots & A_{1+1,0}(v_Q) \\
 A_{1+1,1}(v_1) & \dots & A_{1+1,1}(v_Q) \\
 A_{1+2,0}(v_1) & \dots & A_{1+2,0}(v_Q) \\
 \vdots & & \vdots \\
 A_{N,0}(v_1) & & A_{N,0}(v_Q) \\
 A_{N,1}(v_1) & & A_{N,1}(v_Q)
 \end{bmatrix}
 \begin{bmatrix}
 B_1 \\
 B_2 \\
 B_3 \\
 \vdots \\
 B_{Q-1} \\
 B_Q
 \end{bmatrix}
 =
 \begin{bmatrix}
 A_{1+1,0}(v_{Q+1}) \\
 A_{1+1,1}(v_{Q+1}) \\
 A_{1+2,0}(v_{Q+1}) \\
 \vdots \\
 A_{N,0}(v_{Q+1}) \\
 A_{N,1}(v_{Q+1})
 \end{bmatrix}
 \quad (3.79)$$

which represents a set of  $Q$  inhomogeneous linear equations and can be solved for the unknowns  $B_1, B_2, \dots$ , and  $B_Q$ .

From the mathematical point of view, the set of Eq. (3.79) must give exactly a number of equations equal to the number of unknowns; otherwise it is not solvable. Hence, the following condition must hold

$$Q = 2(N - 1) \quad (3.80)$$

This means that the number of negative eigenvalues is twice the number of segmentations in the positive part of  $\mu$ , i.e.  $\mu \in (0, 1)$ , providing that there is one of the segmentation at  $\mu = 0$ . Clearly, for the general cases of the  $NP_L$  approximation, the number of negative eigenvalues is equal to  $(L+1)$  times the number of the segmentation in  $\mu \in (0, 1)$ . It is important to note here that all the numerical cases which have been tested satisfy this condition.

The total scalar flux  $\psi(x)$  is given by the integration of Eq. (3.73) over the angular variable,  $\mu$ , from  $\mu = -1$  to  $\mu = +1$ . Performing this integration and using the full-range integration of the partial-range Legendre polynomials, Eqs. (2.24) and (2.26), and

the normalization condition of Eq. (3.77) yields

$$\psi(x) = \sum_{n=1}^N [A_{n,0}(v_{Q+1})_0^{-x/v_{Q+1}} + \sum_{k=1}^Q B_k A_{n,0}(v_k)_0^{-x/v_k}], \quad (3.81)$$

which agrees with the previous results<sup>(32)</sup>, viz

$$\psi(x) = \sum_{n=1}^N \phi_{n,0}(x) \quad (3.82)$$

Equation (3.81) represents the total scalar flux as a function of the distance  $x$  from the boundary at  $x = 0$ . The asymptotic flux, which is the dominant part of the above equation far away from the surface, is obtained by retaining the two dominant terms in the above equation. Therefore, the asymptotic flux,  $\psi_{asy}(x)$ , is given by

$$\psi_{asy}(x) = \sum_{n=1}^N [A_{n,0}(v_{Q+1})_0^{-x/v_{Q+1}} + B_Q A_{n,0}(v_Q)_0^{-x/v_Q}]. \quad (3.83)$$

From Eqs. (3.81) and (3.83), we can determine some transport parameters and compare them with the exact values as a test for the method. Some of the parameters which are associated with the vacuum-medium interface at  $x = 0$  are defined as follows<sup>(1-3)</sup>:

- 1) Extrapolated end point  $Z_0$ :

$$\psi_{asy}(Z_0) = 0 \quad (3.84)$$

- 2) Linear extrapolation length  $\lambda$ :

$$\lambda = \frac{\psi_{asy}(0)}{\left. \frac{d\psi_{asy}(x)}{dx} \right|_{x=0}} \quad (3.85)$$

3) Ratio of the asymptotic flux to the total flux at  $x = 0$ ;

$$R = \frac{\psi_{asy}(0)}{\psi(0)} \quad (3.86)$$

These transport parameters have been calculated by the  $3P_1$  approximation with a free angular parameter  $\mu_f$ , given by Eqs. (3.62) and (3.63), for  $c = 0.5$  and three cases of anisotropy;  $f_1 = -0.3, 0$  and  $0.3$ , respectively. The results are given in Figs. 3.8, 3.9 and 3.10, respectively. From these results it is possible to specify an angular segmentation that leads to exact or very accurate results. These angular segmentations vary with the degree of anisotropy and differ in value for the transport parameters under consideration.



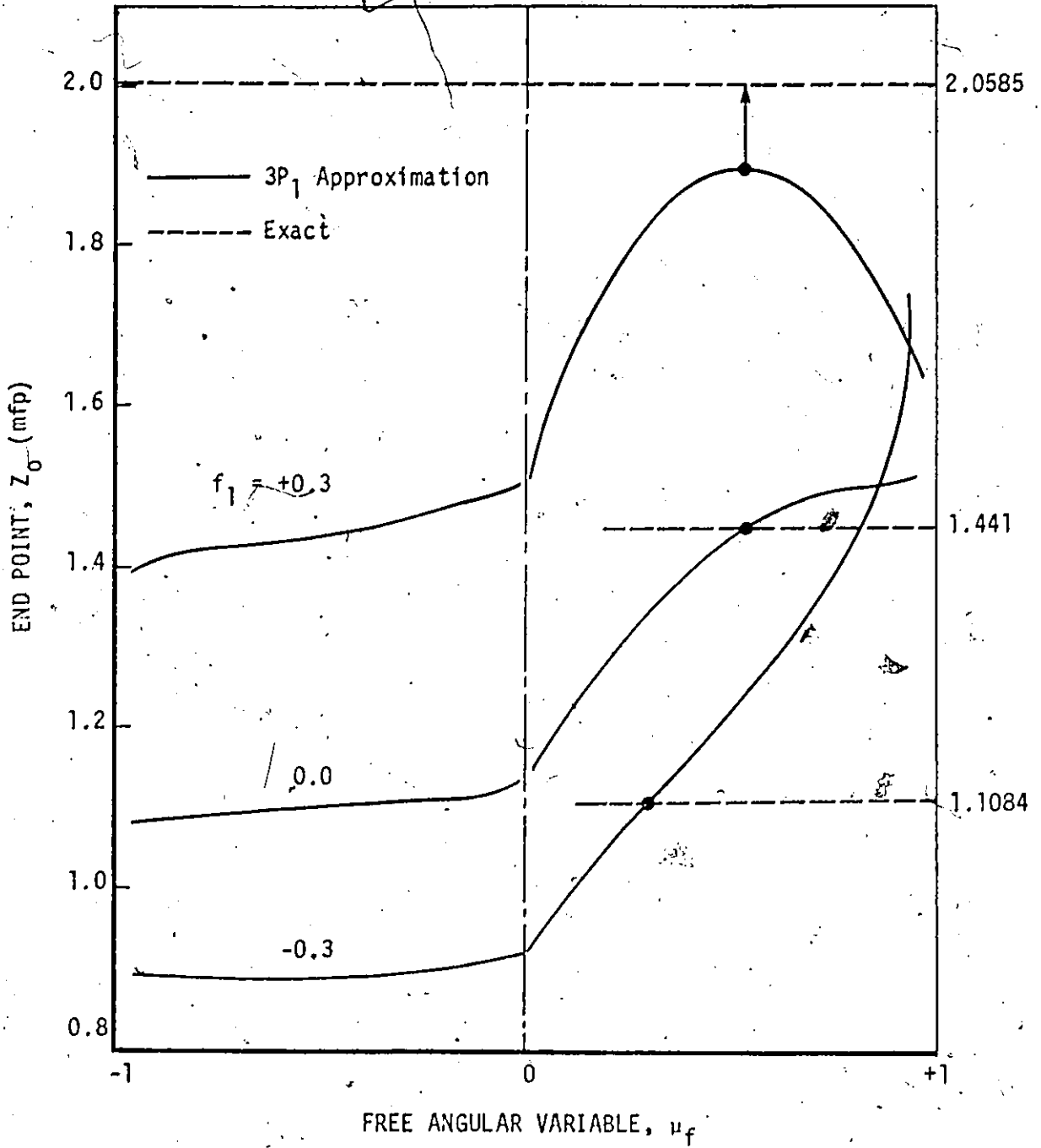


Fig. 3.8: End point of asymptotic flux as a function of the free angular variable for various values of anisotropy and  $c = 0.5$ .

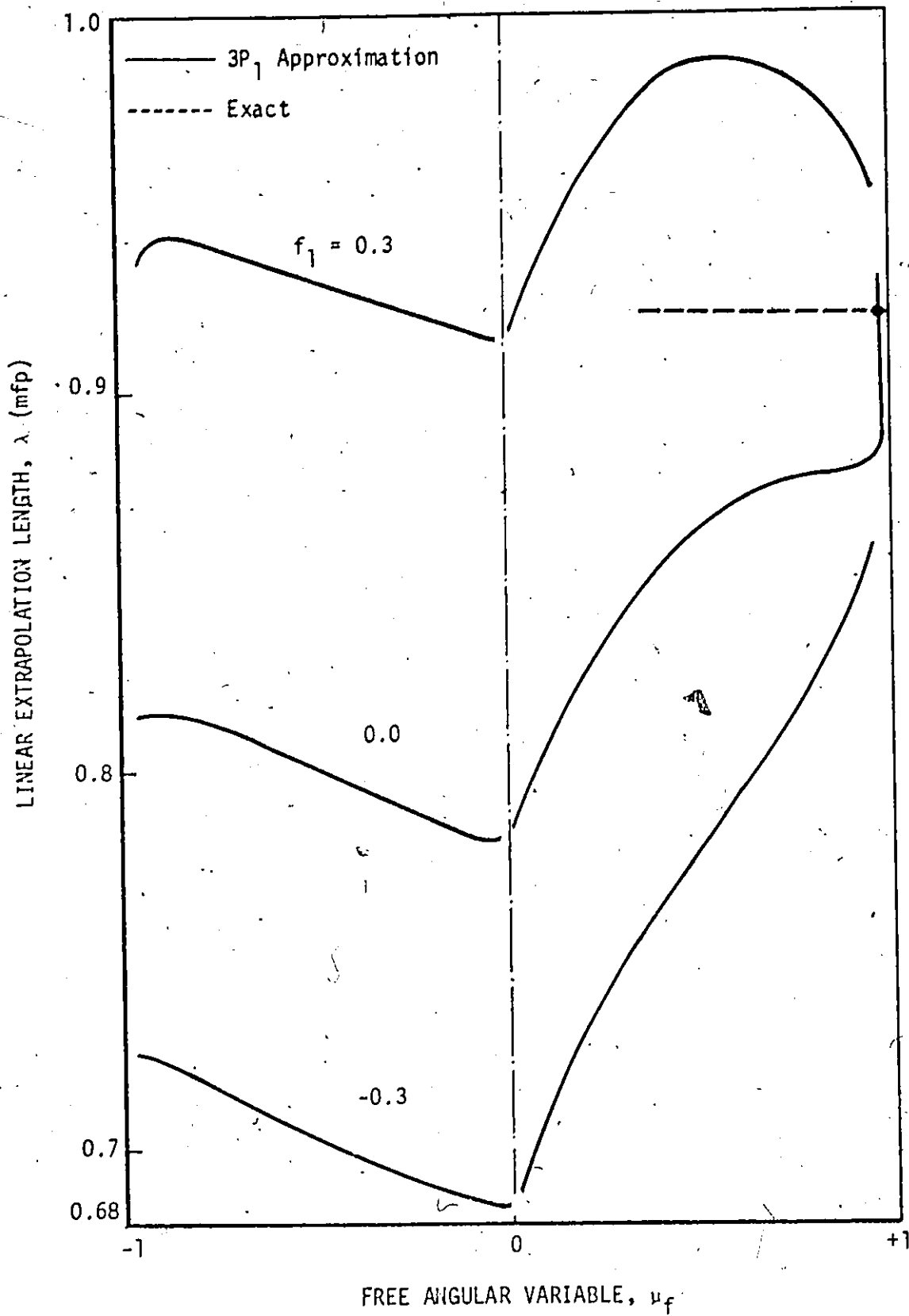


Fig. 3.9: Linear extrapolation length as a function of the free angular variable for various values of anisotropy and  $c = 0.5$ .

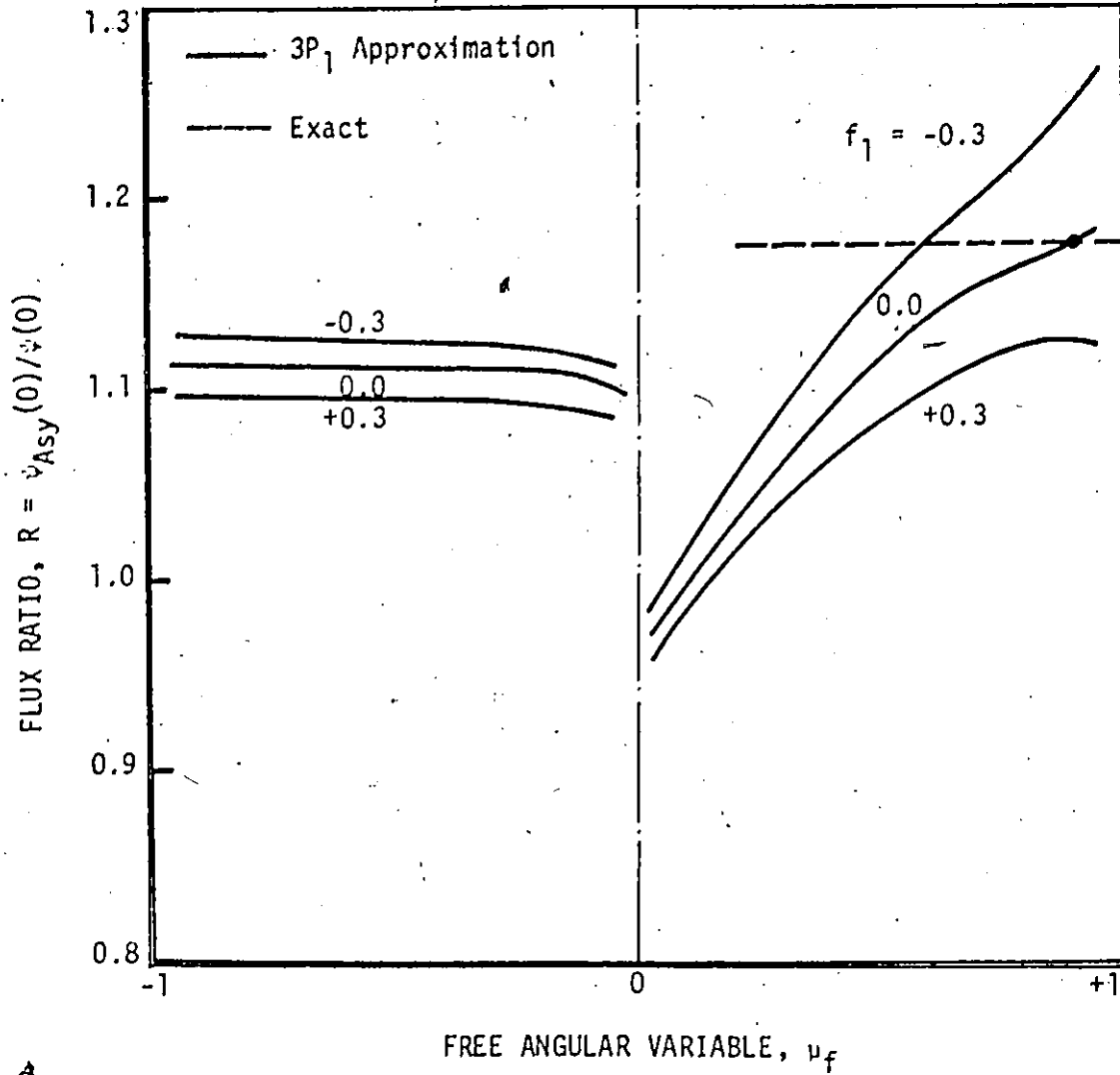


Fig. 3.10: Ratio of asymptotic flux to total flux as a function of the free angular variable for various values of anisotropy and  $c = 0.5$ .

## CHAPTER IV

### PLANE GEOMETRY: PARTIAL-RANGE SCATTERING FUNCTIONS

#### 4.1 Introduction

In this chapter the one-group neutron transport equation with anisotropic scattering for plane geometry will be solved again. However, the approach of representing the scattering function (scattering kernel) is different from the one used in Chapter III. In Chapter III the neutron angular flux  $\psi(x, \mu)$  and the external source of neutrons  $S(x, \mu)$  have been expanded in terms of partial-range Legendre polynomials while the scattering function  $f(\Omega, \Omega')$  has been expanded the usual way in terms of the full-range Legendre polynomials. We have seen in Chapter III that the expansion of neutron flux and external sources in terms of partial-range Legendre polynomials gives better results even with low-order approximations. In the analysis of this chapter, we will extend the usage of partial-range formalism and expand all the pertinent angular functions  $\psi(x, \mu)$ ,  $S(x, \mu)$  and  $f(\Omega, \Omega')$  in terms of partial-range Legendre polynomials. In that sense, this represents a complete partial-range spherical harmonics analysis for the one-group neutron transport equation with anisotropic scattering.

The detailed representation of the scattering function in terms of the partial-range Legendre polynomials as well as some test cases for this new representation will be given in Chapter VI. However, for the purpose of the present chapter it is enough to list this representation

of the scattering function and then apply it within the context of the one-group neutron transport equation for plane geometry. In other words the application of the partial-range representation of the scattering function for the plane geometry one-group neutron transport equation is the main objective of this chapter.

The chosen representation is again based on the arbitrary segmentation of the directional cosine of the scattering angle into  $M$  intervals with nodal points defined by  $\mu_{sm}$ ,  $m = 0, 1, 2, \dots, M$ . Over each interval  $(\mu_{s,m-1}, \mu_{sm})$  we expand the scattering function in terms of the complete orthogonal set of partial-range Legendre polynomials which have been discussed in Chapter II. The scattering function  $f(\underline{\Omega}, \underline{\Omega}')$  is, therefore, written as a double sum expansion

$$f(\underline{\Omega}, \underline{\Omega}') = \sum_{m=1}^M \sum_{\ell=0}^{\infty} \frac{2\ell + 1}{2\pi(\mu_{sm} - \mu_{s,m-1})} f_{m,\ell} P_{m,\ell}(\mu_s) \quad (4.1)$$

Here,  $\mu_s$  is the cosine of the scattering angle. Obviously, the partial-range coefficients  $f_{m,\ell}$  are given by

$$f_{m,\ell} = 2\pi \int_{\mu_{s,m-1}}^{\mu_{s,m}} f(\underline{\Omega}, \underline{\Omega}') P_{m,\ell}(\mu_s) d\mu_s \quad (4.2)$$

The neutron flux  $\psi(x, \mu)$  and the external source of neutrons  $S(x, \mu)$  are expanded the same way of Chapter III; their expansions are given by Eqs. (3.2) and (3.4), respectively. However, the neutron flux and the external source of neutrons have been expanded in terms of the angular variable  $\mu$ , which is the cosine of the angle between the neutron direction and the  $x$ -axis, while the scattering function is

expanded in terms of the cosine of the scattering angle  $\mu_s$ . The angular variable  $\mu$ , therefore, is divided into  $N$  intervals by the following inequalities.

$$-1 \leq \mu_0 < \mu_1 < \dots < \mu_n < \dots < \mu_{N-1} \leq +1, \quad (4.3)$$

while  $\mu_s$  is divided into  $M$  intervals by the following inequalities

$$-1 \leq \mu_{s0} < \mu_{s1} < \dots < \mu_{sm} < \dots < \mu_{sM} \leq +1. \quad (4.4)$$

Of interest here is the feature that the segmentation of the angular variables  $\mu$  and  $\mu_s$  are completely independent of each other. Also, the number of intervals  $N$  is not necessarily equal to the number  $M$ .

#### 4.2 Solution Formalism

The time independent one-group neutron transport equation for plane geometry, Eq. (1.2), is again rewritten here for convenience.

$$\mu \frac{\partial \psi(x, \mu)}{\partial x} + \psi(x, \mu) = c \int_{\underline{\Omega}'} f(\underline{\Omega}, \underline{\Omega}') \psi(x, \mu') d\underline{\Omega}' + \frac{1}{\Sigma} S(x, \mu). \quad (4.5)$$

The notation used here has been defined in Section 1.2. The basis for the formalism here is to expand the neutron flux  $\psi(x, \mu)$ , the neutron sources  $S(x, \mu)$ , and the scattering function  $f(\underline{\Omega}, \underline{\Omega}')$  in terms of orthogonal sets of partial-range Legendre polynomials. The expansions of  $\psi(x, \mu)$  and  $S(x, \mu)$  are given by Eqs. (3.2) and (3.4), respectively, while that of  $f(\underline{\Omega}, \underline{\Omega}')$  is given by Eq. (4.1)

Usually, the next step in this formalism is the substitution of these expansions, Eqs. (3.2), (3.4) and (4.1), into the neutron

transport equation, Eq. (4.5), followed by a multiplication of the partial-range Legendre polynomials over a particular range of  $\mu$  and performing the integration over this range. The most important term in this process is the integral term of the right hand side of Eq. (4.5) because the other terms have been treated in Chapter III. We will designate this integral term by the symbol  $\Gamma$ :

$$\Gamma = \int_{\underline{\Omega}'} f(\underline{\Omega}, \underline{\Omega}') \psi(x, \mu') d\underline{\Omega}' \quad (4.6)$$

Now, suppose that the neutron before the collision possessed a polar angle  $\theta'$  and an azimuthal angle  $\omega'$  and after the collision the neutron has a direction defined by  $\theta$  and  $\omega$ , Fig. 4.1. In this representation  $\theta_s$  is the scattering angle and the cosine of this angle is given by

$$\mu_s = \mu\mu' + (1 - \mu^2)^{1/2}(1 - \mu'^2)^{1/2}\cos(\omega - \omega') \quad (4.7)$$

where

$$\mu_s = \cos\theta_s \quad (4.8)$$

$$\mu = \cos\theta \quad (4.9)$$

and

$$\mu' = \cos\theta' \quad (4.10)$$

Moreover,  $d\underline{\Omega}'$  is given by

$$d\underline{\Omega}' = -d\mu'd\omega' \quad (4.11)$$

For simplicity, let  $(\omega - \omega')$  be given by  $\omega$  since this will not affect the generality of the formalism; then Eqs. (4.7) and (4.11) can be rewritten as

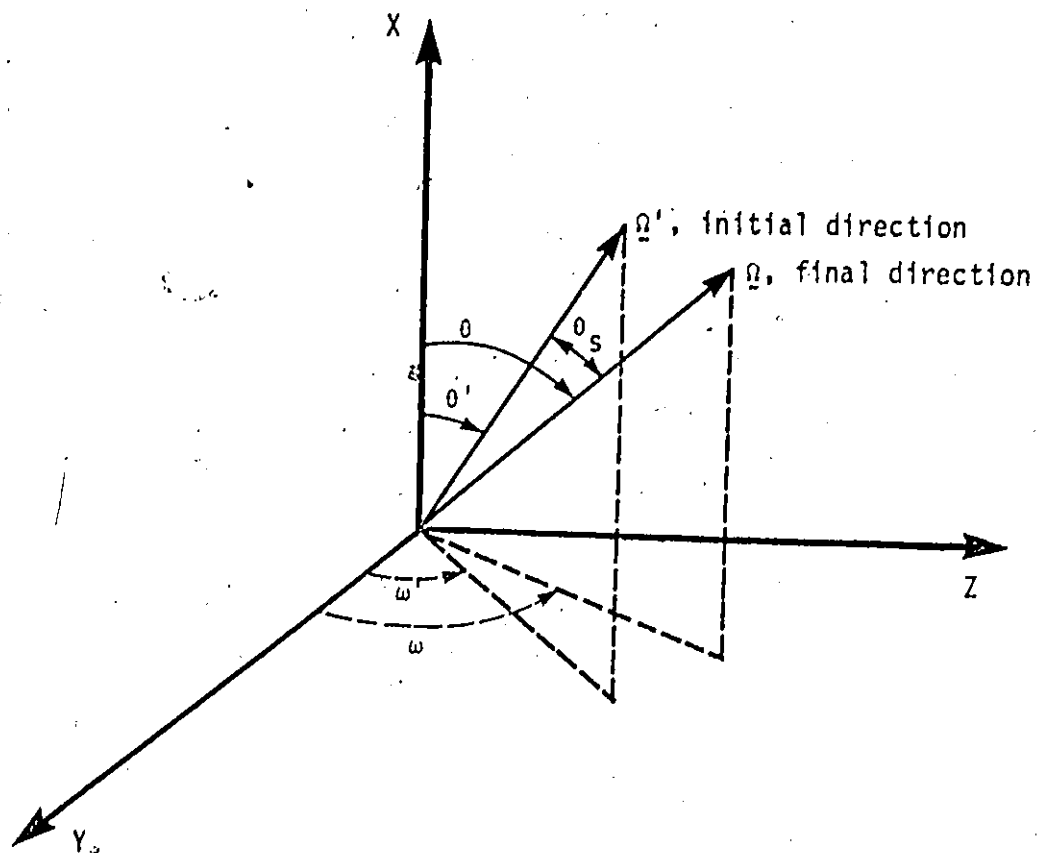


Fig. 4.1: Neutron directions before and after a collision;  $\theta_s$  is the scattering angle.



$$\mu_s = \mu\mu' + (1 - \mu^2)^{1/2}(1 - \mu'^2)^{1/2}\cos\omega, \quad (4.12)$$

and

$$d\Omega' = d\mu'd\omega. \quad (4.13)$$

Substituting Eqs. (3.2), (4.1) and (4.13) into the integral of Eq. (4.6) yields

$$r = \sum_{m=1}^M \sum_{\ell=0}^{\infty} \sum_{n=1}^N \sum_{\ell'=0}^{\infty} \frac{(2\ell+1)(2\ell'+1)}{(\mu_{sm} - \mu_{s,m-1})(\mu_n - \mu_{n-1})} f_{m,\ell} \times \phi_{n,\ell'}(\omega) B_{\ell\ell'}^{mn}(\mu), \quad (4.14)$$

where  $B_{\ell\ell'}^{mn}(\mu)$  is a function of  $\mu$  only and it is defined by

$$B_{\ell\ell'}^{mn}(\mu) = \frac{1}{2\pi} \int_{\omega} \int_{\mu'} P_{m,\ell}(\mu_s) P_{n,\ell'}(\mu') d\mu' d\omega. \quad (4.15)$$

The limits of the integration are determined so that the following conditions are satisfied

$$\mu_{s,m-1} \leq \mu_s \leq \mu_{sm}, \quad (4.16)$$

and

$$\mu_{n-1} \leq \mu' \leq \mu_n \quad (4.17)$$

Hereafter, the integrals of Eq. (4.15) combined with the conditions of Eqs. (4.16) and (4.17) will be written as

$$B_{\ell\ell'}^{mn}(\mu) = \frac{1}{2\pi} \int_{\omega} \int_{\mu'} P_{m,\ell}(\mu_s) P_{n,\ell'}(\mu') d\mu' d\omega \quad (4.18)$$

$$\mu_{s,m-1} \leq \mu_s \leq \mu_{sm}$$

$$\mu_{n-1} \leq \mu' \leq \mu_n$$

The function  $B_{\ell\ell}^{mn}(\mu)$  can have values over the entire range of  $\mu$  from  $\mu = -1$  to  $\mu = +1$  and is not restricted to the segment  $(\mu_n - \mu_{n-1})$ . Because of the expansion of the scattering function in terms of partial-range Legendre polynomials we lose some of the spherical symmetry of the scattering integrals and hence the evaluation of these integrals is much more complicated and more involved than the case of the full-range scattering function studied in Chapter III. Aside from the fact that there are many of these nonsymmetrical spherical surface integrals to be evaluated, the derivation of the complete expansions in terms of partial-range Legendre polynomials is straightforward.

To proceed further, we substitute Eqs. (3.2), (3.4) and (4.14) into the neutron transport equation, Eq. (4.5), multiply by  $P_{n',j}(\mu)$  and integrate over  $\mu$  from  $\mu = \mu_{n'-1}$  to  $\mu = \mu_{n'}$ ; rearranging yields

$$\begin{aligned} & \frac{\mu_n - \mu_{n-1}}{2j+1} \left[ j \frac{d\phi_{n,j-1}(x)}{dx} + (j+1) \frac{d\phi_{n,j+1}(x)}{dx} \right] \\ & + (\mu_n + \mu_{n-1}) \frac{d\phi_{n,j}(x)}{dx} + 2\phi_{n,j}(x) \\ & = 2c \sum_{m=1}^M \sum_{n'=1}^N \sum_{\ell=0}^{\infty} \sum_{\ell'=0}^{\infty} \frac{(2\ell+1)(2\ell'+1)}{(\mu_{sm} - \mu_{s,m-1})(\mu_{n'} - \mu_{n'-1})} \\ & \times f_{m,\ell} \phi_{n',\ell'}(x) A_{j\ell\ell'}^{nmn'} + \frac{2}{\Sigma} s_{n,j}(x); \end{aligned} \quad (4.19)$$

with  $j = 0, 1, \dots, \infty$  and  $n = 1, 2, \dots, N$ , where the constants  $A_{j\ell\ell'}^{nmn'}$  are defined by the following integral.

$$A_{j\ell\ell'}^{nmn'} = \int_{\mu_{n-1}}^{\mu_n} P_{n,j}(\mu) B_{\ell\ell'}^{mn'}(\mu) d\mu. \quad (4.20)$$

In the derivation of Eq. (4.19), excepting the scattering integral term, we have proceeded exactly the same way similar to the derivation of Section 3.2. The left hand side of Eq. (4.19) as well as the source term are exactly the same as that of Eq. (3.18). However, the coupling between the partial-range moments of the flux in the first term of the right hand side is different. This means that the partial-range representation of the scattering function has two effects. First, it reconstructs the scattering function more accurately and, second, it introduces a new way of coupling between the partial-range moments of the flux.

Here, Eq. (4.19) is the general equation which gives the conditions on the partial-range moments of the neutron flux. It is an exact equation without any functional approximations. The general expressions of the integrals  $B_{\ell\ell'}^{mn'}$ , Eq. (4.18), and  $A_{j\ell\ell'}^{nmn'}$ , Eq. (4.20), are quite difficult to obtain and each integral for a certain approximation must be considered individually. This represents the only drawback of the present formalism. Some low-order integrals will be discussed in detail in the following sections where some study cases will be given. Equation (4.19) represents the starting point for any further studies in this chapter.

### 4.3 Special Case: Full-Range Scattering Functions

As mentioned previously, the partial-range representation of the scattering function changes only the scattering term of the right hand side of Eq. (4.19). We will, therefore, consider the first term in the right hand side of Eq. (4.19) and work it out for the special case of full-range scattering function. This special case can be deduced from this general formalism by specifying  $M = 1$  with  $\mu_{s0} = -1$  and  $\mu_{s1} = +1$ . This means that we consider the entire range of the scattering cosine  $\mu_s$  as one interval. Hence the coefficient  $f_{1,\ell}$  of the scattering function is identically equal to  $f_\ell$ . For this special case the first term in the right hand side of Eq. (4.19), designated  $\Gamma$ , reduces to

$$\Gamma = c \sum_{n'=1}^N \sum_{\ell=0}^{\infty} \sum_{\ell'=0}^{\infty} \frac{(2\ell+1)(2\ell'+1)}{\mu_{n'} - \mu_{n'-1}} f_{\ell} P_{n',\ell'}(x) A_{j\ell\ell'}^{n'n'} \quad (4.21)$$

where  $A_{j\ell\ell'}^{n'n'}$ , in this case, is given by

$$A_{j\ell\ell'}^{n'n'} = \int_{\mu_{n'-1}}^{\mu_n} P_{n,j}(\mu) B_{\ell\ell'}^{n'n'}(\mu) d\mu \quad (4.22)$$

and

$$B_{\ell\ell'}^{n'n'}(\mu) = \frac{1}{2\pi} \int_0^{2\pi} \int_{\mu_{n'-1}}^{\mu_n} P_{\ell}(\mu_s) P_{n',\ell'}(\mu') d\mu' d\omega \quad (4.23)$$

From the addition theorem of the spherical harmonics we have

$$P_\ell(\mu_S) = P_\ell(\mu)P_\ell(\mu') + 2 \sum_{m=1}^{\ell} \frac{(\ell-m)!}{(\ell+m)!} P_\ell^m(\mu)P_\ell^m(\mu') \cos(m\omega), \quad (4.24)$$

where  $P_\ell^m(\mu)$  is the associate Legendre polynomial. Substituting Eq. (4.24) into Eq. (4.23) and performing the integration over the azimuthal angle  $\omega$  yields

$$B_{\ell\ell'}^{n'}(\mu) = \int_{\mu_{n'-1}}^{\mu_{n'}} P_\ell(\mu)P_\ell(\mu')P_{n',\ell'}(\mu')d\mu' \quad (4.25)$$

This equation can be written in this form

$$B_{\ell\ell'}^{n'}(\mu) = P_\ell(\mu)a_{n',\ell,\ell'} \quad (4.26)$$

where the constant  $a_{n',\ell,\ell'}$  is defined by Eq. (2.30). Substituting Eq. (4.26) into Eq. (4.22) gives the following expression for  $A_{j\ell\ell'}^{n'n'}$

$$A_{j\ell\ell'}^{n'n'} = a_{n',\ell,\ell'}a_{n,\ell,j} \quad (4.27)$$

Substituting Eq. (4.27) into Eq. (4.21) yields

$$\Gamma = c \sum_{n'=1}^N \sum_{\ell=0}^{\infty} \sum_{\ell'=0}^{\infty} \frac{(2\ell+1)(2\ell'+1)}{\mu_n - \mu_{n-1}} f_\ell \phi_{n',\ell'}(x) \times a_{n',\ell,\ell'}a_{n,\ell,j} \quad (4.28)$$

This equation agrees with the scattering term of Eq. (3.18) which has been derived for this special case from a different starting point in Section 3.2.

#### 4.4 NP<sub>L</sub>-MP<sub>K</sub> Approximation

In this approximation, the angular variable  $\mu$  is divided into  $N$  intervals and over each interval the flux as well as the external neutrons source are represented by the  $L$ 'th partial-range Legendre polynomials. The angular variable of the scattering function  $\mu_s$  is divided into  $M$  intervals and over each interval the scattering function is assumed to be adequately represented by the  $K$ 'th partial-range Legendre polynomial. This means that  $\phi_{n,\ell} = S_{n,\ell} = 0$  for  $\ell > L$  and  $f_{m,\ell} = 0$  for  $\ell > K$ . For this approximation, Eq. (4.19) can be rewritten as

$$\begin{aligned}
 & \frac{\mu_n - \mu_{n-1}}{2j+1} \left[ j \frac{d\phi_{n,j-1}(x)}{dx} + (j+1) \frac{d\phi_{n,j+1}(x)}{dx} \right] \\
 & + (\mu_n + \mu_{n-1}) \frac{d\phi_{n,j}(x)}{dx} + 2\phi_{n,j}(x) \\
 & = 2c \sum_{m=1}^M \sum_{n'=1}^N \sum_{\ell=0}^K \sum_{\ell'=0}^L \frac{(2\ell+1)(2\ell'+1)}{(\mu_{sm} - \mu_{s,m-1})(\mu_{n'} - \mu_{n'-1})} \\
 & \times f_{m,\ell} \phi_{n',\ell'}(x) A_{j\ell\ell'}^{nmn'} + \frac{2}{\Sigma} s_{n,j}(x) ; \quad (4.29)
 \end{aligned}$$

with  $j = 0, 1, \dots, L$ , and  $n = 0, 1, \dots, N$ .

This system of equations represents  $N(L+1)$  first order coupled differential equations in the  $N(L+1)$  partial-range moments of the flux  $\phi_{n,j}(x)$ ;  $j = 0, 1, \dots, L$  and  $n = 1, 2, \dots, N$ . The study of this system for some simple cases is the goal of the following sections.

#### 4.5 DP<sub>0</sub>-DP<sub>0</sub> Approximation

When two partial-range Legendre polynomial expansions are used for the two half-ranges divided by  $\mu = 0$ , the formalism in this case is known as the double- $P_L$  approximation. Moreover, when  $L = 0$  it gives the double- $P_0$  approximation. In this approximation it is possible to satisfy exactly the free-surface boundary conditions and also allow for discontinuities of the angular flux at the interface. Therefore, in the approximation considered in this section we divide both the angular variable of the flux  $\mu$  into two ranges by  $\mu = 0$  and the angular variable of the scattering angle  $\mu_s$  into two ranges by  $\mu_s = 0$ . Over each range we only consider one term of the partial-range Legendre polynomials corresponding to  $l = 0$ . This representation is shown in Fig. 4.2 for the angular flux and the scattering function.

In order to examine this approximation we will consider a source free medium. Equation (4.29) gives for  $n = 1$  and  $n = 2$ , respectively,

$$-\frac{d\phi_{1,0}(x)}{dx} + 2\phi_{1,0}(x) = \alpha_1\phi_{1,0}(x) + \beta_1\phi_{2,0}(x) \quad , \quad (4.30)$$

and

$$\frac{d\phi_{2,0}(x)}{dx} + 2\phi_{2,0}(x) = \alpha_2\phi_{1,0}(x) + \beta_2\phi_{2,0}(x) \quad , \quad (4.31)$$

where the coefficients  $\alpha_i$  and  $\beta_i$  are given by

$$\alpha_i = 2c(f_{1,0}A_{000}^{i11} + f_{2,0}A_{000}^{i21}) \quad , \quad (4.32)$$

and

$$\beta_i = 2c(f_{1,0}A_{000}^{i12} + f_{2,0}A_{000}^{i22}) \quad ; \quad (4.33)$$

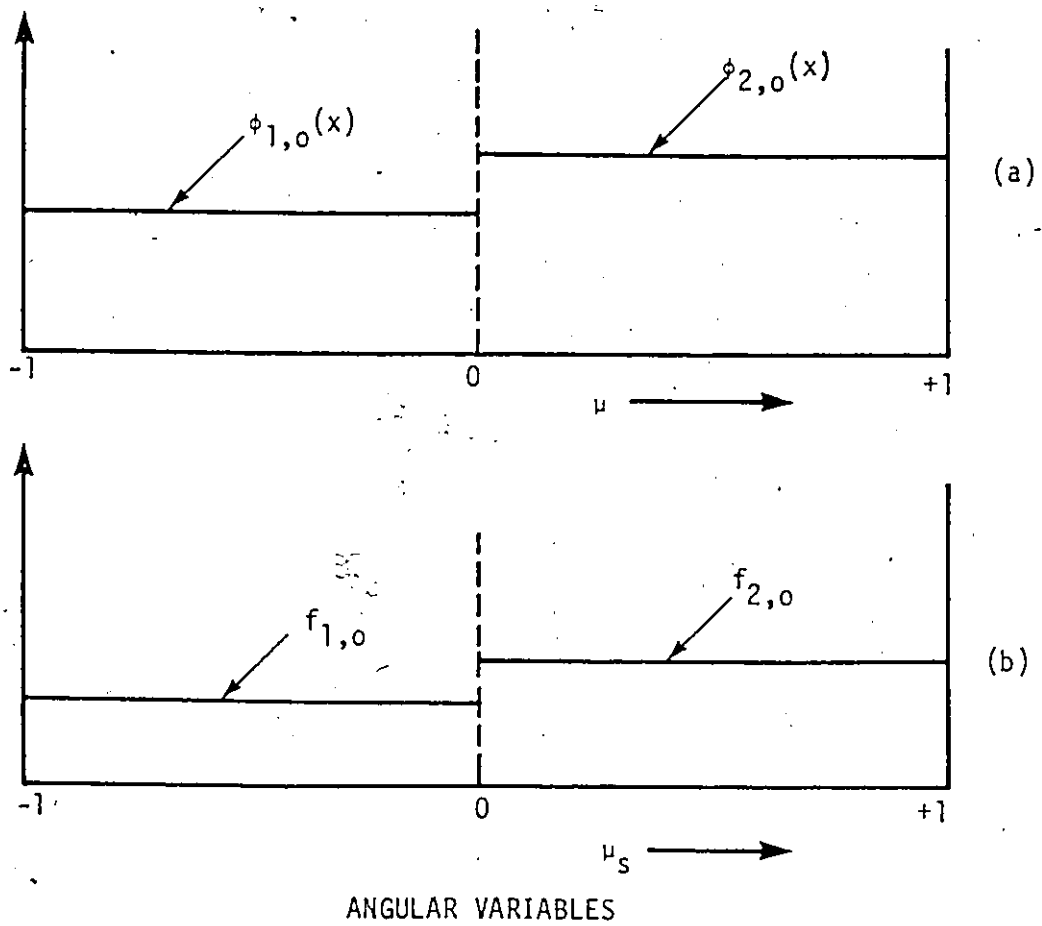


Fig. 4.2: The  $DP_0$ - $DP_0$  representations of (a) angular flux and (b) scattering function.



$i = 1, 2$ . Here, the  $A$ 's are constants defined according to Eq. (4.20) and given by

$$A_{000}^{1jk} = \int_{-1}^0 B_{00}^{jk}(\mu) d\mu, \quad (4.34)$$

and

$$A_{000}^{2jk} = \int_0^1 B_{00}^{jk}(\mu) d\mu; \quad (4.35)$$

$j = 1, 2$  and  $k = 1, 2$ , where the  $B$ 's are functions of  $\mu$  defined according to Eq. (4.18) and given by

$$B_{00}^{11}(\mu) = \frac{1}{2\pi} \iint_{\substack{-1 \leq \mu_s \leq 0 \\ -1 \leq \mu' \leq 0}} d\mu' d\omega, \quad (4.36)$$

$$B_{00}^{12}(\mu) = \frac{1}{2\pi} \iint_{\substack{-1 \leq \mu_s \leq 0 \\ 0 \leq \mu' \leq 1}} d\mu' d\omega, \quad (4.37)$$

$$B_{00}^{21}(\mu) = \frac{1}{2\pi} \iint_{\substack{0 \leq \mu_s \leq 1 \\ -1 \leq \mu' \leq 0}} d\mu' d\omega, \quad (4.38)$$

and

$$B_{00}^{22}(\mu) = \frac{1}{2\pi} \iint_{\substack{0 \leq \mu_s \leq 1 \\ 0 \leq \mu' \leq 1}} d\mu' d\omega. \quad (4.39)$$

Hereafter, for the  $DP_0$ - $DP_0$  approximation, the A's constants will be denoted by  $A_0^\alpha$  and the B's integrals will be designated by  $B_0^\alpha$ . These integrals have been evaluated and their results are given by

$$B_{00}^{11}(\mu) = B_{00}^{22}(\mu) = 1 - \frac{1}{\pi} \cos^{-1} \mu, \quad (4.40)$$

and

$$B_{00}^{12}(\mu) = B_{00}^{21}(\mu) = \frac{1}{\pi} \cos^{-1} \mu. \quad (4.41)$$

The detailed derivation of the  $B_0^\alpha$  functions is given in Appendix A. Using these functions of Eqs. (4.40) and (4.41) into the  $A_0^\alpha$  integrals, Eqs. (4.34) and (4.35) and performing the integrations yields

$$A_{000}^{111} = A_{000}^{122} = A_{000}^{221} = A_{000}^{212} = \frac{1}{\pi}, \quad (4.42)$$

and

$$A_{000}^{121} = A_{000}^{112} = A_{000}^{211} = A_{000}^{222} = 1 - \frac{1}{\pi}. \quad (4.43)$$

Substituting the proper  $A_0^\alpha$  from Eqs. (4.42) and (4.43) into Eqs. (4.32) and (4.33) gives, respectively,

$$\alpha_1 = \beta_2 = 2c \left[ \frac{1}{\pi} f_{1,0} + \left(1 - \frac{1}{\pi}\right) f_{2,0} \right], \quad (4.44)$$

and

$$\alpha_2 = \beta_1 = 2c \left[ \left(1 - \frac{1}{\pi}\right) f_{1,0} + \frac{1}{\pi} f_{2,0} \right]. \quad (4.45)$$

Let us define  $\alpha$  and  $\beta$  as follows:

$$\alpha = \alpha_1 = \beta_2, \quad (4.46)$$

and

$$\beta = \alpha_2 = \beta_1 \quad (4.47)$$

Substituting Eqs. (4.46) and (4.47) into Eqs. (4.30) and (4.31) of the partial-range moments of the flux and rearranging the resultant equations to read, respectively,

$$\frac{d\phi_{1,0}(x)}{dx} = (2 - \alpha)\phi_{1,0}(x) - \beta\phi_{2,0}(x) \quad (4.48)$$

and

$$\frac{d\phi_{2,0}(x)}{dx} = -(2 - \alpha)\phi_{2,0}(x) + \beta\phi_{1,0}(x) \quad (4.49)$$

This system of equations, Eqs. (4.48) and (4.49), will be used to examine the eigenvalues associated with the problem, to discuss the diffusion approximation within this low-order approximation and to study the critical thickness of a slab reactor as a function of anisotropy.

#### 4.5.1 The Eigenvalues

The eigenvalue problem associated with Eqs. (4.48) and (4.49) is obtained by seeking the following solution for the partial-range moments of the flux

$$\phi_{n,0}(x) = A_n e^{-x/\nu} \quad ; \quad n = 1, 2 \quad (4.50)$$

where  $1/\nu$  are the eigenvalues and  $A_n$  are constants which depend on the eigenvalues as well as the boundary conditions of the problem under consideration. Substituting this ansatz, Eq. (4.50), into Eqs. (4.48) and (4.49) we can write the resultant in a matrix form as

$$\begin{bmatrix} -(2 - \alpha) - \frac{1}{v} & \beta \\ -\beta & (2 - \alpha) - \frac{1}{v} \end{bmatrix} \begin{bmatrix} A_1 \\ A_2 \end{bmatrix} = 0 \quad (4.51)$$

From this equation the eigenvalues are given by

$$\left(\frac{1}{v}\right)^2 = 4(1 - c)\left[1 - \frac{1}{2}(\alpha - \beta)\right] \quad (4.52)$$

Substituting the expressions of  $\alpha$  and  $\beta$ , Eqs. (4.44) to (4.47), into the above equation gives

$$\left(\frac{1}{v}\right)^2 = 4(1 - c)\left[1 - \left(1 - \frac{2}{\pi}\right)c\Delta f\right] \quad (4.53)$$

where  $\Delta f$  is the degree of anisotropy of the scattering function and it is, here, defined by

$$\Delta f = f_{2,0} - f_{1,0} \quad (4.54)$$

A positive  $\Delta f$  represents anisotropy in the forward direction and a negative  $\Delta f$  represents anisotropy in the backward direction.

Moreover, we can recognize the following special cases:

- 1)  $\Delta f = 1$  represents a complete forward scattering, where  $f_{1,0} = 0.0$  and  $f_{2,0} = 1.0$ ;
- 2)  $\Delta f = 0$  represents isotropic scattering, where  $f_{1,0} = f_{2,0} = 1/2$ ;
- 3)  $\Delta f = -1$  represents a complete backward scattering, where  $f_{1,0} = 1.0$  and  $f_{2,0} = 0.0$ .

These three special cases are shown in Fig. 4.3. From the normalization of the scattering function we have

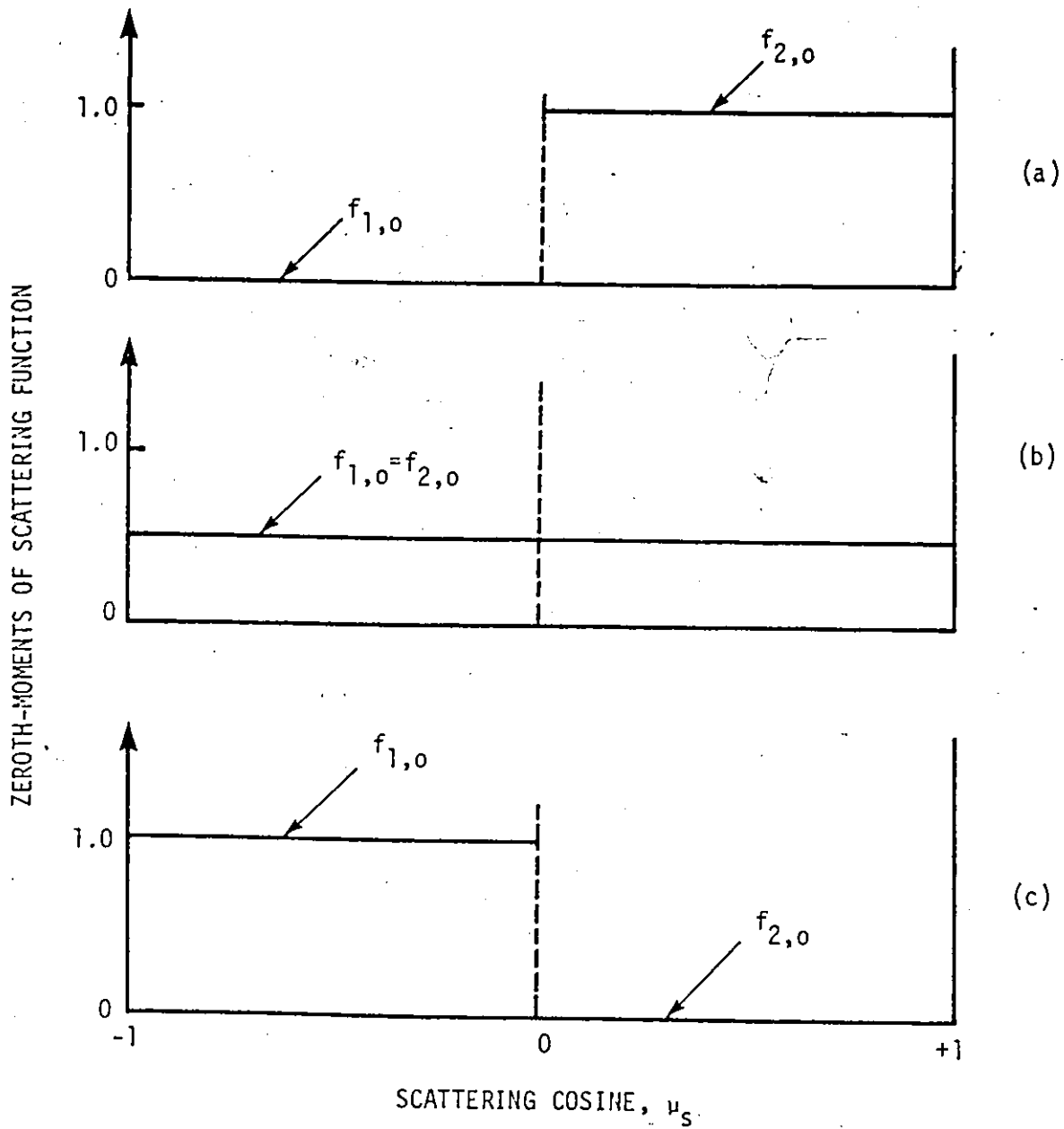


Fig. 4.3: Double- $P_0$  representation of scattering function:  
 (a) complete forward scattering, (b) isotropic scattering, and (c) complete backward scattering.

$$f_{1,0} + f_{2,0} = 1.0 \quad (4.55)$$

Alternatively, this condition implies that the neutrons are conserved in the system.

It is worthwhile to notice that there is a great similarity between this formalism, here, of the  $DP_0$ - $DP_0$  approximation and the Asymptotic Double- $P_0$  Theory<sup>(23,24)</sup>. The main difference between them is that in the present formalism  $f_{1,0}$  and  $f_{2,0}$  are properties of the material of the medium under consideration, while in the Asymptotic Double- $P_0$  Theory they are free parameters.

Also, for the isotropic case of scattering,  $\Delta f = 0$ , Eq. (4.53) reduces to

$$\left(\frac{1}{v}\right)_{iso}^2 = 4(1 - c) \quad (4.56)$$

This result agrees with the eigenvalues of the double- $P_0$  approximation<sup>(2,3)</sup>.

Equation (4.53) has been used to calculate the eigenvalue  $1/v$  as a function of the degree of anisotropy  $\Delta f$ . Figure 4.4 gives the results for values of  $c = 0.1, 0.5, 0.7, 0.9$  and  $0.95$ , respectively. From the figure we can see that the eigenvalue decreases, in general, with increasing anisotropy,  $\Delta f$ . This agrees with the general behaviour of the exact eigenvalue with anisotropy which can be observed in Table 3.1. Also, the decrease or increase in the eigenvalue from that of isotropic scattering, with  $\Delta f$ , is smaller for small  $c$ . However, we cannot say whether this approximation is better for anisotropic scattering or not unless we compare with the exact eigenvalues associated with

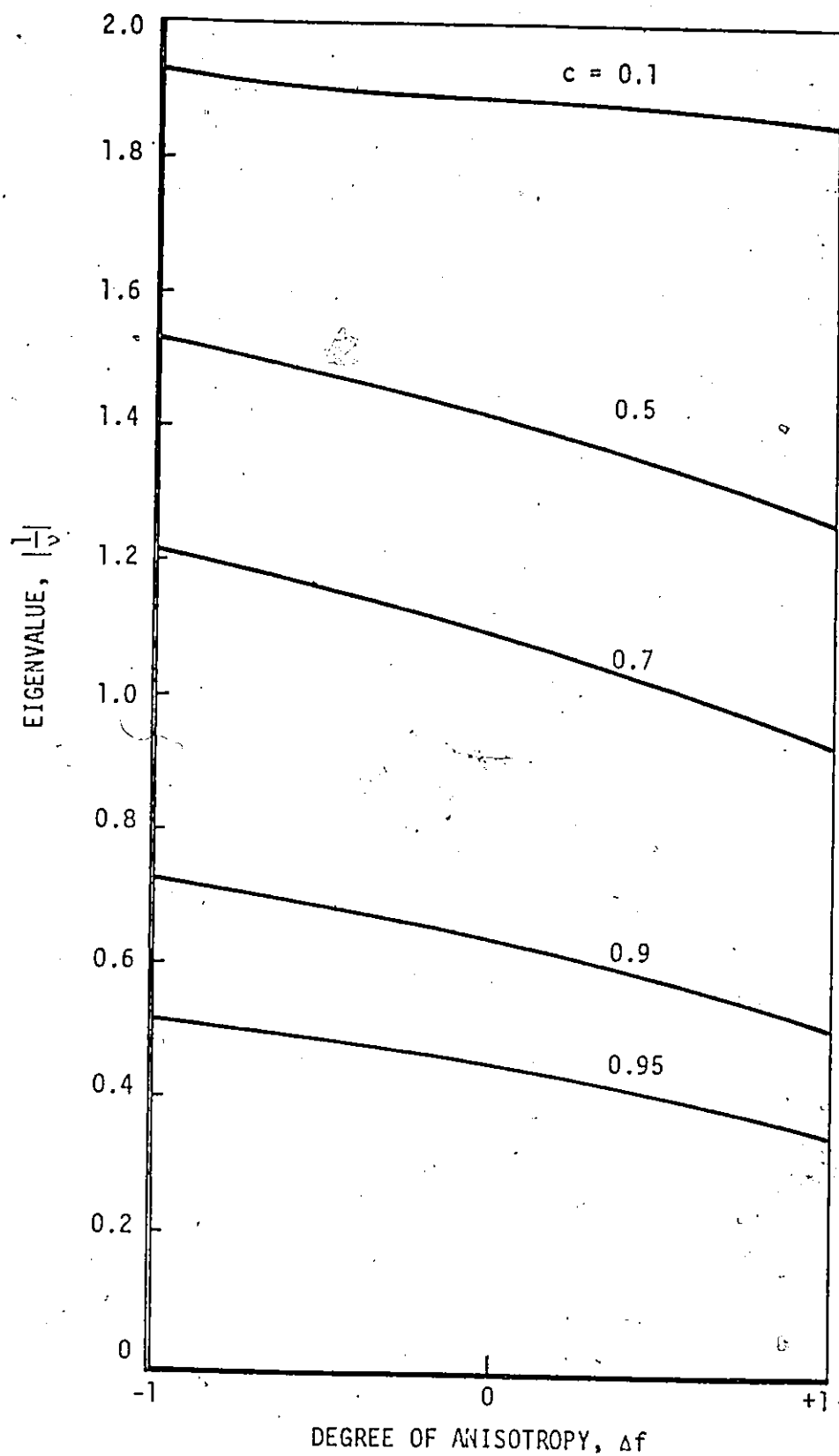


Fig. 4.4: Eigenvalue as a function of degree of anisotropy,  $\Delta f$ , and number of secondaries,  $c$ , for  $DP_0$ - $DP_0$  approximation.

a certain anisotropic function. Section 4.8 will be devoted to this purpose.

#### 4.5.2 Diffusion Approximation

It is possible to express the  $DP_0$ - $DP_0$  equations, Eqs. (4.48) and (4.49), in terms of the scalar flux  $\psi(x)$  and the neutron current  $J(x)$ . Since the scalar flux is given by<sup>(32)</sup>

$$\psi(x) = \phi_{1,0}(x) + \phi_{2,0}(x) \quad , \quad (4.57)$$

and the current is given by

$$J(x) = \frac{1}{2} [\phi_{2,0}(x) - \phi_{1,0}(x)] \quad , \quad (4.58)$$

we can obtain the following equations from Eqs. (4.48) and (4.49) by first subtracting, and substituting the expressions of  $\alpha$  and  $\beta$  of Eqs. (4.44) to (4.47),

$$\frac{d\psi(x)}{dx} + 4\left[1 - \left(1 - \frac{2}{\pi}\right)c\Delta f\right]J(x) = 0 \quad , \quad (4.59)$$

and then adding

$$\frac{dJ(x)}{dx} + (1 - c)\psi(x) = 0 \quad . \quad (4.60)$$

Equation (4.59) can be rewritten in the form of the Fick's rule<sup>(1-3)</sup> which represents the basic relation of the diffusion approximation, i.e.

$$J(x) = -D \frac{d\psi(x)}{dx} \quad , \quad (4.61)$$

where  $D$  is the diffusion coefficient and is given for the present formalism by



$$D = \frac{1}{4[1 - (1 - \frac{2}{\pi})c\Delta f]} \quad (4.62)$$

This relation gives the diffusion coefficient of neutrons as function of the number of secondaries  $c$  and the degree of anisotropy  $\Delta f$ . From Eqs. (4.60) and (4.61) we can write the following diffusion equation

$$\frac{d^2\psi(x)}{dx^2} + B_m^2\psi(x) = 0 \quad , \quad (4.63)$$

where  $B_m^2$  is the material buckling given by

$$B_m^2 = \frac{c - 1}{D} \quad (4.64)$$

Here  $c$  is the average number of secondary neutrons emitted per collision and  $D$  is the diffusion coefficient given by Eq. (4.62).

#### 4.5.3 Critical Bare Slab Reactor

As a final study case for the  $DP_0$ - $DP_0$  approximation, we calculate the critical thickness of a bare slab reactor as a function of the degree of anisotropy  $\Delta f$ , and compare it with the available exact results. The solution of the equivalent diffusion equation, Eq. (4.63), for positive  $B_m^2$ , i.e.  $c > 1$ , gives the neutron flux  $\psi(x)$  as

$$\psi(x) = A\cos(B_m x) \quad , \quad (4.65)$$

where the solution  $\sin(B_m x)$  has been suppressed because of the symmetry required and  $A$  is a constant dependent on the reactor power. The boundary condition for this problem is given by

$$\phi_{1,0}(x_{1/2}) = 0 \quad , \quad (4.66)$$

where  $x_{1/2}$  is the half thickness of the reactor. Clearly, the boundary condition is satisfied exactly. From Eqs. (4.57) and (4.58) we obtain the following relationship for  $\phi_{1,0}(x)$

$$\phi_{1,0}(x) = \frac{1}{2} \psi(x) - J(x) \quad (4.67)$$

where  $\psi(x)$  is the neutron flux given by Eq. (4.65) and  $J(x)$  is the neutron current which is given by Eq. (4.61). Using the boundary condition of Eq. (4.66) into Eq. (4.67) and the definitions of  $B_m$ , Eq. (4.64), and  $D$ , Eq. (4.62), we can write the following relationship for the half-thickness  $x_{1/2}$  of the reactor as a function of  $c$  and  $\Delta f$ ,

$$x_{1/2} = \frac{1}{\sqrt{4(c-1)[1 - (1 - \frac{2}{\pi})c\Delta f]}} \tan^{-1} \sqrt{\frac{1 - (1 - \frac{2}{\pi})c\Delta f}{c-1}} \quad (4.68)$$

This relationship has been used to calculate the reactor thickness ( $2x_{1/2}$ ) as a function of  $\Delta f$  for various values of  $c$  and the results have been shown in Fig. 4.5. From the calculations and the figure we can conclude that for large values of  $c$  ( $c > 2$ ), the reactor thickness does not depend strongly on the anisotropy of neutron generation  $\Delta f$ , but in practical ranges of  $c$  ( $c = 1$  to  $c = 2$ ) the reactor thickness changes considerably with  $\Delta f$ . Therefore, the effect of anisotropy should be taken into consideration in the design of nuclear reactors especially when high anisotropic scattering is involved; a case in hand is the fast reactor.

Further, by examining the formula of  $x_{1/2}$ , Eq. (4.68), we can see that  $x_{1/2}$  is real and finite under the following conditions:

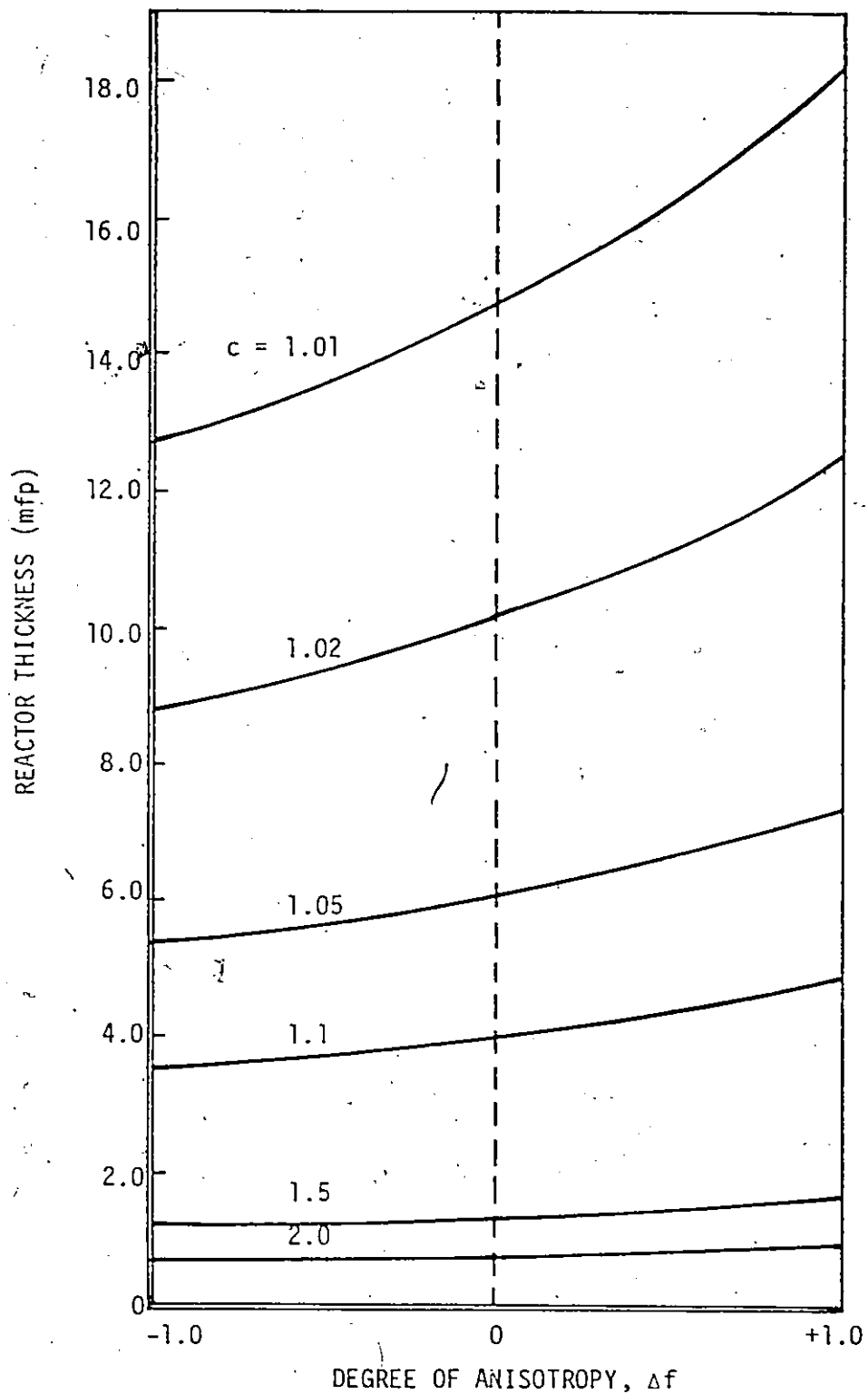


Fig. 4:5: Slab reactor thickness as a function of anisotropy,  $\Delta f$ , for various values of  $c$  using the  $DP_0 - DP_0$  approximation.

- 1)  $c > 1$ ;
- 2)  $[1 - (1 - \frac{2}{\pi})c\Delta f] > 0$ .

The second condition is satisfied for all the negative values of  $\Delta f$ .

However, for positive values of  $\Delta f$  it leads to the following

$$c \geq \frac{1}{(1 - \frac{2}{\pi})\Delta f} \quad (4.69)$$

Figure 4.6 gives the domain of  $c$ - $\Delta f$  space, region I, in which this low-order approximation works and gives real and finite reactor thickness. This range includes all the practical values of  $c$  and  $\Delta f$ . On the other hand, in region II of Fig. 4.6, this approximation yields negative diffusion coefficient and accordingly breaks down.

To compare the results of this low-order approximation with the previous results we present Table 4.1 for the special case of isotropic scattering. The reactor half-thickness has been calculated exactly for this special case<sup>(67,68)</sup>. However, we have compared our results with the benchmark value of the reactor thicknesses<sup>(67)</sup>. In fact, for this special case of isotropic scattering our results reduce to the  $DP_0$  approximation of Yvon<sup>(16,17)</sup> and are in good agreement with the benchmark values. Moreover, the data of Table 4.1 is represented graphically in Fig. 4.7. Of interest is the cross of the results of the present approximation over the benchmark values. From the figure we can observe that for  $c = 1.25$  this low-order approximation gives the same result as the benchmark value.

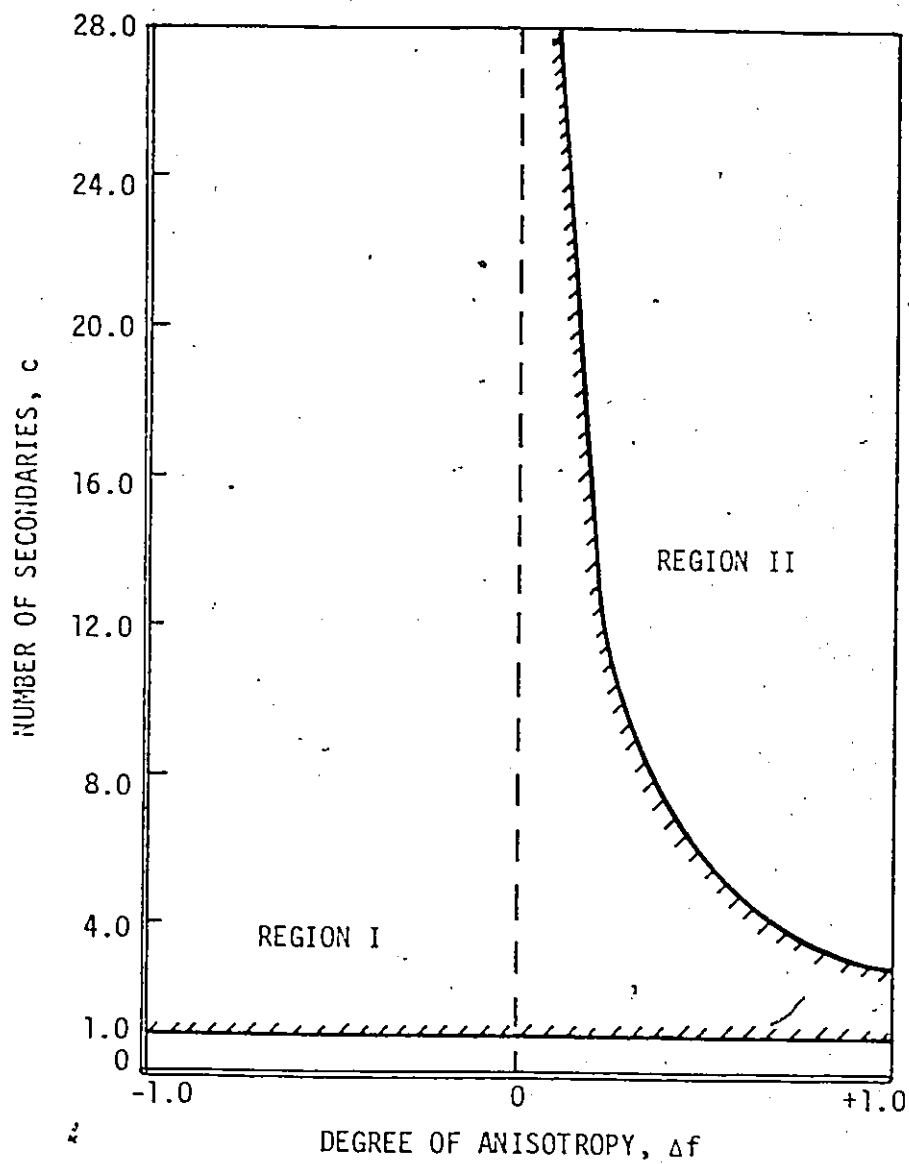


Fig. 4.6: Illustration showing  $c$ - $\Delta f$  domain of real and finite reactor thickness in the context of the  $DP_0$ - $DP_0$  approximation.

c	Benchmark Values	$DP_0 - DP_0$ Approximation (this work)
1.01	8.3295	7.3555
1.02	5.6655	5.0570
1.05	3.3003	3.0205
1.10	2.1233	1.9994
1.20	1.2894	1.2861
1.30	0.9377	0.9765
1.40	0.7366	0.7960
1.60	0.5120	0.5885
2.00	0.3110	0.3927

Table 4.1: Critical half-thickness of slabs for isotropic scattering and various values of the mean number of secondaries per collision.

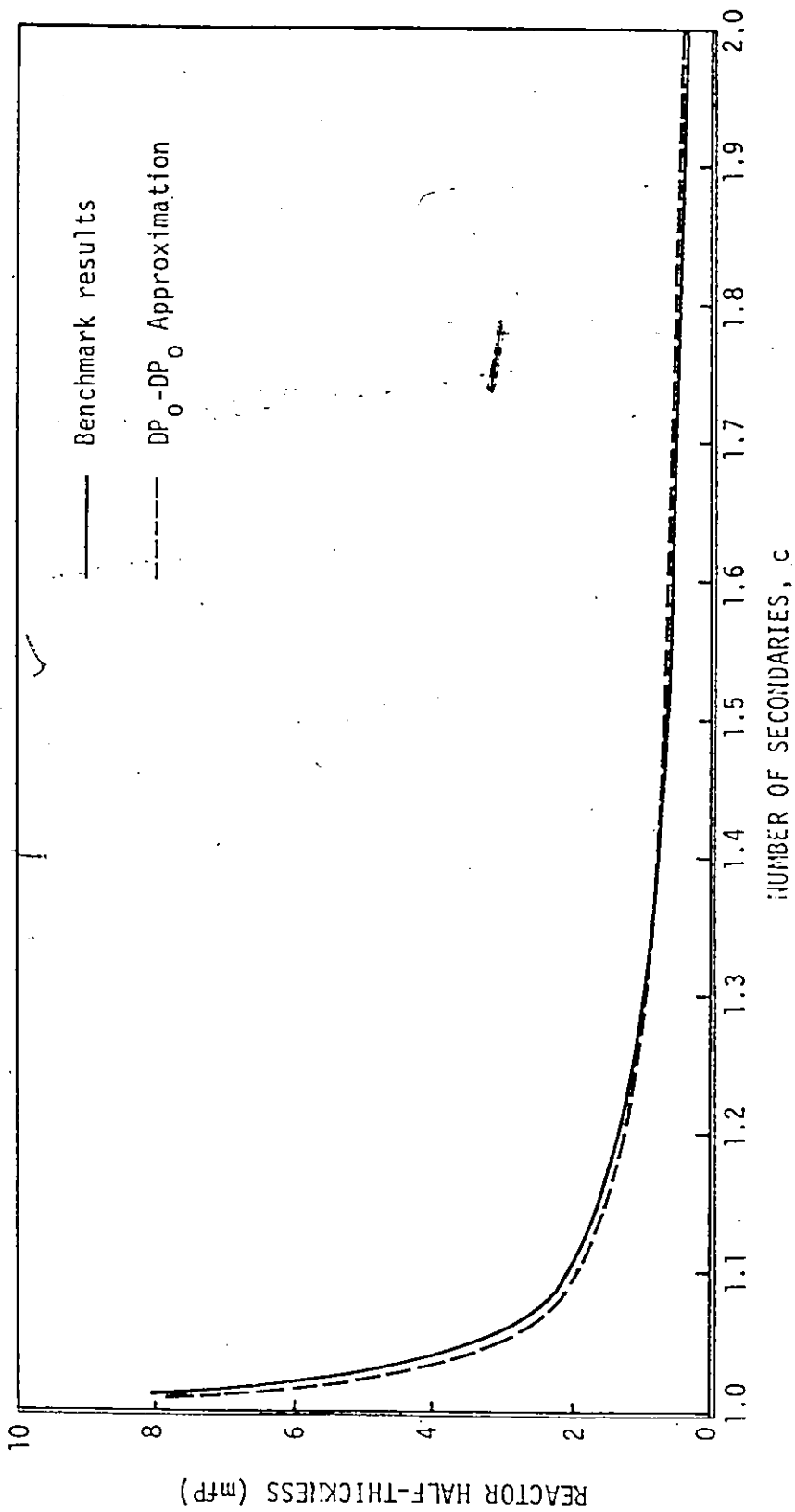


Fig. 4.7: Critical half-thickness of slab reactor as a function of number of secondaries for isotropic scattering.

#### 4.6 DP<sub>0</sub>-2P<sub>0</sub> Approximation

In this section we will develop the DP<sub>0</sub>-2P<sub>0</sub> approximation and use it to calculate the eigenvalue associated with the Milne problem. In the DP<sub>0</sub>-2P<sub>0</sub> approximation the neutron angular flux is represented by the approximation of Section 4.5, DP<sub>0</sub> approximation, while the scattering function is represented by 2P<sub>0</sub> approximation. Figure 4.8 shows the representation of both the neutron angular flux and the scattering function for the DP<sub>0</sub>-2P<sub>0</sub> approximation. Although the scattering function has been represented by isotropic scattering over two intervals given by  $\mu_{s0} = -1$ ,  $\mu_{s1}$  and  $\mu_{s2} = +1$ , we still have  $\mu_{s1}$  as a free parameter which can take any value so that  $-1 < \mu_{s1} < +1$ . This allows us to describe a given scattering function with much more accuracy than is possible with the DP<sub>0</sub> representation.

Starting by Eq. (4.29) and specifying  $\mu_0 = \mu_{s0} = -1$ ,  $\mu_1 = 0$ ,  $\mu_{s1}$  as a free parameter and  $\mu_2 = \mu_{s2} = +1$  we can write the following two equations for  $n = 1$  and 2, respectively,

$$-\frac{d\phi_{1,0}(x)}{dx} + 2\phi_{1,0}(x) = \alpha_1\phi_{1,0}(x) + \beta_1\phi_{2,0}(x) \quad , \quad (4.70)$$

and

$$\frac{d\phi_{2,0}(x)}{dx} + 2\phi_{2,0}(x) = \alpha_2\phi_{1,0}(x) + \beta_2\phi_{2,0}(x) \quad . \quad (4.71)$$

In this case the coefficients  $\alpha_i$  and  $\beta_i$  are given by

$$\alpha_i = 2c \left[ \frac{f_{1,0}^{A_{000}^{i11}}}{1 + \mu_{s1}} + \frac{f_{2,0}^{A_{000}^{i21}}}{1 - \mu_{s1}} \right] \quad , \quad (4.72)$$

and



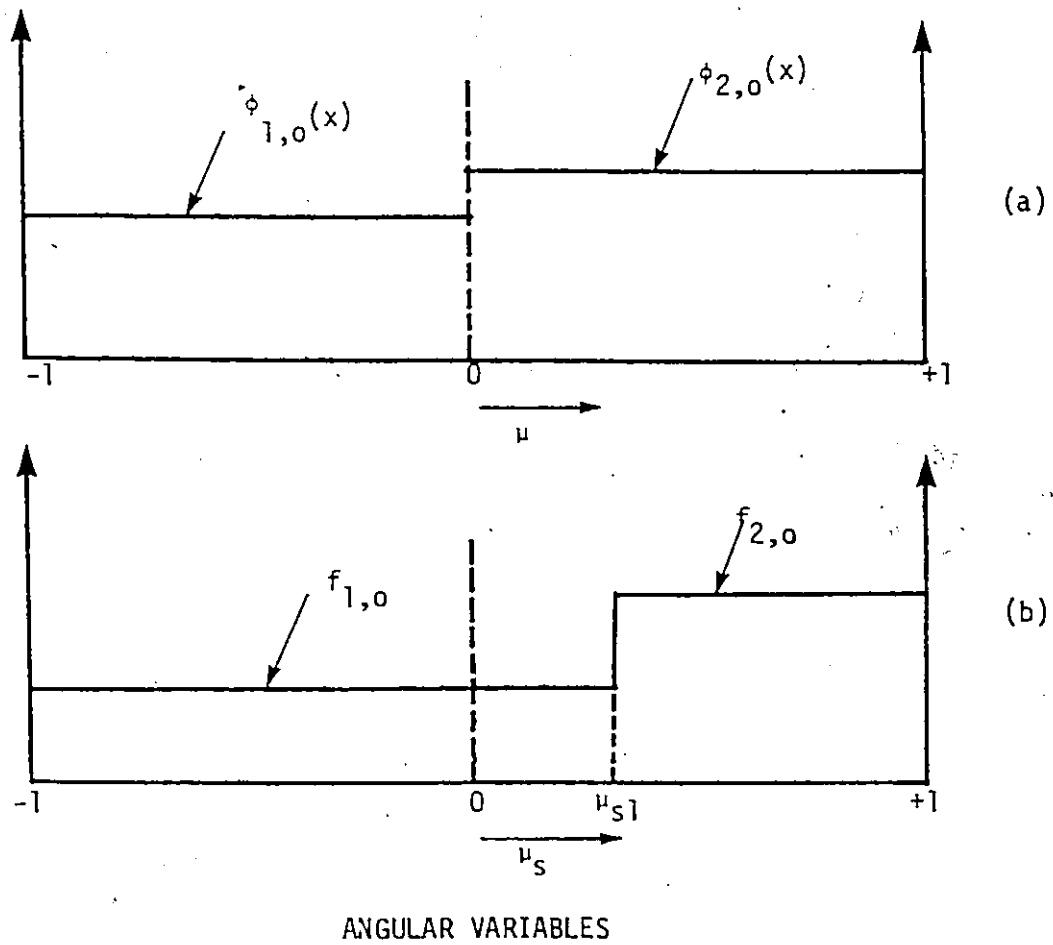


Fig. 4.8: The  $DP_0-2P_0$  representation of (a) angular flux and (b) scattering function.

$$B_i = 2c \left[ \frac{f_{1,0} A_{000}^{i12}}{1 + \mu_{s1}} + \frac{f_{2,0} A_{000}^{i22}}{1 + \mu_{s1}} \right] ; \quad i = 1 \text{ and } 2. \quad (4.73)$$

Again, we have assumed a source free medium and considered the case of  $L = 0$ . For  $\mu_{s1} = 0$  these equations, Eqs. (4.70) to (4.73), reduce to the similar set of equations for the  $DP_0$ - $DP_0$  approximation, Eqs. (4.30) to (4.33). The main difficulties in this approximation arise in the evaluation of the A's integrals which are also defined by Eq. (4.20). For this approximation, we will denote these integrals by  $A_0^B$ .

To evaluate the integrals  $A_0^B$  we will consider first the integrals  $B_0^B$  defined by Eq. (4.18) in some detail. Again  $B_0^B$  stands for the B's integrals of the  $DP_0$ - $DP_0$  approximation. Consider the integral  $B_{00}^{22}(\mu)$  as defined by

$$B_{00}^{22}(\mu) = \frac{1}{2\pi} \iint_{\substack{\mu_{s1} \leq \mu_s \leq +1 \\ 0 \leq \mu' \leq +1}} P_{2,0}(\mu_s) P_{2,0}(\mu') d\mu' d\omega. \quad (4.74)$$

This integral can be rewritten as

$$B_{00}^{22}(\mu) = \frac{1}{2\pi} \iint_{\substack{\mu_s \geq \mu_{s1} \\ \mu' \geq 0}} d\mu' d\omega, \quad (4.75)$$

which represents a nonsymmetrical spherical surface integral. In fact the integral of Eq. (4.75) represents the surface area on the upper hemisphere (radius = 1) which is also enclosed inside a cone of angle  $\theta_{s1} = \cos^{-1} \mu_{s1}$  with the direction  $\underline{\Omega}$  as shown in Fig. 4.9. This integral

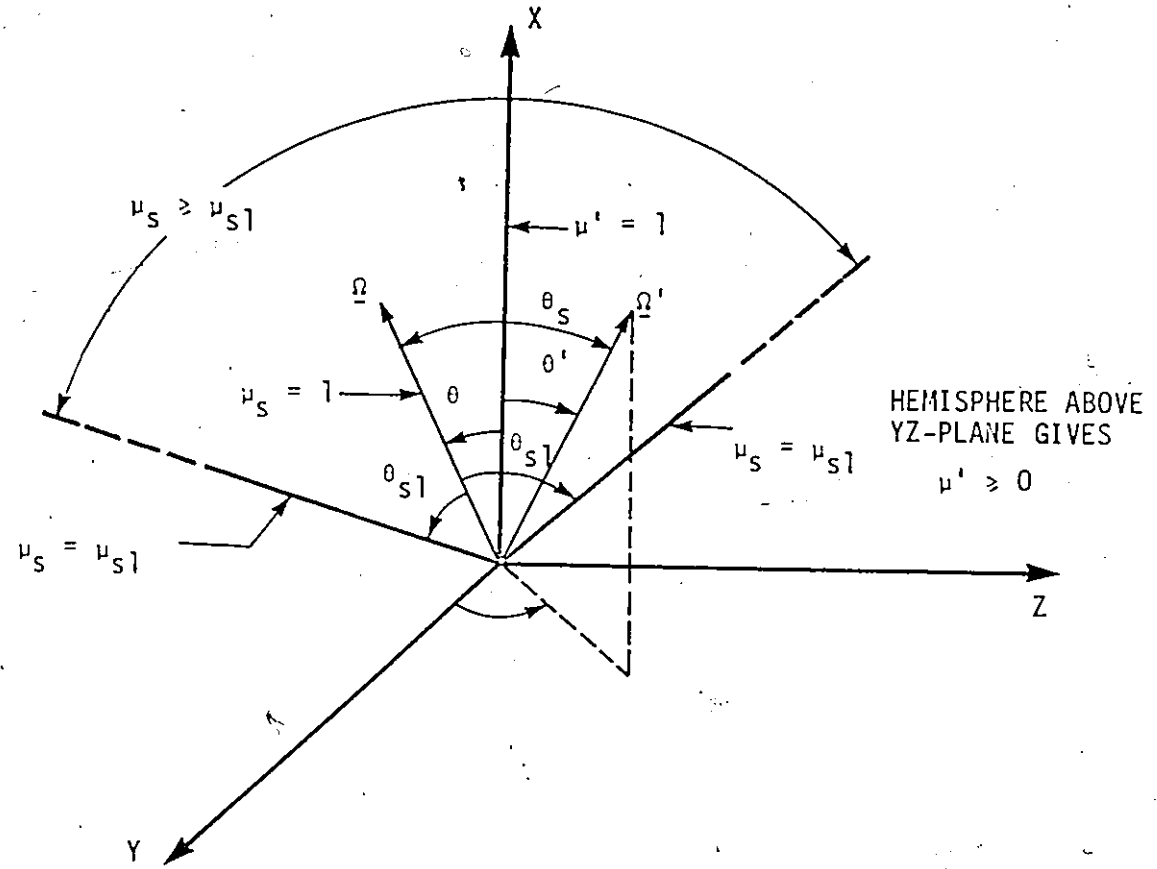


Fig. 4.9: Representation of the integral  $B_{00}^{22}(\mu)$  for  $DP_0-2P_0$  approximation:  $\underline{\Omega}'$  is the initial direction of neutron and  $\underline{\Omega}$  is its final direction;  $\theta_s$  is the scattering angle and  $\theta_{s|} = \cos^{-1} \mu_{s|}$ .

is evaluated in Appendix B. It turns out that it has different expressions depending on the range of  $\theta = \cos^{-1} \mu$  and  $\theta_{s1} = \cos^{-1} \mu_{s1}$ . Figure 4.10 gives the expressions of  $B_{00}^{22}(\mu)$  for the different domains of  $\theta$  and  $\theta_{s1}$  while Fig. 4.11 displays it as a function of  $\mu$  for values of  $\mu_{s1} = -0.8, -0.4, 0.0, 0.4$  and  $0.8$ , respectively.

The complete set of the  $B_0^\beta$  integrals have been evaluated in Appendix B and they are related to  $B_{00}^{22}(\mu)$  by the following

$$B_{00}^{11}(\mu) = \mu_{s1} + B_{00}^{22}(\mu) \quad , \quad (4.76)$$

$$B_{00}^{12}(\mu) = 1 - B_{00}^{22}(\mu) \quad , \quad (4.77)$$

and

$$B_{00}^{21}(\mu) = 1 - \mu_{s1} - B_{00}^{22}(\mu) \quad . \quad (4.78)$$

Now, using the definition of the integrals  $A_0^\beta$ , Eq. (4.20), and the above relationships of the functions  $B_0^\beta$  we can show that the following relationships hold

$$A_{000}^{i11} = \mu_{s1} + A_{000}^{i22} \quad , \quad (4.79)$$

$$A_{000}^{i12} = 1 - A_{000}^{i22} \quad , \quad (4.80)$$

and

$$A_{000}^{i21} = 1 - \mu_{s1} - A_{000}^{i22} \quad ; \quad (4.81)$$

$i = 1$  and  $2$ , where

$$A_{000}^{122} = \int_{-1}^0 B_{00}^{22}(\mu) d\mu \quad , \quad (4.82)$$

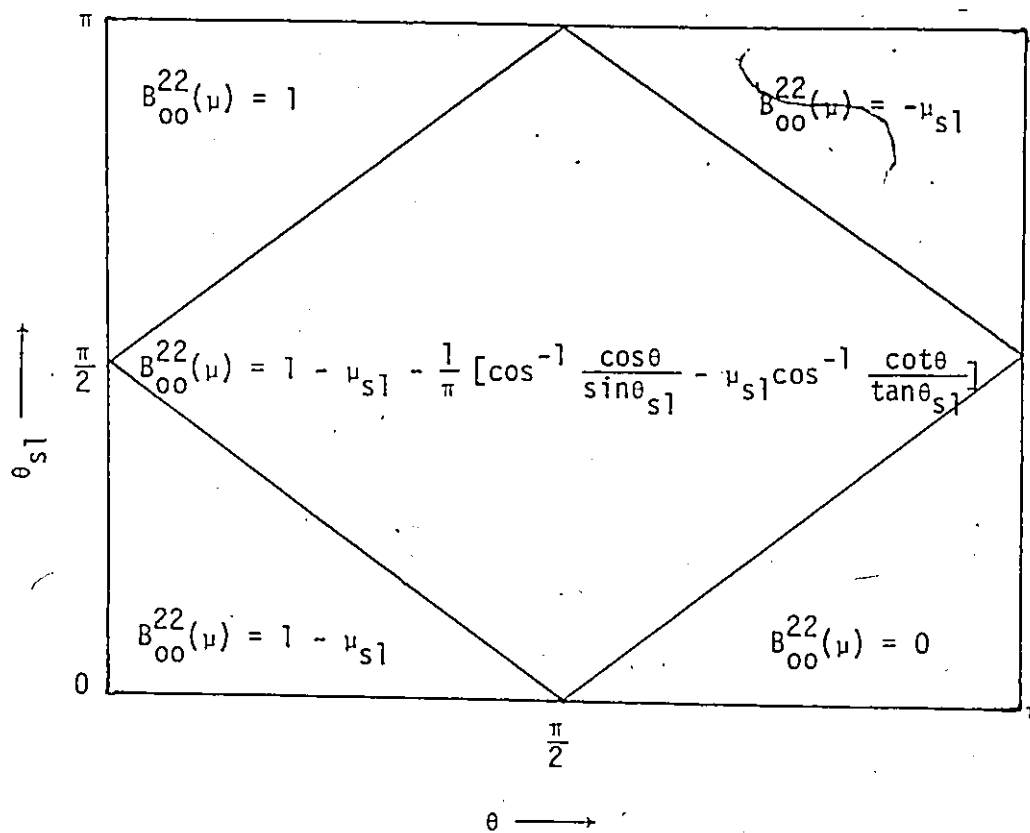


Fig. 4.10: The function  $B_{00}^{22}(\mu)$  as a function of  $\theta = \cos^{-1} \mu$  and  $\theta_{s1} = \cos^{-1} \mu_{s1}$  for the  $DP_0 - 2P_0$  approximation.

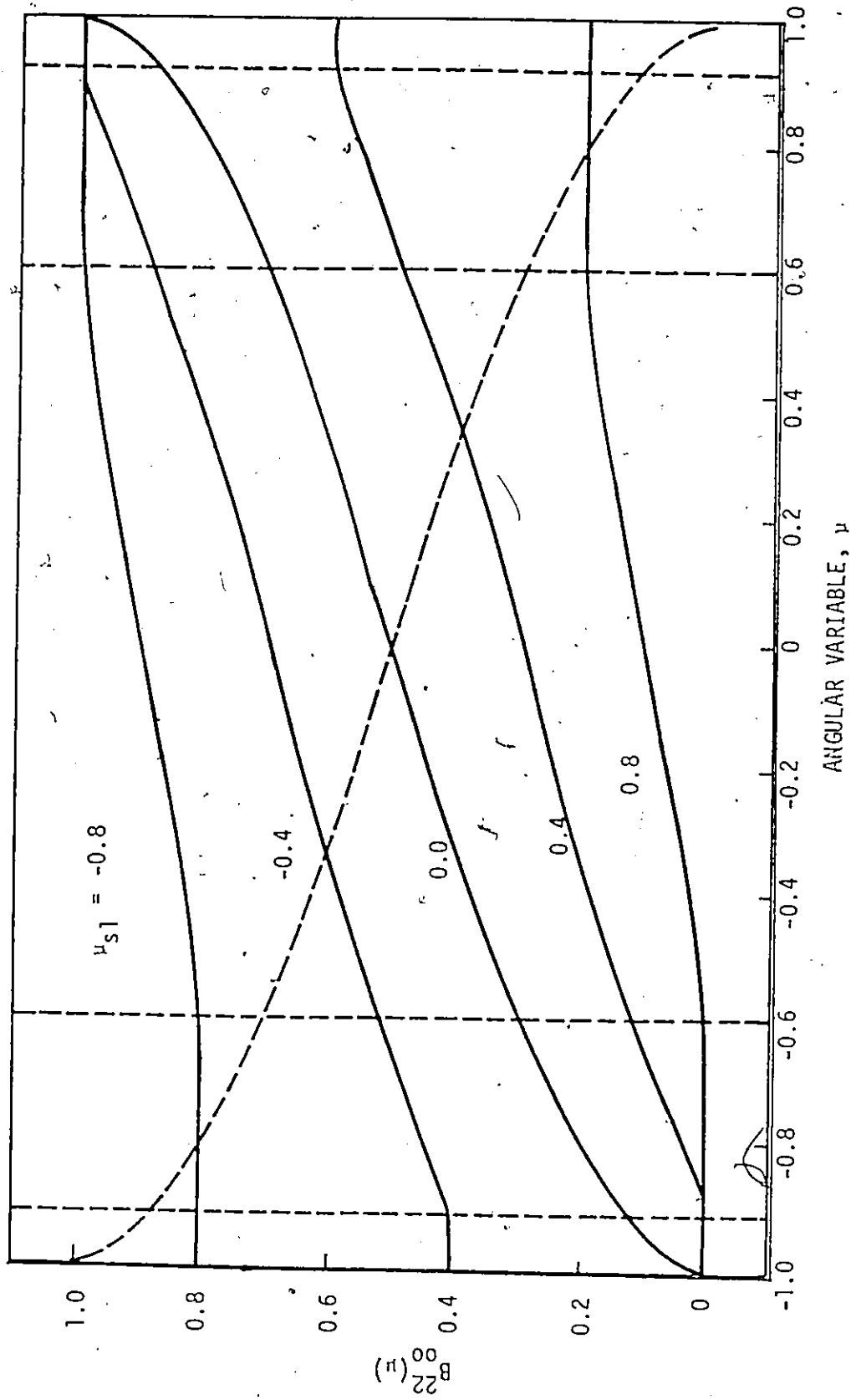


Fig. 4.11: The function  $B_{00}^{22}(\mu)$  as a function of  $\mu$  for various values of  $\nu_{s1}$  for the  $DP_0-2P_0$  approximation; the dashed curve gives  $B_{00}^{11}(\mu)$  for  $\nu_{s1} = 0$ .

and

$$A_{000}^{222} = \int_0^1 B_{00}^{22}(\mu) d\mu \quad (4.83)$$

The integrals of Eqs. (4.82) and (4.83) have been evaluated in Appendix B and the results are given by

$$A_{000}^{122} = \frac{1}{\pi} [\sqrt{1 - \mu_{s1}^2} - \mu_{s1} \cos^{-1} \mu_{s1}] \quad (4.84)$$

and

$$A_{000}^{222} = 1 - \mu_{s1} - A_{000}^{122} \quad (4.85)$$

The expressions of the constants  $A_0^B$ , Eqs. (4.79) to (4.85), have been examined further and the following relationships have been found

$$A_{000}^{111} = A_{000}^{212} \quad (4.86)$$

$$A_{000}^{121} = A_{000}^{222} \quad (4.87)$$

$$A_{000}^{112} = A_{000}^{211} \quad (4.88)$$

and

$$A_{000}^{122} = A_{000}^{221} \quad (4.89)$$

Numerical values for the constants  $A_0^B$  are given in Table 4.2 for the same values of  $\mu_{s1}$  of Fig. 4.11.

In order to examine the accuracy of this approximation we will use it for the calculation of the eigenvalues associated with the Milne problem as a function of the scattering angular segmentation  $\mu_{s1}$  and

$\mu_{s1}$	$A_{000}^{111} = A_{000}^{212}$	$A_{000}^{121} = A_{000}^{222}$	$A_{000}^{112} = A_{000}^{211}$	$A_{000}^{122} = A_{000}^{221}$
-0.8	0.27120	0.97288	0.17288	0.82712
-0.4	0.14413	0.85587	0.45587	0.54413
0.0	0.31831	0.68169	0.68169	0.31831
0.4	0.54413	0.45587	0.85587	0.14413
0.8	0.82712	0.17288	0.97288	0.27120

Table 4.2: The constants  $A_0^\beta$  of the  $DP_0-2P_0$  approximation for various values of  $\mu_{s1}$ .



the degree of anisotropy  $\Delta f$ . Substituting the ansatz of Eq. (4.50) into Eqs. (4.70) and (4.71) results, after some rearrangement, in the following matrix form

$$\begin{bmatrix} -(2 - \alpha_1) - \frac{1}{v} & \beta_1 \\ -\alpha_2 & (2 - \beta_2) - \frac{1}{v} \end{bmatrix} \begin{bmatrix} A_1 \\ A_2 \end{bmatrix} = 0 \quad (4.90)$$

Here,  $1/v$  represents the eigenvalue and  $A_1$  and  $A_2$  are the eigenvectors. From the above matrix the eigenvalues can be shown to be given by

$$\left(\frac{1}{v}\right)^2 = (2 - \alpha_1)(2 - \beta_2) - \alpha_2\beta_1, \quad (4.91)$$

where  $\alpha_i$  and  $\beta_i$  ( $i = 1, 2$ ) are given by Eqs. (4.72) and (4.73), respectively.

Equation (4.91) has been used to calculate the eigenvalue and Fig. 4.12 shows some of the results represented by the eigenvalue as a function of  $\Delta f$  for small, intermediate and large  $c$ , i.e.  $c = 0.1, 0.5$  and  $0.9$ , respectively, for various values of  $\mu_{s1}$ . For small  $c$  the eigenvalue does not change significantly with the degree of anisotropy, but for large  $c$  it does change by a considerable amount. From these results we conclude that this formalism of  $DP_0 - 2P_0$  approximation gives better results for anisotropic scattering and large  $c$ . The reason for this is that the  $DP_0$  approximation for the case of isotropic scattering is accurate for large  $c$ . A comparison of the results of this approximation with the exact ones for a specific scattering function will be given in Section 4.8.

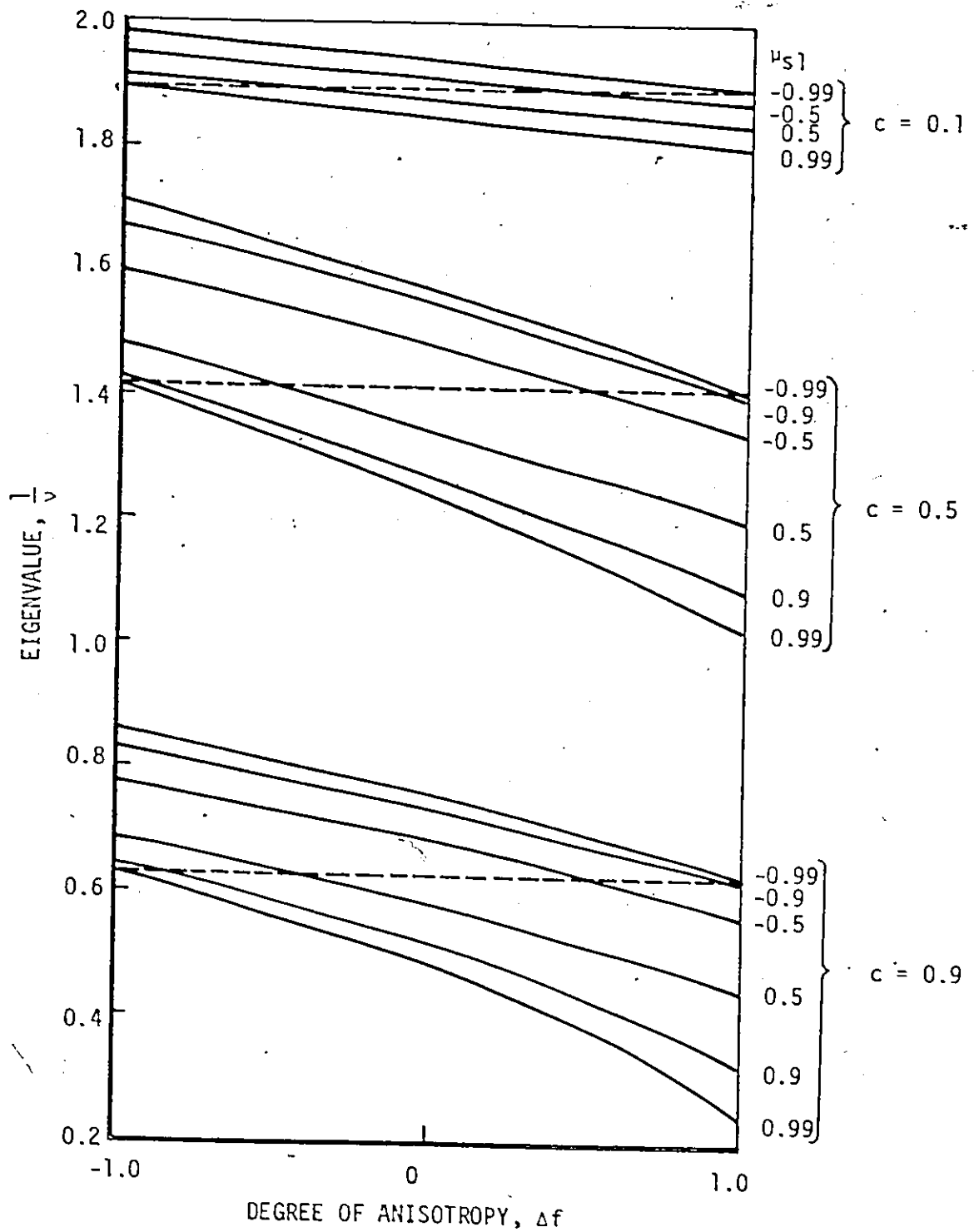


Fig. 4.12: Eigenvalue as a function of degree of anisotropy  $\Delta f$ , scattering angular segmentation  $\mu_{s1}$  and number of secondaries  $c$  using the  $DP_0-2P_0$  approximation; the dashed lines correspond to isotropic scattering.

#### 4.7 $2P_0$ - $2P_0$ Approximation

As a final case of study we consider the  $2P_0$ - $2P_0$  approximation. In this case the angular flux as well as the scattering function are represented by the  $2P_0$  approximation. This representation is schematically shown in Fig. 4.13. The angular variable of the flux  $\mu$  is divided by the segmentation  $\mu_1$  which can take any value between -1 and +1. Similarly, the angular variable of the scattering function  $\mu_s$  is divided by the scattering angular segmentation  $\mu_{s1}$  which can take any value between -1 and +1. Basically,  $\mu_1$  and  $\mu_{s1}$  are independent. However, for the sake of simplicity we will assume that  $\mu_1 = \mu_{s1}$ . It is of interest to observe that for the special case of  $\mu_1 = \mu_{s1} = 0$  this approximation gives the  $DP_0$ - $DP_0$  approximation of Section 4.5.

Starting by Eq. (4.29) and assuming  $\mu_0 = \mu_{s0} = -1$ ,  $\mu_1 = \mu_{s1}$  as free parameter and  $\mu_2 = \mu_{s2} = +1$  we can write the following two equations for a source free medium for  $n = 1$  and  $n = 2$ , respectively,

$$-(1 - \mu_1) \frac{d\phi_{1,0}(x)}{dx} + 2\phi_{1,0}(x) = \alpha_1\phi_{1,0}(x) + \beta_1\phi_{2,0}(x), \quad (4.92)$$

and

$$(1 + \mu_1) \frac{d\phi_{2,0}(x)}{dx} + 2\phi_{2,0}(x) = \alpha_2\phi_{1,0}(x) + \beta_2\phi_{2,0}(x), \quad (4.93)$$

where the coefficients  $\alpha_i$  and  $\beta_i$  are given by

$$\alpha_i = \frac{2c}{1 + \mu_1} \left[ \frac{f_{1,0} A_{000}^{i11}}{1 + \mu_1} + \frac{f_{2,0} A_{000}^{i21}}{1 - \mu_1} \right], \quad (4.94)$$

and

$$\beta_i = \frac{2c}{1 - \mu_1} \left[ \frac{f_{1,0} A_{000}^{i12}}{1 + \mu_1} + \frac{f_{2,0} A_{000}^{i22}}{1 - \mu_1} \right]; \quad i = 1 \text{ and } 2. \quad (4.95)$$

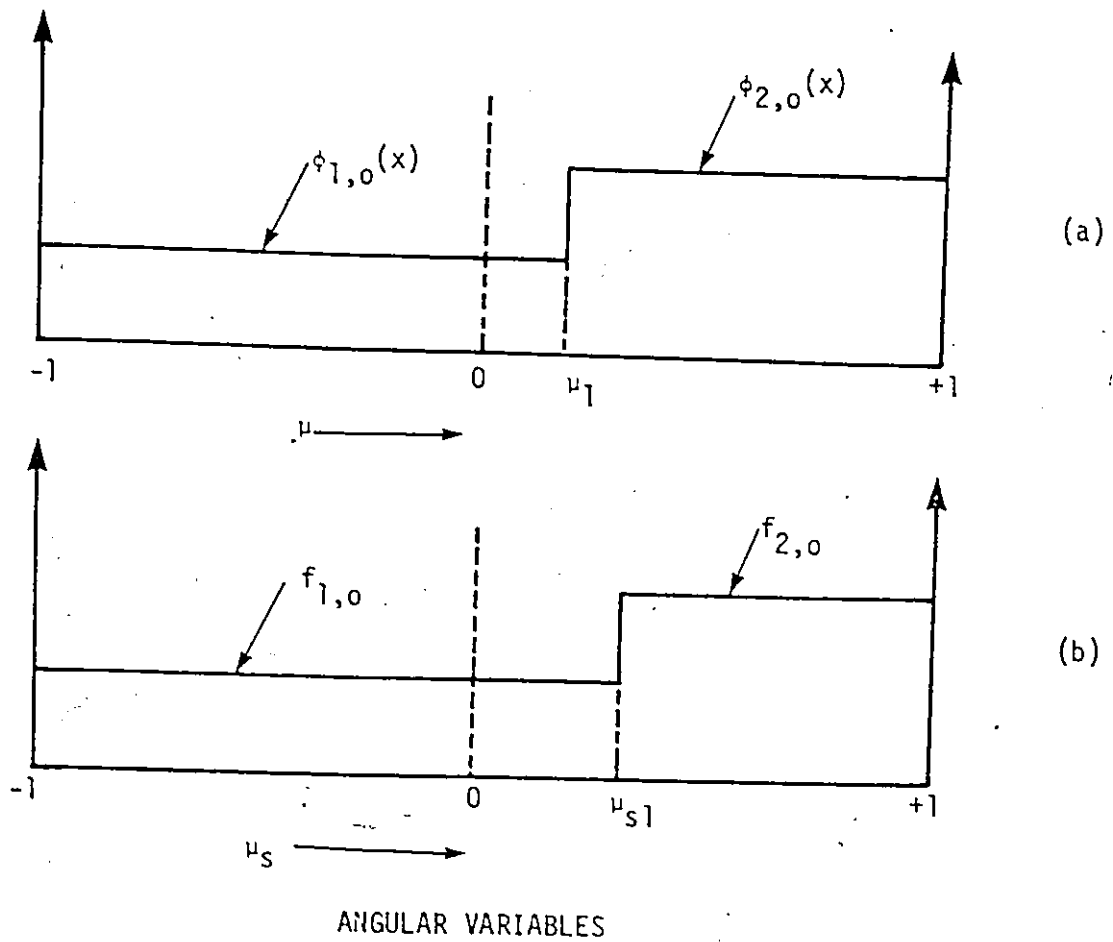


Fig. 4.13: The  $2P_0-2P_0$  representation of (a) angular flux and (b) scattering function.

The main difference between the formulation of the present approximation and the previous two approximations of this chapter is the evaluation of the A's constants which are still defined by Eq. (4.20) but the limits of integrations are different. We will denote these integrals for the  $2P_0-2P_0$  approximation by  $A_0^Y$ .

To evaluate the integrals  $A_0^Y$  we will consider first the integrals  $B_0^Y$  defined by Eq. (4.18). Again  $B_0^Y$  refers here to the  $2P_0-2P_0$  approximation. As an example consider the integral  $B_{00}^{22}(\mu)$  which in this case is given by

$$B_{00}^{22}(\mu) = \frac{1}{2\pi} \iiint_{\substack{1 \geq \mu_s \geq \mu_1 \\ 1 \geq \mu' \geq \mu_1}} d\mu' d\omega \quad (4.96)$$

Graphically, the integral of the above equation represents the area on the surface of a sphere of unit radius enclosed between two cones each of which has an angle of  $\theta_1 = \cos^{-1} \mu_1$  as shown in Fig. 4.14. The evaluation of the integrals  $B_0^Y$  is given in Appendix C. The expressions of the integral  $B_{00}^{22}(\mu)$  for the different domains of  $\theta$  and  $\theta_1$  are given in Fig. 4.15. Furthermore, Fig. 4.16 gives the  $B_{00}^{22}(\mu)$  as a function of  $\mu$  for values of  $\mu_1 = -0.8, -0.4, 0.0, 0.4$  and  $0.8$ , respectively. For all domains of  $\theta$  and  $\theta_1$  the other  $B_0^Y$  integrals are related to  $B_{00}^{22}(\mu)$  by the following relationships

$$B_{00}^{11}(\mu) = 2\mu_1 + B_{00}^{22}(\mu) \quad (4.97)$$

and

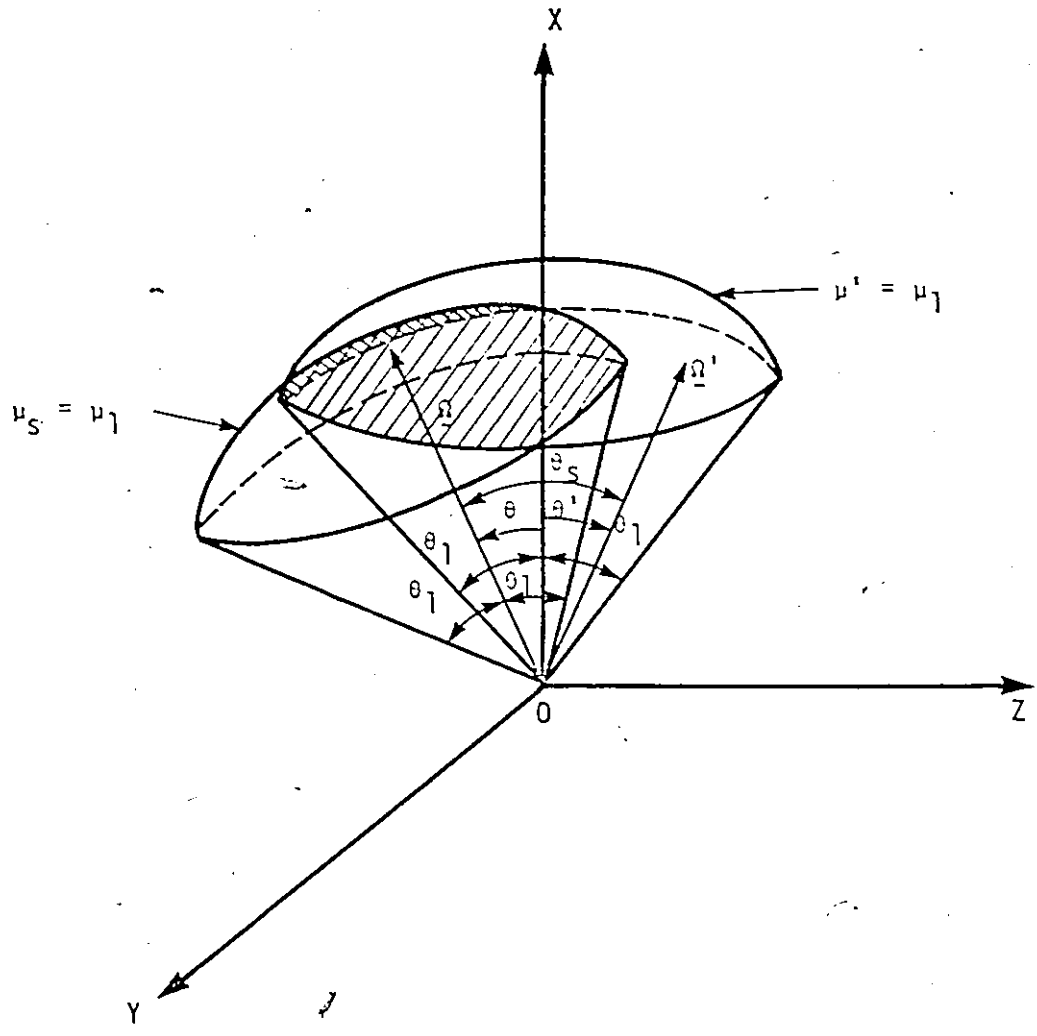


Fig. 4.14: Representation of the integral of  $B_{00}^{22}(\mu)$  for the  $2P_0-2P_0$  approximation; the dashed area represents the integral of Eq. (4.96).

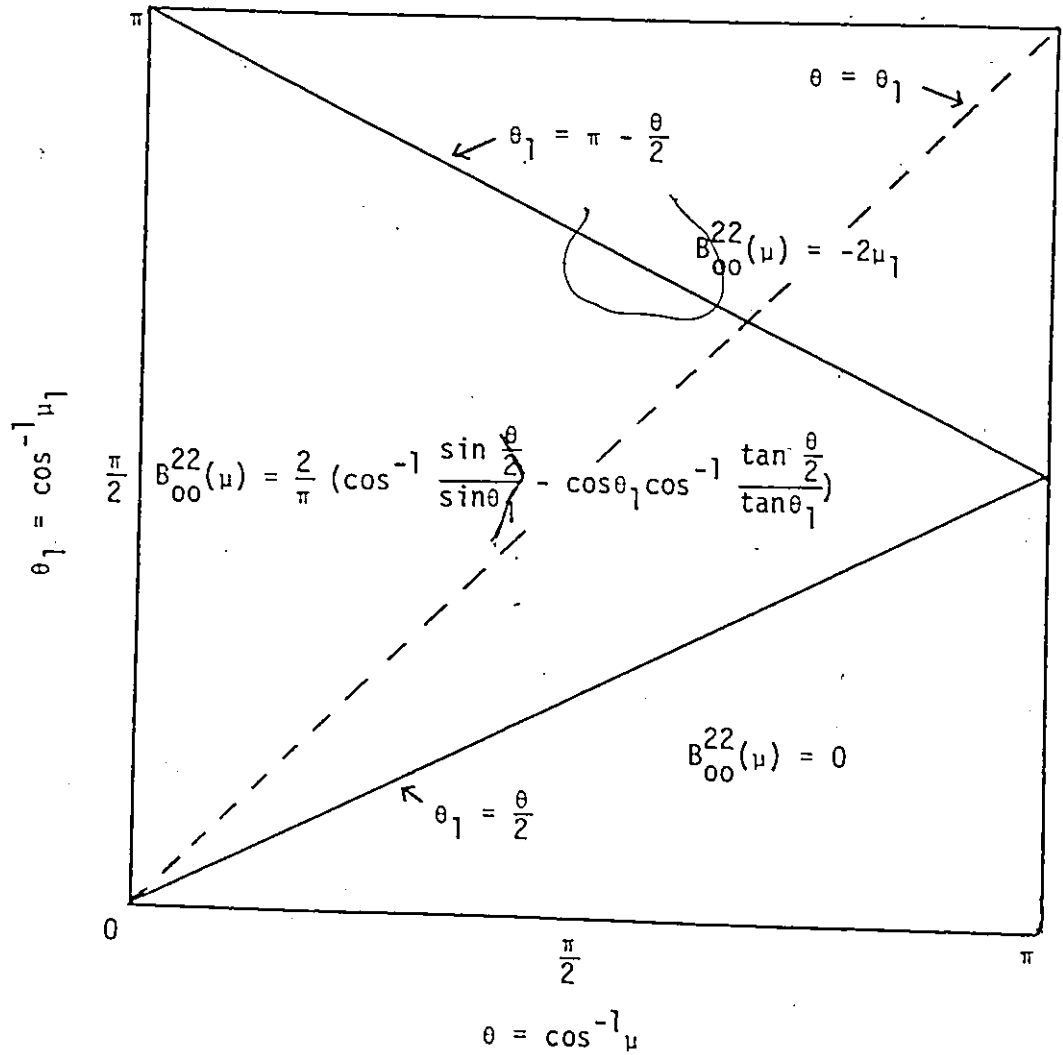


Fig. 4.15: The integral  $B_{00}^{22}(\mu)$  as a function of  $\theta$  and  $\theta_1$  for the  $2P_0-2P_0$  approximation.

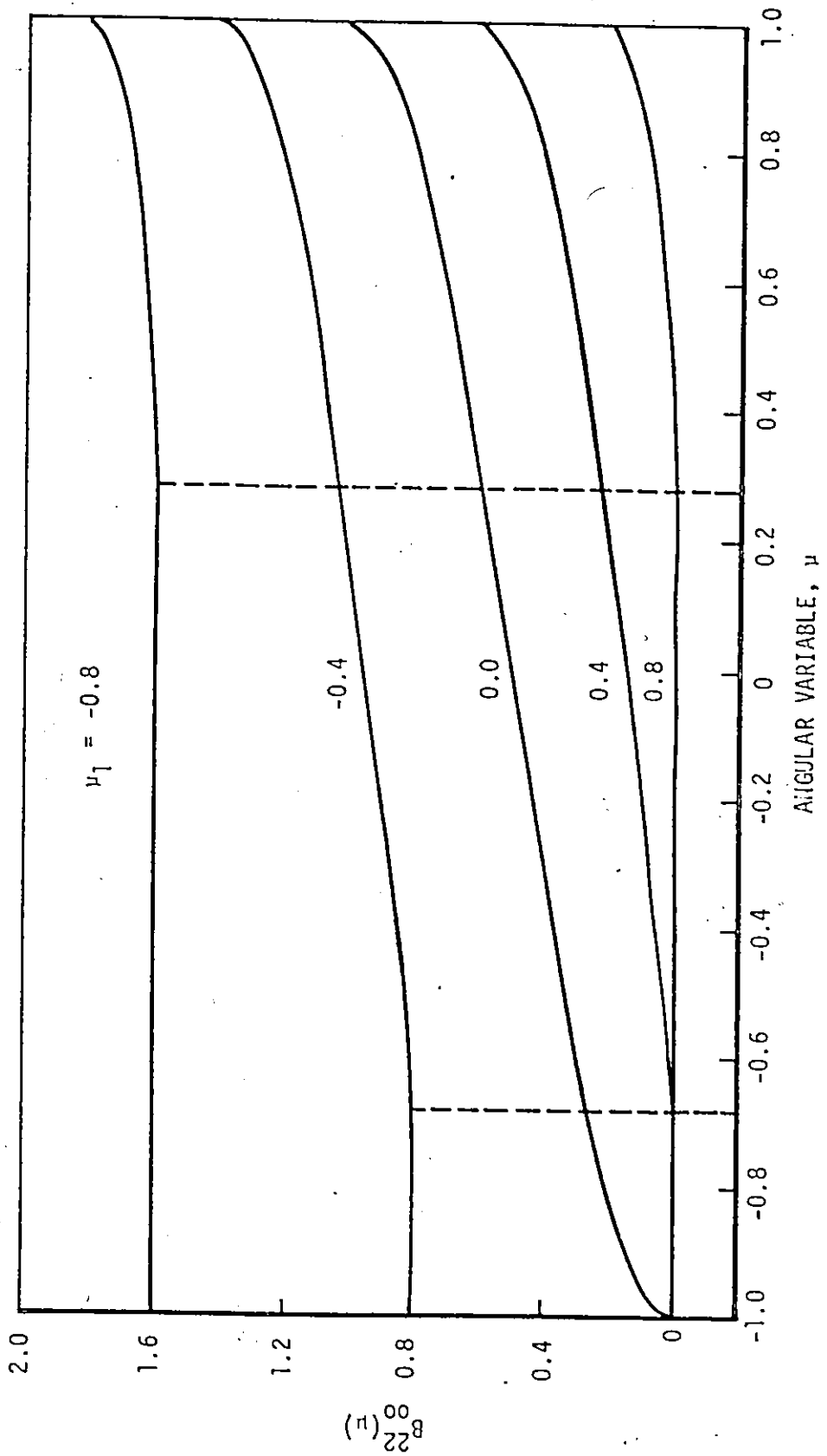


Fig. 4.16: The integral  $B_{00}^{22}(\mu)$  as a function of the angular variable  $\mu$  for various values of angular segmentation  $\nu_1$  for the  $2P_0-2P_0$  approximation.



$$B_{00}^{12}(\mu) = B_{00}^{21}(\mu) = 1 - \mu_1 - B_{00}^{22}(\mu) \quad (4.98)$$

The symmetry in these integrals, Eq. (4.98), appears because of the assumption that  $\mu_1 = \mu_{S1}$  which is, in a sense, similar to the  $DP_0 - DP_0$  integrals, Eq. (4.41).

The integrals  $A_0^Y$  are discussed in Appendix C. The results can be summarized as the following

$$A_{000}^{111} = 2\mu_1(1 + \mu_1) + A_{000}^{122}, \quad (4.99)$$

$$A_{000}^{112} = A_{000}^{121} = 1 - \mu_1^2 - A_{000}^{122}, \quad (4.100)$$

$$A_{000}^{211} = 2\mu_1(1 - \mu_1) + A_{000}^{222}, \quad (4.101)$$

$$A_{000}^{212} = A_{000}^{221} = 1 - \mu_1^2 - A_{000}^{222}, \quad (4.102)$$

where  $A_{000}^{122}$  and  $A_{000}^{222}$  are also functions of  $\mu_1$ . However, their expressions depend on the range of  $\mu_1$  as follows

$$1) \quad +1 > \mu_1 \geq 0$$

$$A_{000}^{122} = \int_{\mu=2\mu_1-1}^{\mu_1} B_{00}^{22}(\mu) d\mu, \quad (4.103)$$

and

$$A_{000}^{222} = \int_{\mu=\mu_1}^1 B_{00}^{22}(\mu) d\mu, \quad (4.104)$$

$$2) \quad 0 \geq \mu_1 \geq -0.5$$

$$A_{000}^{122} = -4\mu_1^3 + \int_{\mu=2\mu_1^2-1}^{\mu_1} B_{00}^{22}(\mu) d\mu, \quad (4.105)$$

and

$$A_{000}^{222} = \int_{\mu=\mu_1}^1 B_{00}^{22}(\mu) d\mu. \quad (4.106)$$

$$3) \quad -0.5 \geq \mu_1 > -1$$

$$A_{000}^{122} = -2\mu_1(1 + \mu_1), \quad (4.107)$$

and

$$A_{000}^{222} = 2\mu_1(1 + \mu_1 - 2\mu_1^2) + \int_{\mu=2\mu_1^2-1}^1 B_{00}^{22}(\mu) d\mu. \quad (4.108)$$

In Eqs. (4.103) to (4.108) the expression of the integral  $B_{00}^{22}(\mu)$  is that of the range  $\pi - \theta/2 \geq \theta_1 \geq \theta/2$  of Fig. 4.15.

A special case of the above integrals is given when  $\mu_1 = 0$ .

This case corresponds to the  $DP_0$ - $DP_0$  approximation of Section 4.5.

For  $\mu_1 = 0$ , Eqs. (4.99) to (4.108) yield

$$A_{000}^{111} = A_{000}^{122} = A_{000}^{212} = A_{000}^{221} = \frac{1}{\pi}, \quad (4.109)$$

and

$$A_{000}^{112} = A_{000}^{121} = A_{000}^{211} = A_{000}^{222} = 1 - \frac{1}{\pi}. \quad (4.110)$$

These results agree with that of the  $DP_0$ - $DP_0$  approximation, Eqs. (4.42) and (4.43), respectively, which have been already derived from a

different starting point in Section 4.5.

The integrals involved in  $A_{000}^{122}$  and  $A_{000}^{222}$  are calculated numerically. The Gaussian quadrature formula with 10 points<sup>(69)</sup> has been used. Table 4.3 gives the constants  $A_0^Y$  for various values of  $\mu_1$  similar to that of Fig. 4.16. From the numerical results of  $A_0^Y$  we have found that

$$A_{000}^{121} = A_{000}^{112} = A_{000}^{211} , \quad (4.111)$$

and

$$A_{000}^{122} = A_{000}^{221} = A_{000}^{212} . \quad (4.112)$$

Again, in order to test the accuracy of this approximation we will use it to calculate the eigenvalues associated with the Milne problem. Introducing the ansatz of Eq. (4.50) for the solution of the partial-range moments of the flux into Eqs. (4.92) and (4.93) and rearranging we obtain the following matrix form

$$\begin{bmatrix} \frac{2 - \alpha_1}{1 - \mu_1} - \frac{1}{\nu} & \frac{\beta_1}{1 - \mu_1} \\ -\frac{\alpha_2}{1 + \mu_1} & \frac{2 - \beta_2}{1 + \mu_1} - \frac{1}{\nu} \end{bmatrix} \begin{bmatrix} A_1 \\ A_2 \end{bmatrix} = 0 , \quad (4.113)$$

where  $1/\nu$  is the eigenvalue and  $A_1$  and  $A_2$  are the eigenvectors. From the above system we can write the following equation governing the eigenvalue

$$\left(\frac{1}{\nu}\right)^2 + a\left(\frac{1}{\nu}\right) + b = 0 , \quad (4.114)$$

where  $a$  and  $b$  are constants given by

$\mu_1$	$A_{000}^{111}$	$A_{000}^{121}$	$A_{000}^{112}$	$A_{000}^{122}$	$A_{000}^{211}$	$A_{000}^{221}$	$A_{000}^{212}$	$A_{000}^{222}$
-0.8	0.0	0.04000	0.04000	0.32000	0.039985	0.32001	0.32001	2.9200
-0.4	0.0065348	0.35347	0.35347	0.48653	0.35340	0.48660	0.48660	1.4734
0.0	0.31831	0.68169	0.68169	0.31831	0.68169	0.31831	0.31831	0.68169
0.4	1.2512	0.70882	0.70882	0.13118	0.70880	0.13120	0.13120	0.22880
0.8	2.8960	0.34404	0.34404	0.015959	0.34404	0.015961	0.015961	0.024039

Table 4.3: The  $A_0^Y$  constants of the  $2P_0-2P_0$  approximation for various values of  $\mu_1$ .

$$a = \frac{2 - \alpha_1}{1 - \mu_1} - \frac{2 - \beta_2}{1 + \mu_1} \quad (4.115)$$

and

$$b = \frac{\beta_1 \alpha_2 - (2 - \alpha_1)(2 - \beta_2)}{1 - \mu_1^2} \quad (4.116)$$

where the  $\alpha$ 's and  $\beta$ 's are given by Eqs. (4.94) and (4.95), respectively.

The eigenvalues are calculated using this approximation and the results are given in Figs. 4.17 to 4.20. Figure 4.17 gives the eigenvalue for  $c = 0.5$  as a function of the angular segmentation  $\mu_1$  for the two extreme cases of anisotropic scattering, i.e.  $\Delta f = +1$  and  $-1$ , respectively. From this figure we can see that the general behaviour of the eigenvalue with  $\mu_1$  and  $\Delta f$  is in agreement with the results of Chapter III, Fig. 3.3. In Figs. 4.18 to 4.20 the eigenvalue is given as a function of the degree of anisotropy  $\Delta f$  for various values of the angular segmentation  $\mu_1$  and three values of  $c$ ; 0.95, 0.5 and 0.1, respectively, representing a high, intermediate, and low value of  $c$ . From these figures we can observe the following characteristics for this particular approximation:

- 1) the eigenvalue varies approximately linearly with  $\Delta f$ ;
- 2) for a particular value of  $\Delta f$  the eigenvalue changes considerably as  $\mu_1$  changes.

The dashed lines in Figs. 4.18 to 4.20 represent the isotropic case of scattering and again it is in agreement with the results given in Chapter III, Figs. 3.2 and 3.3.

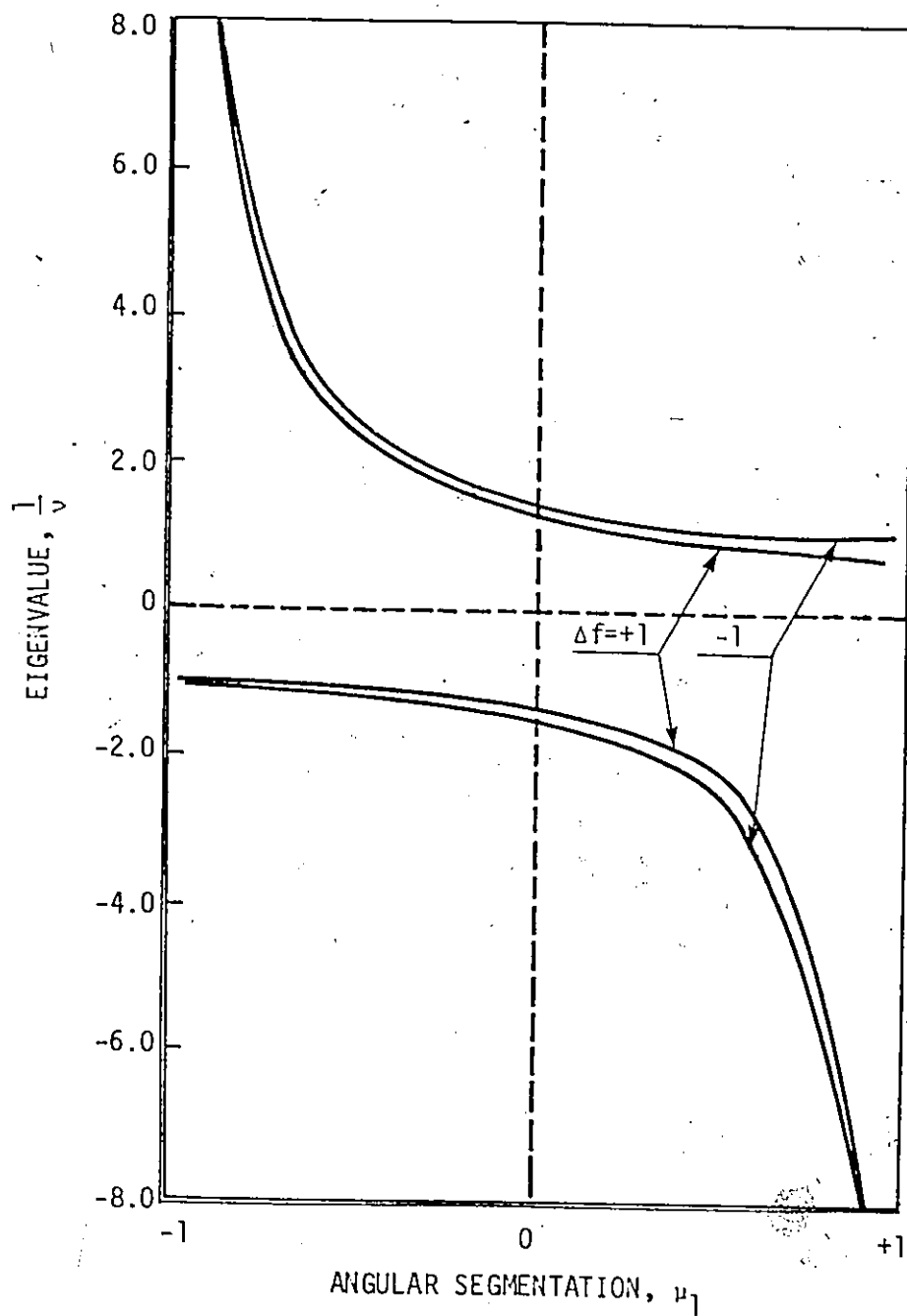


Fig. 4.17: Eigenvalue spectrum as a function of angular segmentation  $\mu_1$  for  $c = 0.5$  and  $\Delta f = +1$  and  $-1$ , respectively.

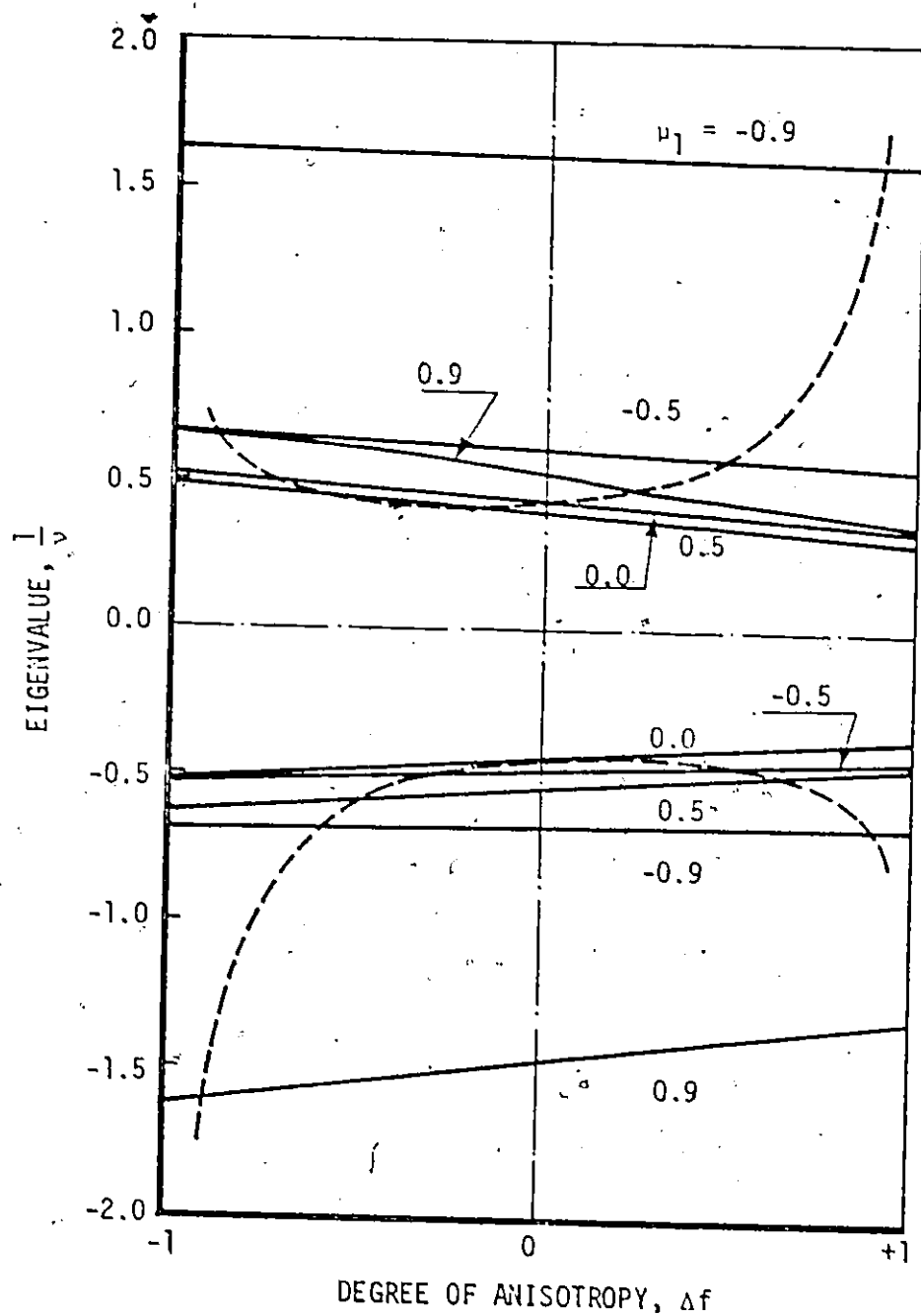


Fig. 4.18: Eigenvalue spectrum as a function of the degree of anisotropy for  $c = 0.95$  and various values of angular segmentation using the  $2P_0 - 2P_0$  approximation; the dashed curves correspond to isotropic scattering.

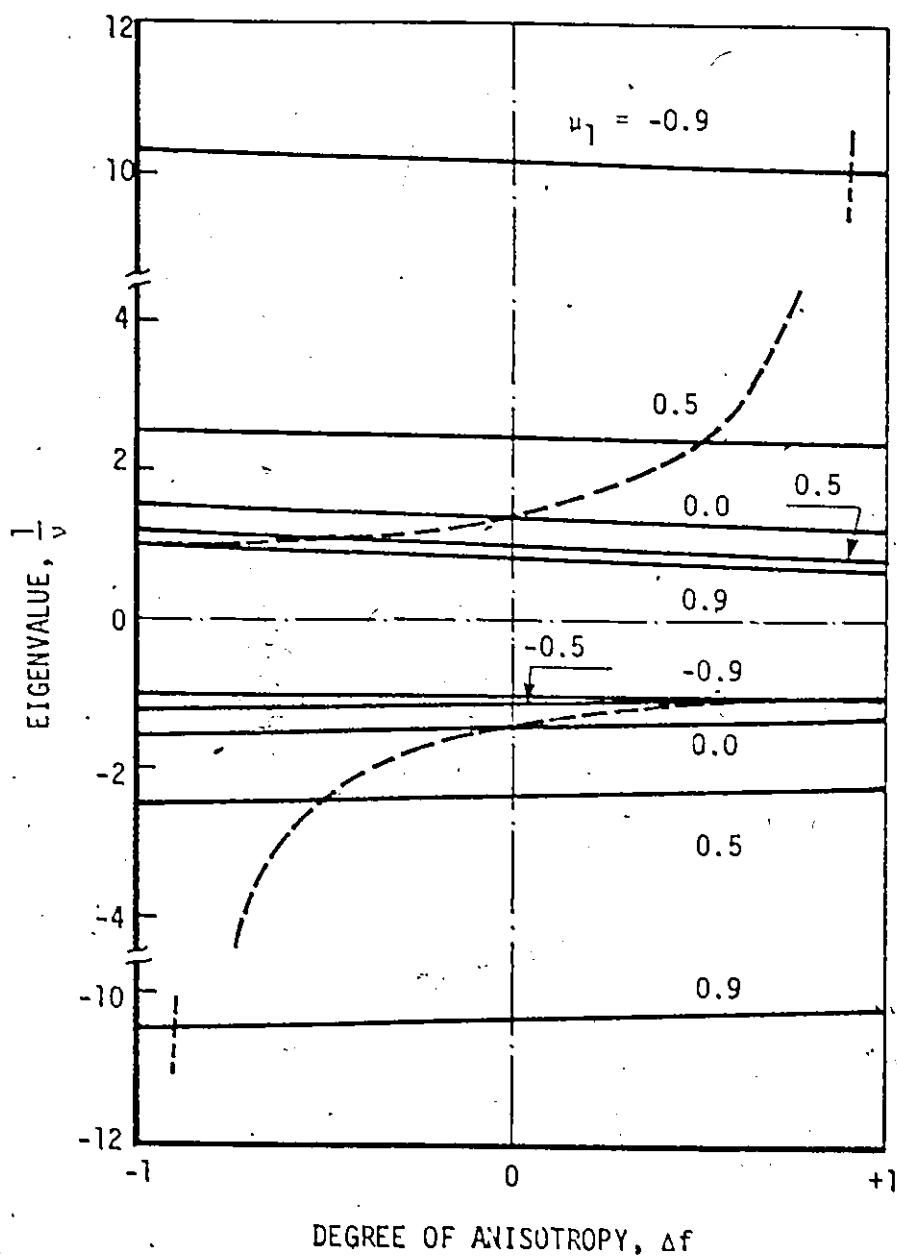


Fig. 4.19: Eigenvalue spectrum as a function of the degree of anisotropy for  $c = 0.5$  and various values of angular segmentation using the  $2P_0 - 2P_0$  approximation; the dashed curves correspond to isotropic scattering.



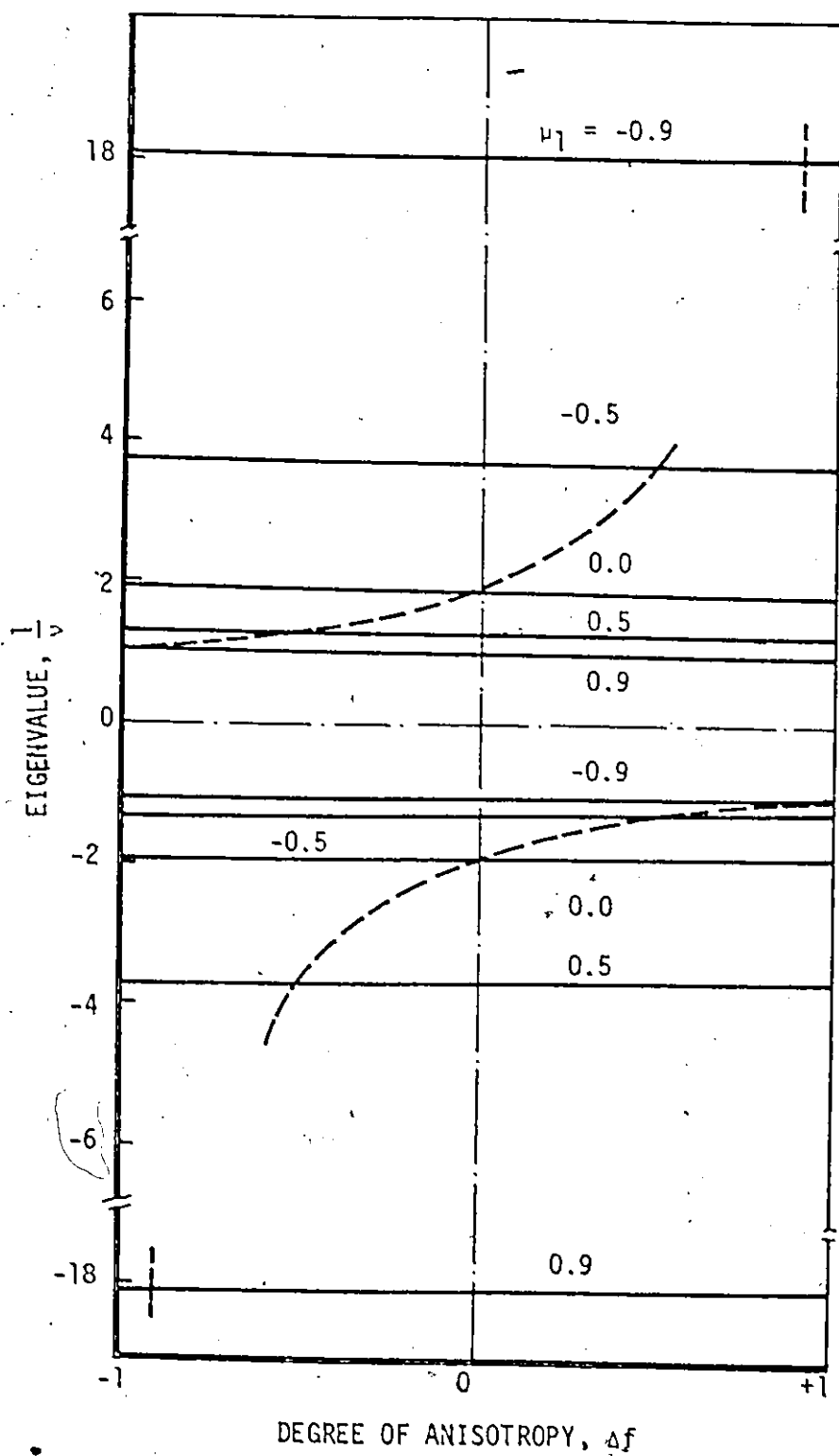


Fig. 4.20: Eigenvalue spectrum as a function of the degree of anisotropy for  $c = 0.1$  and various values of angular segmentation using the  $2P_0-2P_0$  approximation; the dashed curves correspond to isotropic scattering.

#### 4.8 Comparison Between the DP<sub>0</sub>-DP<sub>0</sub>, DP<sub>0</sub>-2P<sub>0</sub> and 2P<sub>0</sub>-2P<sub>0</sub> Approximations

In order to compare the results of the approximations described in the previous sections with the exact solution we have chosen to calculate the eigenvalue associated with the following fictitious scattering function

$$f^{N\pm}(\mu_s) = \frac{N+1}{2^{N+1}} (1 \pm \mu_s)^N, \quad (4.117)$$

where  $\mu_s$  is the cosine of the scattering angle. This scattering function is frequently used for some calculations in neutron transport<sup>(13,29,42,70)</sup>. It becomes increasingly anisotropic in the forward direction (+ sign) or in the backward direction (- sign) as the order of anisotropy  $N$  increases. In Fig. 4.21 the scattering function  $f^{N+}(\mu_s)$  is shown for various orders of anisotropy  $N$ . Very recently the eigenvalue spectrum for the tenth-order forward and backward scattering function for  $c = 0.95$  has been calculated exactly based on the singular eigenfunctions approach<sup>(29)</sup>.

The scattering function, Eq. (4.117), is expanded in terms of the 2P<sub>0</sub> approximation with the angular segmentation  $\mu_{s1}$  as a free parameter which can be any value between -1 and +1. The partial-range coefficients  $f_{1,0}$  and  $f_{2,0}$  are given by

$$f_{1,0} = \begin{cases} \frac{1}{2^{N+1}} (1 + \mu_{s1})^{N+1} & ; \text{ for forward scattering} \\ 1 - \frac{1}{2^{N+1}} (1 - \mu_{s1})^{N+1} & ; \text{ for backward scattering} \end{cases} \quad (4.118)$$

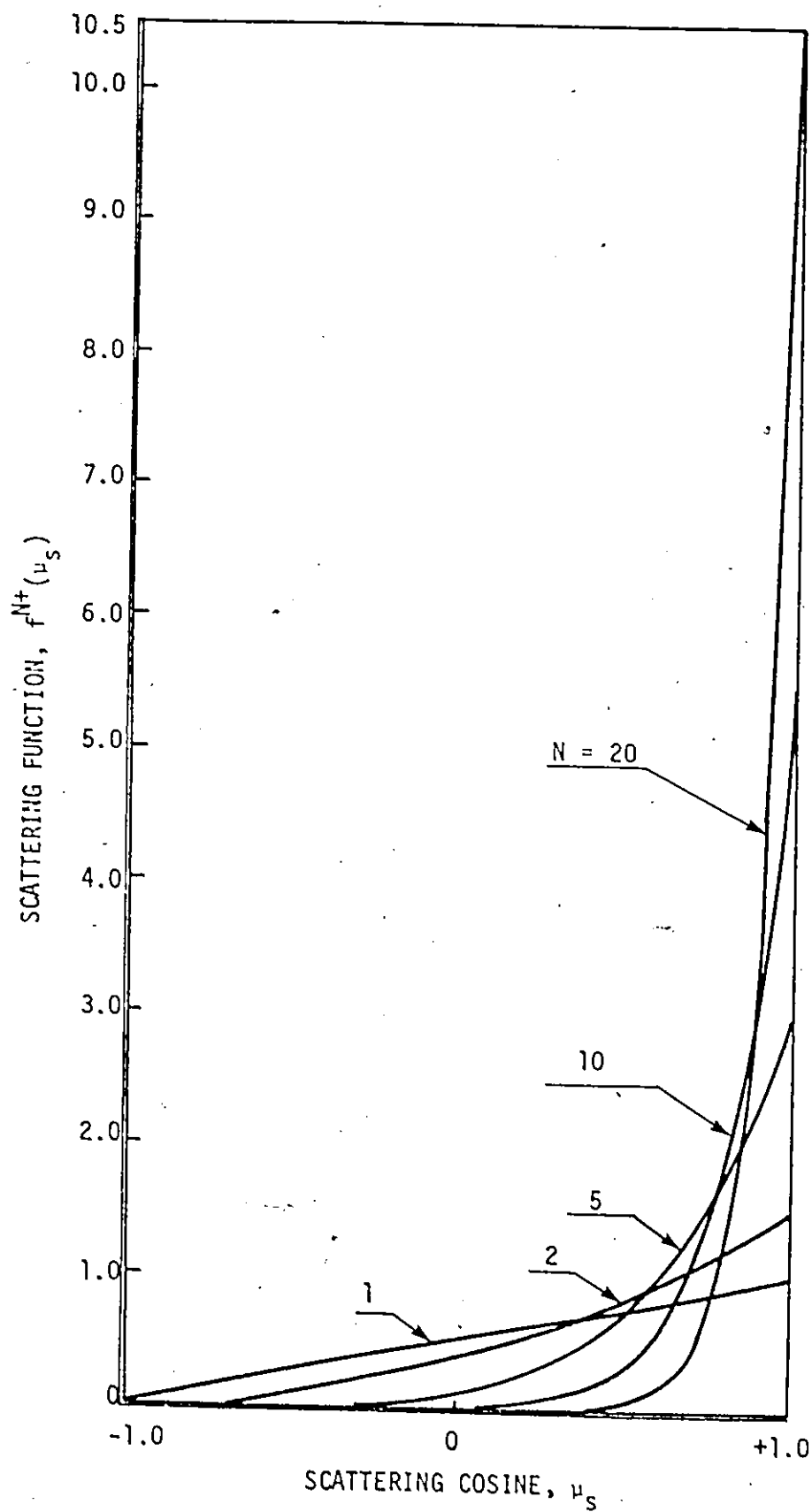


Fig. 4.21: The scattering function  $f^{N+}(\mu_s)$  for various orders of anisotropy.

and

$$f_{2,0} = 1 - f_{1,0} \quad (4.119)$$

For the purpose of this study the angular segmentation  $\mu_{s1}$  has been chosen according to the least-squares error criterion; that is, according to minimizing the function  $\epsilon$

$$\epsilon = \int_{-1}^{+1} \left[ \sum_{n=1}^2 \frac{f_{n,0}}{\mu_{sn} - \mu_{s,n-1}} P_{n,0}(\mu_s) - f(\mu_s) \right]^2 d\mu_s \quad (4.120)$$

For the particular scattering function  $f^{N+}(\mu_s)$  of Eq. (4.117), the function  $\epsilon$  is given by

$$\epsilon = \frac{(N+1)^2}{2(2N+1)} + \left[ \frac{(1+\mu_{s1})^{N+1}}{2^N} - \frac{(1+\mu_{s1})^{2N+1}}{2^{2N+1}} - 1 \right] / (1 - \mu_{s1}) \quad (4.121)$$

The condition  $\mu_{s1}$  which gives minimum  $\epsilon$  is given by the following

$$\begin{aligned} f(\mu_{s1}) &= \frac{1}{2^N} (1 + \mu_{s1})^N (N + 2 - N\mu_{s1}) \\ &- \frac{1}{2^{2N}} (1 + \mu_{s1})^{2N} (N + 1 - N\mu_{s1}) - 1 = 0 \end{aligned} \quad (4.122)$$

The angular segmentation  $\mu_{s1}$  which gives minimum  $\epsilon$  as well as the partial-range coefficients  $f_{1,0}$  and  $f_{2,0}$  corresponding to this angular segmentation for various orders of anisotropy are given in Table 4.4.

A special case is the  $DP_0$  representation of the scattering function which is used in the  $DP_0$ - $DP_0$  approximation. For this approximation, the partial-range coefficients of the tenth-order forward scattering function are given by

Order of Anisotropy	$\mu_{s1}$	$f_{1,0}$	$f_{2,0}$
1	0.0	0.25	0.75
2	0.28078	0.26262	0.73738
3	0.43968	0.26850	0.73150
4	0.58415	0.27191	0.72809
5	0.61196	0.27413	0.72587
10	0.78088	0.27903	0.72097
15	0.84738	0.28082	0.71918
20	0.88292	0.28175	0.71825

Table 4.4: The parameters  $\mu_{s1}$ ,  $f_{1,0}$  and  $f_{2,0}$  for the  $2P_0$  approximation of the scattering function  $f^{ilt}(\mu_s)$ .

$$f_{1,0} = 0.00048828 \quad (4.123)$$

and

$$f_{2,0} = 0.99951172 \quad (4.124)$$

The  $DP_0 - DP_0$ ,  $DP_0 - 2P_0$ , and  $2P_0 - 2P_0$  approximations studied in this chapter have been used to calculate the eigenvalue associated with the tenth-order forward and backward scattering function of Eq. (4.117). For the  $DP_0 - 2P_0$  approximation the segmentation  $\mu_{S1}$  of Table 4.4 is used in representing the scattering function while for the  $2P_0 - 2P_0$  approximation it is used as a segmentation for both the angular flux and the scattering function. The results are compared with the exact values in Table 4.5. From the results of Table 4.5 we can conclude the following:

- 1) Using the angular segmentation  $\mu_{S1} = 0.78088$ , which gives the best representation of the forward scattering function according to the least-squares error criterion, the  $DP_0 - 2P_0$  approximation gives the best eigenvalue for forward scattering based on the comparison with the smallest exact eigenvalue. As observed, Table 4.5, higher forward anisotropic scattering introduces multiple discrete eigenvalues. This makes the comparison difficult because in this case the solution depends on the weight of each discrete eigenvalue.

Approximation	Forward Scattering	Backward Scattering
Exact	$\pm 0.16926775$ $\pm 0.85065254$	$\pm 0.49434330$
$DP_0 - DP_0$ Approximation	$\pm 0.36197401$	$\pm 0.51862782$
$DP_0 - 2P_0$ Approximation	$\pm 0.32651138$	$\pm 0.54165517$
$2P_0 - 2P_0$ Approximation	$+0.40612891$ $-0.80630803$	$+0.97045304$ $-0.57049964$
$DP_0$ Approximation and $P_1$ Scattering Function	$\pm 0.28504385$	$\pm 0.56457949$

Table 4.5: Comparison of the eigenvalue  $(1/\nu)^\pm$  for the tenth-order scattering function  $f^{N^\pm}(\mu_s)$  and  $c = 0.95$ ; the exact results are extracted from reference (29).

2) For backward scattering the  $DP_0-DP_0$  approximation gives the best eigenvalue. This means that the angular segmentation  $\mu_{S1} = -0.78088$ , which gives the best representation of the backward scattering function, does not give the most accurate eigenvalue when used as a segmentation for either the  $DP_0-2P_0$  or  $2P_0-2P_0$  approximations.

We will compare these results with approximations of the same degree of complexity. The approximation we have chosen is the  $DP_0$  approximation of the angular flux with a full-range expansion of the scattering function in two terms. For the calculation of the eigenvalue, we used Eq. (3.40) which is appropriate for this case. The tenth-order scattering function of Eq. (4.117) is expanded in two terms of the full-range Legendre polynomial; the coefficients of expansion are given by<sup>(71)</sup>

$$f_0 = 1.0 \quad , \quad (4.125)$$

and

$$f_1 = \pm 0.83333333 \quad ; \quad (4.126)$$

where the positive sign corresponds to forward scattering and the negative sign for the backward scattering. The results of this approximation are also listed in Table 4.5.

From the table we note that, for backward scattering both the  $DP_0-DP_0$  and  $DP_0-2P_0$  approximations give better results than the  $DP_0$  approximation. For forward scattering the  $DP_0$  approximation is, in a sense, superior over the three other approximations of this formalism.



However, the full-range representation of the scattering function, in two terms gives negative cross section in some portions of the scattering angular space  $\mu_s$ . This negative cross section is not desirable in the neutron transport calculations.

The above results and conclusions suggest the study of the eigenvalue as a function of the angular segmentation  $\mu_{s1}$ , for this particular case of  $c = 0.95$  and the tenth-order scattering function of Eq. (4.117), using both the  $DP_0-2P_0$  and  $2P_0-2P_0$  approximations. Figure 4.22 shows the results of the  $DP_0-2P_0$  approximation while Fig. 4.23 shows that of the  $2P_0-2P_0$  approximation as well as the exact value of the eigenvalue for both cases. Also,  $\mu_{s1b}$  and  $\mu_{s1f}$ , which are the angular segmentations that give the best representation of the scattering function for backward and forward scattering, respectively, are shown in Figs. 4.22 and 4.23.

From Fig. 4.22 we see that it is possible to obtain the exact eigenvalue for backward scattering with two different angular segmentations, but these segmentations are not  $\mu_{s1b}$ . On the other hand, for forward scattering the most accurate eigenvalue we can obtain is the minimum of the curve of forward scattering in this figure. The angular segmentation corresponds to this minimum is also different from  $\mu_{s1f}$ . Here,  $\mu_{s1b}$  and  $\mu_{s1f}$  are the angular segmentations which give the best representation of the backward and forward scattering, respectively, according to the least-squares error criterion. From Fig. 4.23 we observe that only for backward scattering we obtain an exact positive eigenvalue. The most accurate negative eigenvalue is very close to the

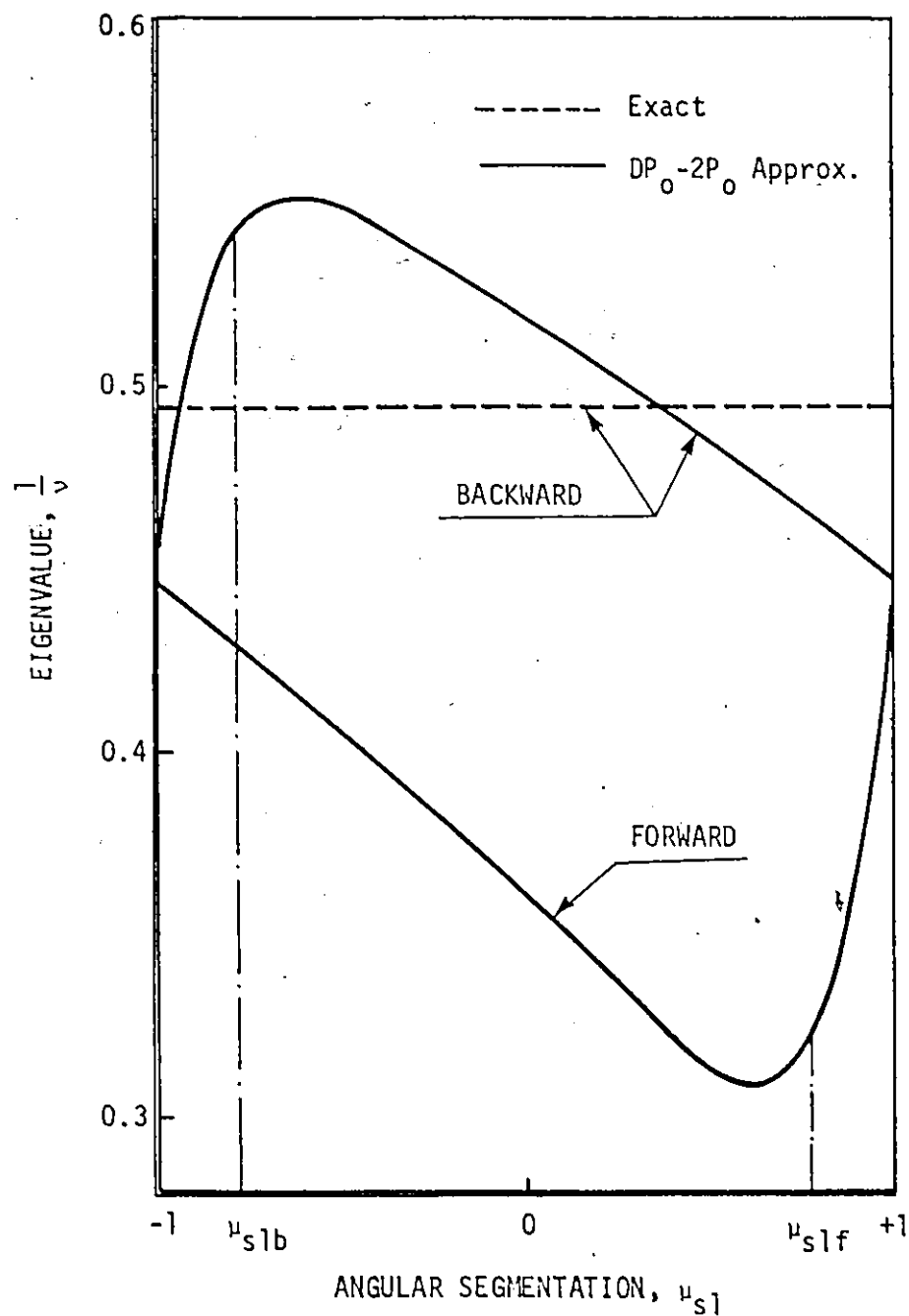


Fig. 4.22: Eigenvalue spectra as a function of scattering angular segmentation for  $c = 0.95$ ;  $\mu_{s1b}$  and  $\mu_{s1f}$  give the best representation for backward and forward scattering, respectively.

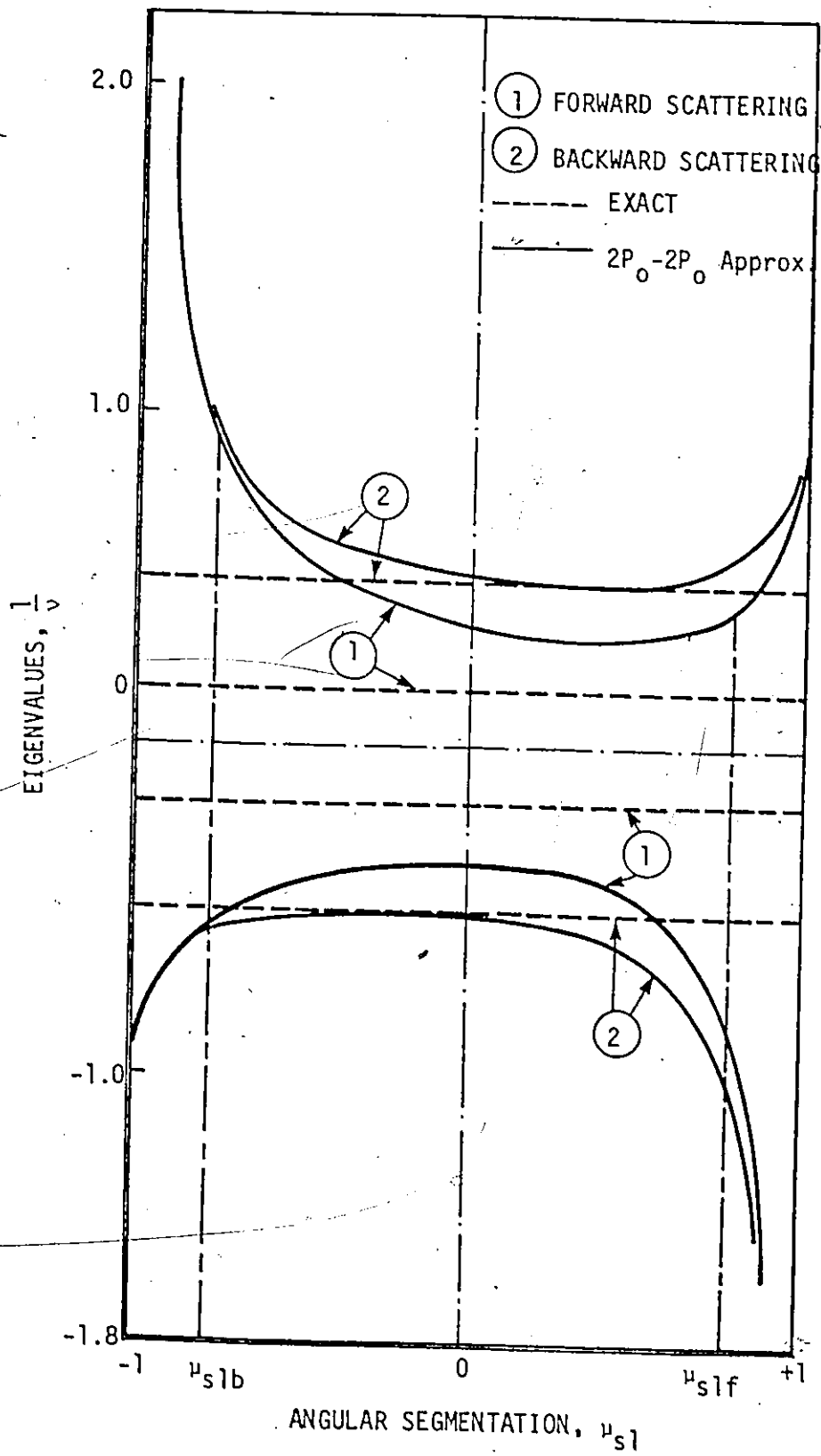


Fig. 4.23: Eigenvalue spectra as a function of angular segmentation for  $c = 0.95$ ;  $\mu_{slb}$  and  $\mu_{slf}$  give the best representation for backward and forward scattering, respectively.

exact one. However, it occurs at  $\mu_{s1}$  which is different from both  $\mu_{s1b}$  and the angular segmentation gives the exact positive eigenvalue. For forward scattering we never obtain the exact eigenvalue and the most accurate eigenvalues are almost as accurate as that of the  $DP_0-2P_0$  approximation. Thus, the conclusion of this comparison study is that the  $DP_0-2P_0$  approximation is the most appropriate approximation to treat such kinds of scattering function compared with the same order of other approximations. In addition, we conclude that the partial-range formalism appears most appropriate for treating the neutron transport equation with backward scattering and acceptable for forward scattering.

## CHAPTER V

### SPHERICAL GEOMETRY: POSITION DEPENDENT POINTS OF DISCONTINUITIES

#### 5.1 Introduction

In this chapter the solution of the one-group neutron transport equation in spherical geometry will be considered using the partial-range spherical harmonics formalism. Although the solutions of neutron transport problems by spherical harmonics are extensively employed in planar geometry, it is noteworthy that they have found little use in spherical geometry. The reasons for this selective avoidance are lucidly described by Gelbard<sup>(35)</sup> and by Bell and Glasstone<sup>(3)</sup>. Basically, difficulties are encountered in spherical systems because of the possibility of having directional discontinuities in either the angular flux or in its directional derivative in position dependent directions. It seems that this difficulty could be overcome if it were possible to establish a harmonic type solution formalism which embodies position dependent directional discontinuities.

The partial-range spherical harmonics, described in Chapter II and employed in the solution of the one-group neutron transport equation for plane geometry in Chapters III and IV, allow for discontinuities at arbitrary fixed directions. However, it is possible to extend this formalism with slight modifications to allow for position dependent directional discontinuities to describe the spherical systems. Here, we will develop a spherical harmonic-type solution of the neutron

transport equation in spherical geometry which allows for a position dependent segmentation of the directional variable. In essence, the solution admits the imposition of partial-range Legendre polynomials over position dependent directional segments.

Let us consider the idealized problem formulated by Gelbard<sup>(35)</sup> and mentioned in Section 1.3, which consists of a black absorbing spherical lump, Region I in Fig. 5.1, contained in a diffusing medium, identified as Region II in the same figure, with a neutron source at infinity to provide neutrons. Everywhere on the surface of the neutronically black sphere we have the following condition on the angular flux  $\psi(r, \mu)$ :

$$\psi(R, \mu) = 0 \quad \text{for} \quad \mu > 0, \quad (5.1)$$

where  $R$  is the radius of the absorbing sphere. Clearly, on the surface of the sphere, the angular flux is discontinuous at  $\mu = 0$ . However, at the point  $P$  in Region II, Fig. 5.1, we can conclude that  $\psi(r, \mu_1)$  is discontinuous at  $\mu_1 \neq 0$ , where

$$\mu_1 = \cos \theta_1 = \cos[\sin^{-1} \frac{R}{r}] ; \quad r \geq R. \quad (5.2)$$

Thus, the point of discontinuity has been shifted from  $\mu = 0$  to  $\mu = \mu_1$ ; indeed, this point  $\mu_1$  is a function of position  $r$ . Obviously this system of two different media possesses one point of directional discontinuity at  $\mu_1$ . This problem can be treated by a partial-range Legendre polynomials with two regions and position dependent segmentation at  $\mu_1$  given by Eq. (5.2).

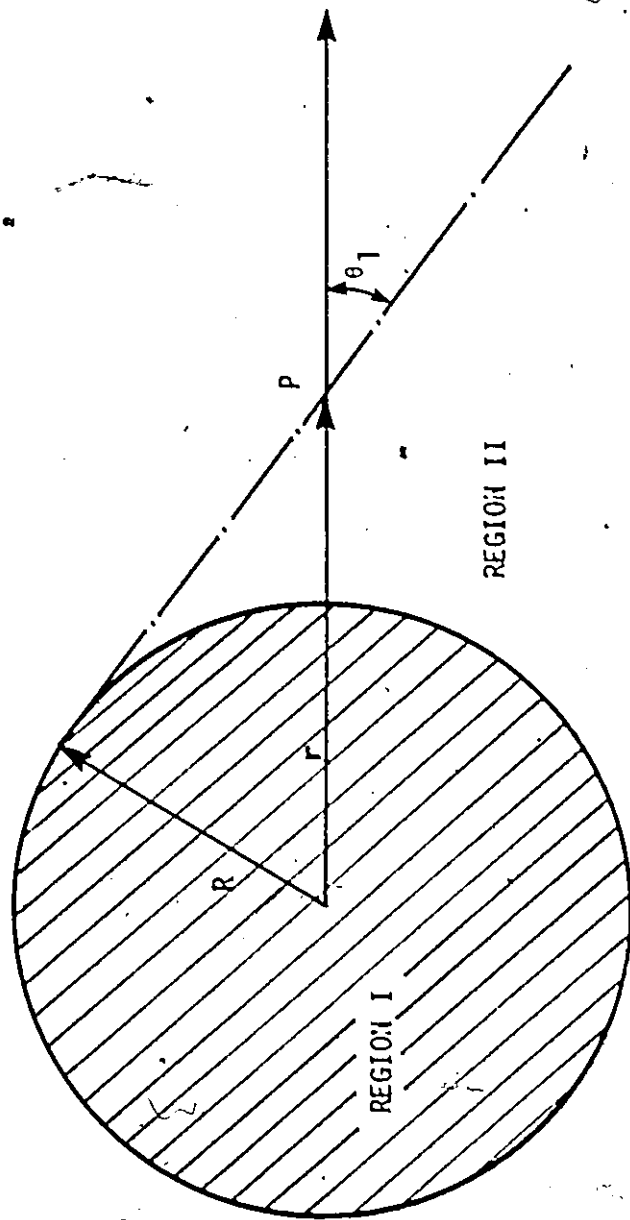


Fig. 5.1: Absorbing sphere in an infinite moderating medium. Region I: Black absorbing sphere;

Region II: Moderator with a source of neutrons at infinity.

Moreover, it is possible to have a spherical system with more than one of position dependent directional discontinuities. In the following we illustrate one such system, possessing a maximum of three directional discontinuities either in the angular flux or in its directional derivative. This system, Fig. 5.2, consists of four concentric spherical regions having different properties and different external sources of neutrons. In Region IV of Fig. 5.2, the discontinuities correspond to the cosines given by

$$\mu_n = \cos\theta_n = \cos\left[\sin^{-1} \frac{R_n}{r}\right]; \quad r \geq R_n, \quad (5.3)$$

where  $n = 1, 2$  and  $3$ . We emphasize that  $\mu_n$  ( $n = 1, 2$  and  $3$ ) are functions of position  $r$ . Clearly, we can have  $N$  numbers of position dependent directional discontinuities in an  $(N+1)$  concentric spherical systems with different properties and sources of neutrons. It is obvious that a partial-range Legendre polynomial formalism with  $N$  position dependent segmentations is required for the treatment of such problems.

## 5.2 Solution Formalism

The time-independent one-group neutron transport equation in spherical geometry for a homogeneous medium is given by Eq. (1.3). For convenience it is rewritten here as

$$\begin{aligned} & \mu \frac{\partial \psi(r, \mu)}{\partial r} + \frac{1 - \mu^2}{r} \frac{\partial \psi(r, \mu)}{\partial \mu} + \psi(r, \mu) \\ & = c \int_{\Omega'} \psi(r, \mu') f(\underline{\Omega}', \underline{\Omega}) d\underline{\Omega}' + \frac{S(r, \mu)}{\Sigma} \end{aligned} \quad (5.4)$$



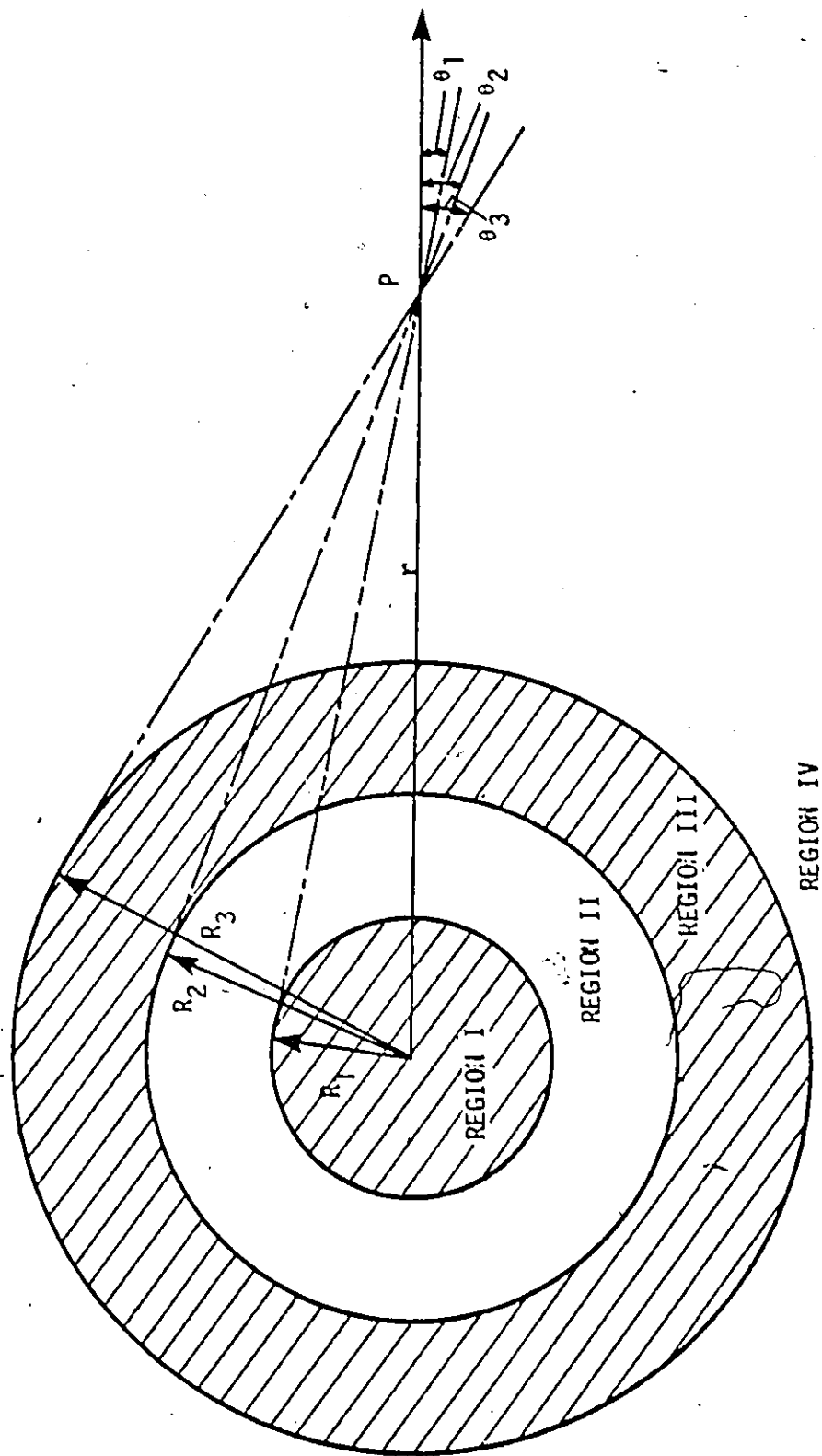


Fig. 5.2: Concentric spherical system possessing three directional discontinuities. Region I: Black absorbing sphere; Region II: Moderator with  $\Sigma_2$  and a source of neutrons  $S_2$ ; Region III: Moderator with  $\Sigma_3$  and a source of neutrons  $S_3$ ; Region IV: Moderator with  $\Sigma_4$  and a source of neutrons  $S_4$ .

To write the above equation, Eq. (5.4), in a form which allows for discontinuities of  $\psi(r, \mu)$  and/or its directional derivative at  $\mu = \mu_n$  requires that its second term be rewritten. It is clear that this term, containing the derivative of  $\psi(r, \mu)$  with respect to  $\mu$  must be proportional to the Dirac delta distribution functions at each  $\mu_n$ . Integrating this proportionality relationship over the range  $(\mu_n - \epsilon, \mu_n + \epsilon)$  results in

$$\left. \frac{1 - \mu^2}{r} \frac{\partial \psi(r, \mu)}{\partial \mu} \right|_{\mu = \mu_n} = \frac{1 - \mu_n^2}{r} [\psi^+(r, \mu_n) - \psi^-(r, \mu_n)] \delta(\mu - \mu_n), \quad (5.5)$$

where,

$$\psi^+(r, \mu_n) = \lim_{\mu \rightarrow \mu_n^+} \psi(r, \mu), \quad (5.6)$$

and

$$\psi^-(r, \mu_n) = \lim_{\mu \rightarrow \mu_n^-} \psi(r, \mu). \quad (5.7)$$

For the general case of  $N$  segmentation, Eq. (5.4), therefore can be rewritten as

$$\begin{aligned} & \mu \frac{\partial \psi(r, \mu)}{\partial r} + \left. \frac{1 - \mu^2}{r} \frac{\partial \psi(r, \mu)}{\partial \mu} \right|_{\mu \neq \mu_n} \\ & + \sum_{n=1}^{N-1} \frac{1 - \mu_n^2}{r} [\psi^+(r, \mu_n) - \psi^-(r, \mu_n)] \delta(\mu - \mu_n) + \psi(r, \mu) \\ & = c \int_{\Omega'} \psi(r, \mu') f(\underline{\Omega}', \underline{\Omega}) d\Omega' + \frac{1}{\Sigma} S(r, \mu) \end{aligned} \quad (5.8)$$

We note here that Eq. (5.8) incorporates discontinuities in the angular flux  $\psi(r, \mu)$  and/or its directional derivatives at  $\mu = \mu_n$ ,  $n = 1, 2, \dots, (N-1)$ . The presence of the delta-functions is associated specifically with the assumption of the discontinuities in the angular flux. We should note that in reality it is not necessary to have these discontinuities all the time.

We now expand the angular flux  $\psi(r, \mu)$  and the neutron source  $S(r, \mu)$  in terms of the partial-range Legendre polynomials as follows

$$\psi(r, \mu) = \sum_{n=1}^N \sum_{\ell=0}^{\infty} \frac{2\ell + 1}{\mu_n - \mu_{n-1}} \phi_{n,\ell}(r) P_{n,\ell}(\mu) \quad (5.9)$$

and

$$S(r, \mu) = \sum_{n=1}^N \sum_{\ell=0}^{\infty} \frac{2\ell + 1}{\mu_n - \mu_{n-1}} s_{n,\ell}(r) P_{n,\ell}(\mu) \quad (5.10)$$

These expansions are similar to those used with plane geometry, Eqs. (3.2) and (3.4), respectively, but here the segmentations are functions of the position  $r$ . The partial-range moments of the flux  $\phi_{n,\ell}(r)$  and the coefficients of the source  $s_{n,\ell}(r)$  are given by similar equations to Eqs. (3.3) and (3.5), respectively. The partial-range Legendre polynomials  $P_{n,\ell}(\mu)$  are defined by Eq. (2.2); the segmentations  $\mu_n$  are functions of the position  $r$  and given by Eq. (5.3) for arbitrary number  $N$ .

The scattering function is expanded in the conventional form in terms of full-range spherical harmonics, Eq. (3.6). Though clearly, it is possible to use partial-range expansion of the scattering function, Eq. (4.1), as well. However, the purpose of the study in this chapter is to emphasize the effect of satisfying the boundary conditions of the

neutron flux exactly within the spherical harmonics approximation.

Proceeding further with Eq. (5.8) requires that the Dirac delta distribution functions be eliminated by expansion in terms of the partial-range Legendre polynomials. From the known properties of the delta function we can write

$$\int_{\mu_{n-1}}^{\mu_n} P_{n,\ell}(\mu) \delta(\mu - \mu_n) d\mu = \frac{1}{2} P_{n,\ell}(\mu_n) \quad (5.11)$$

and

$$\int_{\mu_n}^{\mu_{n+1}} P_{n+1,\ell}(\mu) \delta(\mu - \mu_n) d\mu = \frac{1}{2} P_{n+1,\ell}(\mu_n) \quad (5.12)$$

In the above integrals, we have assumed that the  $\delta$ -function is symmetric about  $\mu = \mu_n$ . In previous work by Wang<sup>(19)</sup>, who employed the double-spherical harmonics approximation in spherical geometry, the effect of distributing the  $\delta$ -function between the forward and backward directions has been discussed. However, for the purpose of this work it appears adequate to assume that the  $\delta$ -function is symmetric about  $\mu = \mu_n$ .

Employing the general orthogonality of the partial-range Legendre polynomials over an arbitrary directional interval  $(\mu_n - \mu_{n-1})$ , Eq. (2.18), together with Eqs. (5.11) and (5.12) results in the following expression for  $\delta(\mu - \mu_n)$

$$\begin{aligned} \delta(\mu - \mu_n) &= \sum_{\ell=0}^{\infty} \frac{2\ell + 1}{2} \left[ \frac{1}{\mu_n - \mu_{n-1}} P_{n,\ell}(\mu) P_{n,\ell}(\mu_n) \right. \\ &\quad \left. + \frac{1}{\mu_{n+1} - \mu_n} P_{n+1,\ell}(\mu) P_{n+1,\ell}(\mu_n) \right] \end{aligned} \quad (5.13)$$

Using the special values of  $P_{n,\ell}(\mu_n)$  and  $P_{n+1,\ell}(\mu_n)$ , Eqs. (2.27) and (2.28), respectively, results in

$$\begin{aligned} \delta(\mu - \mu_n) &= \sum_{\ell=0}^{\infty} \frac{2\ell + 1}{2} \left[ \frac{1}{\mu_n - \mu_{n-1}} P_{n,\ell}(\mu) \right. \\ &\quad \left. + \frac{(-1)^\ell}{\mu_{n+1} - \mu_n} P_{n+1,\ell}(\mu) \right] \end{aligned} \quad (5.14)$$

Equation (5.9) can be used to obtain an expression for the derivative term of  $\psi(r, \mu)$  with respect to the position  $r$ :

$$\begin{aligned} \frac{\partial \psi(r, \mu)}{\partial r} &= \sum_{n=1}^N \sum_{\ell=0}^{\infty} (2\ell + 1) \left\{ \frac{d}{dr} \left( \frac{1}{\mu_n - \mu_{n-1}} \right) \phi_{n,\ell}(r) P_{n,\ell}(\mu) \right. \\ &\quad \left. + \frac{1}{\mu_n - \mu_{n-1}} \left[ \frac{d\phi_{n,\ell}(r)}{dr} P_{n,\ell}(\mu) + \phi_{n,\ell}(r) \frac{dP_{n,\ell}(\mu)}{dr} \right] \right\} \end{aligned} \quad (5.15)$$

Here,  $\mu_n$  and  $\mu_{n-1}$  are functions of the position  $r$  and hence the partial-range Legendre polynomial  $P_{n,\ell}(\mu)$  is a function of  $r$  as well. The segmentation  $\mu_n$  is used as defined by Eq. (5.3) and the first derivative term of Eq. (5.15) is obtained by

$$\frac{d}{dr} \left( \frac{1}{\mu_n - \mu_{n-1}} \right) = \frac{-1}{(\mu_n - \mu_{n-1})^2} \left( \frac{d\mu_n}{dr} - \frac{d\mu_{n-1}}{dr} \right) \quad (5.16)$$

where, using Eq. (5.3),

$$\frac{d\mu_n}{dr} = \frac{1 - \mu_n^2}{r\mu_n} \quad (5.17)$$

Similarly, from Eq. (5.9), the derivative term of  $\psi(r, \mu)$  with respect to  $\mu$ , where  $\mu \neq \mu_n$ , is given by

$$\left. \frac{\partial \psi(r, \mu)}{\partial \mu} \right|_{\mu \neq \mu_n} = \sum_{n=1}^N \sum_{\ell=0}^{\infty} \frac{2\ell + 1}{\mu_n - \mu_{n-1}} \phi_{n,\ell}(r) P'_{n,\ell}(\mu) \Big|_{\mu \neq \mu_n}, \quad (5.18)$$

where,

$$P'_{n,\ell}(\mu) = \frac{dP_{n,\ell}(\mu)}{d\mu} \quad (5.19)$$

Finally, we write the expressions of the discrete term  $[\psi^+(r, \mu_n) - \psi^-(r, \mu_n)]$  of Eq. (5.8) as

$$\begin{aligned} \psi^+(r, \mu_n) - \psi^-(r, \mu_n) &= \sum_{\ell=0}^{\infty} (2\ell + 1) \left[ \frac{1}{\mu_{n+1} - \mu_n} \phi_{n+1,\ell}(r) P_{n+1,\ell}(\mu_n) \right. \\ &\quad \left. - \frac{1}{\mu_n - \mu_{n-1}} \phi_{n,\ell}(r) P_{n,\ell}(\mu_n) \right], \end{aligned} \quad (5.20)$$

which, in view of Eqs. (2.27) and (2.28), is clearly given by

$$\begin{aligned} \psi^+(r, \mu_n) - \psi^-(r, \mu_n) &= \sum_{\ell=0}^{\infty} (2\ell + 1) \left[ \frac{(-1)^\ell}{\mu_{n+1} - \mu_n} \phi_{n+1,\ell}(r) \right. \\ &\quad \left. - \frac{1}{\mu_n - \mu_{n-1}} \phi_{n,\ell}(r) \right]. \end{aligned} \quad (5.21)$$

The equations of the angular flux over the  $N$  intervals of  $\mu$  expressed explicitly in terms of the position dependent partial-range Legendre polynomials are obtained by direct substitution of the appropriate terms into Eq. (5.8). Table 5.1 lists this system of equations.

$$\begin{aligned}
& \mu \sum_{n=1}^N \sum_{\ell=0}^{\infty} (2\ell + 1) \left\{ \frac{d}{dr} \left( \frac{1}{\mu_n - \mu_{n-1}} \right) \phi_{n,\ell}(r) P_{n,\ell}(\mu) + \frac{1}{\mu_n - \mu_{n-1}} \left[ \frac{d\phi_{n,\ell}(r)}{dr} P_{n,\ell}(\mu) \right. \right. \\
& \left. \left. + \phi_{n,\ell}(r) \frac{dP_{n,\ell}(\mu)}{d\mu} \right] \right\} + \frac{1 - \mu^2}{r} \sum_{n=1}^N \sum_{\ell=0}^{\infty} \frac{2\ell + 1}{\mu_n - \mu_{n-1}} \phi_{n,\ell}(r) P'_{n,\ell}(\mu) \Big|_{\mu \neq \mu_n} \\
& + \sum_{n=1}^{N-1} \frac{1 - \mu_n^2}{r} \sum_{\ell=0}^{\infty} (2\ell + 1) \left[ \frac{(-1)^\ell}{\mu_{n+1} - \mu_n} \phi_{n+1,\ell}(r) - \frac{1}{\mu_n - \mu_{n-1}} \phi_{n,\ell}(r) \right] \\
& * \sum_{\ell'=0}^{\infty} \frac{2\ell' + 1}{2} \left[ \frac{1}{\mu_n - \mu_{n-1}} P_{n,\ell'}(\mu) + \frac{(-1)^{\ell'}}{\mu_{n+1} - \mu_n} P_{n+1,\ell'}(\mu) \right] \\
& + \sum_{n=1}^N \sum_{\ell=0}^{\infty} \frac{2\ell + 1}{\mu_n - \mu_{n-1}} \phi_{n,\ell}(r) P_{n,\ell}(\mu) \\
& = c \sum_{k=0}^{\infty} \frac{2k + 1}{2} f_k P_k(\mu) \left[ \sum_{n=1}^N \sum_{\ell=0}^{\infty} \frac{2\ell + 1}{\mu_n - \mu_{n-1}} \phi_{n,\ell}(r) \int_{\mu'} P_k(\mu') P_{n,\ell}(\mu') d\mu' \right] \\
& + \frac{1}{\Sigma} \sum_{n=1}^N \sum_{\ell=0}^{\infty} \frac{2\ell + 1}{\mu_n - \mu_{n-1}} s_{n,\ell}(r) P_{n,\ell}(\mu) .
\end{aligned}$$

Table 5.1: The one-group neutron transport equation in spherical geometry expressed in terms of position dependent partial-range Legendre polynomials.

### 5.3 Partial-Range Spatial Moments.

The conditions on the partial-range spatial moments,  $\phi_{n,\ell}(r)$ , are obtained by, first, multiplying each term of the neutron transport equation, Table 5.1, by  $P_{m,j}(\mu)$ . Each term is subsequently integrated over the  $m$ 'th range of the direction cosine, i.e.  $\mu \in (\mu_{m-1}, \mu_m)$ . The orthogonality and recurrence relationships of the partial-range Legendre polynomials of Chapter II are thereupon used to eliminate the directional dependence resulting in the expression of  $\phi_{n,\ell}(r)$ .

By inspection of terms in Table 5.1, we note that the operations implied above involve integration of products of partial-range Legendre polynomials and/or its derivatives. Some of these integrals have been already evaluated in Chapter III, Eqs. (3.15) and (3.17). However, the other integrals will be considered here. Starting with the following integral

$$I_3 = \int_{\mu_{m-1}}^{\mu_m} (1 - \mu^2) P_{m,j}(\mu) P'_{n,\ell}(\mu) d\mu \quad (5.22)$$

where  $P'_{n,\ell}(\mu)$  is defined by Eq. (5.19). We write Eq. (5.22) as a sum

$$I_3 = b_{j\ell}^{mn} - d_{j\ell}^{mn} \quad (5.23)$$

where,

$$b_{j\ell}^{mn} = \int_{\mu_{m-1}}^{\mu_m} P_{m,j}(\mu) P'_{n,\ell}(\mu) d\mu \quad (5.24)$$

and

$$d_{j\ell}^{mn} = \int_{\mu_{m-1}}^{\mu_m} \mu^2 P_{m,j}(\mu) P'_{n,\ell}(\mu) d\mu \quad (5.25)$$



These integrals are readily evaluated for arbitrary integral values of  $\lambda$ . Several low order terms can be shown to be given by

$$b_{j0}^{mn} = 0 \quad (5.26)$$

$$b_{j1}^{mn} = 2\delta_{j0}\delta_{mn} \quad (5.27)$$

$$d_{j0}^{mn} = 0 \quad (5.28)$$

and

$$d_{j1}^{mn} = \frac{2\alpha_n}{3} \sum_{\lambda=0}^2 a_{n,2,\lambda} \delta_{j\lambda} \delta_{mn} + \frac{2}{3} \delta_{j0} \delta_{mn} \quad (5.29)$$

where the coefficients  $a_{n,2,\lambda}$  have been defined by Eq. (2.30) and extensively discussed in Section 2.4. The interval function  $\alpha_n$  is defined by Eq. (2.13). We have studied the appropriate integrals further and found that the following recurrence relationships exist

$$b_{j\ell}^{mn} = b_{j,\ell-2}^{mn} + 2\delta_{j,\ell-1}\delta_{mn} \quad (5.30)$$

and

$$d_{j\ell}^{mn} = d_{j,\ell-2}^{mn} + \frac{2}{(2j+1)\alpha_n^2} e_{j\ell}^n \delta_{mn} \quad (5.31)$$

where  $e_{j\ell}^n$  is a function given by

$$\begin{aligned} e_{j\ell}^n = & \left[ \frac{(j+1)^2}{2j+3} + \beta_n(2j+1) \right] \delta_{j+1,\ell} + \frac{(j+1)(j+2)}{2j+3} \delta_{j+1,\ell-2} \\ & + 2\beta_n(j+1)\delta_{j+1,\ell-1} + \frac{j(j-1)}{2j-1} \delta_{j-1,\ell} + \frac{j^2}{2j-1} \delta_{j,\ell-1} \\ & + 2\beta_n j \delta_{j,\ell} \quad (5.32) \end{aligned}$$

with  $\beta_n$  given by Eq. (2.14). By Eqs. (5.26) to (5.32) the entire array of integrals of Eq. (5.22) can be evaluated.

The final integral is defined by

$$I_4 = \int_{\mu_{m-1}}^{\mu_m} \mu^{P_{m,j}}(\mu) \frac{dP_{n,\ell}(\mu)}{dr} d\mu \quad (5.33)$$

which, for reasons of subsequent notational convenience, we choose to define it by

$$I_4 = g_{j\ell}^{mn} \quad (5.34)$$

Using the chain rule of differentiation the above integral, Eq. (5.33), can be rewritten as

$$g_{j\ell}^{mn} = \frac{1}{\alpha_n} \left[ \frac{d\alpha_n}{dr} \int_{\mu_{m-1}}^{\mu_m} \mu^{2P_{m,j}}(\mu) P'_{n,\ell}(\mu) d\mu + \frac{d\beta_n}{dr} \int_{\mu_{m-1}}^{\mu_m} \mu^{P_{m,j}}(\mu) P'_{n,\ell}(\mu) d\mu \right] \quad (5.35)$$

which can be rewritten as

$$g_{j\ell}^{mn} = \frac{1}{\alpha_n} \left[ \frac{d\alpha_n}{dr} d_{j\ell}^{mn} + \frac{d\beta_n}{dr} h_{j\ell}^{mn} \right] \quad (5.36)$$

where  $d_{j\ell}^{mn}$  is defined by Eq. (5.25) and  $h_{j\ell}^{mn}$  is given by

$$h_{j\ell}^{mn} = \int_{\mu_{m-1}}^{\mu_m} \mu^{P_{m,j}}(\mu) P'_{n,\ell}(\mu) d\mu \quad (5.37)$$

The above integrals, Eq. (5.37), have been examined further and we can write the following relationship

$$h_{j\ell}^{mn} = \frac{1}{\alpha_n(2j+1)} [(j+1)b_{j+1,\ell}^{mn} + j b_{j-1,\ell}^{mn} + \beta_n(2j+1)b_{j\ell}^{mn}] \quad (5.38)$$

where  $b_{j\ell}^{mn}$  is defined by Eq. (5.24). The parameters  $\alpha_n$  and  $\beta_n$  are used as defined by Eq. (2.13) and (2.14), respectively, but  $\mu_n$  is a function of the position  $r$ . The derivative terms of Eq. (5.36) are obtained as

$$\frac{d\alpha_n}{dr} = \frac{-2}{(\mu_n - \mu_{n-1})^2} \left[ \frac{d\mu_n}{dr} - \frac{d\mu_{n-1}}{dr} \right] \quad (5.39)$$

and

$$\frac{d\beta_n}{dr} = \frac{2}{(\mu_n - \mu_{n-1})^2} \left[ \mu_{n-1} \frac{d\mu_n}{dr} - \mu_n \frac{d\mu_{n-1}}{dr} \right] \quad (5.40)$$

where the derivative  $d\mu_n/dr$  is given by Eq. (5.17).

Following the procedure described earlier in this section and using the integrals  $I_1$ ,  $I_2$ ,  $I_3$  and  $I_4$  of Eqs. (3.15), (3.17), (5.23) and (5.34), respectively, as well as the orthogonality condition of the partial-range Legendre polynomials, Eq. (2.18), the resultant system of equations for the partial-range spatial moments  $\phi_{n,\ell}(r)$  is found in Table 5.2.

#### 5.4 Two-Range Approximation

For the purpose of numerical illustration, the low-order

$$\frac{\nu_n - \nu_{n-1}}{2j+1} \{ (\nu_n - \nu_{n-1}) [j \phi_{n,j-1}(r) + (j+1) \phi_{n,j+1}(r)] + (2j+1)(\nu_n + \nu_{n-1}) \phi_{n,j}(r) \} \frac{d}{dr} \left( \frac{1}{\nu_n - \nu_{n-1}} \right)$$

$$+ \frac{\nu_n - \nu_{n-1}}{2j+1} \left[ j \frac{d \phi_{n,j-1}(r)}{dr} + (j+1) \frac{d \phi_{n,j+1}(r)}{dr} \right] + (\nu_n + \nu_{n-1}) \frac{d \phi_{n,j}(r)}{dr}$$

$$+ \sum_{l=0}^{\infty} \frac{2(2l+1)}{\nu_n - \nu_{n-1}} \phi_{n,l}(r) g_{jl}^{mn} + \frac{2}{r} \sum_{l=0}^{\infty} \frac{2l+1}{\nu_n - \nu_{n-1}} \phi_{n,l}(r) [b_{jl}^{nn} - d_{jl}^{nn}]$$

$$+ \sum_{l=1}^{n-1} \frac{1 - \nu_n^2}{r} \left[ \frac{(-1)^l}{\nu_{n+1} - \nu_n} \phi_{n+1,l}(r) - \frac{1}{\nu_n - \nu_{n-1}} \phi_{n,l}(r) \right] [\delta_{lm} + (-1)^j \delta_{m+1,n}] + 2 \phi_{n,j}(r)$$

$$= c \sum_{l=0}^{n-1} \sum_{k=0}^l \frac{(2l+1)(2k+1)}{\nu_n - \nu_{n-1}} f_{ln,il,j}^a \phi_{n,i,k}(r) + \frac{2}{r} s_{n,j}(r) ;$$

$n = 1, 2, \dots$ , if and  $j = 0, 1, 2, \dots, \infty$ .

Table 5.2: System of equations of partial-range spatial moments  $\phi_{n,l}(r)$  for  $\nu \in (\nu_{n-1}, \nu_n)$ .

approximation case of  $N = 2$  will be considered. By this case of study we are able to describe the two media problem defined by Gelbard<sup>(35)</sup> and explained here in the introduction section and given by Fig. 5.1.

At every point in the space of region II, Fig. 5.1, there are two ranges of the direction cosine from  $-1$  to  $\mu_1$  and from  $\mu_1$  to  $+1$ . Herein, we have chosen to segment the direction cosine by  $\mu_1$ , where  $\mu_1$  is given by Eq. (5.2). For this two-range problem the backward and forward flux moments are given by  $\phi_{1,e}(r)$  and  $\phi_{2,e}(r)$ , respectively, where

$$\phi_{1,e}(r) = \int_{-1}^{\mu_1} \psi(r, \mu) P_{1,e}(\mu) d\mu \quad (5.41)$$

and

$$\phi_{2,e}(r) = \int_{\mu_1}^{+1} \psi(r, \mu) P_{2,e}(\mu) d\mu \quad (5.42)$$

Employing  $N = 2$  in the system of equations of Table 5.2 and writing two equations for  $n = 1$  and  $n = 2$ , respectively, yields the condition on the backward and forward flux moments. The results are listed in Tables 5.3 and 5.4, respectively.

### 5.5 Calculational Analysis

The analysis presented in the previous sections is free of any functional assumptions or approximations. In a calculation application it will of course be necessary to truncate the series expansion at some appropriate order. As a test case for this new formalism we consider the low-order approximation of  $L = 0$  and undertake to calculate the

Range of $\nu$	Conditions on Spatial Moments
$\frac{1}{2}l \leq \nu \leq \nu_1$	$\begin{aligned} & \frac{j(1 + \nu_1)}{2j + 1} \frac{d\phi_{1,j-1}(r)}{dr} + \frac{(j + 1)(1 + \nu_1)}{2j + 1} \frac{d\phi_{1,j+1}(r)}{dr} - (1 - \nu_1) \frac{d\phi_{1,j}(r)}{dr} \\ & + \left[ \frac{j(1 + \nu_1)^2}{2j + 1} \phi_{1,j-1}(r) + \frac{(j + 1)(1 + \nu_1)^2}{2j + 1} \phi_{1,j+1}(r) - (1 - \nu_1^2) \phi_{1,j}(r) \right] \frac{d}{dr} \left( \frac{1}{1 + \nu_1} \right) \\ & + \sum_{l=0}^{\infty} \frac{2(2l + 1)}{1 + \nu_1} \phi_{1,l}(r) g_{jl}^{11} + 2\phi_{1,j}(r) + \frac{2}{r(1 + \nu_1)} \sum_{l=0}^{\infty} (2l + 1) \phi_{1,l}(r) [b_{jl}^{11} - d_{jl}^{11}] \\ & + \frac{1 - \nu_1}{r} \sum_{l=0}^{\infty} (2l + 1) \left[ \frac{(-1)^l}{1 - \nu_1} \phi_{2,l}(r) - \frac{1}{1 + \nu_1} \phi_{1,l}(r) \right] \\ & = c \sum_{\substack{l=j \\ l \neq j}}^{\infty} (2l + 1) f_{\square 1, \square, j}^{a, j} \sum_{l=0}^{\infty} (2l + 1) \left[ \frac{a_{1, \square, l}^j}{1 + \nu_1} \phi_{1,l}(r) + \frac{a_{2, \square, l}^j}{1 - \nu_1} \phi_{2,l}(r) \right] + \frac{2}{r} s_{1,j} \end{aligned}$
	$j = 0, 1, 2, 3, \dots, \infty$

Table 5.3: System of equations of partial-range spatial moments for  $\nu \in (-1, \nu_1)$ .

Range of $\mu$	Conditions on Spatial Moments
$\mu_1 \leq \mu \leq +1$	$\begin{aligned} & \frac{j(1 - \mu_1)}{2j + 1} \frac{d\phi_{2,j-1}(r)}{dr} + \frac{(j + 1)(1 - \mu_1)}{2j + 1} \frac{d\phi_{2,j+1}(r)}{dr} + (1 + \mu_1) \frac{d\phi_{2,j}(r)}{dr} \\ & + \left[ \frac{j(1 - \mu_1)^2}{2j + 1} \phi_{2,j-1}(r) + \frac{(j + 1)(1 - \mu_1)^2}{2j + 1} \phi_{2,j+1}(r) + (1 - \mu_1^2) \phi_{2,j}(r) \right] \frac{d}{dr} \left( \frac{1}{1 - \mu_1} \right) \\ & + \sum_{l=0}^{\infty} \frac{2(2l + 1)}{1 - \mu_1} \phi_{2,l}(r) g_{jl}^{22} + 2\phi_{2,j}(r) + \frac{2}{r(1 - \mu_1)} \sum_{l=0}^{\infty} (2l + 1) \phi_{2,l}(r) [b_{jl}^{22} - d_{jl}^{22}] \\ & + \frac{1 - \mu_1^2}{r} (-1)^j \sum_{l=0}^{\infty} (2l + 1) \left[ \frac{(-1)^l}{1 - \mu_1} \phi_{2,l}(r) - \frac{1}{1 + \mu_1} \phi_{1,l}(r) \right] \\ & = c \sum_{\mu=j}^{\infty} (2\mu + 1) f_{\mu}^a \sum_{l=0}^{\mu} \phi_{2,\mu,l}(r) + \frac{a_{1,\mu,l}}{1 + \mu_1} \phi_{1,l}(r) + \frac{a_{2,\mu,l}}{1 - \mu_1} \phi_{2,l}(r) + \frac{2}{r} s_{2,j} \end{aligned}$ <p style="text-align: center;"><math>j = 0, 1, 2, 3, \dots, \infty</math></p>

Table 5.4: System of equations of partial-range spatial moments for  $\mu \in (\mu_1, +1)$ .

angular flux as well as the total flux for the two media problem defined in the introduction of this chapter, Fig. 5.1. This problem with a neutron source at infinity has been defined by Williams<sup>(45)</sup> as the Milne problem in spherical geometry with boundary conditions, using the notation adopted here in Section 3.9, given by

$$1) \quad \psi(r, \mu) + \bar{\psi}_{0-}(r, \mu)$$

and

$$2) \quad \psi(R, \mu) = 0 ; \mu > 0$$

where  $R$  is the radius of the absorbing sphere, Fig. 5.1, and  $\bar{\psi}_{0-}(r, \mu)$  is the asymptotic angular flux distribution due to a source at infinity. We will consider a medium with linear anisotropic scattering, hence,  $f_2 = 0$  for  $l \geq 2$ .

For  $L = 0$ , the system of equations of Table 5.3 and Table 5.4 reduces to

$$\frac{d\phi_{1,0}(r)}{dr} = \frac{1}{1 - \mu_1} [A_{10}\phi_{1,0}(r) + B_{10}\phi_{2,0}(r)] \quad (5.43)$$

and

$$\frac{d\phi_{2,0}(r)}{dr} = -\frac{1}{1 + \mu_1} [A_{20}\phi_{1,0}(r) + B_{20}\phi_{2,0}(r)] \quad (5.44)$$

where  $A_{10}$ ,  $B_{10}$ ,  $A_{20}$  and  $B_{20}$  are given by

$$A_{10} = \frac{(1 - \mu_1)^2}{r\mu_1} + 2 - \frac{1 - \mu_1}{r} - c(1 + \mu_1) - \frac{3cf_1}{4} (1 - \mu_1)^2(1 + \mu_1) \quad (5.45)$$



$$B_{10} = \frac{1 + \mu_1}{r} - c(1 + \mu_1) + \frac{3cf_1}{4} (1 - \mu_1)(1 + \mu_1)^2, \quad (5.46)$$

$$A_{20} = -\frac{1 - \mu_1}{r} - c(1 - \mu_1) + \frac{3cf_1}{4} (1 - \mu_1)^2(1 + \mu_1), \quad (5.47)$$

and

$$B_{20} = \frac{(1 + \mu_1)^2}{r\mu_1} + 2 + \frac{1 + \mu_1}{r} - c(1 - \mu_1) - \frac{3cf_1}{4} (1 - \mu_1)(1 + \mu_1)^2. \quad (5.48)$$

The above equations, Eqs. (5.43) and (5.44), represent a system of first order differential equations. We note, however, that the coefficients  $A_{10}$ ,  $B_{10}$ ,  $A_{20}$  and  $B_{20}$  are space dependent. This dependency of these coefficients on the position  $r$  is introduced because of the position dependent segmentation  $\mu_1$ . Hence, the equations are singular at  $\mu_1 = 0$  which corresponds to the point  $r = R$  even though the solution need not necessarily be singular at this point. There may be several ways of circumventing this analytical-numerical difficulty. For our present purpose of numerical calculations we have elected to reformulate the problem for a constant although arbitrary  $\mu_1$  and subsequently specified  $\mu_1 = 0$  applicable to the angular flux at the surface of the sphere. In view of the conceptual derivation of this solution formalism, this solution is analogous to the double- $P_1$  solution applicable only at  $r = R$ ; this, incidently, gives the limiting condition of this position dependent partial-range formalism as  $r \rightarrow R$ . Therefore, we have, at the surface of the sphere, the following system of equations which can be obtained by specifying that  $\mu_1$  is constant right from the beginning and

subsequently equal to zero:

$$\frac{d\phi_{1,0}(r)}{dr} = A_{10D}\phi_{1,0}(r) + B_{10D}\phi_{2,0}(r) \quad (5.49)$$

and

$$\frac{d\phi_{2,0}(r)}{dr} = A_{20D}\phi_{1,0}(r) + B_{20D}\phi_{2,0}(r) \quad (5.50)$$

where,

$$A_{10D} = 2 - \frac{1}{R} - c - \frac{3cf_1}{4} \quad (5.51)$$

$$B_{10D} = \frac{1}{R} - c - \frac{3cf_1}{4} \quad (5.52)$$

$$A_{20D} = -\frac{1}{R} - c + \frac{3cf_1}{4} \quad (5.53)$$

and

$$B_{20D} = 2 + \frac{1}{R} - c - \frac{3cf_1}{4} \quad (5.54)$$

The subscript D identifies the usual double- $P_L$  approximation. This approximation has been studied previously by Wang<sup>(19)</sup> and used over the entire space.

The system of equations, Eqs. (5.43) and (5.44), have been solved numerically using the Runge-Kutta method. As an illustration, we show the angular flux distribution as a function of  $\mu$  for several distances from the surface of the sphere, Fig. 5.3. We note that, as expected from the physics of the problem, the present formalism shows a discontinuity in the angular flux at  $\mu_1$  which varies with position, Eq. (5.2). In view of the order of approximation used the flux is constant in the two forward and backward directional domains.

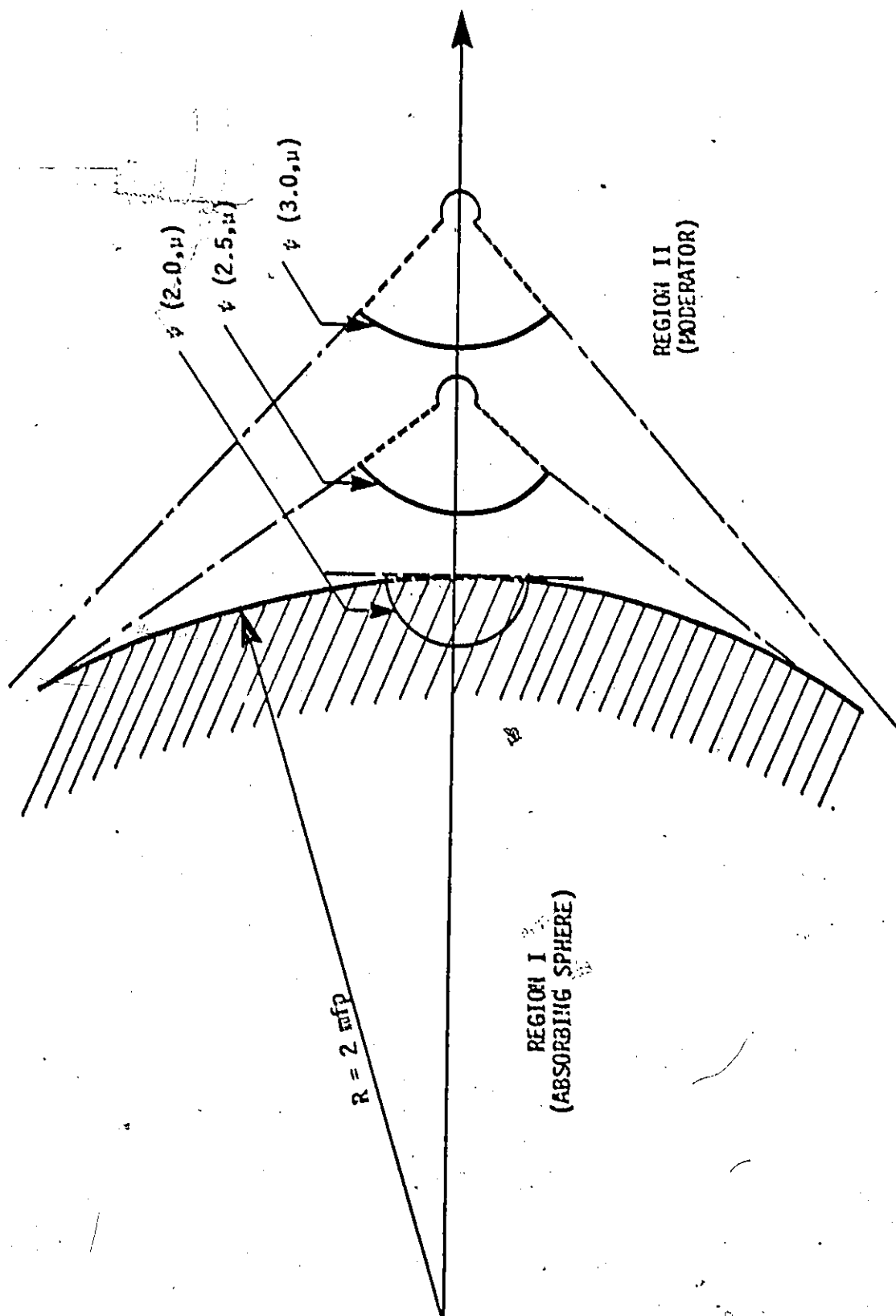


Fig. 5.3: Calculated directionally discontinuous flux  $\psi(r, \mu)$  at positions  $r = 2.0, 2.5$  and  $3.0$  measured in units of mean-free-path from the center of the absorbing sphere. The case considered is that of isotropic scatter with  $c = 1.0$ .

To obtain an indication of the accuracy of this directionally-discontinuous solution we have calculated the total flux for the special case of isotropic scattering with no absorption in the moderator (region II) and compared these results to the equivalent results reported by Sahni<sup>(72)</sup>. This comparison is shown in Table 5.5 where each column of data is normalized to unity at the surface of the sphere. Figure 5.4 displays the data given in Table 5.5. The important feature to note here is that this low-order  $2P_0$  approximation, which is of the same computational complexity as the diffusion approximation, yields more accurate results closer to the surface of the sphere. This suggests that the application of the solution formalism developed here can, in general, provide more accurate results without additional computational effort.

Distance $r$	Transport (Ref. 73)	Diffusion (Ref. 73)	$2P_0$ Approximation (This Work)
0.0	1.0	1.0	1.0
0.1	1.4548	1.1581	1.4350
0.2	1.7539	1.3162	1.6707
0.3	2.0259	1.4743	1.8538
0.4	2.2846	1.6326	2.0058
0.5	2.5357	1.7907	2.1363
0.6	2.7814	1.9487	2.2509
0.8	3.2644	2.2649	2.4453
1.0	3.7397	2.5822	2.6064

Table 5.5: Calculated total flux in the moderating medium normalized to unity at the surface of an absorbing sphere possessing a radius of two mean-free paths. The distance  $r$  is measured from the surface of the sphere in units of the mean-free path.

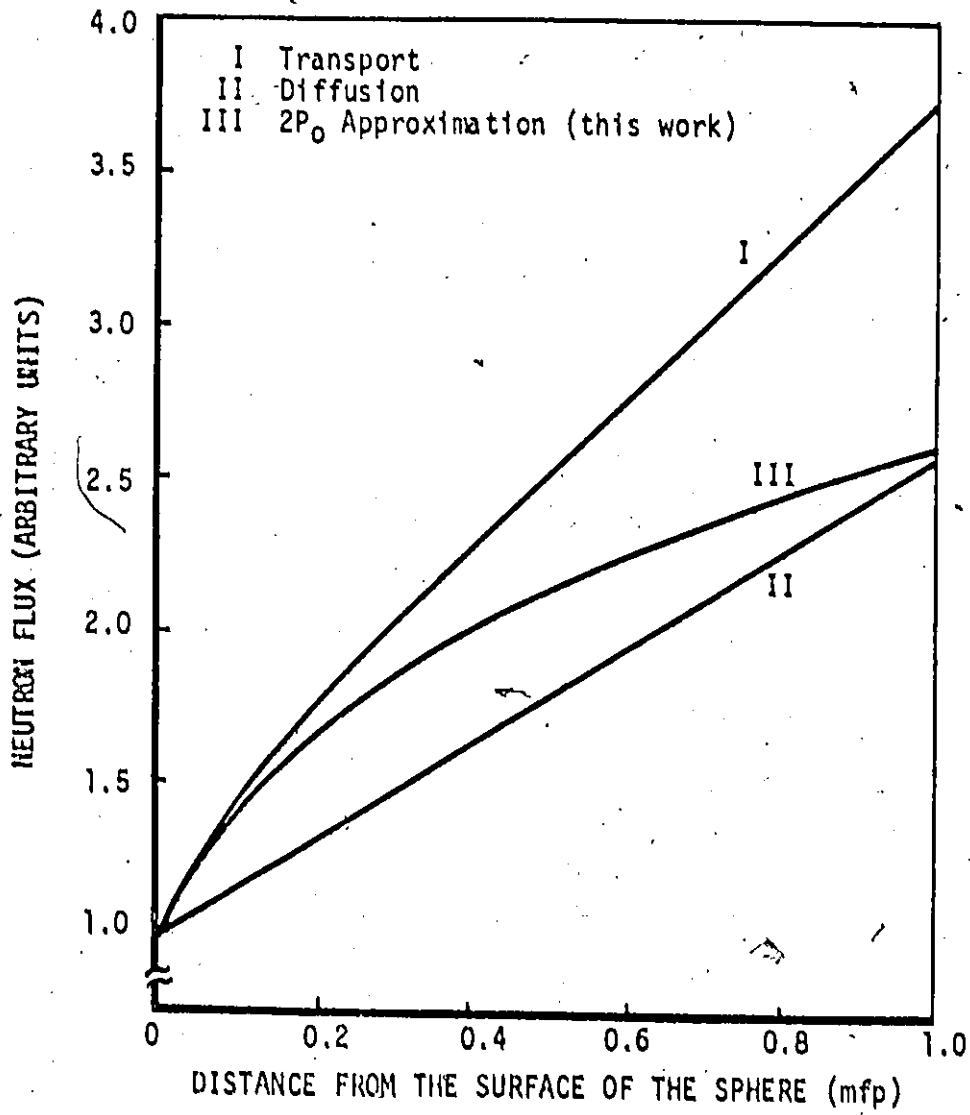


Fig. 5.4: Total flux in the moderating medium normalized to unity at the surface of an absorbing sphere possessing a radius of two mean free paths.

## CHAPTER VI

### SCATTERING KERNELS: REPRESENTATION AND APPLICATIONS

#### 6.1 Introduction

The subject of this chapter is the representation and applications of the scattering kernels based on the use of partial-range Legendre polynomials. This functional approach appears to possess the property of permitting a high order accuracy representation of very anisotropic phenomena in low-order expansions. The representation of both the one-group neutron transport scattering kernel and the group-to-group neutron transfer cross section in the multi-group technique will be considered here.

For neutron-nucleus interaction, we can derive a sufficiently accurate scattering cross section using a quantum mechanical formalism suggested by Van Hove<sup>(73)</sup>. Also, the neutron scattering cross section is measured experimentally for some elements and some neutron energies<sup>(37,38,74)</sup>. As the neutron energy increases or as the mass of the interacting nucleus increases, neutron scattering becomes increasingly anisotropic<sup>(25,37-39)</sup>. In the neutron transport analysis with anisotropic scattering, it is necessary to reconstruct the scattering kernels in a simple analytical formula to be used in the transport equation. Full-range Legendre polynomials are usually used<sup>(1-3)</sup>.

The various difficulties which have been reported can be attributed to the analytical representation of the scattering function in terms of

Legendre polynomials<sup>(1-3)</sup> and in the property that the differential cross sections vary non-monotonically with the scattering angle<sup>(25,37,38)</sup>.

Truncation induced oscillations leading to negative values for the neutron flux<sup>(25,26)</sup> has prompted the introduction of large numbers of Legendre coefficients<sup>(27)</sup> and other ad-hoc methods<sup>(28)</sup>. Moreover, from the study of Chapter IV, we see that the representation of the scattering function in terms of partial-range Legendre polynomials gives more accurate eigenvalues, even with low-order approximations, compared with the full-range representation.

In the following section, we will consider the new representation of scattering kernels, for one-group theory, based on the use of partial-range Legendre polynomials. Section 6.2.2 will give the group-to-group transfer cross section representation. Finally, in Section 6.3 some applications will be given.

## 6.2 Partial-Range Expansion of Scattering Kernels

### 6.2.1 One-Group Neutron Transport

The analysis is again based on the arbitrary segmentation of the directional variable of the scattering angle, i.e.  $\mu_s = \cos\theta_s$ , where  $\theta_s$  represents the scattering angle; see Fig. 4.1. That is, we divide the range of the cosine of the scattering angle into  $N$  arbitrary intervals with nodal points defined by  $\mu_i$ ,  $i = 1, 2, \dots, N$ . Over each interval  $(\mu_{n-1}, \mu_n)$  we expand the scattering function in terms of the complete orthogonal set of partial-range Legendre polynomials. The scattering function  $f(\underline{\Omega}, \underline{\Omega}')$  is thus written as a double sum expansion



$$f(\underline{\Omega}, \underline{\Omega}') = \sum_{n=1}^N \sum_{\ell=0}^L \frac{(2\ell + 1)}{2\pi(\mu_n - \mu_{n-1})} f_{n,\ell} P_{n,\ell}(\mu_s) \quad (6.1)$$

where the  $P_{n,\ell}(\mu_s)$  is the  $\ell$ 'th order partial-range Legendre polynomial over the  $n$ 'th range of the angular variable  $\mu_s$ . The definition and properties of the partial-range Legendre polynomials have been given in Chapter II. The partial-range moments  $f_{n,\ell}$  follow directly as

$$f_{n,\ell} = \int_{\mu_{n-1}}^{\mu_n} f(\mu_s) P_{n,\ell}(\mu_s) d\mu_s \quad (6.2)$$

Here, we made use of the following relationship

$$F(\underline{\Omega}, \underline{\Omega}') = \frac{1}{2\pi} f(\mu_s) \quad (6.3)$$

implying that the scattering function is a function of  $\mu_s$  only. Also, the above relationship leads to the following normalization condition of the scattering function

$$\int_{-1}^1 f(\mu_s) d\mu_s = 1 \quad (6.4)$$

Using the expansion of Eq. (6.1) it is now possible to describe the scattering function  $f(\mu_s)$  to a given degree of accuracy even with a low-order partial-range Legendre polynomials expansion by increasing the number of directional intervals. For example, consider the low order approximation of  $L = 0$  for which Eq. (6.1) and Eq. (6.3) yield

$$f(\mu_s) = \sum_{n=1}^N \frac{1}{(\mu_n - \mu_{n-1})} f_{n,0} P_{n,0}(\mu_s) \quad (6.5)$$

Substituting the expression of the zero-order partial-range Legendre polynomial which is given by Eq. (2.15) into Eq. (6.5) yields

$$f(\mu_s) = \sum_{n=1}^N \frac{1}{(\mu_n - \mu_{n-1})} f_{n,0} \quad (6.6)$$

based on the zero-order moment of the n'th interval,

$$f_{n,0} = \int_{\mu_{n-1}}^{\mu_n} f(\mu_s) d\mu_s \quad (6.7)$$

This low order moment represents the probability of a neutron scattering into the range of the cosine of the scattering angle between  $\mu_{n-1}$  and  $\mu_n$ . We note that Eq. (6.5) implies that the angular variable  $\mu_s$  is divided into N arbitrary intervals and over each interval the scattering function  $f(\mu_s)$  is approximated by a constant. We designate this case as partial-range isotropic scattering. It is obvious that as N increases, the accuracy of Eq. (6.6) increases and it is clear, also, that it is impossible to generate a negative differential cross section in this lowest-order approximation of partial-range representation.

For the second order of approximation  $L = 1$ , Eq. (6.1) and Eq. (6.3) yield

$$f(\mu_s) = \sum_{n=1}^N \frac{1}{(\mu_n - \mu_{n-1})} [f_{n,0} + 3f_{n,1}(\alpha_n \mu_s + \beta_n)] \quad (6.8)$$

Here, we have used the expressions of zero-order and first-order Legendre polynomials given by Eqs. (2.15) and (2.16), respectively. The moment  $f_{n,0}$  is still given by Eq. (6.7) while  $f_{n,1}$  is defined by

$$f_{n,1} = \int_{\mu_{n-1}}^{\mu_n} f(\mu_s) (\alpha_n \mu_s + \beta_n) d\mu_s \quad (6.9)$$

The interval functions  $\alpha_n$  and  $\beta_n$  are given by Eqs. (2.13) and (2.14), respectively. Equation (6.8) implies that the angular variable  $\mu_s$  is divided into  $n$  arbitrary intervals and over each interval the scattering function is approximated by a straight line segment. We denote this case by the partial-range linearly anisotropic case of scattering.

It is useful to place the representation developed thus far into perspective by noting that the usual expansion of the scattering function in terms of the full-range Legendre polynomials is obtained as a special case by setting  $n = 1$ . For this case Eq. (6.1) gives, therefore,

$$f(\underline{\Omega}, \underline{\Omega}') = \sum_{\ell=0}^L \frac{2\ell+1}{2\pi(\mu_1 - \mu_0)} f_{1,\ell} P_{1,\ell}(\mu_s) \quad (6.10)$$

For the full-range description of the scattering function, we require  $\mu_0 = -1$  and  $\mu_1 = +1$  and Eq. (6.10) reduces to

$$f(\underline{\Omega}, \underline{\Omega}') = \sum_{\ell=0}^L \frac{2\ell+1}{4\pi} f_{\ell} P_{\ell}(\mu_s) \quad (6.11)$$

where  $P_{\ell}(\mu_s)$  is the full-range Legendre polynomial and  $f_{\ell}$  is the usual moment of the scattering function given by

$$f_{\ell} = 2\pi \int_{-1}^{+1} f(\underline{\Omega}, \underline{\Omega}') P_{\ell}(\mu_s) d\mu_s \quad (6.12)$$

These latter two equations are the usual description of the scattering function in terms of the full-range Legendre polynomials<sup>(1,2)</sup>.

We now consider the case of isotropic scattering. Clearly, the scattering function  $f(\mu_s)$  satisfies the normalization condition of Eq. (6.4) and is given by

$$f(\mu_s) = \frac{1}{2} , \quad (6.13)$$

which, upon substituting into Eq. (6.7), results in

$$f_{n,0} = \frac{1}{2} (\mu_n - \mu_{n-1}) , \quad (6.14)$$

and  $f_{n,\ell} = 0$  for  $\ell > 0$ .

Using Eq. (6.14) we can write

$$\sum_{n=1}^N f_{n,0} = \frac{1}{2} \sum_{n=1}^N (\mu_n - \mu_{n-1}) = \frac{1}{2} (\mu_N - \mu_0) . \quad (6.15)$$

Assuming a full-range description for the scattering function, that is  $\mu_0 = -1$  and  $\mu_N = 1$ , we obtain

$$\sum_{n=1}^N f_{n,0} = 1.0 . \quad (6.16)$$

This condition, Eq. (6.16), applies for both isotropic and anisotropic scattering. Indeed, it represents the normalization condition of the scattering function, Eq. (6.4).

Of some interest is the special case of  $N = 2$ . In this case, there are two ranges of the scattering variable  $\mu_s$  given by this inequality

$$-1 < \mu_1 < +1 \quad (6.17)$$

Again, we have assumed full-range representation of the scattering function, i.e.  $\mu_0 = -1$  and  $\mu_2 = +1$ . From Eq. (6.14) we can write

$$f_{1,0} = \frac{1}{2} (1 + \mu_1) \quad (6.18)$$

and

$$f_{2,0} = \frac{1}{2} (1 - \mu_1) \quad (6.19)$$

from which the degree of anisotropy  $\Delta f$ , defined by Eq. (4.54), is given by

$$\Delta f = -\mu_1 \quad (6.20)$$

Therefore, even for isotropic scattering, the moments of the scattering function  $f_{1,0}$  and  $f_{2,0}$  are functions of the partition  $\mu_1$ . The condition of Eq. (6.20) has been frequently used in Chapter IV.

### 6.2.2 Multi-Group Neutron Transport

Consideration will now be given to the development of the group-to-group transfer cross section. The exact elastic scattering transfer cross section from group  $g'$  to group  $g$  can generally be written as

$$\sigma_{g' \rightarrow g}(\underline{r}, \mu_s) = \frac{\int_{E_g}^{E_{g-1}} \left\{ \int_{E_{g'}}^{E_{g'-1}} \sigma_s(\underline{r}, E', \underline{\Omega}' \rightarrow E, \underline{\Omega}) \psi(\underline{r}, E', \underline{\Omega}') dE' \right\} dE}{\int_{E_{g'}}^{E_{g'-1}} \psi(\underline{r}, E', \underline{\Omega}') dE'} \quad (6.21)$$

where  $\sigma_s$  is the scattering cross section which is the probability of a neutron having energy  $E'$  at direction  $\underline{\Omega}'$  to be scattered to the direction  $\underline{\Omega}$  with energy  $E$  per unit volume at the position  $\underline{r}$ , and  $\psi(\underline{r}, E', \underline{\Omega}')$  is the

neutron angular flux while the remaining symbols are employed as conventionally used in the literature<sup>(3)</sup>.

The scattering law, that is, a relation between the scattering angle and the energy change of the scattered particle, can be written as<sup>(75,76)</sup>

$$\Omega \cdot \Omega' = \xi(E, E') ; \quad -1 \leq \xi \leq +1 \quad (6.22)$$

This restricts our analysis here to neutron slowing down only, which is represented by Fig. 6.1. The scattering transfer cross section can hence be written in its usual form

$$\sigma_s(\underline{r}, E', \Omega' \rightarrow E, \Omega) = \frac{1}{2} k(E, E') \delta[\Omega \cdot \Omega' - \xi(E, E')] \quad (6.23)$$

where  $k(E, E')$  is a function of the neutron energy before,  $E'$ , and after,  $E$ , the scattering event. For the case of elastic scattering Eqs. (6.21), (6.22) and (6.23) reduce to the following equations, respectively<sup>(41)</sup>,

$$\begin{aligned} \sigma_{g' \rightarrow g}(\underline{r}, \mu_s) &= \frac{2}{1 - \alpha} \int_{E_g}^{E_{g-1}} dE \int_{E_{g'}}^{E_{g'-1}} dE' \frac{\sigma_s(\underline{r}, E')}{E'} f[E', \xi(\mu_s)] \\ &\times \psi(\underline{r}, \Omega', E') \delta[\mu_s - S(E, E')] \\ &\times \frac{H(E - \alpha E') - H(E - E')}{\int_{E_{g'}}^{E_{g'-1}} dE' \psi(\underline{r}, \Omega', E')} \quad (6.24) \end{aligned}$$

and

$$\Omega \cdot \Omega' = S(E, E') \quad (6.25)$$

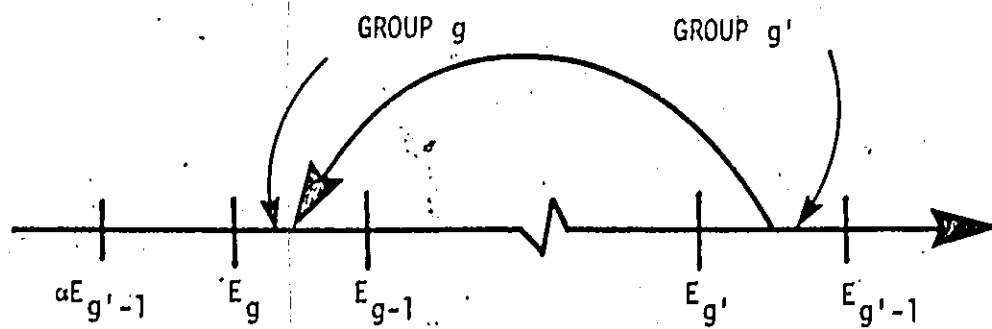


Fig. 6.1: Representation of energy groups  $g$  and  $g'$  illustrating neutron down scattering.

where

$$S(E, E') = \frac{1}{2} [(A + 1)\sqrt{\frac{E}{E'}} - (A - 1)\sqrt{\frac{E'}{E}}] \quad (6.26)$$

The delta function,  $\delta$ , and the unit step function,  $H$ , in Eq. (6.24) describe the angle-energy coupling imposed by elastic scattering.

Here,  $\mu_s$  and  $\xi$  are the cosine of the scattering angles in the laboratory and center-of-mass-system, respectively,  $f[E', \xi(\mu_s)]$  is the differential scattering distribution, and  $\sigma_s(\underline{r}, E')$  is the total scattering cross section. The constant  $\alpha$  is given by

$$\alpha = \left(\frac{A - 1}{A + 1}\right)^2, \quad (6.27)$$

where  $A$  is the relative mass of the scattering isotope to the mass of the neutron.

With the introduction of a multi-group structure, Fig. 6.1, the allowable range of  $\mu_s$  for the transfer of a neutron elastically scattered from a source group  $g'$ , containing  $E'$ , to group  $g$ , containing  $E$ , may not include the entire range of  $\mu_s$   $(-1, +1)$ . Instead the bounds of  $\mu_s$  for the transfer  $g' \rightarrow g$  are given by

$$\mu_{n-1} = \frac{1}{2} [(A + 1)\sqrt{\frac{E_g}{E_{g'-1}}} - (A - 1)\sqrt{\frac{E_{g'-1}}{E_g}}], \quad (6.28)$$

and

$$\mu_n = \frac{1}{2} [(A + 1)\sqrt{\frac{E_{g-1}}{E_{g'}}} - (A - 1)\sqrt{\frac{E_{g'}}{E_{g-1}}}] \quad (6.29)$$

We are considering energy groups which are not directly coupled, that is  $g \neq g' + 1$ . Also, we are considering a case in which the maximum



decrease in neutron energy after elastic scattering is much larger than the width of any energy group. This is particularly applicable for light elements; hence, Eqs. (6.28) and (6.29) are correct providing the following condition holds,

$$\alpha E_{g'-1} \ll E_g \quad (6.30)$$

This condition imposes the following restriction on  $\mu_{n-1}$  and  $\mu_n$ ,

$$-1 \leq \mu_{n-1} < \mu_n < +1 \quad (6.31)$$

It is worthwhile to note that this formalism is correct for all nuclei and any division of energy groups; it is, however, necessary to take care in calculating the allowable range of  $\mu_s$ .

For example, the allowable range of  $\mu_s$  for the in-group cross section is given by

$$\mu_{n-1} = \frac{1}{2} \left[ (A+1) \sqrt{\frac{E_{g'}}{E_{g'-1}}} - (A-1) \sqrt{\frac{E_{g'-1}}{E_{g'}}} \right] \quad (6.32)$$

and

$$\mu_n = +1 \quad (6.33)$$

Moreover, for the contiguous group transfer cross section the allowable range of  $\mu_s$  is given by the lower bound

$$\mu_{n-1} = \frac{1}{2} \left[ (A+1) \sqrt{\frac{E_{g'-1}}{E_{g'+1}}} - (A-1) \sqrt{\frac{E_{g'+1}}{E_{g'-1}}} \right] \quad (6.34)$$

while  $\mu_n$  is unchanged, Eq. (6.33).

From the above discussions, we conclude that the group-to-group

transfer cross section  $\sigma_{g' \rightarrow g}(\underline{r}, \mu_s)$  is not well-behaved in the entire interval of  $\mu_s \in (-1, 1)$ , but it is well-behaved in the allowable range of  $\mu_s \in (\mu_{n-1}, \mu_n)$ ; by this we mean that it is equal to zero everywhere except in the allowable ranges of  $\mu_s$  where it varies monotonically.

The objective, therefore, is to expand the transfer cross section  $\sigma_{g' \rightarrow g}(\underline{r}, \mu_s)$  in terms of a complete set of orthogonal functions over the arbitrary range of  $\mu_s \in (\mu_{n-1}, \mu_n)$ . For this purpose we have chosen the partial-range Legendre polynomials which introduced in Chapter II. Accordingly, the group-to-group transfer cross section of Eq. (6.24) can be expanded as

$$\sigma_{g' \rightarrow g}(\underline{r}, \mu_s) = \sum_{\ell=0}^{\infty} \frac{2\ell + 1}{2\pi(\mu_n - \mu_{n-1})} \sigma_{g' \rightarrow g}^{\ell}(\underline{r}) P_{n,\ell}(\mu_s) \quad (6.35)$$

where, generally,  $\mu_{n-1}$  and  $\mu_n$  are given for the case of elastic scattering, by Eqs. (6.28) and (6.29), respectively, and the

partial-range Legendre polynomial,  $P_{n,\ell}(\mu_s)$ , is given by Eq. (2.2).

The partial-range moment  $\sigma_{g' \rightarrow g}^{\ell}(\underline{r})$  follows directly and is given by

$$\sigma_{g' \rightarrow g}^{\ell}(\underline{r}) = \int_{\underline{\Omega}_s} \sigma_{g' \rightarrow g}(\underline{r}, \mu_s) P_{n,\ell}(\mu_s) d\underline{\Omega}_s \quad (6.36)$$

A similar procedure has recently been applied to the differential Compton scattering cross section of photons<sup>(52)</sup>.

### 6.3 Examples of Applications

#### 6.3.1 Scattering Function Calculations

As an application of the expansion of the scattering function

in terms of the partial-range Legendre polynomials, we consider the elastic scattering of  $U^{238}$  and  $Bi^{209}$  of 14.0 MeV neutrons. The  $U^{238}$  nucleus has been chosen because it displays particularly strong anisotropies at this energy; moreover, this uranium isotope is likely to be used in fusion reactor blankets as a fertile fuel. The choice of  $Bi^{209}$  is based on its very anisotropic scattering cross section to illustrate the expansion formalism. Here, the expansions have been developed and compared with the usual expansion in terms of the full-range Legendre polynomials. The criteria of interest are:

- 1) non-negative cross section from the reconstructed moments;
- 2) the deviation of the expanded cross sections from the experimental values is determined according to the least-squares error criteria, defined by Eq. (4.120) and rewritten again, here, for convenience,

$$\epsilon = \int_{-1}^{+1} \left[ \sum_{n=1}^N \sum_{\ell=0}^L \frac{2\ell + 1}{(\mu_n - \mu_{n-1})} f_{n,\ell} p_{n,\ell}(\mu_s) - f(\mu_s) \right]^2 d\mu_s \quad (6.37)$$

From the definition of the function  $\epsilon$ , it is clear that it is governed by the order of partial-range polynomials,  $L$ , the number of direction intervals,  $N$ , and on the choice of the division  $\mu_n$ .

For a given order of  $L$  and  $N$ , the divisions,  $\mu_n$ , are completely arbitrary. However, one way of choosing these divisions is to minimize the function  $\epsilon$ , by varying the values of  $\mu_n$  for given values of  $N$  and  $L$ . Figure 6.2 depicts the experimental elastic scattering cross section for

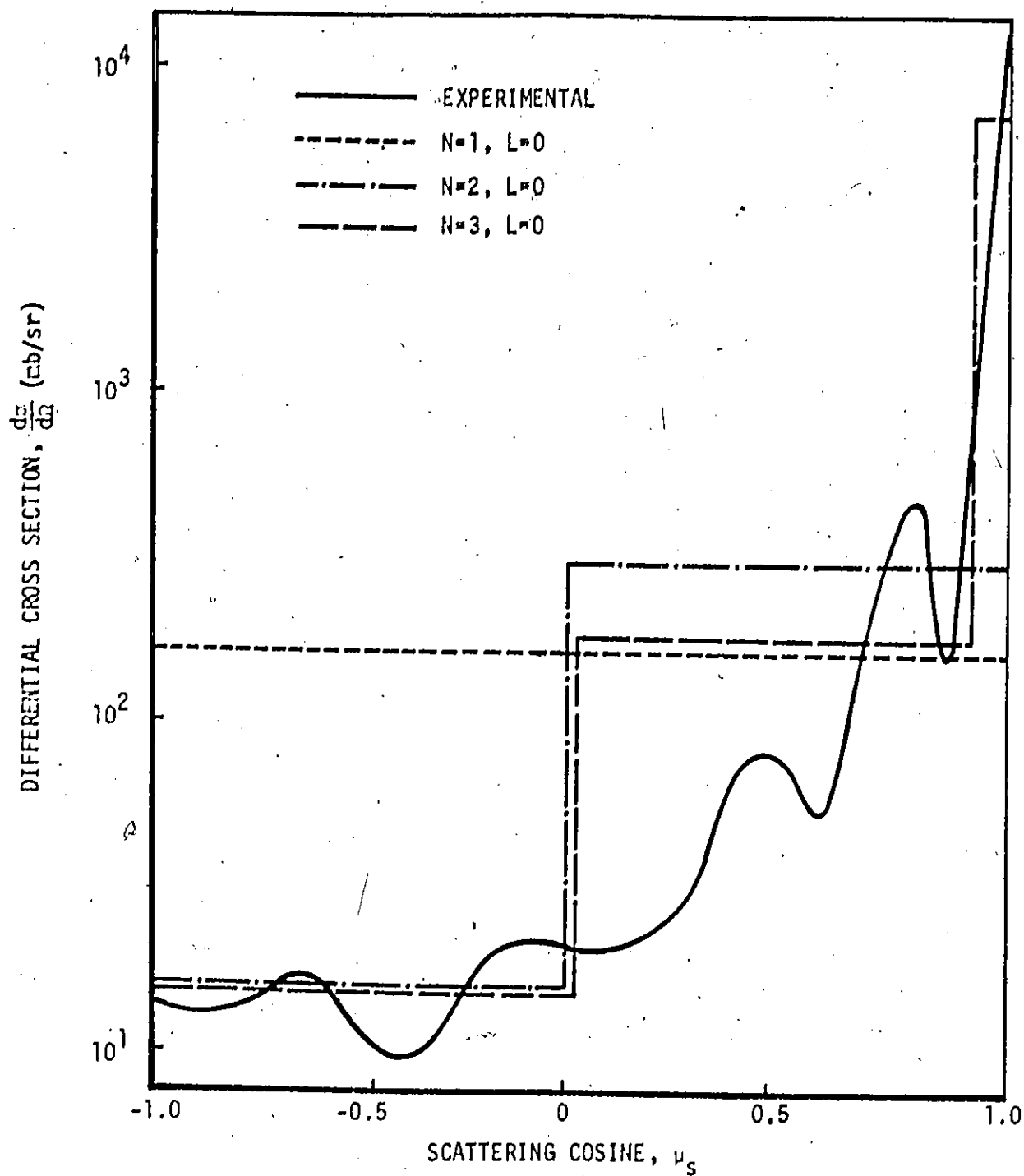


Fig. 6.2: Illustrative comparison between the experimental  $U^{238}$  cross section (14 MeV) and its partial-range Legendre representation for  $L = 0$  while  $N = 1, 2$  and  $3$ .

$U^{238}$  as well as some low-order approximations of the cross section. The case of  $N = 1$  and  $L = 0$  approximates the cross section by an isotropic representation;  $N = 2$  and  $L = 0$  case approximates the cross section by a partial-range isotropic scattering over the two ranges with  $\mu_s = 0$  as a directional partition while the case of  $N = 3$  and  $L = 0$  approximates the cross section by a partial-range isotropic scattering over three ranges with  $\mu_s = 0$  and  $\mu_s = 0.975$  as partitions. The value of  $\mu_s = 0$  in all the approximations of this section has been chosen to be consistent with the choice of  $\mu = 0$  in the partial-range representation of the neutron flux on the basis of exactly satisfying the vacuum-medium boundary conditions in plane geometry<sup>(16)</sup>. The value of  $\mu_s = 0.975$  for the case of  $N = 3$  and  $L = 0$  gives minimum  $c$  for this case. Figure 6.3 displays the approximations of  $N = 3$  with  $L = 2$  and 3, respectively, for  $U^{238}$ .

From these results we note that, as the number  $N$  increases, even with  $L = 0$ , the reconstructed cross sections become closer to the experimental one and the error deviation decreases considerably as tabulated, Table 6.1. Table 6.1 also lists the values of  $c$  for some  $P_L$  approximations for the purpose of comparison. We note that the full-range  $P_8$  approximation yields a negative differential cross section in some intervals of  $\mu_s$ . The value of  $c$ , for this approximation, is comparable with that of the approximation of  $N = 3$  and  $L = 0$  which gives a non-negative cross section.

Figure 6.4 displays the cross section of  $B1^{209}$  for three low-order approximations;  $N = 3$  and  $L = 0, 2$  and 4, respectively. These

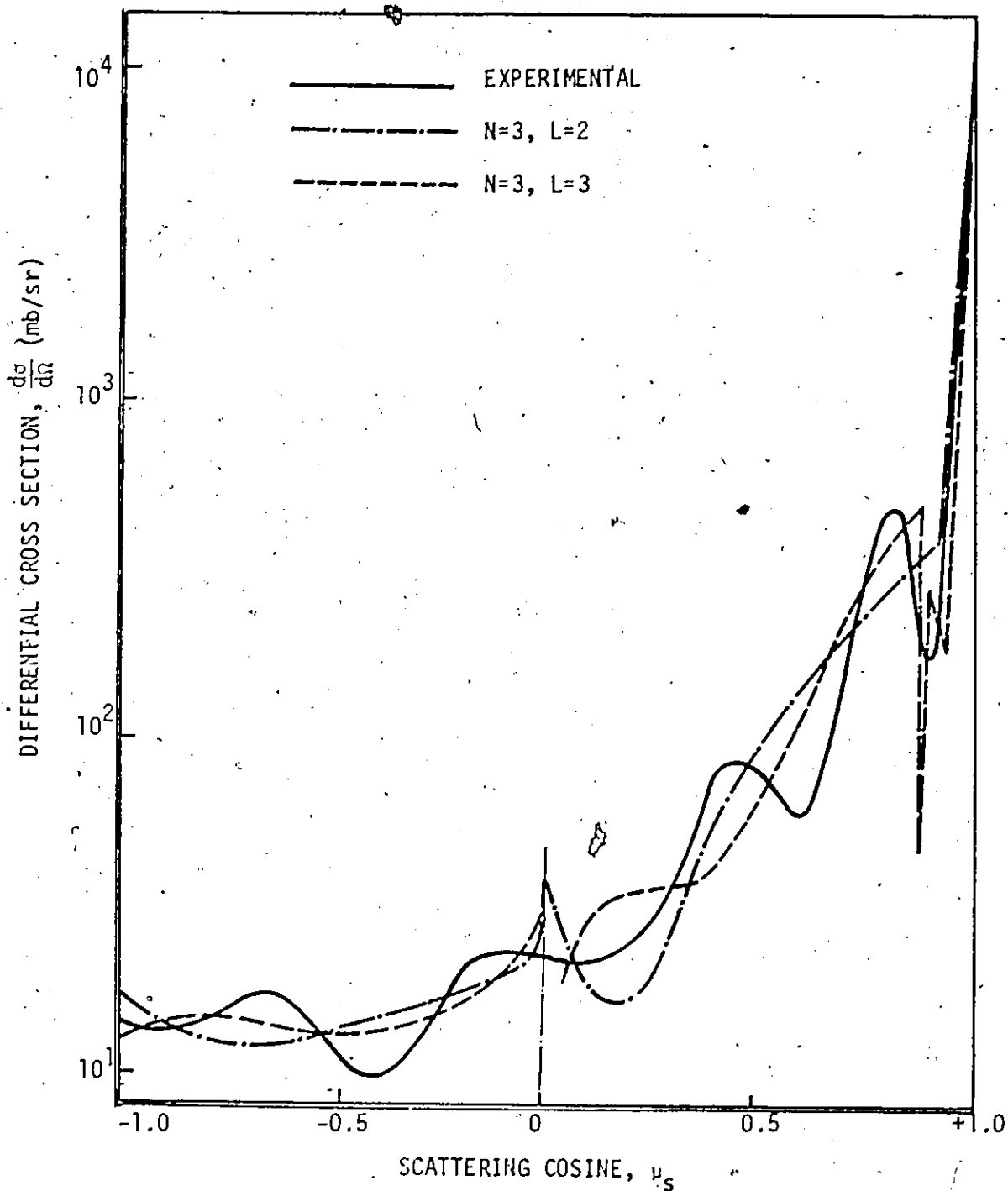


Fig. 6.3: Illustrative comparison between the experimental  $U^{238}$  cross section (14 MeV) and its partial-range Legendre representation for  $L = 2$  and  $3$  while  $N = 3$ . In comparison to Fig. 6.2 this illustrates the effect of integral changes in the order of expansion.

	$\epsilon$ for $U^{238}$	$\epsilon$ for $Bi^{209}$
$P_L$ Approximation	1.0 ( $P_0$ )	1.0 ( $P_0$ )
	0.21* ( $P_8$ )	0.029* ( $P_{13}$ )
This Work	0.96 ( $N=2, L=0$ )	0.98 ( $N=2, L=0$ )
	0.27 ( $N=3, L=0$ )	0.22 ( $N=3, L=0$ )
	0.0055 ( $N=3, L=2$ )	0.0062 ( $N=3, L=2$ )
	0.0018 ( $N=3, L=5$ )	0.0011 ( $N=3, L=6$ )

Table 6.1: Comparison of goodness of fit for the  $U^{238}$  and  $Bi^{209}$  elastic scattering cross sections at 14 MeV with the errors  $\epsilon$  normalized to unity for the  $P_0$  approximation. The symbol \* indicates that a negative cross section was generated.

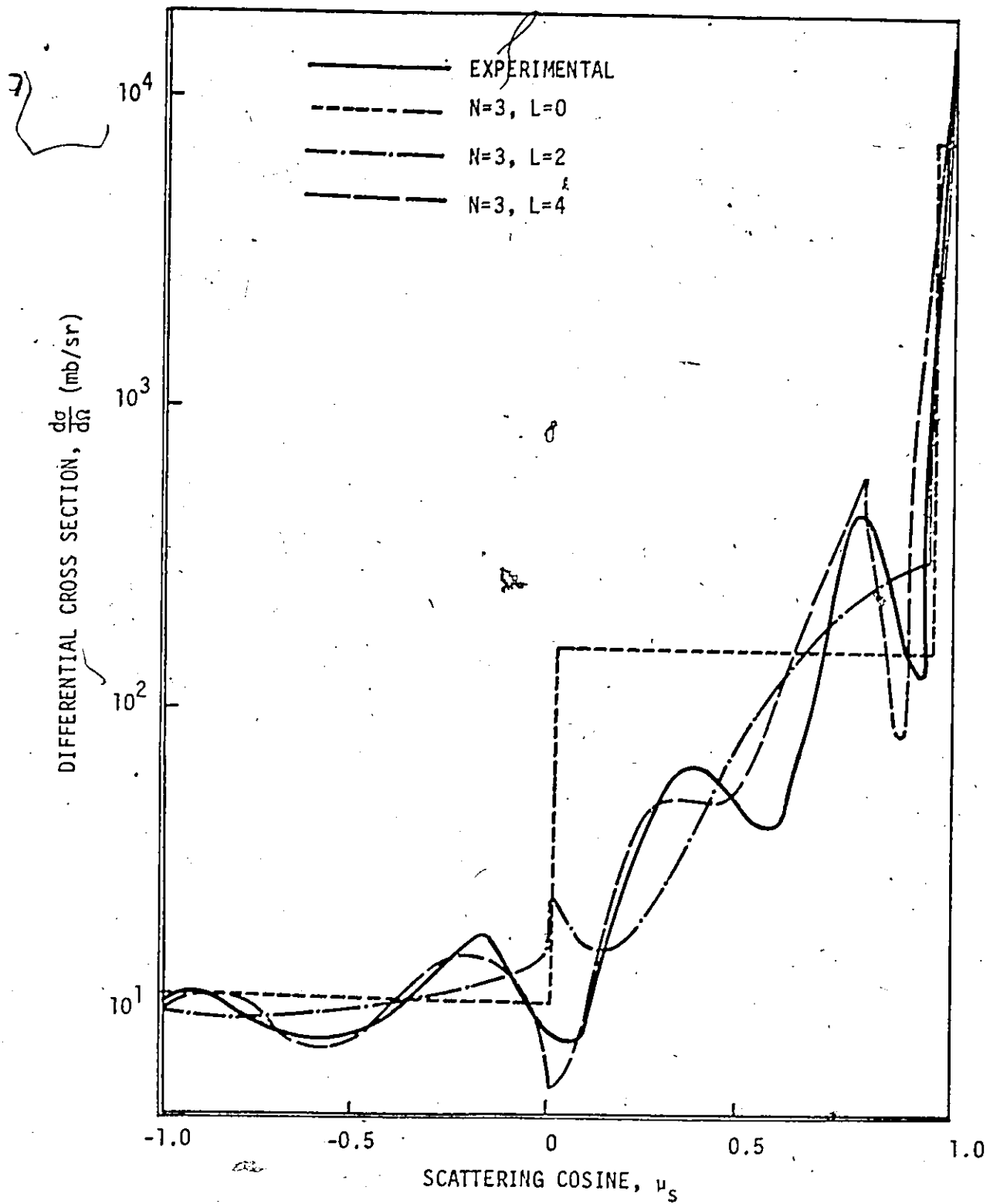


Fig. 6.4: Illustrative comparison between the experimental  $\text{Bi}^{209}$  cross section (14.1 MeV) and its partial range Legendre representation for  $L = 0, 2$  and  $4$  while  $N = 3$ .



approximations do not generate negative cross sections. The error values for  $\text{Bi}^{209}$  are listed in Table 6.1. From the figure and the table we note that this highly anisotropic cross section can be approximated even with a few terms of partial-range polynomials to a high degree of accuracy. The cross sections of  $\text{Bi}^{209}$  have been expanded in terms of the usual full-range Legendre polynomials up to order  $L = 19$  and still yields negative differential cross section in some ranges of  $\mu_s$ ; the only exception occurs at  $L = 0$  and records an attendant large error. Finally, we note the appearance of discontinuities in the reconstructed cross sections at the nodes of the angular segments; this discontinuity is attributable to the inherent property of this expansion formalism of treating each angular interval independently.

### 6.3.2 Group-to-Group Transfer Cross Section Calculations

For the expansion of the group-to-group transfer cross section in terms of the partial-range Legendre polynomial, we consider elastic group-to-group scattering in water from (3.3287 - 3.0119 MeV) to (2.7253 - 2.4660 MeV). The exact transfer cross section between these two groups has been determined for Oxygen and Hydrogen using the data of ENDF/B file<sup>(77)</sup>. The partial-range moments of the transfer cross section have been calculated using the exact data of the cross section then the cross section has been reconstructed from these moments. Using Eqs. (6.28) and (6.29), the allowable range of  $\mu_s$  for Oxygen is  $\mu_s \in (-1.0, 0.2010)$  and for Hydrogen is  $\mu_s \in (0.8609, 0.9510)$ . Figure 6.5 shows a comparison between the exact cross section and various degrees of approximations,  $L = 0, 1$  and  $3$ , respectively, for Oxygen. From this

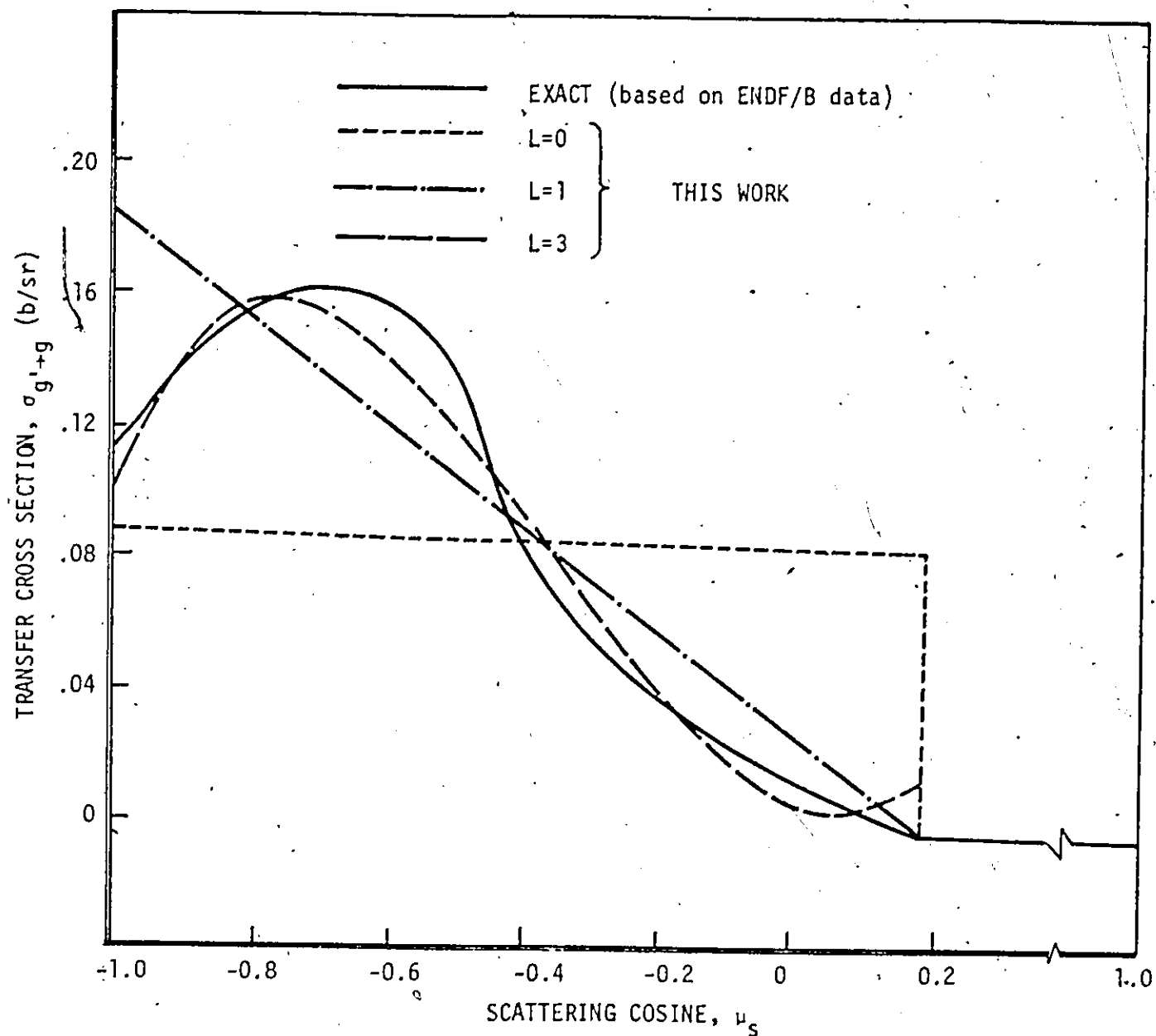


Fig. 6.5: Comparison of oxygen group-to-group elastic scattering cross section from (3.3287 - 3.0119) MeV to (2.7253 - 2.4660) MeV for  $L = 0, 1$  and  $3$  in the partial-range Legendre representation.

figure we observe that the  $L = 3$  approximation gives good representation without any negative values for the cross section. Figure 6.6 shows a similar comparison for Hydrogen using  $L = 0, 2$  and  $4$ , respectively.

To compare the results of this work with the usual expansion of the cross section in terms of the full-range Legendre polynomial, the water group-to-group elastic cross section has been calculated and compared in Fig. 6.7. The results of the eighth order Legendre expansion are taken from reference (41). For water, there are two allowable ranges of  $\mu_s$ ; in the range  $\mu_s \in (-1.0, 0.2010)$  we used  $L = 3$  approximation while for the range  $\mu_s \in (0.8609, 0.9510)$  we used  $L = 4$  approximation. The total number of terms, then are nine which correspond to the same number used in the usual eighth order Legendre expansion. From the figure, we conclude that a partial-range expansion of the same degree of approximation seems to yield much better agreement than the usually employed Legendre expansions. The use of partial-range polynomials thus contributes to a more accurate differential scattering representation and therefore leads to more reliable results.

Finally, we note an additional degree of freedom. It is not necessary to employ the same order of approximation over the various allowable directional ranges of  $\mu_s$ . The order can be varied using the extent of anisotropy of the cross section over each range as the criteria.

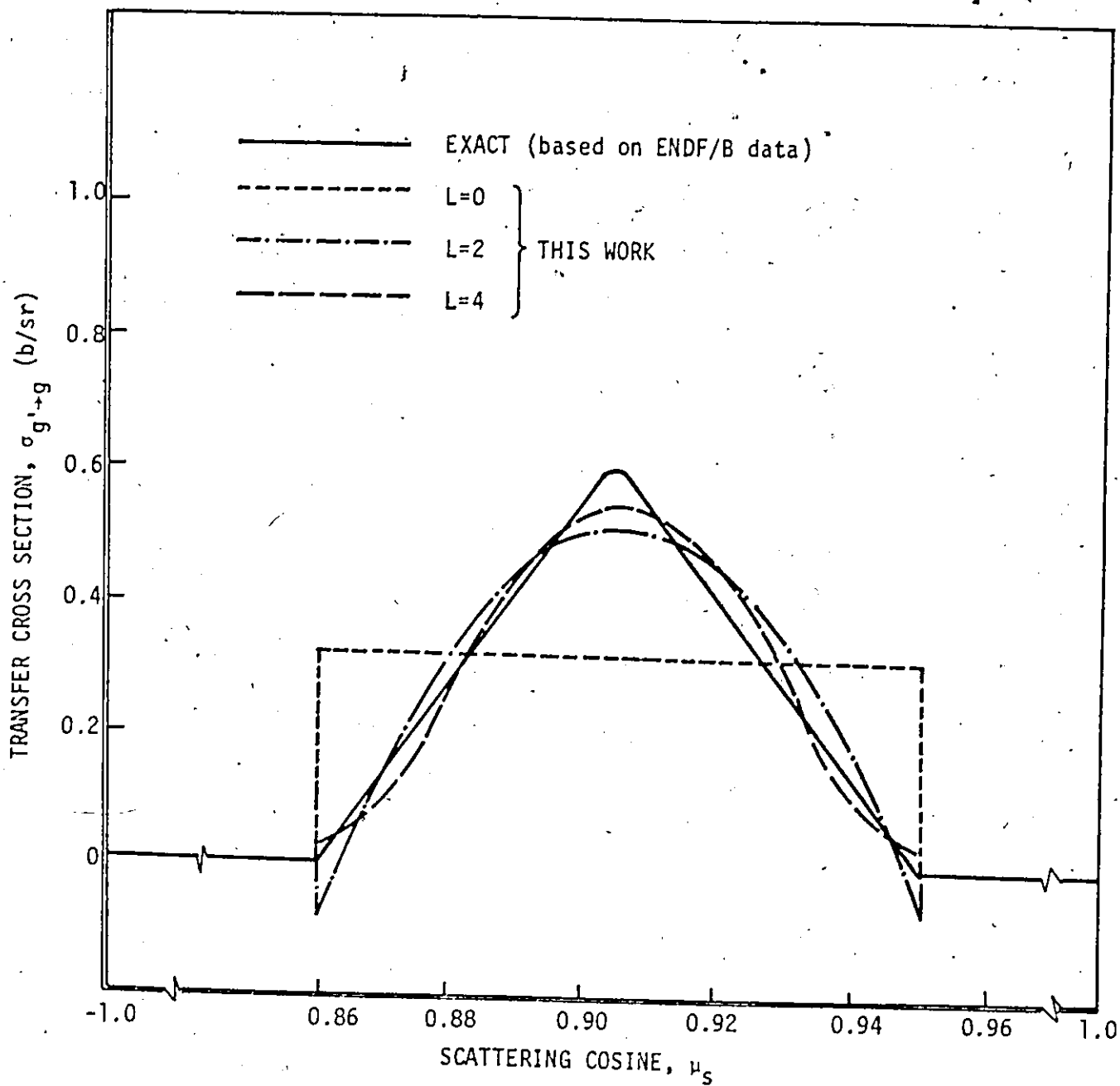


Fig. 6.6: Comparison of hydrogen group-to-group elastic scattering cross section from (3.3287 - 3.0119) MeV to (2.7253 - 2.4660) MeV for  $L = 0, 2$  and  $4$  in the partial-range Legendre representation.

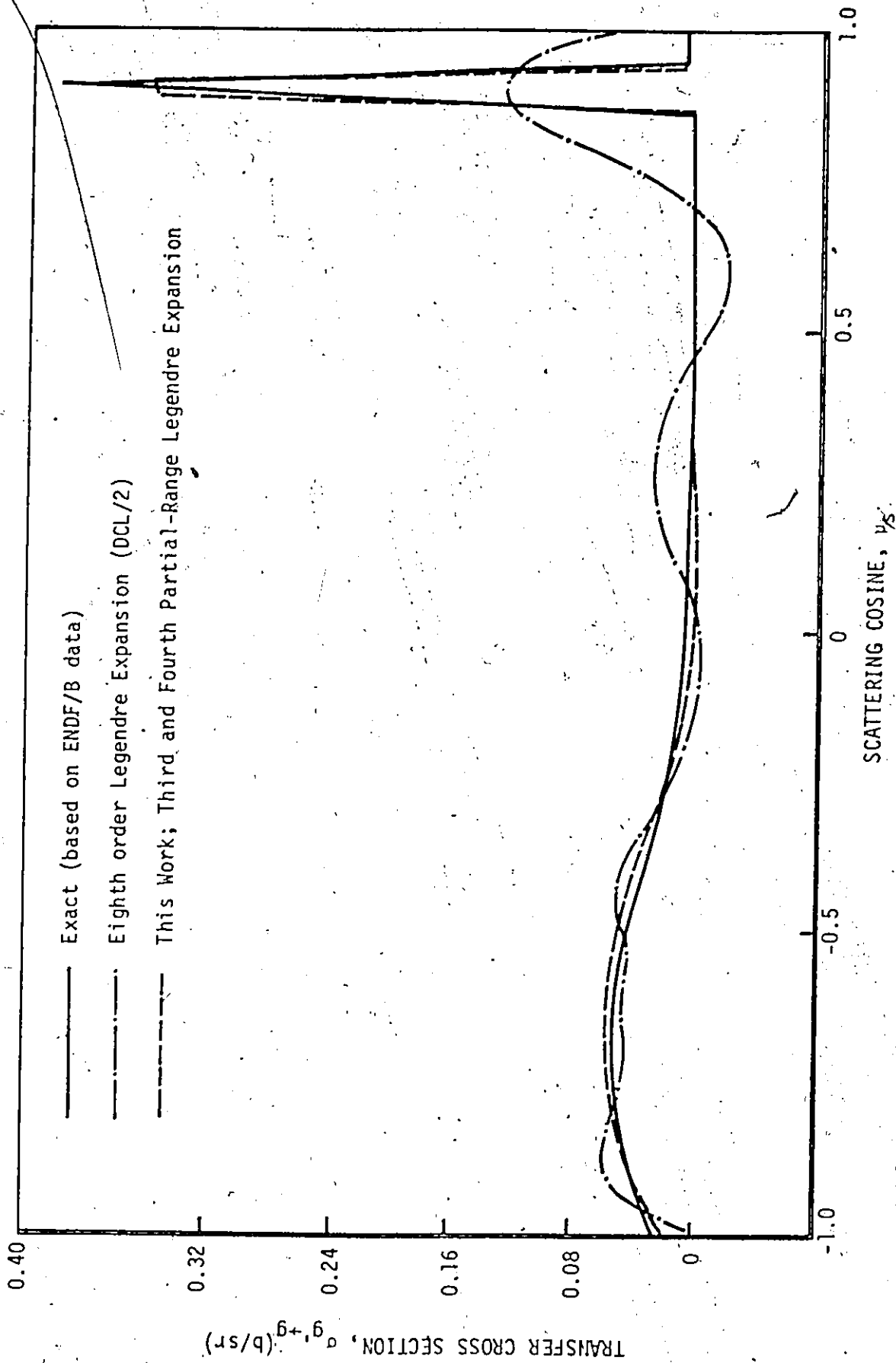


Fig. 6.7: Comparison of water group-to-group elastic scattering cross section from (3.3287 - 3.0119) MeV to (2.7253 - 2.4660) MeV using  $L = 3$  for the oxygen domain and  $L = 4$  for the hydrogen domain in the partial-range Legendre representation.

CHAPTER VII  
SUMMARY AND CONCLUSIONS

The research reported here may be broadly summarized by three related objectives. The first was to systematically develop a new partial-range formalism for solving the time-independent one-group neutron transport equation with anisotropic scattering for plane and spherical geometries. The motivation for this was the recognized limitations of the diffusion theory and the slow convergence of the widely used approximation methods for physical systems with pronounced discontinuities and highly anisotropic scattering processes.

The second objective was to examine and compare the flexibility and accuracy of the low-order approximations of the developed formalism by calculating some neutronic parameters and by studying some problems associated with neutron analysis. For ideal problems, such as the Milne's problem in plane and spherical geometries, the exact solution is known and hence a comparison using the low-order approximations of the developed formalism meaningful and instructive.

The third objective, then, was to apply the partial-range spherical harmonics in the study of some problems of current interest in reactor analysis. We have chosen to reconstruct the highly anisotropic scattering functions within the context of one-group neutron transport

theory. In addition, the reconstruction of the group-to-group transfer cross section within the context of multigroup neutron transport theory, which is not well behaved over the entire range of the scattering angular variable, has been considered.

To attain our objectives, the partial-range polynomials were used to describe the angular dependence of the functions under consideration in this work. Therefore, we devoted Chapter II to the definitions and properties of such polynomials. The partial-range Legendre polynomials were reconstructed using two different approaches namely the Gram-Schmidt orthogonalization theorem and the transformation of variables. The properties of orthogonality, recurrence relationships and full-range integrations have been examined. Also, the generalization of these mathematical definitions and properties has been extended to other polynomials namely Jacobi, Gegenbauer, and Tschebyscheff polynomials.

For plane geometry, we have established two formalisms which are appropriate for media with anisotropic scattering. In both formalisms the neutron angular flux and the external sources of neutrons were expanded in terms of partial-range Legendre polynomials. In the first formalism, Chapter III, the scattering function has been represented in terms of full-range Legendre polynomials; in the second formalism, Chapter IV, it is represented in terms of partial-range Legendre polynomials. In the former formalism, the mathematical analyses were systematic without any mathematical difficulties while the latter has introduced some unsymmetrical spherical surface integrals

which required considerable care in their evaluation.

The two formalisms allow for discontinuities in the angular flux as well as the external neutron sources at arbitrary points of the angular variable. In addition, the partial-range scattering function formalism allows such discontinuities in the scattering function as well. By this flexibility the scattering function can be reconstructed with a higher degree of accuracy even with low-order approximations. It should be pointed out that, although the formalism allows for discontinuities in the scattering function, the physical scattering function need not necessarily be discontinuous.

An indication of the computational usefulness of these formalisms was obtained by calculating some neutronic parameters using low-order approximations. For example, the eigenvalue associated with the homogeneous neutron transport equation, which gives the inverse diffusion length, has been calculated by the low-order approximation of  $N = 2$  and  $L = 0$  for various cases of linear anisotropy. The results show that this low-order approximation, with a proper choice for the angular segmentation, yields very accurate results in the range of small  $c$ . Hence, it is better than the alternative conventional methods which are particularly inaccurate in this range of  $c$ . It has also been found that for backward scattering the  $NP_L$  approximation gives essentially better results than for forward scattering. However, the same order of approximation gives better results for anisotropic than isotropic scattering for high values of  $c$ .

Using the  $3P_1$  approximation, the eigenvalues associated with the homogeneous neutron transport equation have been calculated. This



approximation has been found to yield better results than the  $2P_0$  approximation. Indeed, it is possible to obtain the exact eigenvalue especially for backward scattering. This approximation was also used to calculate the end point, the linear extrapolation length and the ratio of the asymptotic flux to the total flux associated to the vacuum boundary of the Milne's problem in the plane geometry.

Three different low-order approximations of the  $NP_L - MP_K$  analysis of Chapter IV have been examined and used for the calculation of the eigenvalues. A fictitious highly anisotropic scattering function has been used for the calculational purpose. A comparison between the results of the three low-order approximations,  $DP_0 - DP_0$ ,  $DP_0 - 2P_0$ , and  $2P_0 - 2P_0$  approximations and the exact results shows that the  $DP_0 - 2P_0$  approximation gives more accurate results than the others. It gives, moreover, the exact eigenvalues for backward scattering. In addition, it gives better results than the traditional  $2P_0$  approximation which is comparable in complexity.

Generally, we recommend the  $DP_L - 2P_K$  approximation for the analysis of problems with highly anisotropic scattering. This is because this approximation is the simplest one which exactly satisfies the vacuum boundary condition associated with plane geometry. At the same time it describes the scattering function to a very good extent even with low-order approximations. Further, it does not generate a negative cross section which might result in negative fluxes. Finally, it does not present severe difficulties in its mathematical analysis.

The  $DP_0 - DP_0$  approximation is further used to examine the critical thickness of a bare slab reactor. For large values of  $c$  ( $c > 2$ ), the reactor thickness does not depend strongly on the anisotropy of neutrons generation. For practical ranges of  $c$  ( $1 < c \leq 2$ ), however, the reactor thickness changes considerably with the degree of anisotropy. The reactor thickness increases as the anisotropy increases in the forward direction while it decreases as the anisotropy increases in the backward direction. Therefore, the effect of anisotropic scattering must be taken into consideration in the analysis and design of nuclear reactors specially when high anisotropic scattering is involved like the case of fast breeder reactors.

A general formalism, which allows for discontinuities in the neutron angular flux and its angular derivatives at position dependent points of the angular variable, has been established for spherical geometry, Chapter V. This formalism is, in principle, exact and free of any functional assumptions and exactly represents the actual behaviour of the discontinuities in the angular flux. Therefore, it satisfies the boundary conditions exactly; there is, therefore, no need to use approximate boundary conditions.

For the purpose of numerical calculations, the  $2P_0$  approximation has been used to study the spherical Milne's problem for a medium with a linear anisotropic scattering. The results show discontinuities in the angular flux at position dependent angular points. This is consistent with the expectation from the physical process of the problem; numerical calculations for these discontinuities have

apparently not been given previously for such problems. The total neutron flux for the special case of isotropic scattering is calculated and compared with the exact as well as the diffusion theory results. The important feature of this formalism is that the low-order  $2P_0$  approximation, which is of the same computational complexity as the diffusion theory, yields far more accurate results closer to the surface of the sphere. This suggests that the applications of the position dependent partial-range formalism developed herein for the spherical geometry can, in general, provide more accurate results without additional analytical or computational efforts.

Finally, Chapter VI is devoted to some reactor physics problems of current practical interest. It is concerned with the reconstruction of elastic scattering cross sections in terms of partial-range Legendre polynomials. This new representation, even for few terms, circumvents the appearance of negative cross sections which usually are encountered with the traditional methods. This negativity of cross section leads, in many cases, to oscillations in the solution and consequently yields negative fluxes. For a numerical illustration, the elastic scattering cross section of 14.0 MeV neutrons of  $U^{238}$  and  $Bi^{209}$ , which are very highly anisotropic, have been reconstructed. The results show superiority of this new representation over the usual full-range Legendre polynomial representation of the scattering function.

Further, we have established representations of the group-to-group transfer cross section in terms of partial-range Legendre polynomials. The group-to-group transfer cross section is only well-behaved over certain ranges of the scattering angular variable. These

ranges are governed by the kinematics of neutron scattering interactions as well as the boundaries of the energy groups. Because of this characteristic, the partial-range Legendre polynomials are very suitable for the reconstruction of the transfer cross sections. It yields very good results compared to the full-range Legendre polynomials. This has been confirmed by the numerical results of the water group-to-group transfer cross section from (3.3287 - 3.0119) MeV to (2.7253 - 2.4600) MeV using low-order approximations. Finally, this representation provides an additional degree of freedom. It is not necessary to employ the same order of approximation over the various allowable directional ranges of the scattering angular variable. The order can be varied according to the extent of anisotropy of the scattering cross section over each range.

On the periphery of the main thrust of this research, we have established several properties of partial-range spherical harmonics as well as those of other orthogonal polynomials namely Jacobi, Gegenbauer and Tschebyscheff polynomials. Some unsymmetrical spherical surface integrals, due to the introduction of partial-range scattering functions, have been evaluated. These integrals may be of utility in other fields of physics and engineering.

The success of the partial-range formalism presented herein shows the potential for further extensions and applications for related problems. The  $NP_L$  and the  $NP_L-MP_K$  approximations may be further investigated by numerically examining higher order approximations. Of particular interest would be the  $DP_1-2P_1$  and higher order approximations. More realistic applications could include the study

of a critical reactor assuming a scattering function of two components, isotropic and anisotropic. Further, another application is the study of the albedo problem and comparing its results with the other methods of comparable complexity.

For spherical geometry analysis, more numerical investigations of the higher order approximations could be undertaken. In addition, more calculation for anisotropic scattering using  $2P_0$  approximation appears relevant; the numerical calculations could be extended to more than two region problems.

In addition to the above calculational studies, it appears possible to extend this formalism to the multigroup analysis of neutron transport. Of particular interest is the adaptation of the new representation of the group-to-group transfer cross section with the present methods of multigroup analysis. Another problem might involve extending the partial-range formalism to the cylindrical geometry and the realistic cell calculations.

Finally, the partial-range formalism developed herein can be used in alternative transport problems such as radiative transfer problems and more widely in astrophysics problems.

## APPENDIX A

### THE $B_0^\alpha$ INTEGRALS OF THE $DP_0$ - $DP_0$ APPROXIMATION

The  $B_0^\alpha$  integrals of the  $DP_0$ - $DP_0$  approximation are defined in the text by Eqs. (4.36) to (4.39). Consider, first, the integral  $B_{00}^{22}(\mu)$  which is given by

$$B_{00}^{22}(\mu) = \frac{1}{2\pi} \int\int_{\substack{0 \leq \mu_s \leq 1 \\ 0 \leq \mu' \leq 1}} d\mu' d\omega \quad , \quad (A.1)$$

where

$$\mu_s = \cos\theta_s \quad , \quad (A.2)$$

and

$$\mu' = \cos\theta' \quad . \quad (A.3)$$

Here,  $\theta_s$  is the scattering angle,  $\theta'$  and  $\omega$  give the neutron direction before collision while  $\theta$  gives its direction after collision, Fig. A.1. The angle  $\theta$  is assumed to be in the XY-plane; this assumption does not affect the generality of the theory as mentioned in the text.

The integral of Eq. (A.1) represents the integration over the hemisphere above the plane  $\Omega$ , which has the origin as one point and the direction  $\underline{\Omega}$  as its normal, and also, above the  $X = 0$  plane. Figure A.2 illustrates the projection of the integral of Eq. (A.1) along the Z-direction. This integral is given by the area on the surface of the

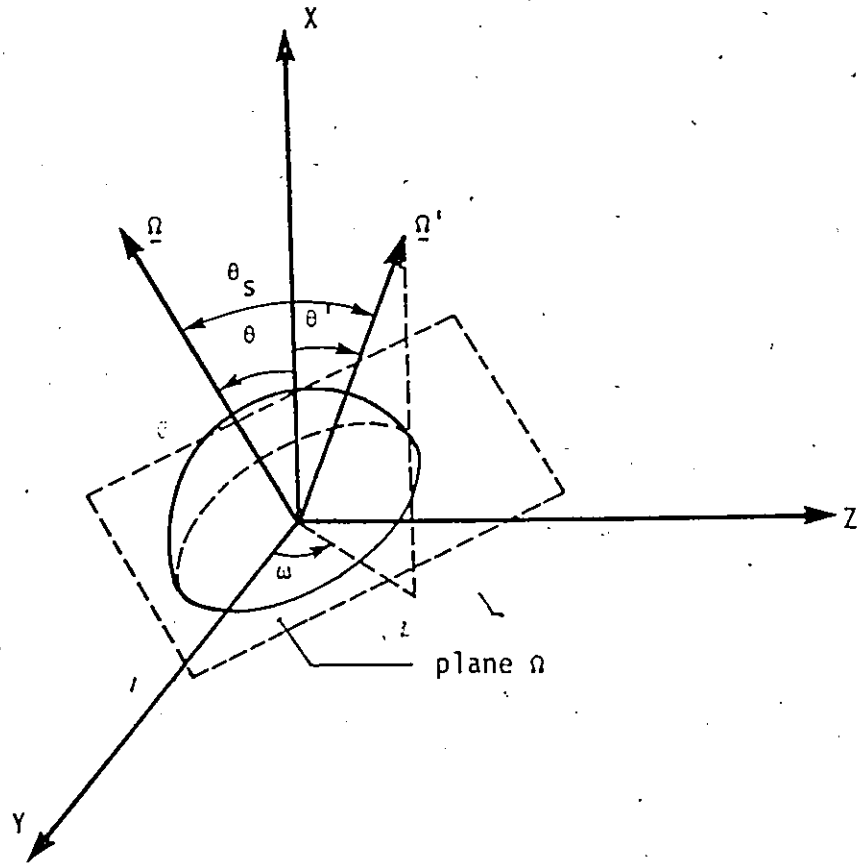


Fig. A.1: Geometrical configuration used in the  $DP_0$ - $DP_0$  approximation;  $\underline{\Omega}'$  is the neutron initial direction,  $\underline{\Omega}$  is the neutron final direction, and  $\theta_s$  is the scattering angle.

sphere (unit radius) corresponding to the solid curve shown in Fig.

A.2. Therefore, we can write

$$B_{00}^{22}(\mu) = \frac{1}{2\pi} (2\pi - 2\theta) = 1 - \frac{1}{\pi} \cos^{-1} \mu \quad , \quad (A.4)$$

where

$$\mu = \cos \theta \quad (A.5)$$

Now, consider the integral  $B_{00}^{21}(\mu)$  which is given by

$$B_{00}^{21}(\mu) = \frac{1}{2\pi} \iint_{\substack{0 \leq \mu_s \leq 1 \\ -1 \leq \mu' \leq 0}} d\mu' d\omega \quad (A.6)$$

This integral represents the integral over the hemisphere above the plane  $\omega$  but below the plane  $X = 0$ . In Fig. A.2, it is given by the area on the surface of the sphere corresponding to the dashed curve. Therefore,

$$B_{00}^{21}(\mu) = \frac{1}{2\pi} \cdot 2\theta = \frac{1}{\pi} \cos^{-1} \mu \quad (A.7)$$

Similarly, the other two integrals,

$$B_{00}^{11}(\mu) = \frac{1}{2\pi} \iint_{\substack{-1 \leq \mu_s \leq 0 \\ -1 \leq \mu' \leq 0}} d\mu' d\omega \quad , \quad (A.8)$$

and

$$B_{00}^{12}(\mu) = \frac{1}{2\pi} \iint_{\substack{-1 \leq \mu_s \leq 0 \\ 0 \leq \mu' \leq 1}} d\mu' d\omega \quad , \quad (A.9)$$



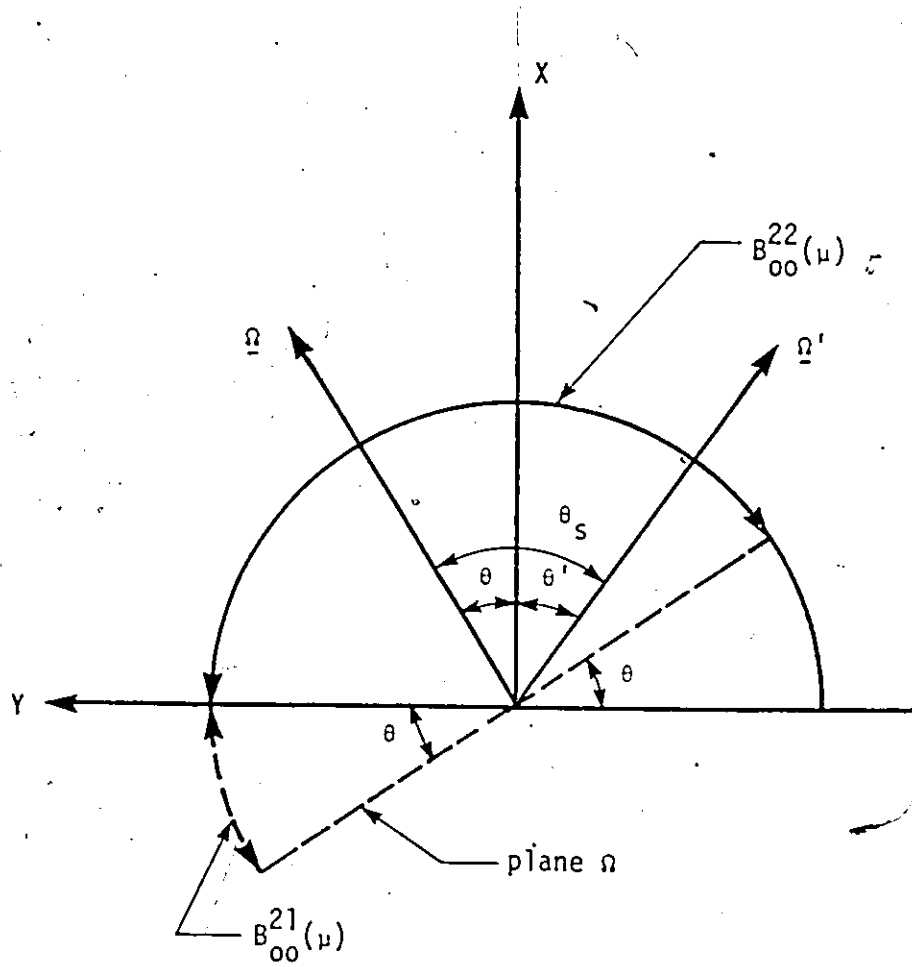


Fig. A.2: One direction projection of the integrals  $B_{00}^{22}(\mu)$  and  $B_{00}^{21}(\mu)$  of the  $DP_0$ - $DP_0$  approximation.

represent the integral over the hemisphere under the plane  $\Omega$ , not shown in Fig. A.1 and at the same time above the  $X = 0$  plane for  $B_{00}^{12}(\mu)$  and below it for  $B_{00}^{11}(\mu)$ , respectively. Therefore, we have

$$B_{00}^{11}(\mu) = 1 - \frac{1}{\pi} \cos^{-1} \mu, \quad (\text{A.10})$$

and

$$B_{00}^{12}(\mu) = \frac{1}{\pi} \cos^{-1} \mu. \quad (\text{A.11})$$

## APPENDIX B

### INTEGRALS OF THE $DP_0-2P_0$ APPROXIMATION

#### B.1 Non Symmetrical Spherical Surface Integral

Before deriving the  $B_0^\beta$  and the  $A_0^\beta$  integrals of the  $DP_0-2P_0$  approximation we need to consider the following non symmetrical spherical surface integral which will be used in their derivation. Consider the area on the surface of a sphere (unit radius), Fig. B.1, which is enclosed between the great circle  $\omega$  and the small circle  $\alpha$  shown in the figure. From Fig. B.1 we can see that the area under consideration is given by

$$A = 2 \int_{\theta=\omega}^{\alpha} \int_{\phi=0}^{\cos^{-1} \frac{\tan \omega}{\tan \theta}} \sin \theta d\theta d\phi \quad (B.1)$$

Performing the integration over the  $\phi$  angle gives

$$A = 2 \int_{\theta=\omega}^{\alpha} \sin \theta \cos^{-1} \frac{\tan \omega}{\tan \theta} d\theta \quad (B.2)$$

Using the integration by parts, the above integral can be shown to be given by

$$A = 2 \left[ \cos^{-1} \left( \frac{\sin \omega}{\sin \alpha} \right) - \cos \alpha \cos^{-1} \left( \frac{\tan \omega}{\tan \alpha} \right) \right] \quad (B.3)$$

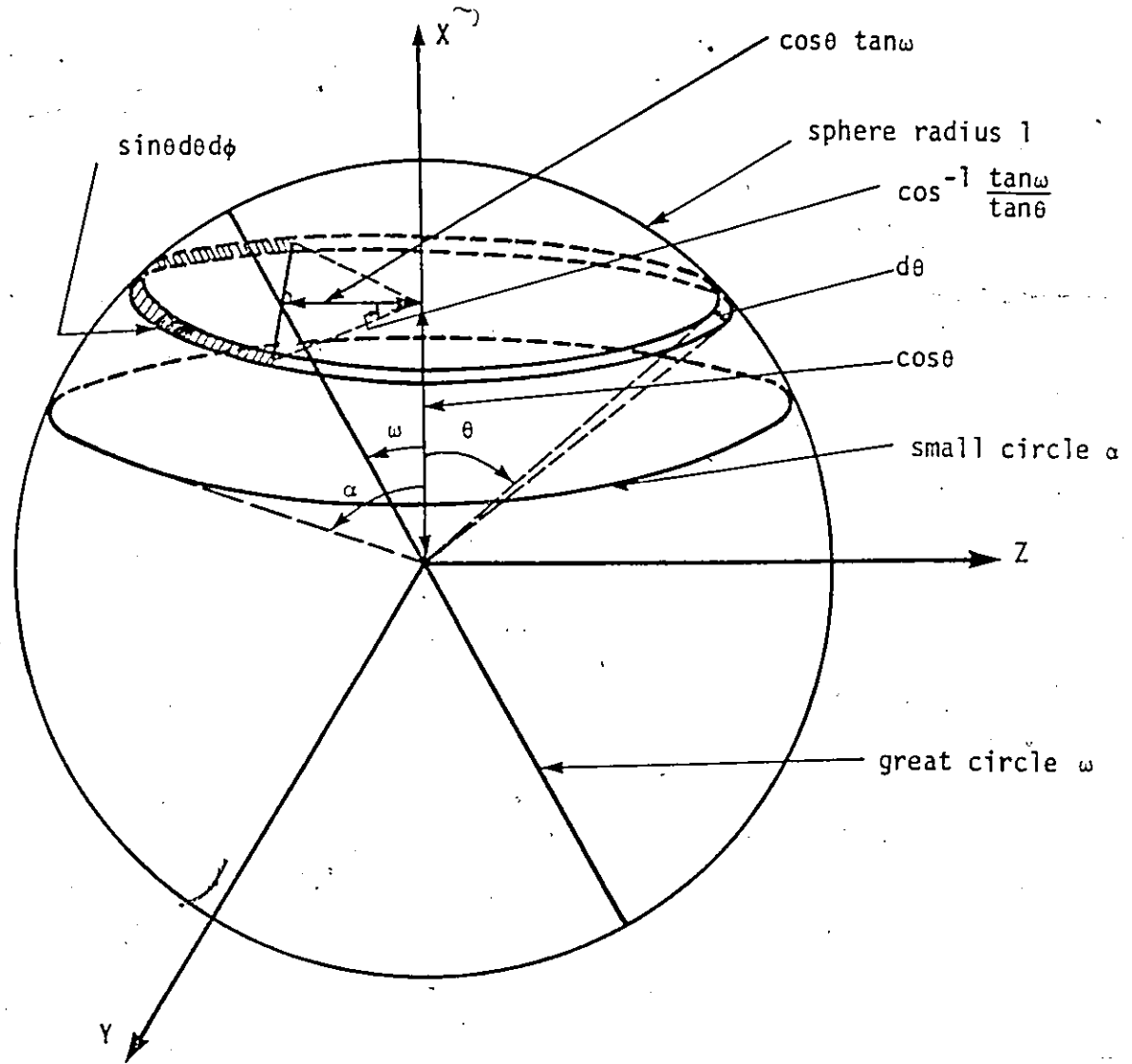


Fig. B.1: A graphical representation of a nonsymmetrical spherical surface integral.

## B.2 The $B_0^\beta$ Integrals

Now, we will consider the  $B_0^\beta$  integrals which are defined by Eq. (4.18) with the appropriate limits of integration for the  $DP_0-2P_0$  approximation. First, let us consider the  $B_{00}^{22}(\mu)$  integral which is given by Eq. (4.75)

$$B_{00}^{22}(\mu) = \frac{1}{2\pi} \iint_{\substack{\mu_{S1} \leq \mu_S \leq 1 \\ 0 \leq \mu' \leq 1}} d\mu' d\omega \quad (B.4)$$

The integral of the above equation represents the area on the surface of a sphere (unit radius) on the upper hemisphere (to satisfy the condition  $1 \geq \mu' \geq 0$ ) and also enclosed inside the cone of the angle  $\theta_{S1} = \cos^{-1} \mu_{S1}$  with the direction  $\underline{\Omega}$  (to satisfy the condition  $1 \geq \mu_S \geq \mu_{S1}$ ) as shown in Fig. B.2.

Similarly, the other integrals of  $B_0^\beta$  can be represented by non symmetrical areas over the surface of a sphere. Consider  $B_{00}^{21}(\mu)$  which is defined by

$$B_{00}^{21}(\mu) = \frac{1}{2\pi} \iint_{\substack{\mu_{S1} \leq \mu_S \leq 1 \\ -1 \leq \mu' \leq 0}} d\mu' d\omega \quad (B.5)$$

The integral of the above equation represents the area on the surface of the sphere of Fig. B.2 on the lower hemisphere and also enclosed inside the cone of the angle  $\theta_{S1}$ . Moreover, the integral of  $B_{00}^{11}(\mu)$

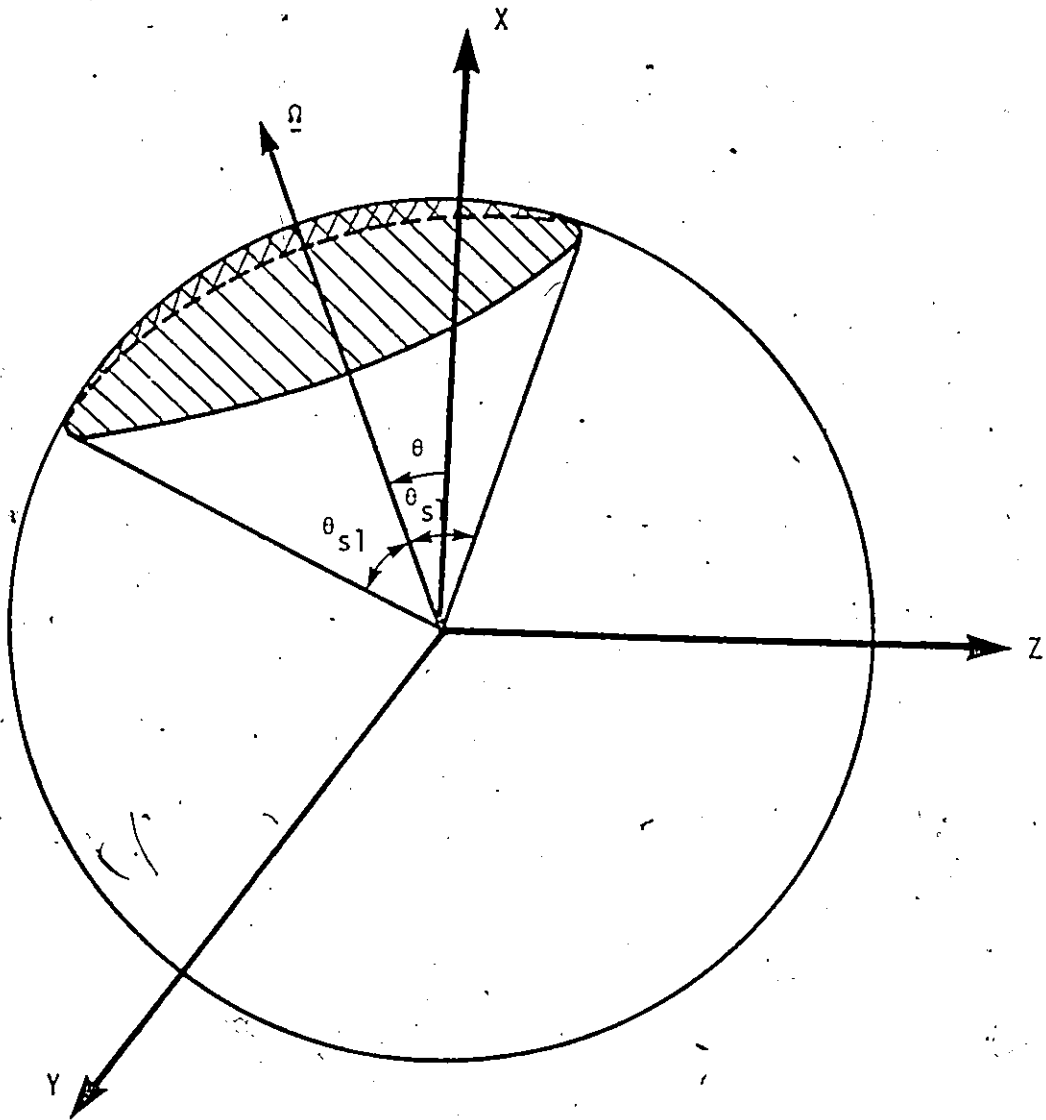


Fig. B.2: Graphical representation of the integral of  $B_{00}^{22}(\mu)$  of the  $DP_0-2P_0$  approximation.

which is defined by

$$B_{00}^{11}(\mu) = \frac{1}{2\pi} \iint_{\substack{-1 \leq \mu_s \leq \mu_{s1} \\ -1 \leq \mu' \leq 0}} d\mu' d\omega, \quad (B.6)$$

represents the area on the surface of the sphere of Fig. B.2 over the lower hemisphere and outside the cone of the angle  $\theta_{s1}$ . Finally, the integral of  $B_{00}^{12}(\mu)$  which is defined by

$$B_{00}^{12}(\mu) = \frac{1}{2\pi} \iint_{\substack{-1 \leq \mu_s \leq \mu_{s1} \\ 0 \leq \mu' \leq 1}} d\mu' d\omega, \quad (B.7)$$

gives the area over the upper hemisphere and outside the cone of the angle  $\theta_{s1}$ . These three integrals, Eqs. (B.5) to (B.7), can be related to the integral  $B_{00}^{22}(\mu)$  as will be given later in this appendix.

From Fig. B.2 we can see that the expression of the integral  $B_{00}^{22}(\mu)$  depends on both the range of the angle  $\theta$  as well as the range of the angle  $\theta_{s1}$ . In the following we will consider all the possible ranges of  $\theta$  and  $\theta_{s1}$  and obtain an expression for  $B_{00}^{22}(\mu)$  in each range.

I)  $\theta \leq \pi/2$ : For this range of  $\theta$ , there are three possible ranges of  $\theta_{s1}$  as follows:

1)  $\theta_{s1} \leq \pi/2 - \theta$ ; Fig. B.3-a:

In this range the integral of  $B_{00}^{22}(\mu)$  is just the area of a cap with an angle  $\theta_{s1}$ . Therefore

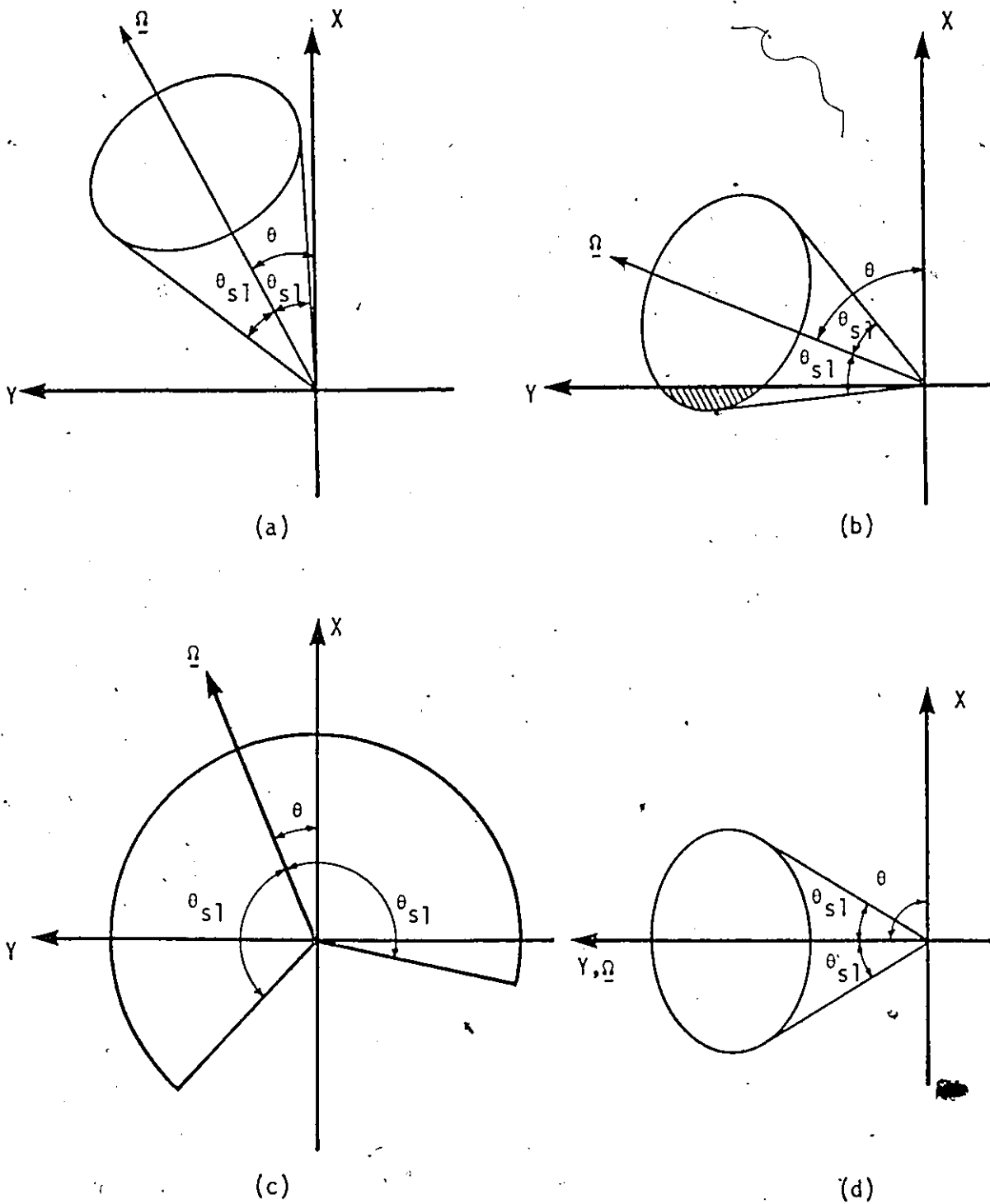


Fig. B.3: Different ranges of  $\theta$  and  $\theta_{s1}$  for the derivation of  $B_{00}^{22}(\mu)$  of the  $DP_0-2P_0$  approximation.



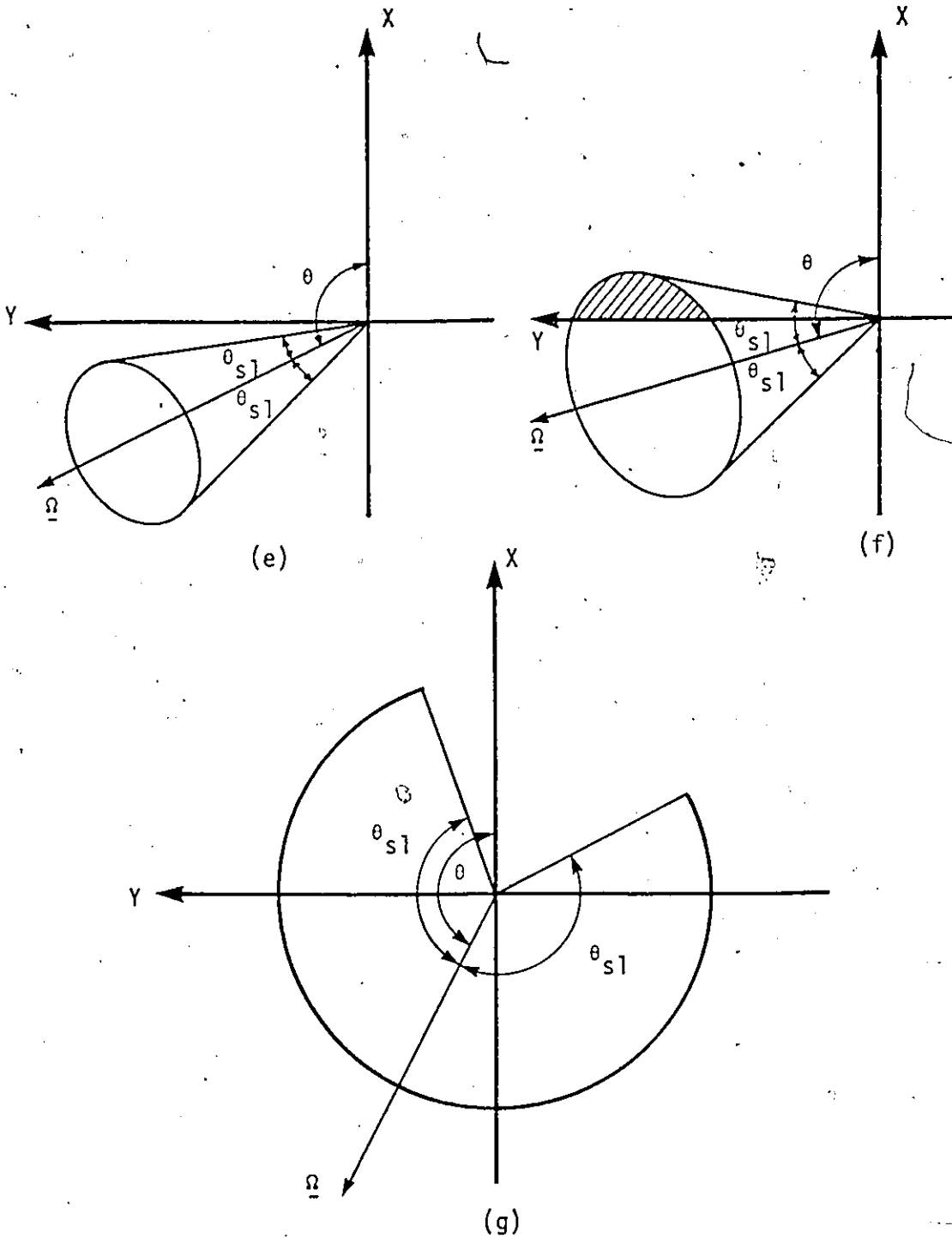


Fig. B.3 (cont'd): Different ranges of  $\theta$  and  $\theta_{s1}$  for the derivation of  $B_{00}^{22}(\mu)$  of the  $DP_0-2P_0$  approximation.

$$B_{00}^{22}(\mu) = 1 - \mu_{s1} \quad (B.8)$$

2)  $\pi/2 + \theta \geq \theta_{s1} \geq \pi/2 - \theta$ ; Fig. B.3-b:

Using Fig. B.3-b and the integral given by Eq. (B.3) we can write  $B_{00}^{22}(\mu)$ , for this range, as

$$B_{00}^{22}(\mu) = 1 - \mu_{s1} - \frac{1}{\pi} \left[ \cos^{-1} \frac{\sin(\frac{\pi}{2} - \theta)}{\sin \theta_{s1}} - \mu_{s1} \cos^{-1} \frac{\tan(\frac{\pi}{2} - \theta)}{\tan \theta_{s1}} \right]. \quad (B.9)$$

The above equation can be rewritten as

$$B_{00}^{22}(\mu) = 1 - \mu_{s1} - \frac{1}{\pi} \left( \cos^{-1} \frac{\cos \theta}{\sin \theta_{s1}} - \mu_{s1} \cos^{-1} \frac{\cot \theta}{\tan \theta_{s1}} \right). \quad (B.10)$$

3)  $\theta_{s1} \geq \pi/2 + \theta$ ; Fig. B.3-c:

In this range the integral of  $B_{00}^{22}(\mu)$  represents the total area of the upper hemisphere. Therefore,

$$B_{00}^{22}(\mu) = 1.0 \quad (B.11)$$

II)  $\theta = \pi/2$ ; Fig. B.3-d: For this particular value of  $\theta$  and for all values of  $\theta_{s1}$  the integral  $B_{00}^{22}(\mu)$  is given by

$$B_{00}^{22}(\mu) = \frac{1}{2} (1 - \mu_{s1}) \quad (B.12)$$

It is of interest to note that this is a special case of all the cases mentioned in part I and that will be given in part III as well.

III)  $\theta \geq \pi/2$ : For this range of  $\theta$ , there are three ranges of  $\theta_{s1}$  as follows:

i)  $\theta_{s1} \leq \theta - \pi/2$ ; Fig. B.3-e:

From the figure we can see that the cap of the cone of the angle  $\theta_{s1}$  is completely on the lower hemisphere. Therefore,

$$B_{00}^{22}(\mu) = 0.0 \quad (B.13)$$

2)  $\theta - \pi/2 \leq \theta_{s1} \leq 3\pi/2 - \theta$ ; Fig. B.3-f:

From the figure and Eq. (B.3) we can write

$$B_{00}^{22}(\mu) = \frac{1}{\pi} \left[ \cos^{-1} \frac{\sin(\theta - \frac{\pi}{2})}{\sin\theta_{s1}} - \mu_{s1} \cos^{-1} \frac{\tan(\theta - \frac{\pi}{2})}{\tan\theta_{s1}} \right] \quad (B.14)$$

which can be rewritten as

$$B_{00}^{22}(\mu) = 1 - \mu_{s1} - \frac{1}{\pi} \left( \cos^{-1} \frac{\cos\theta}{\sin\theta_{s1}} - \mu_{s1} \cos^{-1} \frac{\cot\theta}{\tan\theta_{s1}} \right) \quad (B.15)$$

The above equation is exactly the same as Eq. (B.10).

3)  $\theta_{s1} \geq 3\pi/2 - \theta$ ; Fig. B.3-g:

For this range the integral  $B_{00}^{22}(\mu)$  is given by

$$B_{00}^{22}(\mu) = -\mu_{s1} \quad (B.16)$$

The results of Eqs. (B.8) to (B.16) are summarized in Fig. B.4.

Now, it is straightforward to show that the other  $B_0^B$  integrals, Eqs. (B.5) to (B.7), are related to  $B_{00}^{22}(\mu)$  by the following

$$B_{00}^{11}(\mu) = \mu_{s1} + B_{00}^{22}(\mu) \quad (B.17)$$

$$B_{00}^{12}(\mu) = 1 - B_{00}^{22}(\mu) \quad (B.18)$$

and

$$B_{00}^{21}(\mu) = 1 - \mu_{s1} - B_{00}^{22}(\mu) \quad (B.19)$$

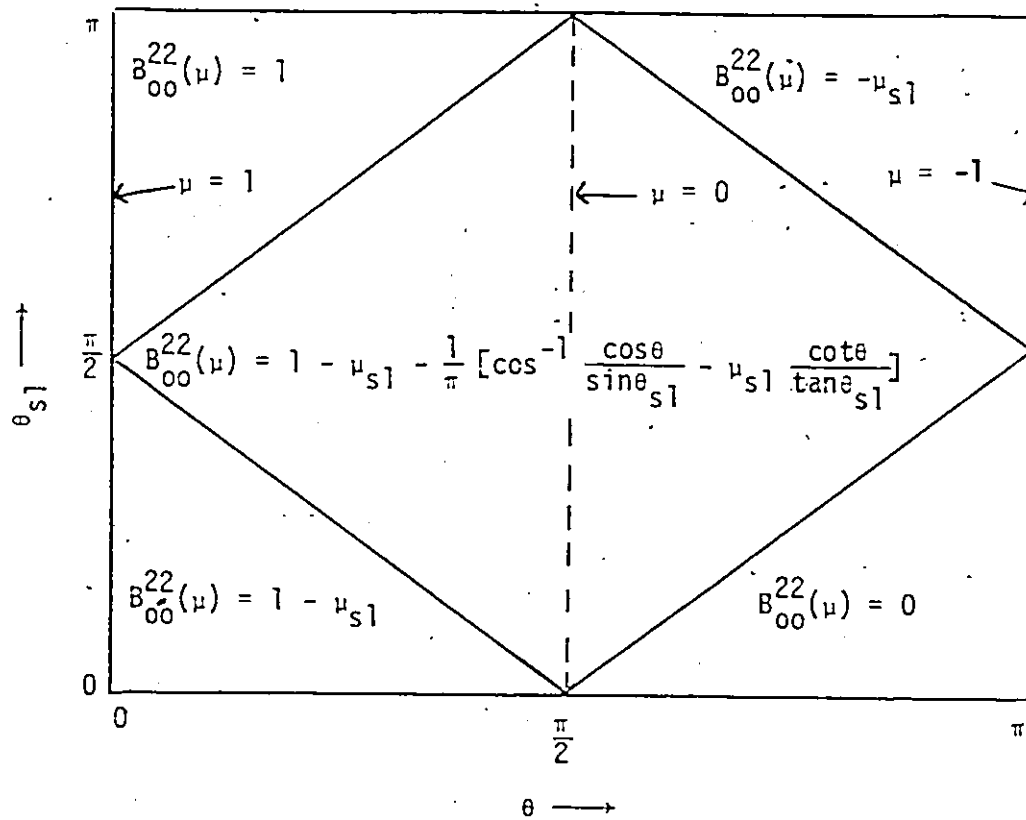


Fig. B.4: The integral  $B_{00}^{22}(\mu)$  as a function of  $\theta = \cos^{-1} \mu$  and  $\theta_{s1} = \cos^{-1} \mu_{s1}$  for the  $DP_0$ - $2P_0$  approximation.

It is of interest to note that these relations are correct for all the ranges of  $\theta$  and  $\theta_{s1}$ .

### 3.3 The $A_0^B$ Constants

In the following we will evaluate the two  $A_0^B$  integrals of the  $D_0^P - 2P_0$  approximation defined by Eqs. (4.82) and (4.83) in the text.

First, consider the integral of Eq. (4.82) which reads

$$A_{000}^{122} = \int_{-1}^0 B_{00}^{22}(\mu) d\mu \quad (B.20)$$

From Fig. B.4 we can see that the above integral depends on the sign of  $\mu_{s1}$ . First, for negative value of  $\mu_{s1}$ , the integral of Eq. (B.20) can be written as

$$A_{000}^{122} = \int_{-1}^{-x} -\mu_{s1} d\mu + \int_{-x}^0 \left[ 1 - \mu_{s1} - \frac{1}{\pi} \left( \cos^{-1} \frac{\cos\theta}{\sin\theta_{s1}} - \mu_{s1} \cos^{-1} \frac{\cot\theta}{\tan\theta_{s1}} \right) \right] d\mu, \quad (B.21)$$

where

$$x = +\sqrt{1 - \mu_{s1}^2} \quad (B.22)$$

Equation (B.21) can be rewritten as

$$A_{000}^{122} = -\mu_{s1}(-x + 1) + I(\mu=0) - I(\mu=-x), \quad (B.23)$$

where the integral  $I$  is defined by

$$I(\mu) = \int \left[ 1 - \mu_{s1} - \frac{1}{\pi} \left( \cos^{-1} \frac{\cos\theta}{\sin\theta_{s1}} - \mu_{s1} \cos^{-1} \frac{\cot\theta}{\tan\theta_{s1}} \right) \right] d\mu. \quad (B.24)$$

The above integral is evaluated and it is given by

$$\begin{aligned}
 I(\mu) = & (1 - \mu_{s1})\mu - \frac{1}{\pi} \left\{ \mu \cos^{-1} \frac{\mu}{\sqrt{1 - \mu_{s1}^2}} \right. \\
 & - \sqrt{1 - \mu_{s1}^2 - \mu^2} - \mu_{s1} \left[ \mu \cos^{-1} \frac{\mu_{s1}\mu}{\sqrt{(1 - \mu^2)(1 - \mu_{s1}^2)}} \right. \\
 & \left. \left. - \sec^{-1} \left( \frac{\sqrt{1 - \mu^2}}{\mu_{s1}} \right) \right] \right\} \quad (B.25)
 \end{aligned}$$

Substituting the limits of  $\mu = 0$  and  $\mu = -x$ , respectively, into the above equation and note that  $\mu_{s1}$  is negative, subsequently substituting into Eq. (B.23), then substituting the expression of  $x$ , Eq. (B.22), and rearranging yields

$$A_{000}^{122} = \frac{1}{\pi} \left( \sqrt{1 - \mu_{s1}^2} - \mu_{s1} \cos^{-1} \mu_{s1} \right) \quad (B.26)$$

Secondly, we will consider the special case of  $\mu_{s1} = 0$ . Substituting  $\mu_{s1} = 0$  into the expression of  $B_{00}^{22}(\mu)$  of Fig. B.4 and subsequently substituting into Eq. (B.20) yields

$$A_{000}^{122} = \int_{-1}^0 \left( 1 - \frac{1}{\pi} \cos^{-1} \mu \right) d\mu = \frac{1}{\pi} \quad (B.27)$$

Note that Eq. (B.27) can be deduced from Eq. (B.26) by specifying  $\mu_{s1} = 0$ . Finally, for positive value of  $\mu_{s1}$ , Eq. (B.20) and Fig. B.4 give

$$A_{000}^{122} = \int_{-x}^0 \left[ 1 - \mu_{s1} - \frac{1}{\pi} \left( \cos^{-1} \frac{\cos \theta}{\sin \theta_{s1}} - \mu_{s1} \cos^{-1} \frac{\cot \theta}{\tan \theta_{s1}} \right) \right] d\mu \quad (B.28)$$

which can be rewritten as

$$A_{000}^{122} = I(\mu=0) - I(\mu=-x) , \quad (B.29)$$

where the integral  $I$  is given by Eq. (B.25) but for positive values of  $\mu_{s1}$ . After some algebraic manipulation Eq. (B.29) can be shown that it reduces to Eq. (B.26).

Now, consider the second integral of  $A_{000}^{222}$  which is defined by

$$A_{000}^{222} = \int_0^1 B_{00}^{22}(\mu) d\mu . \quad (B.30)$$

Proceeding exactly similar to the evaluation of Eq. (B.20) but for the left half of Fig. B.4, the above integral can be shown to be related to  $A_{000}^{122}$  by the following

$$A_{000}^{222} = 1 - \mu_{s1} - A_{000}^{122} , \quad (B.31)$$


for all ranges of  $\mu_{s1}$ .

APPENDIX C

INTEGRALS OF THE  $2P_0$ - $2P_0$  APPROXIMATION

C.1 The  $B_0^Y$  Integrals

Here, we will consider the  $B_0^Y$  integrals of the  $2P_0$ - $2P_0$  approximation which are defined by Eq. (4.18) with the appropriate limits of integration for the present approximation. We will discuss the integral  $B_{00}^{22}(\mu)$  in some detail and then relate the other integrals of  $B_0^Y$  to it. The integral  $B_{00}^{22}(\mu)$  is defined by

$$B_{00}^{22}(\mu) = \frac{1}{2\pi} \iint_{\substack{\mu_1 \leq \mu_s \leq 1 \\ \mu_1 \leq \mu' \leq 1}} d\mu' d\omega \quad (C.1)$$


Here,  $\mu_s$  is again the cosine of the scattering angle, Fig. A.1. The integral of Eq. (C.1) represents the area on the surface of a sphere (unit radius) which is common on the cap inside a cone of an angle  $\theta_1 = \cos^{-1} \mu_1$  with the X-direction (cone 1) and also on the cap inside a cone of an angle  $\theta_1$  with the direction  $\underline{\Omega}$  (cone 2) as shown in Fig. C.1.

From Fig. C.1, we can see that the two small circles of both caps intersect in two points  $\eta$  and  $\xi$  on the surface of the sphere, for the case illustrated in the figure. The area under interest is two times the area between one of these circles and the great circle  $\eta\xi$ . Then,



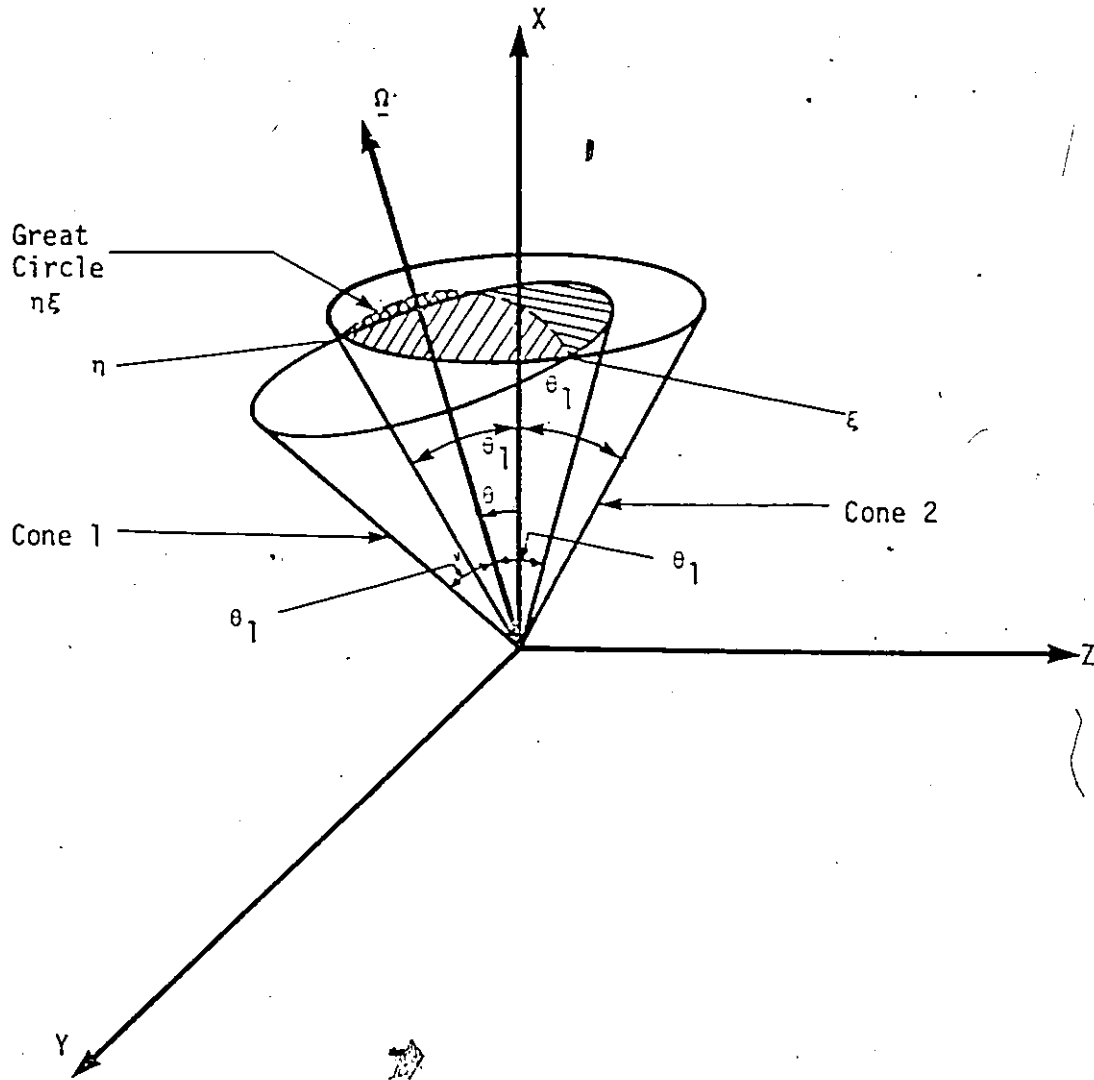


Fig. C.1: Graphical representation of the  $B_{00}^{22}(\mu)$  of the  $2P_0-2P_0$  approximation for the range  $\theta/2 \leq \theta_1 \leq \pi - \theta/2$ .

using Eq. (B.3) with appropriate values for the angles  $\omega$  and  $\alpha$ , we can write

$$B_{00}^{22}(\mu) = \frac{2}{\pi} \left[ \cos^{-1} \frac{\sin \frac{\theta}{2}}{\sin \theta_1} - \mu_1 \cos^{-1} \frac{\tan \frac{\theta}{2}}{\tan \theta_1} \right] \quad (C.2)$$

The above expression holds only for the range of  $\mu_1$  given by

$$\frac{\theta}{2} \leq \theta_1 \leq \pi - \frac{\theta}{2} .$$

For  $\theta_1 \leq \theta/2$ , it is clear from Fig. C.2 that no common area on the two caps under interest. Therefore,

$$B_{00}^{22}(\mu) = 0.0 \quad (C.3)$$

Finally, for  $\theta_1 \geq \pi - \theta/2$  which is shown in Fig. C.3, we can see that the integral under consideration is given by the total area of the sphere excluding the area of the two small caps shown in the figure.

Therefore,

$$B_{00}^{22}(\mu) = -2\mu_1 \quad (C.4)$$

The above results are summarized in Fig. C.4.

Consideration will be given now to the integral of  $B_{00}^{21}(\mu)$  which is defined by

$$B_{00}^{21}(\mu) = \frac{1}{2\pi} \iint_{\substack{\mu_1 \leq \mu_s \leq 1 \\ -1 \leq \mu' \leq \mu_1}} d\mu' d\omega \quad (C.5)$$

The integral of the above equation represents the area on the surface

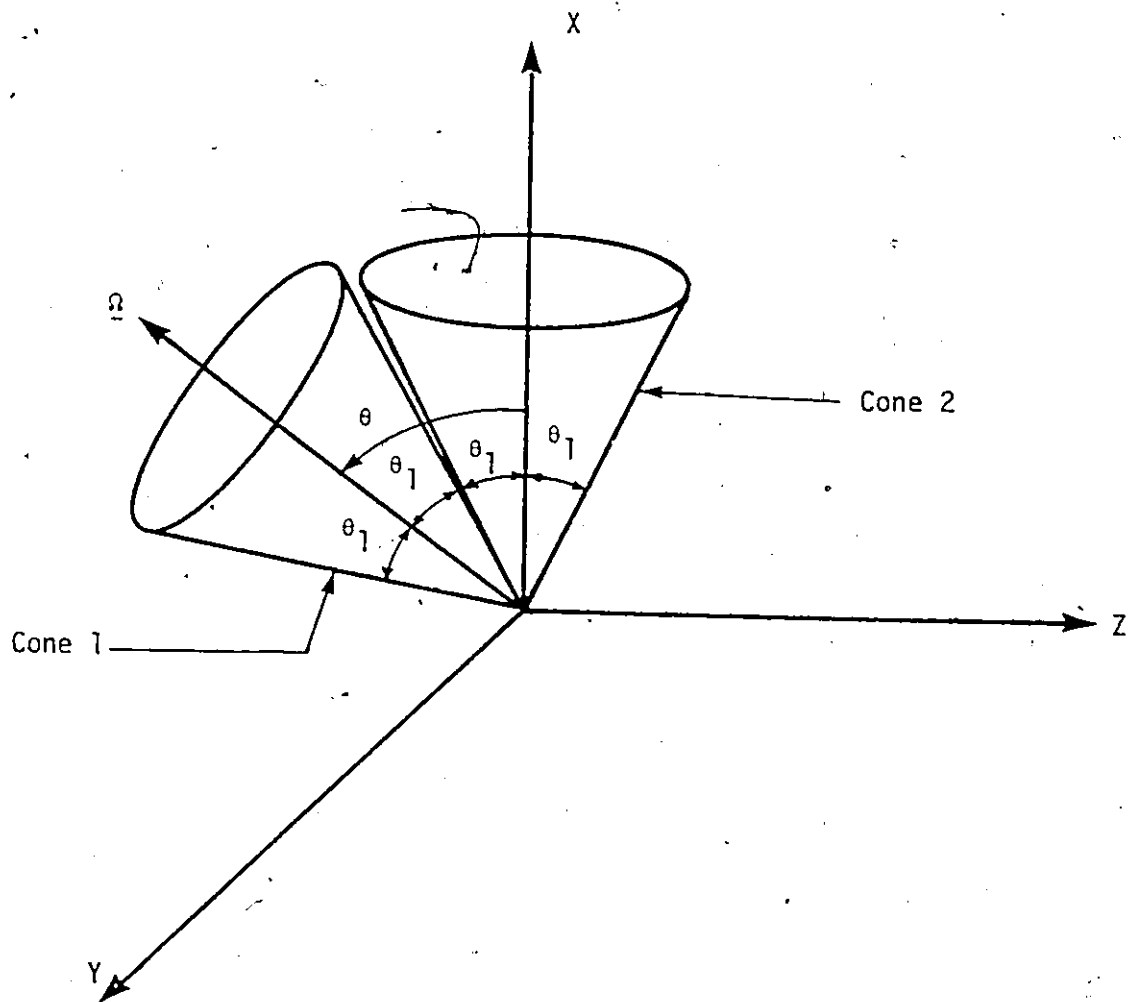


Fig. C.2: Graphical representation of the  $B_{00}^{22}(\mu)$  of the  $2P_0-2P_0$  approximation for the range  $\theta_1 \leq \theta/2$ .

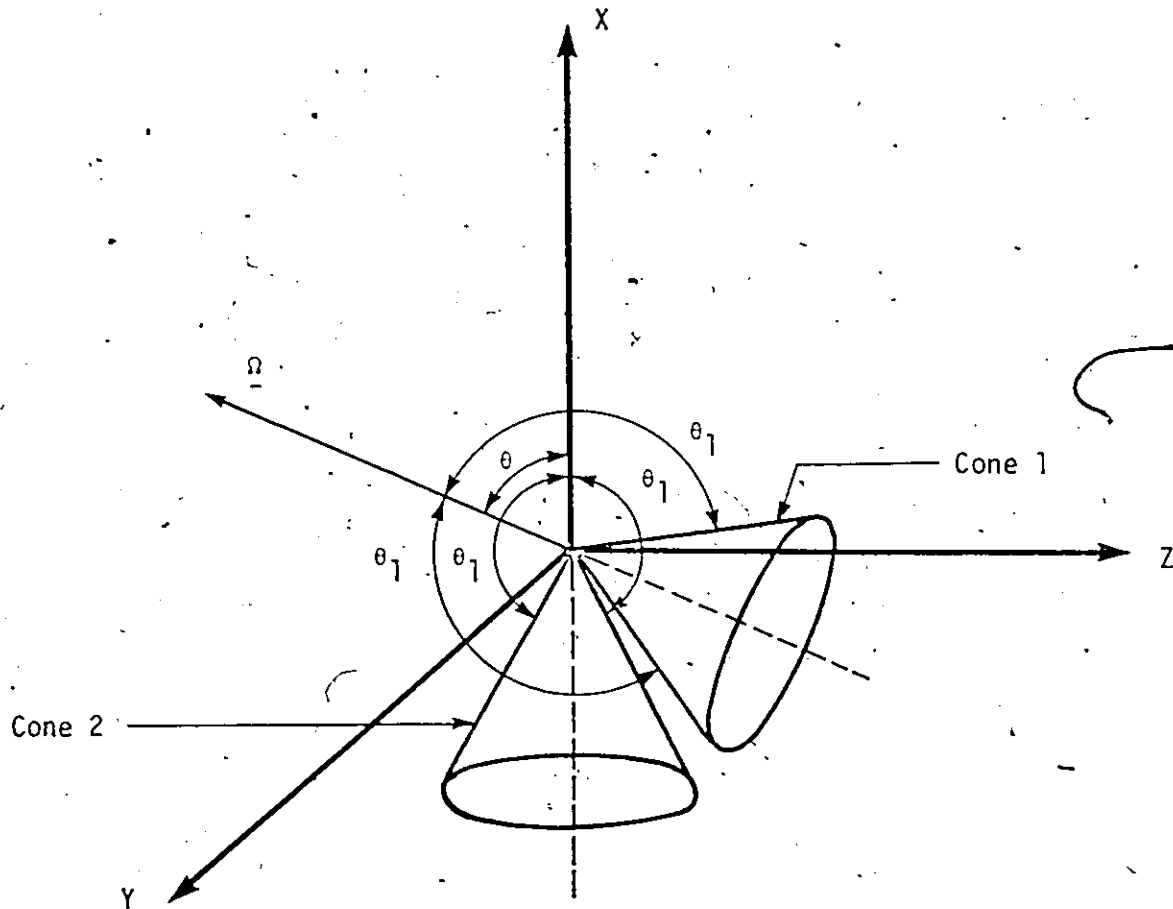


Fig. C.3: Graphical representation of the  $B_{00}^{22}(\mu)$  of the  $2P_0-2P_0$  approximation for the range  $\theta_1 \geq \pi - \theta/2$ .

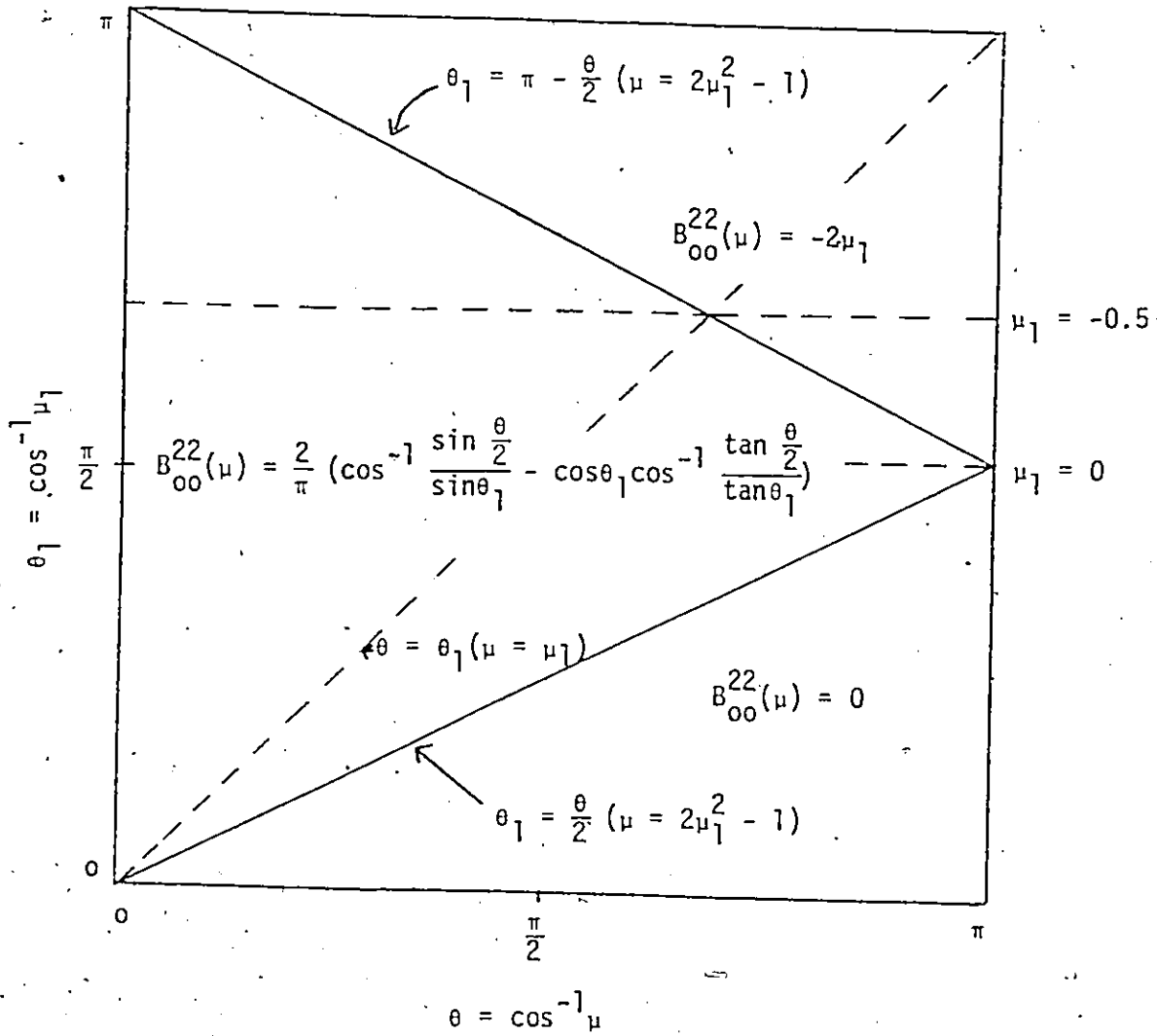


Fig. C.4: The integral  $B_{00}^{22}(\mu)$  as a function of  $\theta$  and  $\theta_1$  for the  $2P_0-2P_0$  approximation.

of the sphere on the cap outside cone 1 and also on the cap inside cone 2, Fig. C.1. Therefore,

$$B_{00}^{21}(\mu) = 1 - \mu_1 - B_{00}^{22}(\mu) \quad (C.6)$$

Next is the integral  $B_{00}^{12}(\mu)$  which is defined by

$$B_{00}^{12}(\mu) = \frac{1}{2\pi} \iint_{\substack{-1 \leq \mu_s \leq \mu_1 \\ \mu_1 \leq \mu' \leq 1}} d\mu' d\omega \quad (C.7)$$

The integral of the above equation represents the area on the surface of the sphere on the cap inside cone 1 and also on the cap outside cone 2 of Fig. C.1. It is clear that this area is symmetric with the area corresponding to the integral of Eq. (C.5). Therefore,

$$B_{00}^{12}(\mu) = B_{00}^{21}(\mu) \quad (C.8)$$

Finally, consider the integral  $B_{00}^{11}(\mu)$  which is defined by

$$B_{00}^{11}(\mu) = \frac{1}{2\pi} \iint_{\substack{-1 \leq \mu_s \leq \mu_1 \\ -1 \leq \mu' \leq \mu_1}} d\mu' d\omega \quad (C.9)$$

The integral of the above equation represents the area on the surface of the sphere of Fig. C.1 on the cap outside cone 1 and also on the cap outside cone 2. Therefore, the integral of Eq. (C.9) can be written as

$$B_{00}^{11}(\mu) = \frac{1}{2\pi} [2\pi(1 + \mu_1) - 2\pi B_{00}^{21}(\mu)] \quad (C.10)$$

Substituting Eq. (C.6) into the above equation and rearranging yields

$$B_{00}^{11}(\mu) = 2\mu_1 + B_{00}^{22}(\mu) \quad (C.11)$$

The integrals of Eqs. (C.5), (C.7) and (C.9) have been examined for the different ranges of  $\theta$  and  $\theta_1$  of Fig. C.4 and the same relationships with  $B_{00}^{22}(\mu)$  hold.

## C.2 The $A_0^Y$ Integrals

In this section we will consider the  $A_0^Y$  integrals of the  $2P_0-2P_0$  approximation which are defined by Eq. (4.20) with the appropriate limits for this approximation. First, consider the integral of  $A_{000}^{111}$  which is defined by

$$A_{000}^{111} = \int_{-1}^{\mu_1} B_{00}^{11}(\mu) d\mu \quad (C.12)$$

Substituting the expression of  $B_{00}^{11}(\mu)$  of Eq. (C.11) into the above equation yields

$$A_{000}^{111} = \int_{-1}^{\mu_1} [2\mu_1 + B_{00}^{22}(\mu)] d\mu \quad (C.13)$$

This equation gives

$$A_{000}^{111} = 2\mu_1(1 + \mu_1) + A_{000}^{122} \quad (C.14)$$

where

$$A_{000}^{122} = \int_{-1}^{\mu_1} B_{00}^{22}(\mu) d\mu \quad (C.15)$$

Secondly, consider the integral  $A_{000}^{121}$  which is defined by

$$A_{000}^{121} = \int_{-1}^{\mu_1} B_{00}^{21}(\mu) d\mu \quad (C.16)$$

Substituting Eq. (C.6) into the above equation and performing the integration of the first term yields

$$A_{000}^{121} = 1 - \mu_1^2 - A_{000}^{122}, \quad (C.17)$$

where  $A_{000}^{122}$  is defined by Eq. (C.15).

Next is the integral of  $A_{000}^{112}$  which is defined by

$$A_{000}^{112} = \int_{-1}^{\mu_1} B_{00}^{12}(\mu) d\mu. \quad (C.18)$$

From Eqs. (C.8), (C.16) and (C.18) we can conclude that

$$A_{000}^{112} = A_{000}^{121}, \quad (C.19)$$

where  $A_{000}^{121}$  is given by Eq. (C.17).

Similarly, we can derive the following relationships for the other  $A_0^Y$  constants

$$A_{000}^{211} = 2\mu_1(1 - \mu_1) + A_{000}^{222}, \quad (C.20)$$

and

$$A_{000}^{212} = A_{000}^{221} = 1 - \mu_1^2 - A_{000}^{222}, \quad (C.21)$$

where  $A_{000}^{222}$  is defined by

$$A_{000}^{222} = \int_{\mu_1}^1 B_{00}^{22}(\mu) d\mu. \quad (C.22)$$

The integrals of  $A_{000}^{122}$  and  $A_{000}^{222}$ , Eqs. (C.15) and (C.22), respectively, depend on the range of  $\mu_1$ . From Fig. C.4, one can recognize the following three ranges:

$$1) \quad +1 > \mu_1 \geq 0:$$

In this range of  $\mu_1$  the integrals of Eqs. (C.15) and (C.22) reduce to

$$A_{000}^{122} = \int_{2\mu_1^2 - 1}^{\mu_1} B_{00}^{22}(\mu) d\mu, \quad (C.23)$$



and

$$A_{000}^{222} = \int_{\mu_1}^1 B_{00}^{22}(\mu) d\mu, \quad (C.24)$$

respectively. The expression of Eq. (C.2) of  $B_{00}^{22}(\mu)$  must be used in the integrals of Eqs. (C.23) and (C.24).

2)  $0 \geq \mu_1 \geq -0.5$ :

In this range we can write

$$A_{000}^{122} = \int_{-1}^{2\mu_1^2-1} -2\mu_1 d\mu + \int_{2\mu_1^2-1}^{\mu_1} B_{00}^{22}(\mu) d\mu, \quad (C.25)$$

which yields

$$A_{000}^{122} = -4\mu_1^3 + \int_{2\mu_1^2-1}^{\mu_1} B_{00}^{22}(\mu) d\mu, \quad (C.26)$$

where  $B_{00}^{22}(\mu)$  is given by Eq. (C.2). The integral of  $A_{000}^{222}$  for this range is unchanged and given by Eq. (C.24).

3)  $-0.5 \geq \mu_1 > -1$ :

Again, from Fig. C.4 we can write

$$A_{000}^{122} = \int_{-1}^{\mu_1} -2\mu_1 d\mu, \quad (C.27)$$

which gives

$$A_{000}^{122} = -2\mu_1(1 + \mu_1). \quad (C.28)$$

Finally,  $A_{000}^{222}$ , for this range is given by

$$A_{000}^{222} = \int_{\mu_1}^{2\mu_1^2-1} -2\mu_1 d\mu + \int_{2\mu_1^2-1}^1 B_{00}^{22}(\mu) d\mu, \quad (C.29)$$

which yields

$$A_{000}^{222} = 2\mu_1(1 + \mu_1 - 2\mu_1^2) + \int_{2\mu_1^2-1}^1 B_{00}^{22}(\mu) d\mu, \quad (C.30)$$

where  $B_{00}^{22}(\mu)$  is given by Eq. (C.2). The integrals,  $\int B_{00}^{22}(\mu) d\mu$ , which are involved in the derivation of  $A_{000}^{122}$  and  $A_{000}^{222}$ , have been calculated numerically in the text for the cases considered.

## REFERENCES

1. B. Davison, Neutron Transport Theory, Oxford University Press, London (1957).
2. K.M. Case and P.F. Zweifel, Linear Transport Theory, Addison-Wesley Publ. Co., Inc., Reading, Massachusetts (1967).
3. G.I. Bell and S. Glasstone, Nuclear Reactor Theory, Van Nostrand Reinhold Co., New York (1970).
4. K.D. Lathrop, "Transport Theory Numerical Methods", CONF-730414-P1, U.S. Atomic Energy Commission (1973).
5. A. Eddington, The Internal Constitution of the Stars, Dover Publ., Inc., New York (1926).
6. E. Amaldi and E. Fermi, Phys. Rev., 50, 899 (1936).
7. M. Verde and G.C. Wick, Phys. Rev., 71, 852 (1947).
8. R.E. Marshak, Rev. Mod. Phys., 19, 185 (1947).
9. B. Davison, "Extension of Feynman's Method of Determining Neutron Energy Spectrum and Spatial Distribution to the Case of Anisotropic Scattering", AERE T/R 590, U.K. Atomic Energy Research Establishment, Harwell (1950).
10. K.M. Case, Ann. Phys., 9, 1 (1960).
11. J.R. Mika, Nucl. Sci. Eng., 11, 415 (1961).
12. A.M. Jacobs, "A Contribution to the Theory of Elementary Solutions of the Neutron Transport Equation", Ph.D. Thesis, The Pennsylvania State University (1963).

13. H.G. Kaper, J.K. Shultis and J.G. Veninga, J. Comp. Phys., 6, 288 (1970).
14. J.K. Shultis, J. Comp. Phys., 11, 109 (1973).
15. E. Oblow, K. Kin, H. Goldstein and J.J. Wagschal, Nucl. Sci. Eng., 54, 72 (1974).
16. Z. Ziering and D. Schiff, Nucl. Sci. Eng., 3, 635 (1958).
17. Y. Yvon, J. Nucl. Energy, 4, 304 (1957).
18. S.A.W. Gerstl, Nucleonik, 8, 101 (1966).
19. Chi-Chung Wang, "The Double Spherical Harmonics Approximation for Cylindrical and Spherical Geometries", Ph.D. Thesis, University of Wisconsin (1967).
20. D.W. Drawbaugh and L.C. Noderer, Nucl. Sci. Eng., 9, 79 (1959).
21. E. Schmidt and E.M. Gelbard, Trans. Am. Nucl. Soc., 9, 432 (1966).
22. R.J. Cerbone and K.D. Lathrop, Nucl. Sci. Eng., 35, 139 (1969).
23. S.T. Huang and E.E. Lewis, J. Nucl. Energy, 26, 232 (1972).
24. S.T. Huang, "Studies of Asymptotic  $P_n$  and Double  $P_n$  Approximations to the Monoenergetic Neutron Transport Equation", Ph.D. Thesis, Northwestern University (1970).
25. H. Brockmann, "Comparison of Different Anisotropic Scattering Techniques in Neutron Transport Codes", 8th SOFT, Noordwijerhout, Netherlands (1974).
26. D.C. Irving, R.R. Coveyou and R.D. MacPherson, "Impossible Legendre Coefficients", CONF-660303, U.S. Atomic Energy Commission (1966).
27. D.H. Timmons, Trans. Am. Nucl. Soc., 16, 350 (1973).
28. D.H. Timmons, Trans. Am. Nucl. Soc., 17, 553 (1973).

29. J.K. Shultis and T.R. Hill, Nucl. Sci. Eng., 59, 53 (1976).
30. S. Chandrasekhar, Radiative Transfer, Dover Publ., Inc., New York (1960).
31. J.P. Odom and J.K. Shultis, Nucl. Sci. Eng., 59, 278 (1976).
32. A.A. Harms, Can. J. Phys., 48, 1007 (1970).
33. A.A. Harms, "Variable Phase-Space Neutron Transport Analysis", Ph.D. Thesis, University of Washington (1969).
34. A.A. Harms and W.J. Garland, "Optimum Angular Segmentations in Neutron Transport Analysis", CONF-720901, U.S. Atomic Energy Commission (1972).
35. E.M. Gelbard, "Spherical Harmonics: The  $P_L$  and Double- $P_L$  Approximations", in Computing Methods in Reactor Physics, H. Greenspan, C.N. Kelber and D. Okrent; eds., Gordon and Breach, New York (1968).
36. A.A. Harms and E.A. Attia, Nucl. Sci. Eng., 56, 310 (1975).
37. P. Kuijper, J.C. Veefkind and C.C. Jonker, Nucl. Phys., A181, 545 (1972).
38. M. Matoba, M. Hyakutaba, H. Tawara, K. Tsuji, H. Hasuyama, S. Matsuki, A. Katase and M. Sonoda, Nucl. Phys., A204, 129 (1973).
39. J.R. Lamarsh, Introduction to Nuclear Reactor Theory, Addison-Wesley Publ. Co., Inc., Reading, Massachusetts (1966).
40. L. Rangaswamy, L.S. Kothari and F. Ahmed, Nucl. Sci. Eng., 59, 261 (1976).
41. J.P. Odom and J.K. Shultis, Trans. Am. Nucl. Soc., 21, 530 (1975).

42. J.P. Odom, "Neutron Transport with Highly Anisotropic Scattering", Ph.D. Thesis, Kansas State University (1975).
43. E.A. Attia and A.A. Harms, Nucl. Sci. Eng., 59, 319 (1976).
44. G.W. Kattawar and G.N. Plass, J. Quant. Spect. Radiat. Transfer, 15, 61 (1975).
45. M.M.R. Williams, Mathematical Methods in Particle Transport Theory, Wiley-Interscience, New York (1971).
46. G.W. Kattawar and G.N. Plass, J. Quant. Spect. Radiat. Transfer, 13, 1065 (1973).
47. G.N. Plass, G.W. Kattawar and J. Binstock, J. Quant. Spect. Radiat. Transfer, 13, 1081 (1973).
48. G.E. Hunt, J. Quant. Spect. Radiat. Transfer, 11, 309 (1971).
49. J. Canosa and H.R. Penafiel, J. Quant. Spect. Radiat. Transfer, 13, 21 (1973).
50. B. Kivel, J. Quant. Spect. Radiat. Transfer, 12, 1659 (1972).
51. H. Jacobowitz, J. Quant. Spect. Radiat. Transfer, 11, 691 (1971).
52. J.T. Ward, Trans. Am. Nucl. Soc., 21, 529 (1975).
53. W.J. Garland and A.A. Harms, Transport Theory and Statistical Physics, 2, 347 (1972).
54. E.A. Attia and A.A. Harms, Nucl. Sci. Eng., 54, 450 (1974).
55. Erwin Kreyszig, Advanced Engineering Mathematics, John Wiley and Sons, Inc., New York (1972).
56. E.W. Cheney, Introduction to Approximation Theory, McGraw-Hill Book Co., New York (1966).
57. W.R. Conkie, Nucl. Sci. Eng., 6, 260 (1959).

58. S. Yabushita, J. Math. Phys., 2, 4 (1961).
59. G.C. Pomraning and M. Clark, Jr., Nucl. Sci. Eng., 17, 8 (1963).
60. V.T. Nonnenmacher, Atomkernenergie, 10, 408 (1965).
61. A.A. Harms and S.A. Kushneriuk, Nucl. Sci. Eng., 51, 76 (1973).
62. M. Abramowitz and I.A. Stegun, Handbook of Mathematical Functions,  
Dover Publ., Inc., New York (1964).
63. G. Goertzel and W. Tralli, Some Mathematical Methods of Physics,  
McGraw-Hill Book Co., Inc., New York (1960).
64. E.A. Attia, A.A. Harms and S.A. Kushneriuk, Can. J. Phys., 53,  
825 (1975).
65. B. Davison, "Milne Problem in a Multiplying Medium with a Linearly  
Anisotropic Scattering", CRT-358, National Research Council  
of Canada (1946).
66. E. İnönü and P.F. Zweifel, Development in Transport Theory, Academic  
Press, New York (1967).
67. H.G. Kaper, A.J. Lindeman and G.K. Leaf, Nucl. Sci. Eng., 54, 94  
(1974).
68. G.J. Mitsis, Nucl. Sci. Eng., 17, 55 (1963).
69. V.J. Krylov, Approximate Calculation of Integrals, McMillan,  
New York (1962).
70. T.R. Hill, J.K. Shultis and J.O. Mingle, J. Comp. Phys., 15, 2  
(1974).
71. Private communication with Dr. J.K. Shultis, Department of Nuclear  
Engineering, Kansas State University, Manhattan, Kansas.
72. D.C. Sahni, J. Nucl. Energy, A/B 20, 915 (1966).

73. L. Van Hove, Phys. Rev., 95, 249 (1954).
74. P. Guenther, A. Smith and J. Whalen, Nucl. Sci. Eng., 59, 106 (1976).
75. S.A.W. Gerstel and W. Kofink, Nucl. Sci. Eng., 33, 249 (1968).
76. S.A.W. Gerstel, Nukleonik, 10, 227 (1967).
77. Private communication with Dr. J.P. Odom, Applied Physics Division,  
Argonne National Laboratory, Argonne, Illinois.